Studying the neurochemical determinants of antipsychotic efficacy and side effect profile: a translational dopamine D2 and serotonin 2a neuroimaging approach

Tsartsalis, Stergios

UNIVERSITÉ DE GENÈVE
FACULTÉ DE MÉDECINE

DOCTORAT EN NEUROSCIENCES
des Universités de Genève
et de Lausanne

UNIVERSITÉ DE GENÈVE

FACULTÉ DE MEDECINE

Professeur MILLET Philippe, directeur de thèse

TITRE DE LA THESE

STUDYING THE NEUROCHEMICAL DETERMINANTS OF ANTIPSYCHOTIC EFFICACY AND SIDE EFFECT PROFILE: A TRANSLATIONAL DOPAMINE D_2 AND SEROTONIN 2A NEUROIMAGING APPROACH

THESE
Présentée à la
Faculté de Médecine

de l'Université de Genève

pour obtenir le grade de
Docteur en Neurosciences

par

Stergios TSARTSALIS

de Grèce

Thèse N° 255

Genève

Editeur ou imprimeur : Université de Genève

2019

UNIVERSITÉ DE GENÈVE
FACULTÉ DE MÉDECINE
Secrétariat des étudiants

oaa accredited in Switzerland

DOCTORAT EN NEUROSCIENCES

des Universités de Genève et de Lausanne

Thèse de

Stergios TSARTSALIS
originaire de Grèce
Intitulée

STUDYING THE NEUROCHEMICAL DETERMINANTS OF ANTIPSYCHOTIC EFFICACY AND SIDE EFFECT PROFILE: A TRANSLATIONAL DOPAMINE D_2 AND SEROTONIN 2A NEUROIMAGING APPROACH

Soutenue le : 28 août 2019

La Faculté de médecine, sur préavis du jury de thèse formé par :

Professeur Alexandre Dayer, Faculté de médecine, Université de Genève, Président du jury
Professeur Philippe Millet, Faculté de médecine, Université de Genève, directeur de thèse
Professeur Stephan Eliez, Faculté de médecine, Université de Genève, expert
Docteure Marie-Claude Grégoire, Australian Nuclear Science and Technology organization, experte
Docteur Michel Bottlaender, Commissariat à l'énergie atomique et aux énergies alternatives, Institut des sciences du vivant Frédéric Joliot, CEA Paris-Saclay, France, expert

Autorise l'impression de la présente thèse, sans prétendre par là émettre d'opinion sur les propositions qui y sont énoncées.

Genève, le 28 octobre 2019

Thèse n° 255

Professeur Cem Gabay
Doyen

*N.B. La thèse imprimée doit porter la déclaration précédente * et remplir les conditions énumérées dans les « Informations aux étudiants relatives aux thèses de doctorat à l'Université de Genève ».*

Acknowledgements

For this work, I would like to thank, first of all, Professor Philippe Millet, my thesis supervisor, for giving me this opportunity, for his constant trust and inspiration. I feel gratitude for Doctor Benjamin Tournier, an excellent colleague without whom this thesis could not have been realized. With Philippe and Benjamin, I have had the immense luck to have found two great colleagues but, most importantly, two very close friends.

A special thank you is addressed to Professor Nathalie Ginovart, who supervised the biological part of my thesis and shared her expertise on the subject. She provided excellent comments and advice.

I wish to thank the members of my thesis committee, Professor Dayer, Doctor Bottlaender, Professor Eliez and Professor Grégoire. They accepted to evaluate my work and provided excellent comments for its improvement.

This work was graciously supported by the Swiss National Science Foundation, the Geneva Neuroscience Center, the Departments of Psychiatry of the Geneva University Hospitals and the University of Geneva, the Greek National Scholarship Foundation (Maria Zaousi Memorial scholarship to the author of this thesis) and the Swiss Association for Alzheimer's Research.

I want to thank all the colleagues and friends of the laboratory in which I realized this thesis, Maria Surini, Marouane Ben-Ammar, Eniko Kovari, Constantinos Bouras, Pia Lovero, Yessica Gloria, Meriem Ben Hamadi, Selim Habiby, Cristina Barca, Karl Aoun, and others. An exceptional thanks to Doctor Yves Charnay, with whom I started working in this lab, a great friend and an example of a researcher for me.

This work could not have been possible without the support of the direction of the Department of Psychiatry of the Geneva University Hospitals. They allowed me to realize a significant part of my Ph.D. studies while pursuing my clinical training in Psychiatry.

My colleagues at the Mood Disorders Unit, led by Dre Hélène Richard-Lepouriel, and the Division of Psychiatric Specialties, led by Prof Jean-Michel Aubry, for being so understanding and patient with my administrative work's lateness these last months. I thank them very much.

I would like to thank my parents, my brother, and the rest of my family for their support and for teaching me to focus on doing my best, not on the result itself. The same goes for all my friends. A special thanks to Eva, a source of strength and encouragement, whose contribution has been crucial to the success of this thesis during these last months.

Abstract

The present thesis describes the development of a translational study combining *ex vivo* and *in vivo* imaging as well as behavioral experiments in rats to address the hypothesis that a 5-HT_{2A} receptor antagonism is one of the substrates of atypicality, i.e. enhanced efficacy and reduced side effect burden of atypical vs typical antipsychotic agents. A major part of this work was dedicated to the development of simple imaging approaches to study the $D_{2/3}$ and the 5-HT_{2A} receptors in the rat brain. Most importantly, a simultaneous, dual-radiotracer methodology was validated, to allow the quantification of $D_{2/3}$ and 5-HT_{2A} receptors in the same *in vivo* Single Photon Emission Computed Tomography (SPECT) scan. This methodology was employed in the biological part of this thesis. In this study, the effect of the co-administration of MDL-100,907, a selective 5-HT_{2A} receptor antagonist, along with a chronic treatment with various clinically relevant doses of haloperidol, a typical antipsychotic agent was assessed with a series of behavioral tests in rats. Dual radiotracer SPECT imaging allowed to measure 1) the occupancy of the $D_{2/3}$ and 5-HT_{2A} receptor by haloperidol and MDL-100,907, respectively and 2) the alterations in the density of $D_{2/3}$ and 5-HT_{2A} receptors by the chronic treatment with their respective antagonists. Co-administration of MDL-100,907 partially reduced the haloperidol-induced catalepsy (a phenomenon corresponding to acute extrapyramidal side effects of antipsychotics) and was associated with a tendency towards a higher efficacy of haloperidol in the dizocilpine-disrupted prepulse inhibition of the startle reflex (a test that is indicative of efficacy of an antipsychotic agent against psychotic symptoms). However, MDL-100,907 co-administration failed to reverse the haloperidol-induced vacuous chewing movements (a symptom corresponding to tardive dyskinesia). Regarding the neurochemical alterations induced by these chronic treatments, haloperidol induced an upregulation of the $D_{2/3}$ receptor in the striatum of rats, while MDL-100,907 had no effect. Similarly, the present study included a previously unappreciated finding: an upregulation of the 5-HT_{2A} receptors in various frontal cortical regions and the VTA, which was induced by a moderate dose of haloperidol. Overall, this thesis underlines the interest of the validation and use of translational SPECT neuroimaging. It points to a -partial- implication of a 5-HT_{2A} receptor antagonism to the mechanism of action of atypical antipsychotic drugs and emphasizes the need to employ clinically pertinent doses of antipsychotics in fundamental psychopharmacological research.

Résumé

Cette thèse décrit le développement d'une étude translationelle, combinant l'imagerie *ex vivo* et *in vivo,* ainsi que des tests comportementaux chez le rat, afin d'évaluer l'hypothèse que l'antagonisme du récepteur 5-HT_{2A} est un des substrats de l'atypicité, i.e. d'une efficacité augmentée et d'un risque réduit d'effets secondaires des antipsychotiques atypiques comparés aux typiques. Une partie importante de cette thèse a été dédiée au développement de méthodes de quantification simplifiées des récepteurs $D_{2/3}$ et 5-HT_{2A}. Une contribution importante de ce travail concerne la validation d'une méthode d'imagerie par Tomographie par Émission Monophotonique (TEMP) *in vivo* de deux récepteurs en simultané, dans la même séance TEMP. Cette approche a été employée dans la partie biologique de la thèse. Dans cette partie, l'effet de la co-administration du MDL-100,907, un antagoniste sélectif du récepteur 5-HT_{2A}, avec un traitement chronique par de multiples doses, cliniquement pertinentes, d'haloperidol a été évalué, sur une série de tests comportementaux chez le rat. Une imagerie SPECT a permis de mesurer 1) l'occupation de récepteurs $D_{2/3}$ et 5-HT_{2A} par l'haloperidol et le MDL-100,907, respectivement et 2) les altérations au niveau de la densité de ces récepteurs suite au traitement chronique par leurs antagonistes. La co-administration du MDL-100,907 a partiellement réduit la catalepsie induite par l'haloperidol (un test qui correspond aux effets extrapyramidaux aigus des antipsychotiques) et a été associée à une tendance de l'haloperidol à être plus efficace dans le test du déficit de l'inhibition du réflexe de sursaut (PPI) induit par la dizocilpine (ce test est un indicateur de l'efficacité de traitements antipsychotiques face aux symptômes psychotiques). Cependant, la co-administration du MDL-100,907 n'a pas prévenu l'apparition de mouvements de mastication induits par l'haloperidol (un test qui correspond à la dyskinésie tardive). Concernant les altérations au niveau de la densité des récepteurs, l'haloperidol a provoqué une augmentation de la densité du récepteur $D_{2/3}$ dans le striatum, un effet qui n'a pas été modifié par la co-administration du MDL-100,907. De plus, notre étude a mis en évidence pour la première fois, une augmentation de la densité du récepteur 5-HT_{2A} dans de régions corticales frontales et l'aire tegmentale ventrale, induite par une posologie modérée d'haloperidol. En conclusion, cette thèse démontre l'intérêt de l'utilisation de la neuroimagerie TEMP dans des études translationnelles. Elle suggère une implication -partielle- de l'antagonisme du récepteur 5-HT_{2A} dans l'atypicité et souligne l'importance d'employer de doses d'antipsychotiques cliniquement pertinentes dans la recherche fondamentale.

Table of contents

1. Introduction

1.1. Schizophrenia and antipsychotic medication

Schizophrenia is a chronic psychiatric disorder, affecting roughly 1% of the population with an invalidating character at the individual level and a major socio-economic impact. At a clinical level, symptoms develop along three well described axes: (i) positive symptoms, i.e. disorganized and/or delusional thought and perception deficits (hallucinations), (ii) negative symptoms, i.e. blunted affect, anhedonia, amotivation and poverty of speech and (iii) cognitive symptoms, i.e. deficits of executive functions, attention, working and verbal memory (Ginovart and Kapur, 2012; Lewis and Lieberman, 2000). Its etiology comprises a wide spectrum of genetic, developmental and environmental factors (Lewis and Lieberman, 2000). The most studied pathophysiological aspect of schizophrenia, in a simplified form, suggests a deficiency in the dopaminergic neurotransmission at the mesocortical level and a “hyperactivity” of the dopaminergic transmission at the mesolimbic level (Demjaha et al., 2012; Fusar-Poli and Meyer-Lindenberg, 2013; Ginovart and Kapur, 2012; Howes et al., 2012; Howes and Kapur, 2009; Kambeitz et al., 2014; Lewis and Lieberman, 2000; McCutcheon et al., 2018; Slifstein et al., 2015). The development of this theory, the “dopaminergic hypothesis” of schizophrenia was based on the fact that the first effective treatment against positive symptoms (and the majority of treatments ever since) was mainly a D_2 receptor antagonist. However, the dopaminergic hypothesis has been modified, if not largely replaced, since its first formulation with new pathophysiological aspects that are currently under study. Genomic and epigenetic studies attempt to shed light on the etiology of the disease that goes way beyond the dopaminergic system. With the advent of new genomic analysis technologies, a polygenic risk score may be determined (Kuehner et al., 2019; Zhuo et al., 2019). Transcriptomic analyses allow the elucidation of gene expression alterations and the identification of the cellular populations that produce these alterations, thus demonstrating potentially causal links between a distinct cell type and an aspect of the disease pathology (Skene et al., 2018). Beyond molecular imaging techniques, a wide range of brain imaging methods, such as functional and structural Magnetic Resonance Imaging (MRI) (McCutcheon et al., 2019), diffusion tensor imaging (Collin and Keshavan, 2018) and electroencephalography (EEG) (Lavoie et al., 2019), extend our knowledge on brain structure and function in health and

disease and intend to provide an arsenal of biomarkers to inform studies on the development of new therapeutics and to serve as indicators of the efficacy of the various therapeutic interventions. The research on the field is further fueled by preclinical animal models that reproduce particular aspects of the disease and pathophysiological mechanisms such as inflammation and oxidative stress (Gumusoglu and Stevens, 2019; Marissal et al., 2018). Overall, these studies have demonstrated that the pathophysiology of schizophrenia is much more than an imbalanced outflow of dopamine to cortical and subcortical areas and that a wider range of brain networks are implicated.

Despite the developments in the understanding of the etiopathology of schizophrenia, antipsychotic agents still constitute the cornerstone of schizophrenia treatment. Based on their pharmacology and their clinical profile they are characterized as typical ("first generation") and atypical ("second generation") agents. Typical antipsychotics (e.g. haloperidol) are efficient against positive symptoms but can induce side effects such as acute (parkinsonism, akathisia and dystonia) and later-onset (tardive dyskinesia) extrapyramidal syndromes (EPS), hyperprolactinemia and effects on cognition and affects (dysphoria/anhedonia, depressed mood and slowed mentation). Atypical antipsychotics are efficient against positive symptoms and probably have a reduced side effect burden (Ginovart and Kapur, 2012). Despite the fact that the actual superiority of atypical over typical antipsychotics is debated (Lewis and Lieberman, 2008), recent meta-analyses suggest lower prevalence of extrapyramidal side effects of atypical agents compared to typical ones (Table 2) (Leucht et al., 2013; Martino et al., 2018).

1.1.1 Atypical antipsychotic medication

The main pharmacodynamic characteristic of all antipsychotic agents is a $D_{2/3}$ receptor blockade. Multiple clinical imaging studies have established a precise relationship between the level of $D_{2/3}$ receptor occupancy and the efficacy/side effect profile of the antipsychotic agents. It is thus generally admitted that, for most of these agents, a $D_{2/3}$ receptor occupancy between 65 and 80% is associated with an efficacy against positive symptoms. Beyond an 80% occupancy level, the propensity for EPS is increased, whereas no greater efficacy is observed (Kapur and Remington, 2001; Uchida et al., 2011). The emergence of such side effects greatly reduces compliance with the treatment, leading to a high symptom relapse risk (Casey, 2006; Dossenbach

et al., 2005).

Concerning the pharmacological determinants of atypicality, multiple theories have been developed. According to the most extensively studied among them, atypical antipsychotics bind to a large spectrum of receptors, over multiple neurotransmitter systems and this is their defining characteristic. Indeed, most typical antipsychotics have relatively limited target-receptor spectrum and their actions are mostly associated with the $D_{2/3}$ receptor blockade. More precisely, a strong antagonism of the 5-HT_{2A} receptor has been proposed as a major determinant of antipsychotic atypicality (Kuroki et al., 1999; Meltzer, 2004; Meltzer et al., 2003). Whereas 5-HT_{2A} antagonism *per se* is not considered as conferring antipsychotic efficacy (Ebdrup et al., 2011), one leading hypothesis proposes that a combined blockade of D_2 and 5-HT_{2A} receptor is responsible for the efficacy and the reduced side effect liability of atypical versus typical agents.

1.1.2 Evidence linking 5-HT_{2A} receptor antagonism to atypicality

The 5-HT_{2A} receptor is widely expressed in the CNS, especially in layer I and IV-V of the cerebral cortex, with frontal areas presenting the highest receptor concentration, as well as, to a lesser extent, in subcortical areas, such as the striatum. They exert their effect via different intracellular signaling pathways, such as the $G_{\alpha q}$ - PLC-IP_3 pathway, the $G_{\alpha q}$-mediated PLC_{β}/IP_3 /calcineurin pathway and the $G_{\alpha 12/13}$-phospholipase A_2 signal transduction pathway, which promotes arachidonic acid release. In addition, 5-HT_{2A} receptors may act via non-G-protein pathways, such as via the β-arrestin2/phosphoinositide 3- kinase/Src/Akt cascade (Zhang and Stackman, 2015). The 5-HT_{2A} receptor is potentially associated to the pathophysiology of schizophrenia. *Post mortem* studies have demonstrated an overall decrease in the 5-HT_{2A} receptor binding (Rasmussen et al., 2010; Selvaraj et al., 2014) along with an increase in the active conformation of 5-HT_{2A} receptor binding the prefrontal cortex of schizophrenic patients (Muguruza et al., 2013). 5-HT_{2A} antagonism may be important in a subset of patients, as genetic variability may induce a differential role of this receptor in the pathophysiology of the disease and the response to treatment (Blasi et al., 2015; Kanno-Nozaki et al., 2018; Kaur et al., 2017)

From a physiological perspective, with a particular focus on the mechanism of action of antipsychotic drugs, 5-HT_{2A} receptors expressed on pyramidal cells of the prefrontal cortex (Santana et al., 2004) project to the ventral tegmental area (VTA) (Vazquez-Borsetti et al., 2008) and the nucleus accumbens (NAcc) (Mocci et al., 2014).

In this way, they may modulate the activity of the dopaminergic projections of the VTA (Bortolozzi et al., 2005). Blockade of the 5-HT_{2A} receptor has been associated with an increase in dopamine release in the prefrontal cortex, compared to the striatum, suggesting that the transmission in the mesocortical system, already deficient in schizophrenic patients may be relatively preserved under atypical antipsychotic treatment, while the “hyperactive” mesolimbic system is safely reduced (Ginovart and Kapur, 2012; Huang et al., 2014; Ichikawa et al., 2001; Ichikawa and Meltzer, 1995; Kuroki et al., 1999; Liegeois et al., 2002). However, a recent study found that dopamine release in prefrontal cortex requires 5-HT_{1A} receptors, not 5-HT_{2A} (Bortolozzi et al., 2010). 5-HT_{2A} antagonism locally in the midbrain may be associated with a preferential blockade of the mesolimbic neurotransmission, while the nigrostriatal system (whose blockade leads to EPS) is relatively spared (Olijslagers et al., 2005). Atypical antipsychotic administration is also associated with a down-regulation of 5-HT_{2A} receptor in rodents (Choi et al., 2017; Huang et al., 2007; Lian et al., 2013; Moreno et al., 2013; Steward et al., 2004; Tarazi et al., 2002; Yadav et al., 2011) and this effect is considered implicated in their superior efficacy compared to typical antipsychotics.

The 5-HT_{2A} receptor remains the object of extensive research in the field of the psychopharmacology of schizophrenia and psychotic disorders, especially in terms of their side effect profile. Newer antipsychotic agents, such as cariprazine (Fleischhacker et al., 2019; Herman et al., 2018; Wesolowska et al., 2018), braxpiprazole (McEvoy and Citrome, 2016), lumateperone (Vanover et al., 2019) and pimavanserine (Nasrallah et al., 2019), have a moderate or high 5-HT_{2A} binding. Overall, the interest for the 5-HT_{2A} receptor remains “alive” in modern psychopharmacology and in this context, the evaluation of the role of this receptor in the clinical profile of antipsychotic medication is warranted.

Receptor affinities

Medications	D2	5HT1A	5HT2A	5HT2C	alpha1	alpha2	H1	M1	M3	M4
Clozapine	210	160	2.59	4.8	6.8	158	3.1	1.4	204	27
Amisulpride	1.3	10000	2000	10000	7100	1600	10000	n/A	n/A	n/A
Olanzapine	20	610	1.5	4.1	44	280	0.08	2.5	622	350
Risperidone	3.77	190	0.15	32	2.7	8	5.2	10000	10000	10000
Paliperidone	2.8	480	1.2	48	10	80	3.4	10000	10000	10000
Zotepine	11	330	2.7	3.2	3.4	180	0.62	18	140	77
Haloperidol	2.6	1800	61	4700	17	600	260	10000	10000	10000
Quetiapine	770	300	31	3500	8.1	80	19	120	630	660
Aripiprazole	0.66	5.5	8.7	22	26	74	30	6780	3510	1520
Sertindole	2.7	2200	0.14	6	3.9	190	440	5000	n/A	n/A
Ziprasidone	2.6	1.9	0.12	0.9	2.6	154	4.6	300	10000	10000
Chlorpromazine	3	3115	5.4	30	2.6	750	9	25	215	40
Asenapine	8.9	8.6	10.15	10.46	8.9	9.5	9	5.09	4.5	5.09
Lurasidone	1.7	6.8	2	415	48	11	10000	10000	10000	10000
Iloperidone	3.3	33	0.2	14	0.31	3	12.3	4.898	3.311	8318

Table 1. Receptor affinity profiles (Ki values) for various neurotransmitter receptors (Olten et al., 2018).

However, it is impossible to dissociate the effects of the 5-HT_{2A} receptor in either clinical or preclinical studies in which the commercially available antipsychotic agents are employed. All these agents have considerable affinities for a wide spectrum of receptors (as presented in Table 1 (Olten and Bloch, 2018)). This underlines the importance of conducting studies with highly specific agents for the receptor of interest. In this context, preclinical paradigms and animal models that study aspects of antipsychotic pharmacology with a high translational potential are of particular interest.

1.1.3 Preclinical experimental paradigms to study the role of 5-HT2A in antipsychotic atypicality

A multitude of preclinical and clinical studies have examined the role of the 5-HT_{2A} receptor in the mechanism of action of atypical antipsychotic agents. Generally, when examining the properties of antipsychotic agents in a preclinical context, several experimental paradigms and models are employed, covering multiple aspects of their efficacy profile and the side effects. These experimental paradigms have a high translational potential: indeed, the efficacy and side effect liability of a pharmacological agent in these tests follows the same pattern with respect to the D_2 receptor-occupancy "window" described above, meaning that a treatment that occupies 65-80% of the $D_{2/3}$ receptors in the rat striatum will be efficient in these tests without any side effects, whereas an occupancy beyond 80% will be associated to the appearance of side effects. In addition, these models are useful in the study of the "atypical" antipsychotic profile, as the differences between various typical and atypical antipsychotics that are observed clinically are generally present when the same agents are evaluated preclinically with these tests (Johnson et al., 2014; Wadenberg et al., 2001b). The existing literature using these paradigms with respect to the role of 5-HT_{2A} in antipsychotic atypicality is reviewed in the following paragraphs.

1.1.4 Evaluation of antipsychotic efficacy

In preclinical paradigms that evaluate the antipsychotic efficacy, 5-HT_{2A} blockade, when added to a treatment with a typical antipsychotic agent may potentiate its effect. One example is the suppression of the Conditioned Avoidance Response (CAR), an established paradigm of atypical antipsychotic efficacy against positive symptoms with a high predictive validity. In this test, rats are trained to avoid an unconditioned stimulus (a mild electric shock) when a conditioned stimulus (a sound) is presented. The disruption of this conditioned avoidance response by a pharmacological agent predicts that this agent will be efficient against positive psychotic symptoms in patients (Wadenberg, 2010). Wadenberg and colleagues demonstrated adding a selective 5-HT_{2A} receptor antagonism to a typical antipsychotic agent potentiated its effects (Wadenberg et al., 2001a; Wadenberg et al., 1998). However, 5-HT_{2A} antagonism with MDL-100,907 at 0.5 mg/kg and 1 mg/kg failed to enhance the effect of a low acute dose of haloperidol (0.05 mg/kg) on the conditioned avoidance response in

a more recent study (Gao et al., 2019).

Another well-established translational paradigm of antipsychotic efficacy is the disruption of the prepulse-inhibition of the startle response (Bakshi and Geyer, 1998; Swerdlow et al., 2008; Wadenberg et al., 2000). In this paradigm, rats are exposed to a strong, high-volume auditory stimulus, which produces a startle response. A lower-volume auditory stimulus that precedes the high-volume one diminishes the magnitude of the startle response. This prepulse inhibition (PPI) of the startle response is disrupted by a pretreatment with dizocilpine (MK-801), an NMDA antagonist. Several antipsychotic agents reverse this disruptive effect of dizocilpine and this property is also associated with an efficacy against psychotic symptoms in a clinical setting. Atypical antipsychotics have generally been shown to efficiently block this disruption (Bubenikova et al., 2005; Hudson et al., 2016; Li et al., 2016; Varty and Higgins, 1995; Zangrando et al., 2013) and are probably superior to haloperidol in this respect (Feifel and Priebe, 1999; Varty and Higgins, 1995), while a 5-HT2A antagonism *per se* shows antipsychotic efficacy in this particular paradigm (Varty et al., 1999). In light of these results, it is possible that the variable level of 5-HT_{2A} antagonism across the different antipsychotic agents could explain these differential effects and one could hypothesize that further enhancing the 5-HT_{2A} antagonism properties of an antipsychotic agent could enhance its efficacy on the dizocilpine-disrupted PPI.

1.1.5 Evaluation of motor side effects

Antipsychotic medication is associated to a risk of motor side-effects, such as parkinsonism and tardive dyskinesia. Atypical antipsychotics have a lower risk of inducing these phenomena (Carbon et al., 2017; Carbon et al., 2018; Correll, 2017; Hartling et al., 2012; Leucht et al., 2013; Martino et al., 2018). In the rat, the acute extrapyramidal side effects are assessed using the catalepsy test. An animal is placed on an inclined surface and an increased latency in moving its paws is indicative of an extrapyramidal syndrome. The catalepsy paradigm has a high translational potential: a $D_{2/3}$ receptor occupancy of >80% is associated to a high risk of positivity in this test, as is the risk of induction of an EPS in human subjects treated with equivalent doses of antipsychotic agents (Johnson et al., 2014). Assuming that 5-HT_{2A} antagonism is a substrate of atypicality, one may hypothesize that adding a 5-HT_{2A} antagonism to a $D_{2/3}$ antagonism should alleviate the cataleptogenic effect of the latter treatment. The actual literature is controversial on the impact of 5-HT_{2A} antagonism on the cataleptic effects of

a $D_{2/3}$-receptor antagonism (Creed-Carson et al., 2011; McOmish et al., 2012; Naumenko et al., 2010; Reavill et al., 1999; Wadenberg et al., 2001a).

In addition to acute EPS that are assessed with the catalepsy test, the phenomenon of tardive dyskinesia may be studied with a relevant animal model: chronic treatment with $D_{2/3}$-receptor antagonists induces vacuous chewing movements (VCM) in rats and mice along with an up-regulation of the $D_{2/3}$ receptor in the striatum (Turrone et al., 2003a, b) and decreases in the levels of monoaminergic neurotransmitters in the rat brain (Bishnoi et al., 2007). A potent 5-HT_{2A} blockade may prevent the up-regulation of $D_{2/3}$ receptor in the striatum, induced by chronic blockade of this receptor (Ishikane et al., 1997; Kusumi et al., 2000), suggesting that such a treatment may prevent the VCM, a finding that, in the actual literature is particularly debated (Egan et al., 1995; Fdez Espejo and Gil, 1997; Ikeda et al., 1999; Marchese et al., 2004; Naidu and Kulkarni, 2001).

Prevalence of Movement Disorders	Medication	NbN Classification
High	Haloperidol	D2 receptor antagonist
	Chlorpromazine	D2 and 5-HT2 receptor antagonist
	L-sulpiride	D2 receptor antagonist
Moderate-to-high	Ziprasidone	D2 and 5-HT2 receptor antagonist
	Aripiprazole	D2 and 5-HT1A partial agonist and 5-HT2A receptor antagonist
	Risperidone	D2, 5HT2A and NE-alpha 2 receptor antagonist
	Amisulpride	D2 receptor antagonist
Moderate-to-low	Olanzapine	D2 and 5-HT2A receptor antagonist
	Paliperidone	D2, 5HT2A and NE-alpha 2 receptor antagonist
	Asenapine	D2, 5HT2A and NE-alpha 2 receptor antagonist
Low	Clozapine	D2, 5HT2A and NE-alpha 2 receptor antagonist
	Quetiapine	D2 and 5HT2A receptor antagonist – norepinephrine transporter inhibitor

The table indicates also their classification based on Principal Mode of Action, according to the neuroscience-based nomenclature (NbN).

Table 2. Summary Table of the Classification of Antipsychotic Agents into Four Groups and Mode of Action Based on Prevalence Estimates of Acute Movement Disorders (Martino et al, 2018).

1.1.6 Evaluation of cognitive side effects

Results from the CATIE trial, a large clinical study comparing the effects of typical and atypical antipsychotics showed that high $D_{2/3}$ receptor occupancy was associated with cognitive side effects (Sakurai et al., 2013) and a PET study found that extrastriatal $D_{2/3}$ receptor blockade is associated with cognitive impairment in schizophrenic patients (Nørbak-Emig et al., 2016). Haloperidol (Lustig and Meck, 2005) and sulpiride (Naef et al., 2017) have been associated with working memory deficits in healthy volunteers. Working memory alterations were also induced by high-occupancy of the $D_{2/3}$ receptor by aripiprazole (Kim et al., 2013). Karl et al found that both haloperidol and an atypical agent, risperidone, impaired working memory in rats (Karl et al., 2006) and this observation has been made in clinical studies of the cognitive side effects of both typical and atypical antipsychotics, pointing to a deleterious effect of $D_{2/3}$. Nevertheless, the effect of a 5-HT_{2A} blockade on this side effect has not been thoroughly assessed.

1.1.7 Towards a multi-modal imaging approach

A particularly high number of studies has assessed the role of the 5-HT_{2A} receptor on the efficacy and side effect profile of antipsychotic agents. However, the actual literature, described in the previous paragraphs, suffers from several technical and conceptual limitations. First of all, as mentioned in paragraph 1.1.2., the dissection of the role of the 5-HT_{2A} receptor on the antipsychotic pharmacology is difficult to perform in clinical studies, mainly because the antipsychotic agents that are actually clinically prescribed or under study act on a wide spectrum of receptors other than the 5-HT_{2A}. Furthermore, in clinical studies and for ethical reasons, only a limited range of antipsychotic dosages may be employed, always remaining within the 65-80% “window” of $D_{2/3}$ receptor occupancy.

Such a study is technically more feasible to perform on rodents and its results, both in terms of behavioral experiments and imaging technics can be highly translatable, as exposed in paragraphs 1.1.3 to 1.1.6. However, concerning these preclinical studies, a major limitation in the actual literature has to do with the absence of clinical relevance of the doses of antipsychotics that are employed. In the vast majority of the preclinical studies described above, a unique dose of haloperidol (1 mg/kg) has been used, with no evaluation of the actual $D_{2/3}$ occupancy ratio. If such doses induces irrelevantly high $D_{2/3}$ occupancy in the striatum, its results are not

necessarily translatable in a clinical setting: indeed, clinical data suggests that, even for atypical agents, their distinct efficacy and side effect profile is most likely to be observed only when their occupancy of the D_2 receptor lies within or "close to" the 65-80% "window". Under this assumption, it is still necessary to evaluate if a 5-HT_{2A} receptor antagonism could alter the profile of a clinically relevant $D_{2/3}$ receptor occupancy. In addition, in several studies in the literature, mixed 5-$HT_{2A/2C}$ antagonists were employed, thus failing to distinguish between the effects of each one of these receptors, given that 5-HT_{2C} could well be another substrate of the antipsychotic atypicality (Creed-Carson et al., 2011; Pogorelov et al., 2017; Reavill et al., 1999). Another limitation in the existing literature concerns the duration of the treatment, given that many of the studies use short-term regimens, even single doses of the antipsychotic agents. Overall, few if any of these studies have directly assessed the relationship between receptor-occupancy, behavioral effects of the treatment and the neurochemical alterations induced by this treatment in the level of the implicated receptors.

In this context, the present thesis proposes an evaluation of the effects of a chronic treatment with a typical $D_{2/3}$-specific antagonist, haloperidol, with and without a 5-HT_{2A} blockade by a highly specific antagonist, MDL-100,907. Haloperidol will be given at different, clinically relevant, doses along the occupancy ratio spectrum. The effects of these chronic treatments will be assessed in the following preclinical paradigms of: 1) antipsychotic efficacy, as measured with the ability of the treatments to reverse the dizocilpine-induced deficits in the PPI of the startle response, 2) acute extrapyramidal side effects using the catalepsy test, 3) tardive dyskinesia using the vacuous chewing movements paradigm and finally, 4) cognitive side effects with the Y maze test.

These behavioral experiments will be combined with small animal Single Photon Emission Tomography (SPECT), which will be employed to: 1) measure *in vivo* the occupancy of the $D_{2/3}$ and 5-HT_{2A} receptors by the respective treatments, which is the "gold-standard" approach in neuropharmacology, 2) in a second series of scans, *in vivo* SPECT imaging will be employed to assess the neurochemical alterations, which are induced after the aforementioned chronic treatments. In the following paragraphs, the molecular neuroimaging techniques that were used in this thesis are presented.

1.2 Molecular neuroimaging in the service of biology

SPECT and PET are two powerful molecular imaging modalities enabling the *in vivo* study of various molecular processes by quantifying molecules of interest, ranging from neurotransmitter receptors (e.g. the $D_{2/3}$ receptor) to pathological proteins in the brain (e.g. Aβ deposits). SPECT and PET are the only neuroimaging modalities that may actually quantify molecules in the living brain, with a picomolar sensitivity (Cunningham et al., 2004; Frankle et al., 2005; Gunn et al., 2001; Phelps, 2000; Slifstein and Laruelle, 2001). In the current project, SPECT imaging has been employed to image 1) the occupancy of the $D_{2/3}$ and the 5-HT_{2A} receptors from the respective antagonist molecules and 2) the alteration in these receptors' concentration after chronic treatment with those antagonists, as mentioned in the previous section.

The following paragraphs aim to shed light on the methodological challenges that had to be addressed in the present project. First, a delineation of the molecular imaging quantification approaches is necessary.

1.2.1 Why use kinetic modeling in molecular neuroimaging?

In a SPECT or PET study of a brain target (hereon, a receptor or a target), a radiotracer that binds to the receptor with a high specificity is intravenously injected into very small, "tracer" amounts. At this quantity, the radiotracer is occupying a very low proportion of the receptors (< 5%). This is a basic principle of molecular imaging, which implies that at this low level of receptor occupancy, the biological system under study is not perturbed by the imaging process. After injection, a proportion of the radiotracer molecules may be bound to plasma proteins and/or metabolized. Then, its physicochemical properties determine the kinetics of blood-brain barrier penetration, association to the receptor, dissociation from it and return to the blood circulation for elimination. So, the radiotracer may be found in various states, namely, (1) free (non-bound to any protein) in the plasma, (2) bound to plasma proteins, (3) free in the brain tissue, (4) bound specifically to its target-protein and (5) bound to other proteins non-specifically. It is evident that the images obtained from the scan do not directly correspond to the number of receptors in the brain (Bailey et al., 2006; Millet and Lemoigne, 2008; Morris et al., 2004) but to an "average" of all these states in which the radiotracer may be found (Figure 1 (Morris et al., 2014; Pellerin and Magistretti, 1994)).

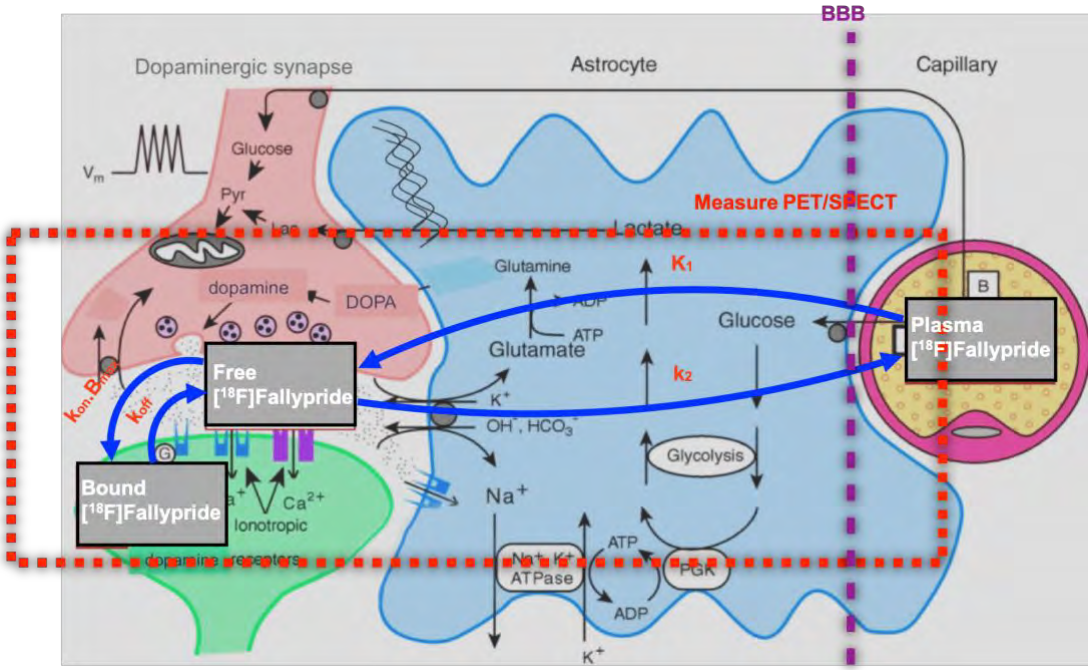

Figure 1. The PET or SPECT measure is an “average” measurement of the concentration of the radiotracer may be found in the brain, i.e. in the plasma of the brain vessels, in a “free” state in the tissue and bound to its receptor. Modified from Morris et al., 2014 and Pellerin et al., 1994. Courtesy of P. Millet.

For this reason, an important number of different methods for quantification, that take all the aforementioned parameters into account, have been developed over the years. These methods allow to “disentangle” the information pertaining to the quantity of receptors from the non-relevant components of the images. In its most classical form, i.e. “kinetic” methods employ dynamic scans, i.e. obtaining a series of images of a very short duration (usually 30 sec to several minutes), which are called frames. The total number of frames required depends on the properties of the tracer. In parallel, serial arterial blood samples are collected, as the knowledge of radiotracer plasma concentration kinetics is a prerequisite in the application of this method of quantification. We may thus follow the kinetic pattern of the concentration of the radiotracer (described by time-activity curves-TACs) in the plasma and in the brain over time (Figure 2). The knowledge of this kinetic pattern is of capital importance for the quantification.

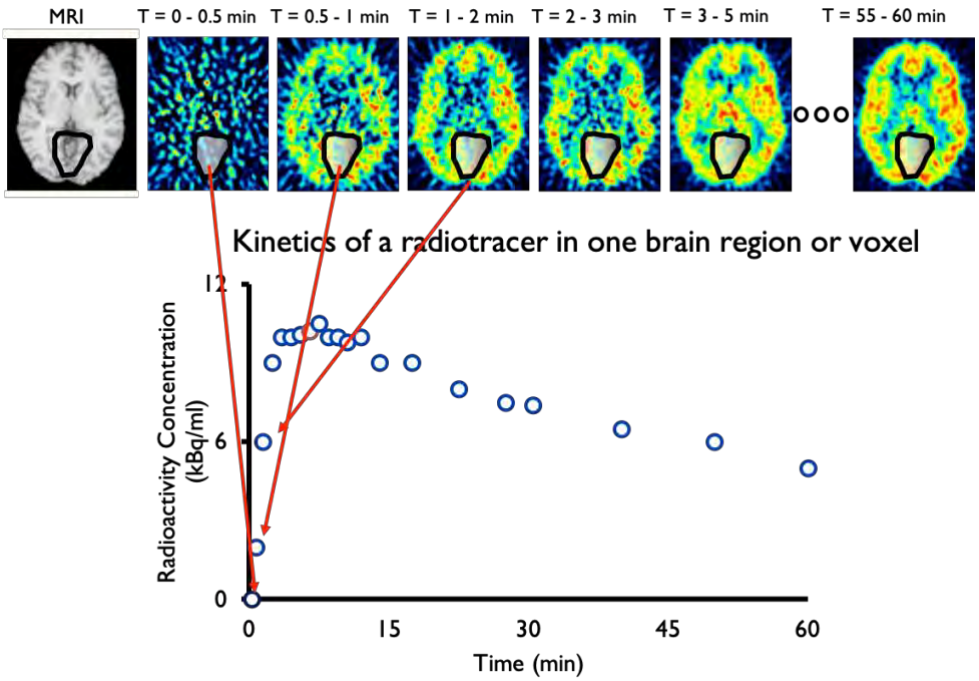

Figure 2. A dynamic PET study: a number of sequential scan acquisitions allows to follow the concentration of the radiotracer over time in a given brain region (pre-defined on an MRI image on the left) or even a voxel. This dynamic information is of utmost importance for the quantification. Courtesy of P. Millet.

Indeed, in the classical form of PET and SPECT image quantification, the biological processes governing the pharmacokinetic properties of the tracer into study, i.e. the exchanges of the radiotracer between its different states, as well as its interactions with the target receptor are expressed mathematically with the use of pharmacokinetic models. In pharmacokinetic modeling, the various states in which the radiotracer may be found in the body (described above and presented in Figure 1) are called compartments. The exchanges of the radiotracer between the various compartments of the model are governed by kinetic constants (represented by the blue arrows in Figure 1). Overall, the ultimate goal of the quantification procedure is to identify these kinetic transfer or exchange constants, among which are the two most important parameters, the absolute quantity of the receptor (B_{avail} or B_{max}) and the affinity of the radiotracer for the receptor.

In its most detailed form, a pharmacokinetic model includes the following compartments, as presented in Figure 3: the plasma compartment $C_p(t)$ represents the non-metabolized, non-protein bound radioligand, i.e. the fraction of tracer that is available for entry in the brain and eventually interaction with the target receptor, that is

measurable with arterial plasma sampling during the scan. The exchange rate between the plasma compartment and the free tracer in the tissue ($M_f(t)$) are governed by the K_1 and k_2 transfer constants. Similarly, k_{on} and k_{off} determine the rate of association and dissociation of the tracer to and from the receptor, respectively. Finally, a fraction of the tracer in the tissue presents non-specific binding to targets other than the receptor-of-interest ($M_{ns}(t)$) and in order to distinguish this compartment we have to introduce two more parameters in the model (k_5 and k_6). In general, "what is known" i.e. what PET scan measures is the activity that is included in the aforementioned tissue compartments, as well as a fraction of the plasma compartments that corresponds to the activity in brain tissue capillaries (F_v) (all these components are delineated with the dashed red rectangle in Figure 1). Using this information, the constants of the model – "what we want to know"- are estimated.

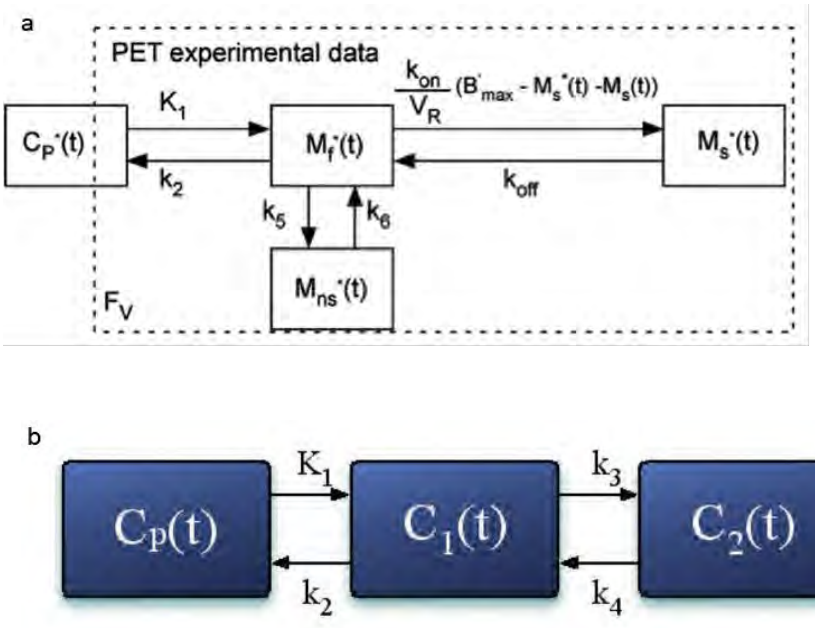

Figure 3. (a) The 3T-7k model used in analysis of PET time–concentration curves obtained from the multi-injection protocol in the Millet et al., (2012) study. The model at the top describes the kinetics of the radioligand (quantities denoted with a star superscript). Parameters K_1 and k_2 are associated with the exchanges between the plasma and free ligand compartment; B_{avail} (here depicted as B'_{max}) represents the concentration of receptors available for binding; k_{on} and k_{off} are the association and dissociation rate constants respectively; k_5 and k_6 are the rate constants associated with non-specific binding. (b) A more simplified model with two-tissue compartments and four parameters to be estimated. $C_1(t)$ stands for both "free" and "non-specific binding" compartments. $C_2(t)$ stands for specific binding of radiotracer on the receptor. Courtesy of P. Millet.

This estimation is performed by non-linearly fitting the kinetic pattern of the radiotracer (the TACs) to a pharmacokinetic model (Bailey et al., 2006; Cunningham et

al., 2004; Frankle et al., 2005; Gunn et al., 2001; Millet and Lemoigne, 2008; Morris et al., 2004; Phelps, 2000; Slifstein and Laruelle, 2001). As illustrated in Figure 4, multiple sets of kinetic parameters (represented by the red solid line) are fitted against the actual measured data (the TAC, represented by the blue dots). The pharmacokinetic model that best fits the data (meaning that the red line is most closely corresponding to the TAC), gives the quantitative parameters that we seek to obtain. The fitting procedure may be applied either in the level of regions defined *a priori* or at the voxel level, on the ensemble of voxels that constitute the brain PET image.

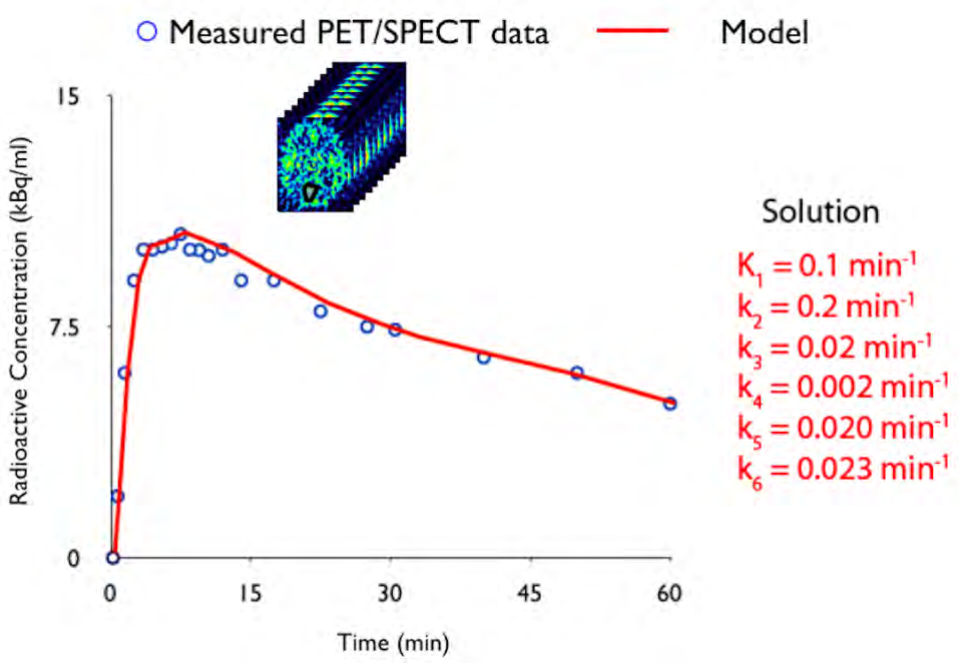

Figure 4. The fitting procedure. The actual PET or SPECT-measured data (unfilled blue dots) are fitted with an iterative procedure with a pharmacokinetic model (represented by the solid red line). Each iteration tries to fit a different "line" and each line is described by a unique set of parameters (shown on the right). The "line", i.e. the set of parameters that best fits the actual data is the one which provides the quantitative parameters of the quantification. Courtesy of P. Millet.

There are, nevertheless, some exceptions to the aforementioned rule. In fact, in several cases, some of the parameters to be estimated present a high level of inter-correlation, that makes it impossible for them to be separately estimated without a non-negligible error or without impeding model fitting overall. In these cases, and as long as none of these parameters is necessary to be known individually for receptor quantification (e.g. K_1 and k_2), we may fix them into values known *a priori* (from preliminary experiments *in vivo* or *in vitro,* see (Tsartsalis et al., 2014) for an example). This permits fitting of the model and precise estimation of the "essential" parameters,

i.e. the parameters that give information about receptor quantity in the tissue.

1.2.2 Pharmacokinetic modeling: from the absolute concentration to the binding potential

In the most complex form of a pharmacokinetic model, the absolute quantity of the receptors in a given area may be estimated. B_{avail} is a parameter that is explicitly included in the model. Similarly, affinity of the radiotracer for the receptor is also estimated, given by the ratio: affinity= k_{on}/k_{off}. The inverse of the affinity is called the dissociation constant, appK_d or K_d appK_d=1/affinity. Naturally, a model that provides such an extensive range of parameters requires a complex PET scan protocol that will provide a sufficient amount of information about the pharmacokinetic properties of the tracer. In this particular case of model, a multi-injection dynamic scan is employed with three distinct injections of the tracer together with various concentrations of the exact same molecule of the tracer, but non-radiolabelled (the cold ligand, as it is called) (Millet et al., 2012). Figure 5 depicts an example of TACs obtained from the Caudate-Putamen (CP) region from a multi-injection experiment. A first injection of the radioligand at a "tracer-dose" (meaning negligible quantity of the cold ligand) is followed by a co-injection of radiolabeled and cold ligand. A third injection contains a receptor-saturating mass of the cold ligand only, aiming the complete displacement of the radiolabeled compound. The complexity of the multi-injection experiment, subjecting the system to two "extreme" situations (one with negligible and the other with a saturating mass of cold compound), as well as an intermediate situation of the co-injection of radiolabeled and cold ligand, gives the maximum amount of information about the pharmacokinetic and pharmacodynamic "behavior" of the radiotracer and thus permits the maximum number of kinetic transfer constants to be individually identified. Apart from the multi-injection protocol, other approaches exist to estimate the B_{avail} and the appK_d, based on the same principle, of multiple injections of the radiotracers along with variable quantities of the cold compound (Carson, 2000; Morris et al., 1999; Morris et al., 2004).

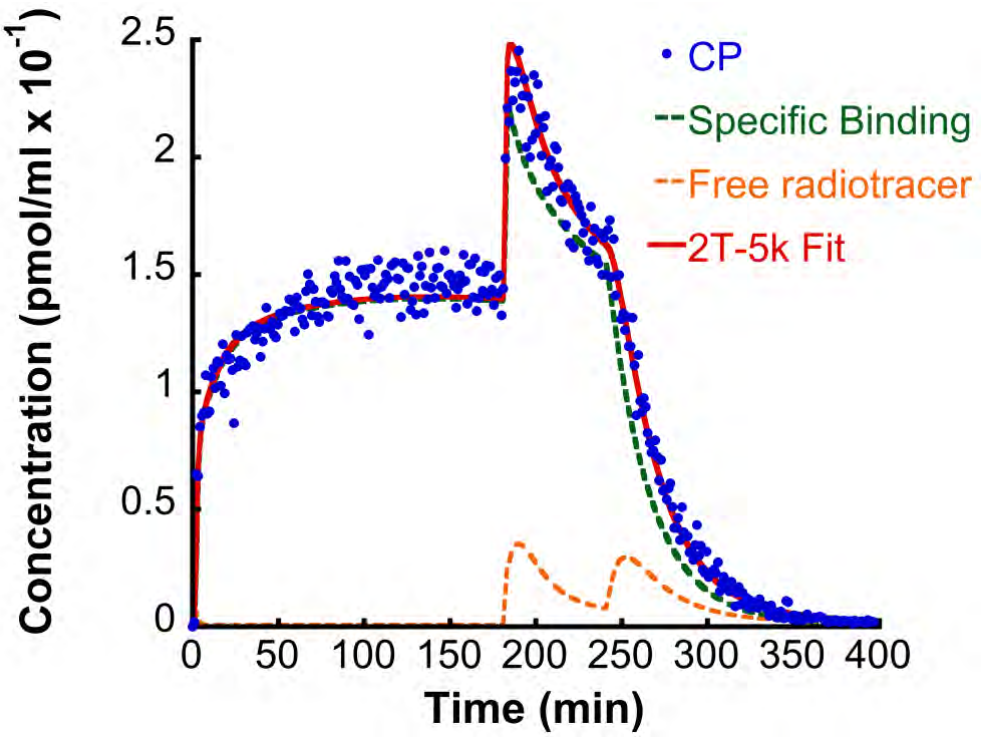

Figure 5. TACs from a multi-injection experiment (Tsartsalis et al., 2017). The first injection of a labeled radiotracer only induces an uptake of the radiotracer from the brain. The second injection of labeled and "cold" ligand (at around 180 min of scan) induces a rapid increase in the radioactivity uptake with an equally rapid decrease. Finally, a third injection (at around 260 min of scan) of the "cold" ligand alone displaces the radioactivity from the brain.

The aforementioned method is particularly laborious and, apart from a few exceptions, not applicable in routine preclinical and especially in clinical research. In addition, injections of the radiotracer's molecule at pharmacological doses (i.e. non-tracer quantities) may exert side effects. Thus, in clinical and experimental PET, pharmacokinetic models are substantially simplified and the number of tissue compartments, as well as the parameters to be estimated are reduced (for an example, Figure 3b). This permits estimations to be performed using a single radiotracer injection and a dynamic PET scan of a considerably shorter duration (0.5-3 h, compared to multi-injection that may require up to 6 h). The most important simplification of this kind of models is that the B_{avail} and the $appK_d$ are no longer distinguishable. Consequently, an index of the quantity of receptor in the brain, called binding potential (BP) (Innis et al., 2007; Millet and Lemoigne, 2008; Slifstein and Laruelle, 2001; Tsartsalis et al., 2014) is obtained. It is estimated as $BP= B_{avail} / appK_d$ and, as the affinity may be considered constant across experimental conditions and subjects, the BP presumably reflects B_{avail} in the vast majority of cases and has been established as the most popular index in PET receptor quantification. Indeed, the vast majority of the quantification approaches

used in routine clinical and preclinical molecular neuroimaging research use the BP as their outcome.

1.2.3 Further simplifying the quantification approach: use of a “reference region” and “delayed activity” scans

As described above, the absolute quantification in PET and SPECT implicates the use of complex protocols with the need for arterial catheterization to measure the input function of the pharmacokinetic model. A first level of simplification, also described in the previous paragraph, permits the estimation of the BP with the use of a single-injection experiment with a significantly shorter scan duration. However, even with this approach, arterial plasma sampling is necessary because the arterial plasma-derived input function is essential in the pharmacokinetic modeling approach. To render molecular neuroimaging quantification non-invasive, another level of simplification has been proposed and extensively validated.

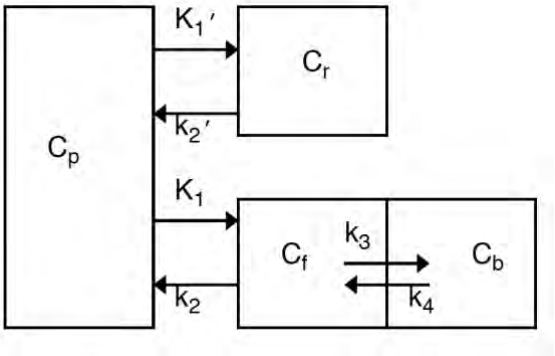

Figure 6. The simplified reference tissue model (SRTM).

These approaches are based on the principle that, for some receptors in the brain, there exist regions in which these receptors are minimally or not expressed at all (Cunningham et al., 2004; Gunn et al., 2001; Gunn et al., 1997; Lammertsma and Hume, 1996; Logan et al., 1996; Millet and Lemoigne, 2008; Morris et al., 2004). In such regions, termed “reference-regions”, the binding that is measured on the PET or SPECT images belongs exclusively to the free and non-specific compartments (Figure 6). With the assumption that the binding in these two compartments is similar in all the regions of the brain, the binding in the reference-region gives us directly the free and non-specific binding in the “target” regions. As a result, taking these components into account in the pharmacokinetic modeling, permits to reveal the specific binding in the target regions and, consequently, the BP. In this case, the BP is termed “non-displaceable” (because the free and non-specific binding jointly form the non-displaceable binding component),

hence the term BP_{ND}. The development of these reference-tissue approaches has considerably improved the feasibility of brain molecular imaging studies, rendering more accessible to research groups and much less invasive for the patients/participants.

The reference-tissue approaches need dynamic scans (lasting up to 3 hours) for the quantification to be valid. The duration of the scan still constitutes a certain drawback in the realization of clinical and experimental research. In this context, an ultimate level of simplification has been proposed and extensively validated, called “standardized uptake ratio (SUR) or delayed-activity approach (Millet et al., 2002b; Millet and Lemoigne, 2008; Morris et al., 2004; Tsartsalis et al., 2014). This consists in the use of static scans, at late time-points after the injection of the radiotracer, of a short duration (usually 10-60 min), along with the employment of a reference region (hence there is no need for arterial catheterization). The quantification is based on the principle that at later time-points, the rate of clearance of the radiotracer from the target and the reference region is stable, thus the radiotracer is found at a “pseudo-equilibrium” at these brain regions. In this condition, the ratio of the radioactivity at the target to the radioactivity at the reference region (Standardized Uptake Ration, SUR) is equivalent to the BP_{ND}, which was described above. The mathematical validation of this approach is out of the scope of this description.

It is important to note that these simplified approaches may introduce significant bias in biological studies if not properly validated (Shrestha et al., 2012) against the “gold-standard” quantitative neuroreceptor estimates obtained with full pharmacokinetic modeling. An overall presentation of the various quantification approaches, their technical characteristics and the outcome measures is presented in Table 3.

Approach	Type of scan	Arterial plasma sampling	Duration	Pharmacokinetic models/Outcome measures
Multi-injection protocol	Dynamic, multiple injections	yes	3-6 hours	2T5k, 3T7k/ B_{avail}, $appK_d$, k_{on}, k_{off}, K_1, k_{2-6}
Single-injection protocol	Dynamic, one injection	yes	usually < 3 hours	2T5k, 3T7k/BP, K_1, k_{2-6}
Single-injection « non-invasive » protocol	Dynamic, one injection	no	usually < 3 hours	SRTM, Logan "reference-region" model/BP_{ND}
Single-injection « non-invasive » protocol	Static, one injection	no	10-60 min	SUR/BP_{ND}

Table 3. Summary Table of the most characteristic and commonly employed quantification approaches in molecular neuroimaging. The 2T5k and 3T7k described the complexity of the pharmacokinetic model and the number of parameters obtained.

1.2.4 Optimization of dynamic image quality: denoising with factor analysis

In nuclear imaging, various physical effects (scatter, partial volume effects and crosstalk) give rise to overlapping phenomena between regions of interest. Therefore, time activity curves (TACs) obtained from ROI measurements can involve activities from different overlapping components. Factor analysis (FA) is a method used to extract a few elementary components from a series of dynamic images (Di Paola et al., 1982). Using FA, information underlying an image sequence is broken down into several pieces of meaningful information which are easier to interpret, while disregarding the irrelevant information such as noise. FA is used for the extraction of "pure" TACs from a series of PET or SPECT dynamic images (Barber, 1980; Buvat et al., 1993; Di Paola et al., 1982) and has been mainly applied in cardiology for extracting the "pure" arterial TAC from kinetic PET data (Kim et al., 2006; Kim et al., 2003; Wu et al., 1995) and for noise removal (Bruyant et al., 1999; Tsartsalis et al., 2014).

In neuroreceptor brain imaging, we have shown that FA is a very efficient tool for improving image quality (Figure 7) (Millet et al., 2012; Tsartsalis et al., 2014; Tsartsalis et al., 2018). Indeed, the crucial role of an image in nuclear imaging is to provide the functional information and the accurate physiological parameters of a specific radiotracer for the whole brain. However, the noise level is generally very high in

nuclear imaging compared to other imaging modalities. Noise removal is therefore essential to improve image quality and to allow parametric imaging (Millet et al., 2002b; Millet et al., 2000b; Millet and Lemoigne, 2008; Tsartsalis et al., 2014; Tsartsalis et al., 2018).

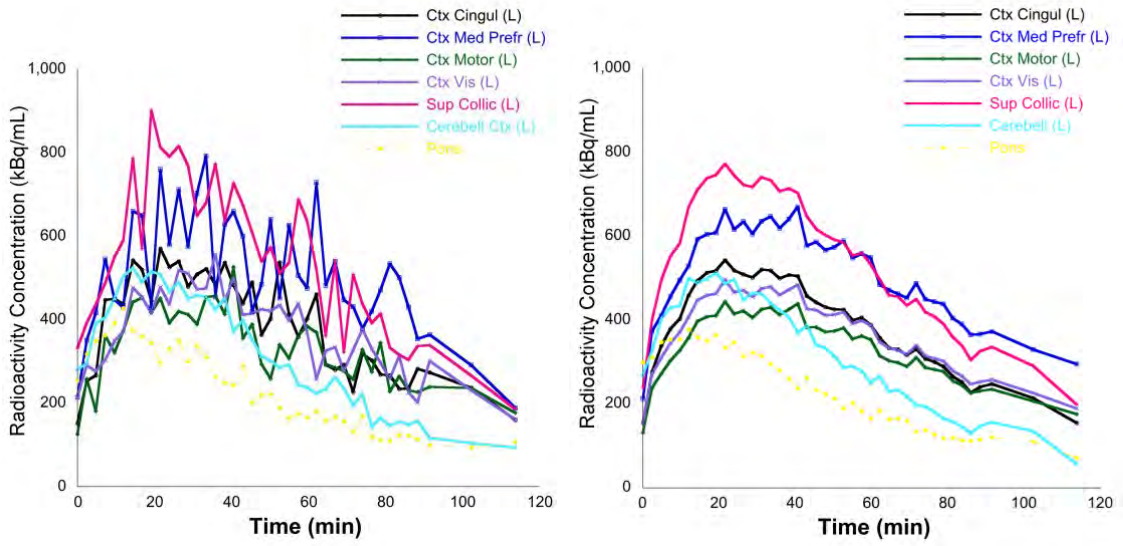

Figure 7. TACs from a SPECT experiment (Tsartsalis et al., 2014). Raw images (left side) present a relatively high level of noise. TACs from the same regions of the same experiment after FA-treatment considerably diminishes the impact of noise (right side).

1.3 Methodological developments for molecular imaging $D_{2/3}$ and 5-HT_{2A} receptors. What can we learn about brain function?

A major component of this work was dedicated to the development of methodological approaches to study the dopaminergic and serotoninergic systems, using SPECT radiotracers for the $D_{2/3}$ and the 5-HT_{2A} receptors, respectively. This development was oriented in four major axes:

1) the validation of a simplified methodology to quantify (i.e. estimate the BP_{ND}) the $D_{2/3}$ receptor using [^{123}I]IBZM. This methodology, never previously validated for rat [^{123}I]IBZM studies, constituted the basis for all the $D_{2/3}$ quantification experiments in the biological part of the project, which served for the measurement of the receptor's occupancy ratio by haloperidol and the quantification of the alteration in the $D_{2/3}$ receptor binding after chronic treatment with haloperidol and MDL-100,907. In the same axis, we further studied [^{123}I]IBZM and validated an approach to separately estimate the absolute receptor concentration B_{avail} and the appK_d parameter using a partial saturation

approach in a simple SPECT scan, as described in section 1.3.1.

2) [^{123}I]IBZM has a low-affinity for the $D_{2/3}$ receptor and thus binds only to the striatal $D_{2/3}$ receptor. To overcome this limitation, we validated an approach that allows a more “in-depth” mapping of the $D_{2/3}$ receptor in the whole brain, using a high-affinity SPECT radiotracer, the [^{123}I]epidepride. This radiotracer allows imaging of the $D_{2/3}$ receptor in the whole brain, however, no methodology existed so far for its quantification, as explained in section 1.3.2. We thus employed a similar partial saturation approach as with [^{123}I]IBZM. This methodology developed for [^{123}I]epidepride SPECT imaging was not employed in the biological part of this thesis. Nevertheless, we employed it in a preliminary study of the effects of a chronic haloperidol treatment on the absolute quantity of the $D_{2/3}$ receptor in the brain.

3) To image the 5-HT_{2A} receptor, we employed [^{123}I]R91150. This radiotracer, whose quantification has already been described by the Millet group (Dumas et al., 2015) is a substrate of P-glycoprotein (P-gp, or Multi-drug resistance protein, Mdr1) and its influx in the brain is severely limited in rats, as explained in section 1.3.3. We thus studied two different approaches to overcome this limitation by either (i) using a P-gp inhibitor treatment during the SPECT scans or (ii) performing the biological study on rats that do not express the P-gp at all.

4) Finally, we describe a SPECT imaging approach that allows a simultaneous, dual-radiotracer imaging of both $D_{2/3}$ and 5-HT_{2A} receptors at the same scan session and under the exact same conditions using [^{123}I]IBZM and [^{123}I]R91150.

1.3.1 [^{123}I]IBZM: simplified BP_{ND} estimation and a protocol for separate identification of B_{avail} and $appK_d$

SPECT imaging of the $D_{2/3}$ receptor is more frequently performed using [^{123}I]IBZM, a low-affinity $D_{2/3}$ radiotracer, which was employed in the biological part of this thesis. Given its low affinity, [^{123}I]IBZM binds to striatal receptors only with no specific binding in extrastriatal $D_{2/3}$ receptors. SPECT imaging with [^{123}I]IBZM permits the *in vivo* study of striatal $D_{2/3}$ receptors in human and translational studies with a particular interest in psychosis and addiction (Abi-Dargham et al., 2009; Murnane and Howell, 2011).

For the biological part of the present thesis, we first performed a validation of a simplified approach to estimate the BP_{ND} of [^{123}I]IBZM, that has never been performed before for rat brain imaging. A full quantification of [^{123}I]IBZM using the multi-injection

approach served as a “gold-standard” for the validation of this simplified methodology for the quantification of the $D_{2/3}$ receptor, as well as of its % occupancy by antipsychotic agents.

Secondly, we used the multi-injection approach to validate another quantification approach, which went beyond the scope of the biological part of this thesis. As mentioned above, full pharmacokinetic modeling allows the estimation of B_{avail} and $appK_d$, thus dissociating the absolute receptor concentration and the affinity of the radiotracer for the receptor (Delforge et al., 1989, 1990). However, the established multi-injection protocol is impractical for use in biological studies, in which a composite index of these parameters, BP is used (for a reminder, $BP=B_{avail}/appK_d$) (Innis et al., 2007).

The use of BP as a quantitative measure in *in vivo* molecular neuroimaging could be indicative of the B_{avail} of the receptor under study only when the $appK_d$ is not altered by the physiological or pathological conditions under study. However, the radiotracer’s affinity is most likely variable. This is notably because of the effect of the endogenous ligand (e.g. the neurotransmitter). Indeed, a radiotracer and the endogenous neurotransmitter are binding to the receptor in a competitive manner. Various physiological and pathological conditions have been shown to alter the concentration of the endogenous neurotransmitter in the vicinity of the receptor, thus directly interfering with the radiotracer’s binding and thus altering $appK_d$ (Kugaya et al., 2000; Kuwabara et al., 2012; Narendran and Martinez, 2008; Vaessen et al., 2015; Volkow et al., 2009a). This implies, that alterations in $appK_d$ may alter BP, even in the absence of alterations in the B_{avail}. Using BP thus over-simplifies the study of such complex phenomena. In this context, a simplified method of *in vivo* estimation of B_{avail} and $appK_d$ would be of utmost value.

A simplified estimation of both B_{avail} and $appK_d$, separately, in the same imaging session is feasible, as it has been described by Delforge and colleagues (Delforge et al., 1996; Delforge et al., 1997; Delforge et al., 1993; Vivash et al., 2014. In this approach, a quantity of unlabeled (cold) radiotracer compound is co-injected with the labeled radiotracer to partially occupy (i.e. “saturate”, thus “partial saturation” approach). Delforge et al. suggested to employ doses of cold compound that occupy of at least 50% of the receptors in order to permit a relatively rapid decrease in specific binding during the scan duration. The B_{avail} and $appK_d$ parameters are estimated as follows: the ratio of specific to non-displaceable binding of the radiotracer is plotted against the specific binding and has a linear form (the “Scatchard” plot, as it is well known in basic

chemistry and experimental pharmacology). The B_{avail} is the intercept of the Scatchard plot to the "specific-binding" axis and the appKd is deduced from the slope of the plot. Ideally, receptor occupancy should not exceed 70% so that a relatively large number of points are aligned within the regression line. A reference region devoid of receptor gives an estimate of the non-displaceable binding, further simplifying the quantification. This protocol has been recently employed (Wimberley et al., 2014a; Wimberley et al., 2014b) for $D_{2/3}$ imaging using [^{11}C]raclopride in small animals.

1.3.2 [^{123}I]epidepride: a protocol for brain-wide mapping of the absolute $D_{2/3}$ receptor concentration

In the methodological part of this thesis, we aimed at the study of a second dopaminergic radiotracer, for reasons exposed here: The various $D_{2/3}$-specific radiotracers that have been developed and routinely used in research settings are generally divided in high- and low-affinity radiotracers. Low-affinity radiotracers such as [^{11}C]raclopride and [^{123}I]IBZM are perhaps the most widely employed in PET and SPECT imaging of the dopaminergic system, respectively. Their low affinity only allows imaging of the striatal receptors. Indeed, in extrastriatal brain regions, the quantity of $D_{2/3}$ receptors is (relatively) so small, that the noise from the imaging procedure is actually more than the specific signal related to the radiotracer's binding to the receptor (i.e. these radiotracers present a low "signal-to-noise" ratio in extrastriatal regions) (de Paulis, 2003; Laruelle, 2000).

Among these radiotracers, [^{123}I]epidepride presents a particularly high affinity for the receptor (Kessler et al., 1991; Leslie et al., 1996). [^{123}I]epidepride's potent binding to the $D_{2/3}$ receptor allows extrastriatal $D_{2/3}$ receptor binding quantification. However, this advantage comes with a cost: its high affinity produces particularly slow pharmacokinetics in striatal regions. The quantification of a receptor necessitates the whole pharmacokinetic profile to be studied (i.e. the influx of the radiotracer from the arterial blood to the brain region, its association and dissociation from the receptor and finally, its efflux from the tissue. With [^{123}I]epidepride, obtaining the whole pharmacokinetic profile in the striatum would require impractically long scan durations both for small-animal and especially, for clinical imaging. For example, in rats, an 8 hour-long scan would still not capture this pharmacokinetic profile (unpublished results from the Millet group). As a result, [^{123}I]epidepride is only used for imaging of extrastriatal receptors in human SPECT imaging (Fagerlund et al., 2013; Fujita et al.,

1999; Fujita et al., 2000; Kegeles et al., 2008; Lehto et al., 2009; Nørbak-Emig et al., 2016; Norbak-Emig et al., 2016; Tuppurainen et al., 2006; Tuppurainen et al., 2009; Varrone et al., 2000).

A methodology that would allow the quantification of $D_{2/3}$ receptors using [^{123}I]epidepride would be of interest. Firstly, imaging of both striatal and extrastriatal receptors would be possible at the same time, in the same SPECT scan session. Secondly, its high-affinity and thus the high signal-to-noise ratio allows a better sensitivity for the quantification of biological changes compared to lower-affinity radiotracers. For this reason, we evaluated the partial saturation approach described above for [^{123}I]IBZM (Delforge et al., 1996; Delforge et al., 1997) to quantify striatal and extrastriatal $D_{2/3}$ receptors in the rat, an approach that may be used as a complementary tool for the cartography of $D_{2/3}$ receptors in the whole brain with respect to the effects of antipsychotic agents that are studied in the present thesis.

1.3.3 Multi-drug resistance protein and radiotracer influx to the brain: a (blood-brain) barrier to 5-HT$_{2A}$ quantification

This part of the methodological study focused on the optimization of the 5-HT$_{2A}$ receptor SPECT imaging in the rat brain, which is necessary for the biological part of this thesis. In PET and SPECT imaging of the brain, transport across the blood-brain barrier (BBB) is a critical part of the pharmacokinetic behavior of a radiotracer. This transport is mainly performed by passive diffusion. However, for multiple radiotracers, passive diffusion is not the only mechanisms of transfer across the BBB. In the case of these radiotracers, a family of proteins expressed on the cells of the BBB is actively transporting molecules out of the brain. In this way, the quantity of the radiotracer that is available for binding is lower (Doze et al., 2000; Loscher and Potschka, 2005). P-gp, which is present on the brain capillary endothelial cells is a major representative of this group of proteins. In human, one isoform of the protein exists, whereas in rodents two isoforms exist, Mdr1a and Mdr1b. Mdr1a is expressed in brain capillary endothelial cells and Mdr1b is expressed in the brain parenchyma (Loscher and Potschka, 2005).

The activity of P-gp activity is a limiting factor for the successful use of a wide spectrum of radiotracers: for some of them, the activity of P-gp limits their brain uptake to such a degree, that a very a low signal-to-noise ratio to a nearly non-detectable radioactivity concentration is obtained in *in vivo* imaging (Buiter et al., 2013; Dumas et al., 2014). P-gp activity may also be altered in several disease of the CNS (e.g. in

epilepsy) and thus, apparent variations of radiotracer binding may actually not reflect brain pathology but merely this altered brain uptake of the radiotracer (Froklage et al., 2012). Several approaches to overcome the impact of P-gp activity on PET and SPECT preclinical and clinical imaging have been proposed, predominantly with a pharmacological inhibition of P-gp. Previous studies have evaluated two P-gp inhibitors, cyclosporine A (CsA) (Blanckaert et al., 2009; Doze et al., 2000; Kroll et al., 2014; Passchier et al., 2000) and tariquidar (TQD) (Froklage et al., 2012; la Fougere et al., 2010; Zoghbi et al., 2008) regarding their capacity to enhance the brain uptake of radiotracers and ameliorate the signal-to-noise ratio, thus making feasible to use these radiotracers in *in vivo* PET and SPECT studies.

However, enhancing the brain uptake of radiotracers that are substrates of P-gp may induce bias in the quantitative parameter estimations. Indeed, some studies have demonstrated that P-gp inhibitors may not act homogeneously across the various brain regions (Kroll et al., 2014; Lacan et al., 2008). In this case, differences in radiotracer binding at the regional level may not reflect actual differences in the quantity of the receptor under study but the differences in the uptake of the radiotracer. This lack of homogeneity may have an even greater impact when simplified quantification methods are employed, i.e. reference-region approaches (Kroll et al., 2014). As these methods are perhaps the most popular in nuclear neuroimaging, the impact of an inhomogeneous P-gp inhibition is considerable.

TQD is a potent inhibitor of P-gp (Fox and Bates, 2007) compared to CsA. This superior efficacy in terms of P-gp inhibition suggests that its effect could be homogeneous over the different brain regions, thus contributing to unbiased receptor quantification with radiotracers that are P-gp substrates (Froklage et al., 2012). The 5-HT_{2A}-specific radiotracer that we employ in this thesis is a P-gp substrate (Blanckaert et al., 2009; Dumas et al., 2015; Dumas et al., 2014). [^{123}I]R91150 is a well-studied SPECT radiotracer, evaluated in clinical and preclinical studies related to schizophrenia and the atypical antipsychotic mechanism of action (Audenaert et al., 2001; Catafau et al., 2011; Dumas et al., 2014; Jones et al., 2001; Mertens et al., 1994). Given the limiting role of P-gp activity in the feasibility of a biological study using [^{123}I]R91150, an evaluation of the effect of TQD on the quantification with this radiotracer was a prerequisite for the SPECT studies undertaken here. The specific question that this methodological study aimed to answer, was if TQD could lead to a homogeneous P-gp inhibition and thus unbiased and robust quantification results. In the case where this is not true, a Mdr1a knock out rat strain, previously employed by the Millet group for 5-

HT_{2A} quantification with small animal SPECT, would be used in the biological study described in this thesis.

1.3.4 Dual-radioisotope SPECT: a tool to simultaneously image two neuroreceptors

A multitude of protein-targets in the brain can be quantified with PET and SPECT, given the wide range of available radiotracers. The complexity of brain physiology and pathology necessitates the study of multiple targets (Cselenyi et al., 2004; Fakhri, 2012). In the context of the biological part of the present thesis, a joint evaluation of $D_{2/3}$ and 5-HT_{2A} is necessary to measure the occupancy of these receptors by their respective antagonists and the alterations in the concentration of these receptors after chronic antagonism (Ginovart and Kapur, 2012; Howes et al., 2012; Selvaraj et al., 2014). However, studying multiple targets on the same animal presents a technical difficulty with the actual quantification approaches. In the absence of methods that allow a simultaneous quantification using two radiotracers in the same SPECT scan, two different scan sessions are required. Nevertheless, this is particularly time-consuming. Indeed, the two SPECT scan sessions may need to be separated by hours or even days, for the radioisotope of the first scan to decay before the second scan and thus prevent bias in the radioactivity measurements. Additional variability may also be introduced, given the dynamic nature of the biological phenomena under study, that may rapidly evolve or even depend on each other (Fakhri, 2012). As an example, $D_{2/3}$ imaging with radiotracers such as [^{123}I]IBZM may be subject to the effect of endogenous dopamine, that competes with the binding of the radiotracer to its receptor, thus altering the quantitative estimates (Laruelle, 2000). Endogenous dopamine concentration is highly variable, with respect to physiological and pathological conditions. Apart from these biological variations, other parameters, inherent to the imaging methods, such as the effect of anesthetic agents may alter the radiotracers' binding (McCormick et al., 2011). Overall, when two receptors are studied at different scan sessions, their joint interpretation is particularly difficult, given the confounding factors described above. To overcome these confounders, the two receptors have to be studied at the same scan session, thus under the exact same conditions.

Simultaneous, dual-radiotracer molecular imaging is theoretically feasible in SPECT. The radioisotopes employed in SPECT emit photons in a particular energy spectrum. Two (or more) radioisotopes may thus be simultaneously employed in a

single scan session. The detectors of the SPECT camera distinguish the photons with respect to their energy spectra (Akutsu et al., 2009; Antunes et al., 1992; Bruce et al., 2000; Ichihara et al., 1993). This is the case for two iodine isotopes used in SPECT. ^{123}I has a principal energy emission spectrum of 143.1-179.9 keV and ^{125}I an energy spectrum of 15-45 keV. The majority of radiotracers used in SPECT studies of the central nervous system (CNS) is radioiodinated (Baeken et al., 1998; De Bruyne et al., 2010; Dumas et al., 2015; Dumas et al., 2014; Ji et al., 2015; Kessler et al., 1991; Kung et al., 1989; Mattner et al., 2011; Mattner et al., 2008; Ordonez et al., 2015; Pimlott and Ebmeier, 2007; Sehlin et al., 2016; Tsartsalis et al., 2015; Tsartsalis et al., 2014). Nevertheless, ^{123}I also emits photons at a secondary energy spectrum that overlaps with the one of ^{125}I and the resulting cross-talk of emissions impedes the accurate quantification of ^{125}I. A methodology allowing the correction of this cross-talk is of major importance for the present thesis, as it will permit the simultaneous quantification of the $D_{2/3}$ and the 5-HT_{2A} receptors and the occupancy of these receptors by their respective antagonists (haloperidol and MDL-100,907), by labeling each one of their respective radiotracers with one of the available iodine radioisotopes.

1.4 Objectives of the present work

1.4.1 Methodological study

1) To propose a simplified methodology for a full quantification of the $D_{2/3}$ receptor in the rat striatum using [^{123}I]IBZM.

2) To propose a simplified methodology for a full quantification of the $D_{2/3}$ in the whole rat brain using [^{123}I]epidepride.

3) To assess the effect of P-gp inhibition on 5-HT_{2A} receptor imaging using [^{125}I]R91150 and to propose an approach to overcome the effect of P-gp, which will be employed in the biological study.

4) To develop a simplified methodology that allows a simultaneous, dual-radiotracer SPECT imaging of $D_{2/3}$ and 5-HT_{2A} receptors in the rat brain.

1.4.2 Biological study

1) To evaluate the effects of a chronic treatment with haloperidol in the rat, inducing various levels of striatal D_2-receptor occupancy, on experimental paradigms of antipsychotic efficacy and side effects.

2) To assess if an addition of a high 5-HT_{2A} receptor occupancy may alleviate the side effects and enhance the efficacy of the aforementioned haloperidol treatment. *In vivo* SPECT imaging will be used to assess the receptor occupancy.

3) To assess the effects of these chronic treatments on the *in vivo* quantity of $D_{2/3}$ and 5-HT_{2A} receptors, with the hypothesis that a chronic haloperidol treatment will induce a $D_{2/3}$ up-regulation and that addition of a 5-HT_{2A} antagonism will reverse this effect.

2. Results

2.1 First Article

2.1.1 Brief summary of the results

In this study, we describe a partial saturation approach for the *in vivo* estimation of B_{avail} and $appK_d$ with [^{123}I]IBZM SPECT using a single-scan protocol in the region- and voxel-level. This method is validated against the results of full pharmacokinetic modeling with a multiple-injection protocol that provides the “gold-standard” estimates of all kinetic parameters along with B_{avail} and $appK_d$. Other simplified methods to estimate BP without an input function estimation are validated. Indeed, a simple static scan of 30 minutes, obtained between 80 and 110 minutes after the injection of the radiotracer allows an accurate estimation of the BP_{ND} (SUR) of [^{123}I]IBZM.

2.1.2 Contribution

In this paper, I contributed in the conception of the experiments (along with Philippe Millet), participated in the realization of the imaging experiments (with the help of Benjamin Tournier), analyzed the imaging data (with the help of Philippe Millet), performed the statistical analyses and drafted the first version of the manuscript.

2.2 Second Article

2.2.1 Brief summary of the results

In this paper, we firstly perform a full-quantification of [^{123}I]epidepride kinetics using a multi-injection imaging protocol (Delforge et al., 1990; Millet et al., 2012; Tsartsalis et al., 2014; Tsartsalis et al., 2017), which separately identifies B_{avail} and $appK_d$. The results of the multi-injection protocol serve as a “gold-standard” for the validation of the partial saturation approach, which is applied at the region- and at the voxel-level. We find that scan of less than 180 minutes allows the quantification of the $D_{2/3}$ receptor in the whole brain.

2.2.2 Contribution

In this article, I contributed in the conception of the experiments (along with Philippe Millet), participated in the realization of the imaging and surgical procedures (with the help of Benjamin Tournier), analyzed the imaging data (with Philippe Millet), performed the statistical analyses and drafted the first version of the manuscript.

2.3 Third Article

2.3.1 Brief summary of the results

To address the hypothesis that an efficient inhibition of P-gp with TQD will allow an unbiased quantification of the 5-HT_{2A} receptor, we evaluated the effect of TQD pretreatment on [^{123}I]R91150 *ex vivo* and *in vivo* imaging of 5-HT2A receptors in the rat brain. We used full-kinetic modeling and a simplified tissue ratio method to quantify the receptor (Dumas et al., 2015). As a "gold-standard" of quantification under complete P-gp inhibition, we employed a Mdr1a knock out (Mdr1a KO) rat strain. We showed that inhibition of P-gp with tariquidar induced a region-dependent increase in the radiotracer's uptake, thus an inhomogeneous effect over the various brain regions. In addition, wild type, tariquidar-treated rats had higher SUR estimates, compared to Mdr1a knock out rats, and, most importantly, a much higher variability (in terms of % CV). Consequently, with such a high variability and biased SUR estimates the statistical power of biological studies of the [^{123}I]R91150 could be compromised. This prompted us to use Mdr1a knock out rats for the biological study, in order to be able to use *in vivo* imaging of the 5-HT_{2A} receptor.

2.3.2 Contribution

In this article, I contributed in the conception of the experiments, participated in the realization of the imaging (*in vivo* and *ex vivo*) experiments, analyzed the imaging data, performed the statistical analyses (with the help of Benjamin Tournier) and drafted the first version of the manuscript.

2.4 Fourth Article

2.4.1 Brief summary of the results

SPECT imaging with two radiotracers at the same time is feasible if two different radioisotopes are employed, given their distinct energy emission spectra. In the case of ^{123}I and ^{125}I, dual SPECT imaging is not straightforward: ^{123}I emits photons at a principal energy emission spectrum of 143.1-179.9 keV. However, it also emits at a secondary energy spectrum (15-45 keV) that overlaps with the one of ^{125}I and the resulting cross-talk of emissions impedes the quantification of ^{125}I. In this paper, we described three different methods for the correction of this cross-talk and the simultaneous *in vivo* [^{123}I]IBZM and [^{125}I]R91150 imaging of $D_{2/3}$ and 5-HT_{2A} receptors in the rat brain. A simple subtraction of the fraction of the ^{123}I-emitted signal from the signal measured at the energy window of ^{125}I allows the estimation of valid BP_{ND} (SUR) values. In addition, we applied this approach to the study of the relationship between the $D_{2/3}$ and 5-HT_{2A} receptors in the striatum and found a positive correlation in the nucleus accumbens, which we also confirmed *ex vivo*.

2.4.2 Contribution

In this article, I contributed in the conception of the experiments, participated in the realization of the imaging (*in vivo* and *ex vivo*) experiments, analyzed the imaging data (along with Philippe Millet), performed the statistical analyses (with the help of Benjamin Tournier) and drafted the first version of the manuscript.

2.5 Fifth Article

2.5.1 Brief summary of the results

A considerable amount of studies has suggested that an antagonism at the 5-HT_{2A} receptor, shared by many atypical antipsychotic agents, may provide a more favorable efficacy and side-effect profile in the antipsychotic treatment. However, no study so far has performed a thorough evaluation of the effect of adding a 5-HT_{2A} antagonism on a chronic treatment with haloperidol, a typical agent, administered at clinically-relevant doses. Here, we chronically treated male Mdr1a knock out rats with several doses of haloperidol alone or haloperidol with a saturating dose of a pure 5-HT_{2A} receptor antagonist, MDL-100,907. The occupancy of the receptors at clinically relevant levels was validated with a dual-radiotracer *in vivo* SPECT imaging to assess $D_{2/3}$ and 5-HT_{2A} receptor occupancy, simultaneously, at the same scan session. A range of well-validated experimental tests of efficacy and side effects was performed (dizocilpine-disrupted prepulse inhibition of the startle response (PPI), catalepsy, vacuous chewing movements (VCM) measurement and Y-maze). Finally, a second dual-radiotracer *in vivo* SPECT scan was performed at the end of the treatment period to assess neurochemical changes at the level of $D_{2/3}$ and 5-HT_{2A} receptor binding with respect to the chronic treatment regimes. Chronic haloperidol treatment failed to reverse the disruption of the PPI by dizocilpine, whilst administration of MDL-100,907 along with haloperidol was associated with a tendency towards the reversal of the effect of dizocilpine. Haloperidol at 0.5 mg/kg/day and at 1 mg/kg/day induced a strong catalepsy that was significantly reversed by co-treatment with MDL-100,907 only in the case of 0.5 mg/kg/day. These two highest doses of haloperidol induced VCM that were not reversed by MDL-100,907 co-administration. Chronic haloperidol treatment, event at doses as low as 0.1 mg/kg/day induced a significant upregulation of the $D_{2/3}$ receptor in the striatum, that failed to be reversed by MDL-100,907 co-administration. Finally, a previously unappreciated upregulation of the 5-HT_{2A} receptor after chronic haloperidol treatment at a moderate dose only (0.25 mg/kg/day) was demonstrated with *in vivo* statistical parametric mapping and confirmed *ex vivo.* These results point to a partial contribution of the 5-HT_{2A} receptor to the amelioration of the efficacy and side-effect profile of haloperidol in preclinical behavioral paradigms, whilst the antagonism at this receptor fails to alter the neurochemical changes that such a chronic haloperidol

treatment induces.

2.5.2 Contribution

In this article, I contributed in the conception of the experiments (along with Nathalie Ginovart, for the biological experiments and Philippe Millet for the dual radiotracer SPECT imaging experiments), performed the surgical experiments (along with Marouane Ben-Ammar), performed the imaging experiments (*in vivo* and *ex vivo*) with Benjamin Tournier and Nathalie Ginovart, the analysis of images, the statistical analysis of the results and drafted the first version of the manuscript.

3. Discussion

3.1 Overview: going from complex neuroimaging approaches to simple methods to address biological questions

The results of the present thesis are discussed in detail in the relevant sections of the individual articles. In the following paragraphs, the major discussion points are exposed, allowing the reader to gain insight into the strengths and limitations of the undertaken experiments from a methodological and biological standpoint. Especially concerning the methodology (sections 3.2 to 3.5), the following discussion focuses on the aspects that are more relevant to its application in the biological part of this thesis (section 3.6).

3.2 Full quantitative modeling of [^{123}I]IBZM and simplified quantification

This thesis described, for the first time, the full pharmacokinetic modeling of [^{123}I]IBZM *in vivo* in the rat using the multi-injection protocol. This step was necessary for the validation of simpler quantification approaches. B_{avail} values (i.e. the absolute concentration of the receptor) in the Caudate-Putamen and the Nucleus accumbens are highly similar to the values described in the literature (Mauger et al., 2005; Millet et al., 2012; Wimberley et al., 2014b). The multi-injection approach allows a quantification of all the kinetic parameters that describe a pharmacokinetic model and it provides a “gold-standard” for the validation of other quantification approaches (Delforge et al., 1990; Dumas et al., 2015; Millet et al., 2002a; Millet et al., 2000a; Millet et al., 2006; Millet et al., 2012).

The development and validation of simplified methodologies is a prerequisite for the realization of biological studies, especially in the context of preclinical imaging. Indeed, scans of a short duration (less than 30 min), that require no arterial catheterization and are quantified in a straightforward manner are necessary. For this reason, using the B_{avail} values from the multi-injection approach, we validated the results of the estimation of a Standardized Uptake Ratio value (SUR, also referred to as BP_{ND} in the articles of this thesis) using a “delayed-activity” approach and the cerebellum as reference region. A SPECT scan obtained between 80 and 110 minutes after radiotracer injection gave the highest correlations of the SUR values with the B_{avail}

values (see Figure 2 of Article 1). Previously, such an approach was employed in the literature to quantify the $D_{2/3}$ receptor in using [^{123}I]IBZM but this is the first study to actually validate its results against a full quantitative approach (Crunelle et al., 2012; Meyer et al., 2008a, b; Meyer et al., 2008c; Nikolaus et al., 2011; Scherfler et al., 2005; Verhoeff et al., 1991). Apart from its technical simplicity, this simplified approach has the advantage to provide robust estimates with minimal variability (Lyoo et al., 2015; Tsartsalis et al., 2016). Consequently, this validated simplified approach was employed in the biological study of the present thesis.

3.3 Estimating B_{avail} and $appK_d$ non-invasively using the partial saturation approach with [^{123}I]IBZM and [^{123}I]epidepride

In molecular neuroimaging, the quantitative parameter that is provided by the vast majority of approaches is a conjoint estimation of the B_{avail} (the absolute receptor concentration) and the $appK_d$ (with $1/appK_d$ being the affinity of the radiotracer for the receptor and can be considered an indirect index of the endogenous ligand, e.g. dopamine in this case), named BP ($BP=B_{avail}/appK_d$, see sections 1.2.1 to 1.2.3 and Table 3 in the Introduction for a detailed description). Nevertheless, when the BP is the outcome measure in human and small animal neuroimaging studies, valuable information may be lost. Indeed, several authors have stressed the difficulty to interpret the results of biological studies, given that both the absolute quantity of the receptors and the endogenous transmitter levels (which are indissociable when BP is the outcome of the quantification) may be altered in a physiological or pathological condition (Egerton et al., 2009; Hillmer et al., 2014; Howes et al., 2009; Howes et al., 2012; Martinez et al., 2012; Tomasi et al., 2016; Vaessen et al., 2015; Vivash et al., 2014; Volkow et al., 2007; Volkow et al., 2009b; Volkow et al., 2008; Wang et al., 1997; Wiers et al., 2016; Wooten et al., 2012; Wooten et al., 2013).

In the present thesis, to separately estimate the B_{avail} and $appK_d$ in $D_{2/3}$ receptor imaging, we employed a partial saturation approach (for a detailed description, see section 1.3.1 in the Introduction), proposed by Delforge et al., for the quantification of $GABA_A$ receptor with [^{11}C]flumazenil (Bouvard et al., 2005; Delforge et al., 1996; Delforge et al., 1997; Freeman et al., 2015). This approach requires no blood sampling, as the cerebellum is employed as reference region. Another advantage of this approach is that it may provide the B_{avail} and $appK_d$ values using SPECT scans of a considerably shorter duration than that needed with more complex full quantitative methods, i.e. the

multi-injection protocol. We described this approach for both [^{123}I]IBZM and [^{123}I]epidepride. The advantage of [^{123}I]IBZM is the feasibility of its use and its sensitivity towards variations of the endogenous dopamine levels (Laruelle, 2000). However, quantification with [^{123}I]IBZM may only be performed in the striatum. On the other hand, [^{123}I]epidepride presents the undeniable advantage of being able to quantify both striatal and extrastriatal $D_{2/3}$ receptors. In the following paragraphs, the results of the quantification with these two radiotracers will be discussed.

3.3.1 [^{123}I]IBZM partial saturation quantification

The B_{avail} and appK_d values obtained with the partial saturation method correlate well with the corresponding values obtained with the multi-injection protocol. An apparent overestimation of the B_{avail} values in the Caudate Putamen compared to the respective values from the multi-injection experiment is observed (see Tables 2 and 4 of Article 1). This could be explained by the fact that, in the partial saturation, as in all simplified, non-invasive approaches (Slifstein et al., 2000), the cerebellum is employed as a reference region and the kinetics in this region are used as an approximation of the kinetics of the radiotracer in the arterial plasma. The arterial plasma, on the contrary, is directly measured in the multi-injection approach. The cerebellar kinetics in our study were scaled by a factor r. This r parameter served in the correction of the TAC of the cerebellum (the reference region). Indeed, in the partial saturation approach, the free and non-specific binding in the reference region (C_{CER}) are employed as an approximation of the free and non-specific binding in the target regions (C_{ND}). The r parameter corrects the cerebellar TAC so that C_{ND}= r x C_{CER}, to more accurately reflect the kinetics of the free radioligand in the striatum, as previously suggested (Delforge et al., 1996; Wimberley et al., 2014b). The r parameter value was estimated using the results of the full quantification using the multi-injection approach (r=1.55) and validated with an experimental approach (r=1.68) that yielded a similar value. In addition, this value corroborates the results from a previous paper on the application of the partial saturation protocol on another $D_{2/3}$-binding radiotracer, [^{11}C]raclopride (Wimberley et al., 2014b). The major limitation of SPECT imaging with [^{123}I]IBZM lies on the fact that this radiotracer, due to its low affinity for the receptor, may only quantify the striatal regions. For this reason, we proceeded to the development of a similar approach with a radiotracer that allows whole-brain imaging, the [^{123}I]epidepride, as described in section 3.3.3.

3.3.2 A demonstration of the potential of the partial saturation approach to study the dopaminergic system with [^{123}I]IBZM

As a preliminary evaluation of the sensitivity of the partial saturation approach, we performed two experiments: firstly, a unilateral overexpression of the D_2 receptor was induced in the striatum of one rat (shown in Figure 6b of Article 1). The quantification with the partial saturation approach confirmed, as expected, an increase of the B_{avail} of about 18% (as the overexpression of this receptor should increase its concentration), while appK_d remained stable (as the concentration of the endogenous dopamine should remain stable) (Laruelle, 2000). This result is a mere demonstration of the potential of the method, having been performed in one rat. An application in a group of rats with a proper statistical analysis should confirm this preliminary finding.

Secondly, we evaluated the efficacy of the partial saturation method to detect simultaneous changes in both the receptor concentration and the level of endogenous dopamine. For this purpose, we employed a well-established imaging protocol, which consists in the realization of two separate [^{123}I]IBZM SPECT scans. The second scan is identical to the first but it is preceded by an amphetamine injection to induce dopamine release (thus augmenting the appK_d) (Ginovart, 2005; Laruelle, 2000) and $D_{2/3}$ receptor endocytosis (thus reducing the B_{avail}) (Ginovart et al., 2004; Jongen et al., 2008; Skinbjerg et al., 2010; Sun et al., 2003). Amphetamine induced a 16.93% decrease in B_{avail} and a 39.12% increase in appK_d. This finding corresponds to a previous study using [^{11}C]raclopride in cats, where a 28% decrease in B_{avail} and a 36% increase in appK_d were found (Ginovart et al., 2004). These results suggest the potential of the partial saturation approach to be used to an in-depth evaluation of the $D_{2/3}$ receptor and its interaction with endogenous dopamine.

3.3.3 Brain-wide cartography of B_{avail} and appK_d using [^{123}I]epidepride and a partial saturation protocol

The partial saturation protocol, as described above for [^{123}I]IBZM, was employed for the quantification of [^{123}I]epidepride SPECT scans. The major development with this approach for [^{123}I]epidepride lies on the fact that, as described in the Introduction

(section 1.3.2), there is no methodology described so far to quantify the $D_{2/3}$ using this radiotracer. The multi-injection protocol was also employed as the "gold-standard" for the validation of the results of the partial saturation study. The correlation of the results of these two approaches were high (Figure 6, Article 2). The validity of the results of the partial saturation study was also confirmed by comparing them to previous results from our group, notably Article 1 using [^{123}I]IBZM (Tsartsalis et al., 2017), and a previous work using a PET radiotracer, [^{18}F]fallypride (Millet et al., 2012), which yielded highly similar B_{avail} values.

The high-affinity of [^{123}I]epidepride allows to obtain excellent quality images. Figure 9 of Article 2 illustrates the superiority of the quality of a [^{123}I]epidepride SPECT image compared to an image obtained with the low-affinity [^{123}I]IBZM. The binding of [^{123}I]epidepride is considerably higher than the binding of [^{123}I]IBZM (note the difference in the range of radioactive concentrations, 0-10 and 0-2.5 KBq/ml, respectively). The high binding of [^{123}I]epidepride also allows an adequate anatomical delineation of the striatal substructures and notably the distinction of the Nucleus Accumbens from the Caudate Putamen Nucleus, which is not possible with [^{123}I]IBZM.

The quality of the radioactive signal and the robustness of the quantitative parameters that are obtained with the partial saturation approach with [^{123}I]epidepride are supported by the low standard deviations and percent coefficients of variance (CV) of the B_{avail} values (Table 2 of Article 2): indeed, the CV of these values obtained with [^{123}I]epidepride in the Caudate-Putamen is 5.87% and in the Nucleus accumbens it is 24.14%. In the extrastriatal regions, CV values range from 10 to 35%. In comparison, the same approach with [^{123}I]IBZM yielded B_{avail} values with a CV of 25.43% and 58% in the Caudate/Putamen and the Nucleus accumbens, respectively (Article 1). Using the same approach and the low-affinity PET radiotracer [^{11}C]raclopride, Wimberley et al found B_{avail} values with a CV around 40% in mice (as roughly depicted in Figure 8 of the aforementioned paper) (Wimberley et al., 2014b). In rat PET imaging with [^{18}F]fallypride (Millet et al., 2012), CV of BP values were also higher than the CV of B_{avail} values presented here. Overall, the robustness of the quantitative parameters obtained with the partial saturation approach in [^{123}I]epidepride SPECT suggests that biological studies using this radiotracer may provide high statistical power compared to other available PET and SPECT imaging modalities of the dopaminergic system.

As in the case of [^{123}I]IBZM (Article 1) and other partial saturation studies (Delforge et al., 1996; Wimberley et al., 2014b), the kinetics of the radiotracer in the cerebellum were scaled by a r parameter, estimated from the multi-injection study.

Contrary to [^{123}I]IBZM, the r parameter in the case of [^{123}I]epidepride, also takes into account a minimal, but non negligible, specific binding in the cerebellum. This could be a limitation in some applications of [^{123}I]epidepride imaging (Pinborg et al., 2007). For this reason, before a biological study is performed, the stability of this specific binding in the cerebellum across the different experimental groups has to be confirmed. If a condition under study alters the specific binding in the cerebellum, the results of the quantification, especially in the extrastriatal regions, may be biased (as illustrated in the simulation study in section 2.4.4 in Article 2).

3.3.4 A preliminary biological application of the partial saturation approach with [^{123}I]Epidepride

A preliminary evaluation of the potential of [^{123}I]epidepride to be used in biological studies was performed. With a chronic haloperidol treatment identical to the protocol described in Article 5, an upregulation of the $D_{2/3}$ receptor's binding was induced in the striatum (Ginovart et al., 2008; Turrone et al., 2003a). Chronic haloperidol treatment led to an increase in the B_{avail} of [^{123}I]epidepride of 17.97% in the left CP and of 13.84% in the right CP. The p values of the comparison with a two-samples t test between the B_{avail} values in haloperidol- vs vehicle-treated rats were 0.07 and 0.12, respectively, i.e. not statistically significant using a conventional two-tailed threshold of p=0.05. This study, merely illustrative in the present thesis, was limited by a small sample size (4 rats in the control and 3 in the haloperidol treatment group), which suggests a limited statistical power. In spite of this limitation, this preliminary study underlines the potential of using [^{123}I]epidepride and a partial saturation protocol in carefully chosen antipsychotic-treated groups of rats to gain a more in-depth evaluation of changes in the absolute concentration of $D_{2/3}$ receptor and the endogenous dopamine levels in response to the chronic antipsychotic treatments, as described in the Discussion of the biological part of this thesis (Article 5).

3.4 Overcoming the effect of P-gp on 5-HT_{2A} SPECT imaging with [^{125}I]R91150

In the present thesis, the second neurotransmitter receptor under study was the 5-HT_{2A}, which was imaged with [^{125}I]R91150. Several radiotracers used in PET and SPECT are substrates of the P-gp, which compromises the quality of quantification, by

reducing the availability of these radiotracers in the brain. This is the case for [^{125}I]R91150. Human and animal studies have consistently demonstrated that inhibiting P-gp may ameliorate the quantification process because it augments signal-to-noise ratio and enhances the kinetic parameter identifiability (Doze et al., 2000; Kroll et al., 2014; la Fougere et al., 2010; Lacan et al., 2008; Liow et al., 2007).

One of the means of overcoming this issue would be the pharmacological inhibition of P-gp, which, ideally, should have a complete and homogenous effect across brain regions. Nevertheless, this does not seem to be the case: Kroll et al., (Kroll et al., 2014) have shown that [^{18}F]altanserin, a 5-HT$_{2A}$-binding radiotracer is a substrate of P-gp. CsA pretreatment (50 mg/kg) augmented the radiotracer's uptake in the brain. However, BP_{ND} (another term essentially describing SUR in the present thesis) values were modified in a region-dependent manner, suggesting that inhibition of P-gp may induce a bias in the quantification. For this reason, we studied the effect of tariquidar (TQD)-mediated inhibition of P-gp activity, which is more selective and potent inhibitor of the P-gp (Bansal et al., 2009). We compared the results to these of the quantification of [^{123}I]R91150 in Mdr1a knock out rats (Dumas et al., 2015; Dumas et al., 2014), in which there is a complete absence of the transporter. Kinetic analysis with arterial plasma-derived input function and *ex vivo* autoradiography quantification was performed.

The principal finding of this study was that TQD-inhibition induces a region-dependent increase in the radiotracer's uptake, thus an inhomogeneous effect over the various brain regions. The cerebellum, the reference region used in the simplified estimation of the SUR was particularly affected, a finding similar to the results of another study with cyclosporin A (CsA) (Kroll et al., 2014), despite the fact that the TQD dose that was administered here was a saturating one (Kroll et al., 2014; Wagner et al., 2009). Wild type-TQD rats had higher SUR estimates, compared to Mdr1a knock out rats, and, most importantly, a much higher variability (in terms of % CV). Consequently, with such a high variability and biased SUR estimates the statistical power of biological studies of the [^{123}I]R91150 could be compromised (Winterdahl et al., 2014).

Alternatively, the use of Mdr1a knock out rats in translational biological studies could rule out the deficient brain penetration of [^{125}I]R91150 and allow the extraction of robust quantitative estimates, if the biological system under study is not perturbed by the absence of P-gp. This would be a certain limitation of using this rat strain. However, the present and previous studies of our group (Dumas et al., 2015; Dumas et al., 2014) gave no argument in favor of a supposed effect of the absence of P-gp on brain

receptor binding. For this reason, the Mdr1a knock out strain was employed in the biological study of this thesis.

3.5 A dual-radiotracer SPECT imaging approach to simultaneously study $D_{2/3}$ and 5-HT_{2A} receptors in the brain

3.5.1 Validation

Perhaps the most important development of the present thesis was the methodology to quantify two neurotransmitter receptors simultaneously, under identical conditions in the same SPECT scan session. This is not technically possible either in SPECT or PET because of a cross-talk (i.e. a "contamination" of the measured radioactive signal of one radiotracer by the signal of the other). In SPECT, many radiotracers of interest for neuroimaging are labeled with iodine radioisotopes. Even if there exist two different iodine radioisotopes that may be used in SPECT imaging, ^{123}I and ^{125}I, which emit photons at distinct energy emission spectra, no simultaneous imaging with these two radioisotopes may be performed. Indeed, a part of the radioactive signal of ^{123}I is emitted at the same energy window as of ^{125}I. Thus, while the signal from the ^{123}I-labeled radiotracer may be directly quantified because it is not "contaminated", the signal of the ^{125}I-labeled radiotracer suffers from the effect of cross-talk. Article 4 described three different methods that allow this dual-radiotracer quantification, using [^{123}I]IBZM and [^{125}I]R91150, with the correction of the signal measured at the ^{125}I spectrum to remove the "contaminating" ^{123}I signal. A group of rats was employed in a single-radiotracer [^{123}I]R91150 imaging study and served as a "gold-standard". All three of these methods provided equally valid results and SUR values of [^{125}I]R91150 from dual-radiotracer experiments correlated highly with values obtained from single-radiotracer [^{123}I]R91150 experiments and are similar to values from the literature (Dumas et al., 2015; Tsartsalis et al., 2017; Tsartsalis et al., 2016). Here, we will focus on the 1st of them, the dual-energy window (DEW) approach, which was the most extensively studied approach in Article 4 and, most importantly, the one that was finally employed in the biological part of this thesis (Article 5).

Indeed, the DEW approach is particularly straightforward and technically feasible. It consists simply in subtracting a stable fraction of the measured ^{123}I-emitted radioactive signal from the measured ^{125}I-emitted signal. This ratio is determined by the α coefficient, which is defined the ratio of the radioactivity from ^{123}I that is emitted at the

secondary energy window (the one that contaminates the ^{125}I signal) to the radioactivity from ^{123}I that is emitted at the principal energy window. As such, the DEW approach has no statistical noise. In the present study, the quantitative parameter values (SUR) from the dual-radiotracer experiments had excellent test-retest variability of 14% for both [^{123}I]IBZM and [^{125}I]R91150 (see section S2.1 of Article 4), which is highly acceptable for small animal imaging studies (Catafau et al., 2008; Constantinescu et al., 2011).

To our knowledge, the present thesis is the first to employ this method in brain imaging (Lee et al., 2015; Lee et al., 2013). One disadvantage of the DEW method is the fact that the α coefficient is determined by the interaction of the emitted photons with matter, i.e. the cerebral and extra-cerebral tissue, as it has been described for another pair of SPECT-employed radioisotopes, ^{111}In^{111} and ^{177}Lu (Hijnen et al., 2012). This implies that the value of this coefficient will likely vary across the different brain regions. Importantly, in our experiments, the effect of the interaction with matter is quite homogeneous across the brain VOI and across rats with a coefficient of variation of α at 17%. This variation in the α parameter values, albeit non-negligible per se, probably has a little impact in the context of this study. Indeed, looking into the value of this parameter in individual VOI across rats shows that in cortical, receptor-rich regions, as well as in the striatum and the CER, α values are less variable (with a coefficient of variation <10% as described in section 3.1 of Article 4 and close to the average value that was used in the application of the DEW method).

Another limitation of the work described in Article 4 lies on the fact that neither scatter nor attenuation correction was performed in the *in vivo* imaging studies. Both corrections are important (Andersen et al., 2014; Lee et al., 2015), especially regarding ^{125}I, which is more sensitive to attenuation and scatter effects than ^{123}I (Feng et al., 2007; Gregor et al., 2007). Indeed, a slight overestimation of the SUR values with [^{125}I]R91150 from the dual-radiotracer experiments, compared to the “gold-standard” [^{123}I]R91150 experiments could be attributed to a differential effect of scatter and attenuation on the various brain regions. However, as stated above, despite a bias in the absolute SUR values, [^{125}I]R91150 SUR values from dual-radiotracer experiments correlate well with [^{123}I]R91150 SUR values from single-radiotracer experiments and do not differ significantly from them. In our experiments, acquiring computed tomography data was not possible, so no attenuation correction could be performed. Regarding scatter, a preliminary correction performed in part of our data yielded highly similar SUR values than these without scatter correction (data not shown). Given this result, the fact that scatter correction may be time-consuming and that scatter correction alone without

attenuation correction may add further bias (Hutton et al., 2011), we chose not to implement scatter correction in our DEW methodology. In any case, our proposed methods may be optimized with the correction of the scatter and attenuation effects (Lee et al., 2015), which was out of the scope of the present thesis.

The work undertaken here, being the first description of a dual-radiotracer imaging procedure with iodinated radiotracers in the brain, is an important addition in the field. Dual radiotracer SPECT has already been described with radiotracer couples that do not emit photons at overlapping spectra (Akutsu et al., 2009; Antunes et al., 1992; Bruce et al., 2000; Hijnen et al., 2012; Ichihara et al., 1993), notably in the study of multiple aspect of cardiovascular pathophysiology (Akutsu et al., 2004). Similar efforts have been made in PET imaging. In this modality, the emission spectrum of all radiotracers is identical, so the correction of the cross-talk between the two radiotracers' signals has to be based on the differences in the kinetics of the two radiotracers (El Fakhri et al., 2013; Fakhri, 2012; Kadrmas et al., 2013; Koeppe et al., 2001). Overall, the development of multi-radiotracer methods is expected to enhance the neuroimaging research in both translational and clinical settings.

3.5.2 An application of the simultaneous, dual-radiotracer SPECT approach to study the relationship between $D_{2/3}$ and 5-HT_{2A} receptor binding in the striatum

Understanding brain physiology and pathology with molecular imaging may be enhanced by the simultaneous study of multiple molecular targets. For this reason, we applied dual-radiotracer [^{123}I]IBZM and [^{125}I]R91150 imaging and provided preliminary evidence for an association of $D_{2/3}$ and 5-HT_{2A} receptors in the nucleus accumbens. Using the DEW method, a positive correlation between $D_{2/3}$ and 5-HT_{2A} binding in the nucleus accumbens, both at the VOI- and at the voxel-level was found. Evidently, we suspected that this correlation is an artefact of the dual-radiotracer imaging approach. This gave us the opportunity to perform a series of simulation and experimental studies (see Supplement 1 in Article 4) that, to our view, conclusively excluded the possibility the dual-radiotracer approach considerably distorts the quantification results to artificially produce this correlation. In addition, the literature provides some evidence to support the correlation between the $D_{2/3}$ and 5-HT_{2A} receptor found in this study, which could be the result of a co-expression of these two receptors on the same cells (Ma et al., 2006), or of a formation of functional heterodimers (Albizu et al., 2011; Borroto-

Escuela et al., 2014; Lukasiewicz et al., 2010; Varela et al., 2015). Although the absence of biological data from this study to support this correlation is a clear limitation, the intention of this preliminary study was to illustrate the potential of simultaneous, dual-radiotracer imaging.

3.6 Assessment of the impact of 5-HT_{2A} antagonism using MDL-100,907 to the effect of haloperidol on behavioral paradigms of efficacy and side effects

3.6.1 Overview of the in vivo imaging approach and the design of the study

This study presents an evaluation of the impact of 5-HT_{2A} antagonism on multiple aspects of the efficacy and side effect profile of haloperidol. To enhance its translational potential, various doses of haloperidol were administered. They induced levels of occupancy of the $D_{2/3}$ receptors in the striatum that were, to our view, clinically pertinent. Indeed, we employed doses ranging from relatively low (0.1 mg/kg/day) to particularly high (1 mg/kg/day). The 0.1 mg/kg/day produces an occupancy of around 60% of the $D_{2/3}$ receptors in the striatum, i.e. at the lowest end of the 65-80% occupancy window that is considered optimal in a clinical and a translational setting (Ginovart and Kapur, 2012; Kapur et al., 2000). This occupancy was confirmed both *ex vivo* and *in vivo* (Figure 2a and 2b of Article 5). At this occupancy, the 0.1 mg/kg/day dose is supposed to be marginally efficient, without any side effects. The 0.25 mg/kg/day produces a $D_{2/3}$ receptor occupancy that largely lies within the 65-80% occupancy window, thus being efficient and inducing minimal side effects. These two doses allowed to assess the hypothesis that the addition of an MDL-100,907 chronic treatment would ameliorate the efficacy of the haloperidol treatment (i.e. in the dizocilpine-disrupted PPI). The two highest haloperidol doses (0.5 and 1 mg/kg/day) produce a maximal $D_{2/3}$ receptor occupancy, that lies largely beyond the highest end of the 65-80% occupancy window. Both doses induce side effects and were important for the assessment of the hypothesis that the addition of an MDL-100,907 chronic treatment would alleviate the haloperidol-induced side effects. The 1 mg/kg/day dose, in particular, was included in the design of this study to allow a direct comparison with the majority of previous studies in the literature. The use of a 1 mg/kg/day dose of haloperidol (which has been criticized as unreasonably high (Kapur et al., 2000)) may "conceal" any ameliorative effects of co-administered substances, such as the MDL-

100,907. On the contrary, the use of a 0.5 mg/kg/day dose almost saturates the $D_{2/3}$ receptors in the striatum (Figure 2, Article 5), induces clinically relevant side effects (e.g. catalepsy and VCM) and allows to demonstrate potential ameliorative effects of MDL-100,907, that were previously unappreciated in the literature (discussed thoroughly in section 4.2 of Article 5).

The haloperidol and MDL-100,907 treatment were chronically administered using osmotic minipumps, an administration route that induces a continuous receptor occupancy, thus providing a relatively good resemblance to the pharmacokinetics of haloperidol in human (Ginovart et al., 2008; Kapur et al., 2000; Turrone et al., 2003a). *In vivo* and *ex vivo* imaging was employed to assess the level of occupancy of the receptors from the chronic treatments, using the simultaneous, dual-radiotracer imaging approach described in Article 4 (see section 3.5 of the present thesis). The same imaging method allowed to assess the changes in the $D_{2/3}$ and 5-HT_{2A} receptors' binding induced by the chronic treatment.

3.6.2 5-HT_{2A} antagonism partially alleviates haloperidol-induced catalepsy but has no effect on vacuous chewing movements (VCM)

As expected, chronic treatment with haloperidol at high doses (0.5 and 1 mg/kg/day) induced catalepsy in rats (Creed-Carson et al., 2011; Karl et al., 2006; McOmish et al., 2012; Reavill et al., 1999; Wadenberg et al., 2001b). Interestingly, co-administration of MDL-100,907, along with haloperidol, managed to reduce catalepsy but only at the 0.5 mg/kg/day dose of haloperidol, not at the 1 mg/kg/day dose. This lack of efficacy of 5-HT_{2A} antagonism to alleviate the catalepsy induced by the highest dose of haloperidol has already been reported in the literature (Creed-Carson et al., 2011; McOmish et al., 2012). However, it is the first time, to our knowledge, that the effect of MDL-100,907 on catalepsy with a lower dose (of 0.5 mg/kg/day) is evaluated. This finding suggests that a 5-HT_{2A} antagonism may be beneficial against the extrapyramidal side effects that are induced by high doses of haloperidol but this beneficial effect is lost when particularly high doses of this agent are administered. To our view, the 0.5 mg/kg/day dose of haloperidol, which already induces a high $D_{2/3}$ occupancy (>85%) in the striatum, is more clinically pertinent than the supersaturating dose of 1 mg/kg/day. Previous studies using the 0.5 mg/kg/day dose of haloperidol to assess the effects of MDL-100,907 on catalepsy have yielded negative results. This apparent contradiction with the results of the present study may be explained by the difference in the

administration schemes (acute administration of haloperidol and MDL-100,907 in previous studies (Creed-Carson et al., 2011; Mombereau et al., 2017) vs chronic in our study). Indeed, the mode of administration of haloperidol has been shown to differentially impact the cataleptic response, with the same dose inducing a milder response when administered chronically, than when administered acutely (Osborne et al., 1994; Turrone et al., 2003a).

Regarding the second motor side effect that was studied, our results confirm previous reports associating a chronic high occupancy of the $D_{2/3}$ receptor to vacuous chewing movements (VCM) in rats (Glenthoj, 1993; Karl et al., 2006; Turrone et al., 2003a, b). Previous reports had indeed shown that a pure 5-HT_{2A} antagonism with MDL-100,907 had no effect on VCM that was induced by a particularly high dose of haloperidol (1 mg/kg/day) but no study evaluated the effect when a lower dose was employed. Here, we extend the existing literature by using the more clinically pertinent 0.5 mg/kg/day dose of haloperidol and show that MDL-100,907 not only failed to reduce the VCM but was associated with a tendency to augment them (Figure 5, Article 5).

Overall, our results suggest that a 5-HT_{2A} antagonism has a partial contribution to the reduction of (acute) extrapyramidal side effects of haloperidol. Other receptors, such as the 5-HT_{2C}, which is also a common target of atypical antipsychotics, might contribute along with 5-HT_{2A} to the reduced motor side effect burden of these agents, compared to typical antipsychotics, as proposed by previous studies (Carbon et al., 2018; Creed-Carson et al., 2011; Di Giovanni and De Deurwaerdere, 2016; Egan et al., 1995; Egerton et al., 2008; Ikeda et al., 1999; Liegeois et al., 2002; Lucas et al., 2000; Marchese et al., 2004; Naidu and Kulkarni, 2001; Reavill et al., 1999; Rosengarten and Quartermain, 2002; Wadenberg et al., 2001a; Wadenberg and Ahlenius, 1995).

3.6.3 Impact of 5-HT_{2A} antagonism on the effect of haloperidol in the dizocilpine-disrupted prepulse inhibition (PPI)

PPI is a physiological phenomenon observed both in human and rodents. In preclinical research, disruption of this phenomenon by glutamatergic and dopaminergic agents is used in studies of the efficacy of antipsychotic agents (Bakshi and Geyer, 1998; Swerdlow et al., 2008; Wadenberg et al., 2000). Here, we chose a glutamatergic agent (dizocilpine) to disrupt the PPI, as it has been shown that its mechanism of action might be more relevant for the study of antipsychotic agents (Geyer et al., 2001). In this model, haloperidol has been found inefficient to reverse the effect of dizocilpine, while

atypical antipsychotics manage to do so (Bubenikova et al., 2005; Feifel and Priebe, 1999; Hudson et al., 2016; Li et al., 2016; Varty and Higgins, 1995; Zangrando et al., 2013). Consequently, our hypothesis was that, if a 5-HT_{2A} antagonism is one of the substrates of atypicality, the co-treatment with MDL-100,907 may render haloperidol capable of reversing the disruption of PPI by dizocilpine, thus more efficient overall. Our results of the MANOVA indeed showed that MDL-100,907 and the interaction of the effect of haloperidol and MDL-100,907 had a significant effect on the dizocilpine treated rats, partially restoring the PPI (Figure 3, Article 5). This is in accordance with a recent paper that demonstrated that a 5-HT_{2A} antagonism may act synergistically with a 5-HT_6 antagonist to reverse the effect of dizocilpine on the PPI (Fijal et al., 2014). A limitation of our study was the high variability of our data. Indeed, the *post hoc* assessments of the effect of the various treatment groups on the PPI failed to reach significance. Despite this limitation, the results of the PPI experiments provide further argument in favor of the efficacy of a 5-HT_{2A} antagonism by MDL-100,907 along with haloperidol in the reversal of dizocilpine-disruption of the PPI. This suggests that an antagonism of the 5-HT_{2A} receptor by atypical antipsychotics may contribute in their increased efficacy over typical agents. However, further research is needed to confirm this hypothesis both in the setting of small animal and clinical studies.

3.6.4 Effect of haloperidol and MDL-100,907 on the Y-maze test of spatial working memory

The present study failed to detect any significant effect of either antagonist, haloperidol or MDL-100,907 on the spatial working memory (Ott and Nieder, 2016). This finding differs from results of clinical and preclinical studies, which suggest that haloperidol induces a working memory deficit (Csomor et al., 2007; Hutchings et al., 2013; Karl et al., 2006; Kim et al., 2013; Lustig and Meck, 2005; Naef et al., 2017; Nielsen et al., 2015; Nørbak-Emig et al., 2016; Sakurai et al., 2013; Xu et al., 2012). The discrepancy between our findings and the findings of previous small animal studies may be explained by the higher doses of haloperidol (up to 2 mg/kg/day) (Xu et al., 2012) and the different tests of working memory that were employed in previous studies (Karl et al., 2006). It is interesting to note that antipsychotic agents (both typical and atypical) have also been found to exert a beneficial action in the cognitive deficits of schizophrenic patients (Desamericq et al., 2014; Goozee et al., 2016; Shin et al., 2018; Steen et al., 2016; Takano, 2018; Williams et al., 2002; Zhang and Stackman, 2015;

Zhou et al., 2018). To our view, these findings suggest that the complexity of cognitive processes and the -probably- differential effect of antipsychotic agents in healthy individuals and schizophrenic patients impose that the impact of antipsychotic treatment on cognition, at the preclinical level, should be studied in animal models of schizophrenia (Castner et al., 2000) and not in healthy rats.

3.6.5 Effect of chronic treatment with haloperidol and MDL-100,907 on the $D_{2/3}$ and 5-HT_{2A} receptor binding

Chronic $D_{2/3}$ antagonism by haloperidol (at each one of the administered doses) led to a significant increase in the binding of this receptor in the caudate-putamen nucleus and the nucleus accumbens (Figure 6, Article 5), in accordance with the relevant literature (Inoue et al., 1997; Ishikane et al., 1997; Kusumi et al., 2000; Mahmoudi et al., 2014; Silvestri et al., 2000; Turrone et al., 2003a, b; Varela et al., 2014). The literature also suggests that this $D_{2/3}$ upregulation is present to a lesser extent, if at all, with atypical antipsychotics, notably clozapine (Kusumi et al., 2000; Lidow and Goldman-Rakic, 1994; Tarazi et al., 1997a; Tarazi et al., 1997b), leading us to hypothesize that a 5-HT_{2A} antagonism, if it is a substrate of atypicality, should prevent the haloperidol-induced $D_{2/3}$ upregulation. No study so far has addressed this hypothesis. A first interesting finding of the present study was that haloperidol upregulated the $D_{2/3}$ receptors in the striatum at all doses (even the lowest one, of 0.1 mg/kg/day). This finding challenges the theory that an upregulation of these receptors is causally linked to VCM in haloperidol-treated rats (Turrone et al., 2003a, b) suggesting that a $D_{2/3}$ receptor upregulation is not a sufficient condition for the induction of this symptom. Indeed, only rats treated with 0.5 and 1 mg/kg/day of haloperidol presented this symptom, while all the doses of haloperidol were associated to an upregulation of the $D_{2/3}$ receptors. MDL-100,907 co-administration with haloperidol in this study failed to reverse its effects, suggesting that other mechanisms than a 5-HT_{2A} receptor antagonism should be responsible for the finding that atypical antipsychotics do not upregulate the $D_{2/3}$ receptor (Ishikane et al., 1997).

Our study also showed that a moderate dose of haloperidol (0.25 mg/kg/day) and not any of the other doses, induced an upregulation of the 5-HT_{2A} receptor in frontal cortical areas and the ventral tegmental area (VTA) *in vivo* and *ex vivo* (section 4.6 and Figure 7, Article 5). This is a surprising finding, given the fact that only atypical antipsychotics have been shown to alter the 5-HT_{2A} receptor binding in rodents

(inducing a downregulation). No study has associated haloperidol to any alteration of the 5-HT_{2A} receptor before. (Amato et al., 2011; Choi et al., 2017; Huang et al., 2007; Kurita et al., 2012; Lian et al., 2013; Moreno et al., 2013; Steward et al., 2004; Tarazi et al., 2002; Yadav et al., 2011). This could be explained by the fact that higher doses than 0.25 mg/kg/day were employed in all these studies. The present study, given the absence of any 5-HT_{2A} binding properties of haloperidol, points to an indirect modulation possibly via an alteration of serotonin release. If serotonin release is diminished, this transmitter competes less with the [^{125}I]R91150 radiotracer for binding to the receptor and the binding of this radiotracer is augmented. Several hypothesis may be formulated to explain this finding, mainly regarding: 1) that D_2 receptor activation mediates the effects of several agents on serotonin release (Amargos-Bosch et al., 2007; Amargos-Bosch et al., 2003; Amargós-Bosch et al., 2004; Amargos-Bosch et al., 2006; Maejima et al., 2013; Mendlin et al., 1998), 2) the fact that a haloperidol treatment has been associated to a reduction in the concentration of serotonin and one of its metabolites (Bishnoi et al., 2007; Burnet et al., 1996), 3) haloperidol may possibly alter the formation of D_2/5-HT_{2A} heteromers, thus altering the affinity of the 5-HT_{2A} receptor for [^{125}I]R91150 (Albizu et al., 2011) and 4) a differential effect of low- versus high-haloperidol doses on $D_{2/3}$ autoreceptors and heteroreceptors (i.e. the 0.25 mg/kg/day dose of haloperidol might act solely on the autoreceptors, while the higher doses of this agent probably act on both auto- and heteroreceptors).

3.6.6 Limitations of the biological part of this thesis (Article 5)

The main limitation of this study lies on the use of Mdr1a knock out rats. We had to use this strain to be able to employ [^{125}I]R91150 for the *in vivo* imaging of 5-HT_{2A}. This radiotracer has minimal brain penetration in wild-type rats, impeding the *in vivo* use in SPECT imaging (Dumas et al., 2015; Dumas et al., 2014; Tsartsalis et al., 2016). However, Mdr1a knock-out and wild type rats present identical $D_{2/3}$ and 5-HT_{2A} receptor binding in the brain (confirmed by *ex vivo* imaging, Article 3), and identical dose-occupancy curves for haloperidol (Natesan et al., 2005; Wadenberg et al., 2001b). In addition, the behavioral responses to haloperidol were highly comparable to those observed in previous studies. It also has to be noted among the limitations of this study that the results on 5-HT_{2A} upregulation by moderate doses of haloperidol and not by high doses of this typical antipsychotic are mostly exploratory. No inference on a causal contribution on the effect of this antipsychotic agent may be formulated in the present

study and further research is required to shed light on the implications of this neurochemical alteration.

3.7 General discussion and perspective for future studies

The present thesis emphasized the potential of molecular imaging approaches in neuropsychiatric research. The work performed here covered the development of new approaches to neuroreceptor quantification using small animal SPECT and the optimization of existing ones. The validation of the quantification approaches is a major prerequisite to obtain consistent and reproducible results in biological studies using SPECT or PET imaging. As described in the introduction of this thesis, SPECT and PET images can be obtained and quantified with a wide variety of scan protocols, ranging from long scans of several hours to short scans of a few minutes. The complexity of the scan may vary as well, going from a multi-injection scan that requires an arterial catheterization for the measurement of the arterial plasma concentration of the radiotracer at multiple time-points to simple, non-invasive scans (see sections 1.2.1 to 1.2.3 and Table 3 in the Introduction for a detailed description). The use of simplified approaches provides high throughput and robust quantification results with relatively low variability, hence augmenting the feasibility and statistical power of imaging studies. However, using simplified approaches indiscriminately for every radiotracer without prior validation may lead to serious errors and even the opposite results in different imaging studies of the same clinical population, as it has been criticized by the review paper of Shrestha et al, in the case of studies of the 5-HT_{1A} receptor in major depressive disorder (Shrestha et al., 2012).

Convinced of the primordial role of methodological developments in molecular imaging, we firstly proceeded to the optimization of the quantification approach of the $D_{2/3}$ receptor using [^{123}I]IBZM and of the 5-HT_{2A} receptor using [^{125}I]R91150. In the case of [^{123}I]IBZM, a methodology that employs a short scan, between 80 and 110 minutes after the administration of the radiotracer, without the need of arterial plasma catheterization was validated against the results of a complex approach with established validity, the multi-injection approach (Delforge et al., 1990). Regarding the 5-HT_{2A} receptor quantification, having the inability to employ the [^{125}I]R91150 imaging *in vivo* given the very low influx of the radiotracer in the brain, we established that using a Mdr1a knock out rat strain led to more robust results than attempting to inhibit the activity of Mdr1a pharmacologically. Secondly, we proceeded to the development of a

simplified approach to the in-depth study of the $D_{2/3}$ receptor. Using a partial saturation approach (Delforge et al., 1996; Delforge et al., 1993) we proposed a method that allowed a separate estimation of the absolute quantity of the $D_{2/3}$ receptor and the affinity of the radiotracer for the receptor, which gives an index of the dynamics of endogenous dopamine. This approach was validated for the study of the striatal (using [^{123}I]IBZM) and whole-brain (using [^{123}I]epidepride) $D_{2/3}$ receptor. Finally, the simultaneous study of both $D_{2/3}$ and 5-HT_{2A} receptors in the same SPECT scan, under the same conditions was rendered possible with a methodology that simply consists in subtracting a stable proportion of the [^{123}I]IBZM-emitted radioactivity from the [^{125}I]R91150-emitted radioactivity to deal with the contamination of the signal of the latter radiotracer by the former.

These approaches ultimately allowed the study of a biological question, regarding the role of 5-HT_{2A} receptor in the efficacy and side-effect profile of the antipsychotic agents. The results indicated that antagonism at the 5-HT_{2A} receptor may reduce the catalepsy induced by a typical antipsychotic agents, haloperidol, and lead to enhanced efficacy of this agent in the experimental paradigm of dizocilpine-disrupted PPI. Finally, a previously unappreciated upregulation of the 5-HT_{2A} receptor binding induced by a narrow range of haloperidol doses was demonstrated.

Overall, this thesis describes all the stages of development of a translational imaging project. The methodological approaches proposed here may be applied to the study of a wide variety of targets in the brain, well beyond the $D_{2/3}$ and the 5-HT_{2A} receptor and the study of antipsychotic agents. The partial saturation approach may be applied to a more in-depth study of the dopaminergic system and provide more information about how a chronic antipsychotic treatment alters the quantity of the $D_{2/3}$ receptors at the whole-brain level, as well as the alterations of endogenous dopamine in this context. The study of extrastriatal regions with [^{123}I]epidepride in particular, such as the frontal cortex and the mesencephalic structures would be of particular interest in the context of the study of antipsychotic agents. Similarly, after a proper validation, the partial saturation approach could be applied to [^{123}I]R91150 imaging. This would permit a better understanding of the upregulation of 5-HT_{2A} receptor that the chronic haloperidol treatment induces and conclusively answer if this upregulation is due to an increase in the absolute quantity of 5-HT_{2A} receptors or, as hypothesized, a reduction in the endogenous serotonin. The simultaneous, dual-radiotracer imaging approach may be applied in the study of any given couple of iodine-labeled radiotracers, most importantly, without the need for any further validation.

As a conclusion, the results of the biological part of the present thesis underline the interest of further study of the 5-HT_{2A} receptor in the action of antipsychotic agents. This thesis had the advantage of employing approaches of translational interest, i.e. the behavioral tests that have a demonstrated validity to predict the clinical effects of antipsychotic agents and molecular imaging approaches that can be used in clinical research. However, it is important to note that, in order to conclusively elucidate the substrates of atypicality and confirm causal relationships, further in-depth studies have to be performed. These include genetic manipulations of the various receptors and the downstream pathways that relate to these receptors, as well as of the neural circuits that are implicated in the mechanism of action of antipsychotic agents. In the present thesis, we worked on the hypothesis that 5-HT_{2A} antagonism, as one of the mechanisms of action of atypical antipsychotic agents is a “friend” for their clinical profile. However, there is evidence that 5-HT_{2A} antagonism may be the “foe” with respect to several major side effects, such as weight gain and sedation (Joshi et al., 2017; Joshi et al., 2019; Rasmussen et al., 2014). These aspects haven’t been treated at all here and have to be addressed in subsequent studies. Most importantly, the results of this thesis have to be confirmed in animal models of schizophrenia and of other disorders in which these agents are clinically used. They also need to be confronted to studies of other putative mechanisms of atypicality, such as 1) other serotoninergic receptors (Olten and Bloch, 2018), 2) other neurotransmitter systems (Choy et al., 2016), 3) epigenetic changes via alteration of the activity of histone deacetylase inhibitors (González-Maeso et al., 2008; Kurita et al., 2012), 4) implication of receptor dimers (Szlachta et al., 2018), 5) activation of alternative cellular signaling pathways downstream of the $D_{2/3}$ receptor, with the prominent example of the arrestin-dependent pathway (Donthamsetti et al., 2018; Schmid et al., 2014; Urs et al., 2016). We believe that the developments undertaken in the present thesis provide a solid framework for further studies in the field of psychopharmacology and the pathophysiology of neuropsychiatric disorders.

4. References

Abi-Dargham, A., van de Giessen, E., Slifstein, M., Kegeles, L.S., Laruelle, M., 2009. Baseline and amphetamine-stimulated dopamine activity are related in drug-naive schizophrenic subjects. Biol Psychiatry 65, 1091-1093.

Akutsu, Y., Kaneko, K., Kodama, Y., Li, H.L., Nishimura, H., Hamazaki, Y., Suyama, J., Shinozuka, A., Gokan, T., Kobayashi, Y., 2009. Technetium-99m pyrophosphate/thallium-201 dual-isotope SPECT imaging predicts reperfusion injury in patients with acute myocardial infarction after reperfusion. Eur J Nucl Med Mol Imaging 36, 230-236.

Akutsu, Y., Shinozuka, A., Kodama, Y., Li, H.L., Kayano, H., Hamazaki, Y., Yamanaka, H., Katagiri, T., 2004. Usefulness of simultaneous evaluations of contractile reserve, perfusion, and metabolism during dobutamine stress for predicting wall motion reversibility (myocardial stunning) after successful PTCA. Jpn Heart J 45, 195-204.

Albizu, L., Holloway, T., Gonzalez-Maeso, J., Sealfon, S.C., 2011. Functional crosstalk and heteromerization of serotonin 5-HT2A and dopamine D2 receptors. Neuropharmacology 61, 770-777.

Amargos-Bosch, M., Adell, A., Artigas, F., 2007. Antipsychotic drugs reverse the AMPA receptor-stimulated release of 5-HT in the medial prefrontal cortex. J Neurochem 102, 550-561.

Amargos-Bosch, M., Adell, A., Bortolozzi, A., Artigas, F., 2003. Stimulation of alpha1-adrenoceptors in the rat medial prefrontal cortex increases the local in vivo 5-hydroxytryptamine release: reversal by antipsychotic drugs. J Neurochem 87, 831-842.

Amargós-Bosch, M., Adell, A., Bortolozzi, A., Artigas, F., 2004. Stimulation of α1-adrenoceptors in the rat medial prefrontal cortex increases the local in vivo 5-hydroxytryptamine release: reversal by antipsychotic drugs. J Neurochem 87, 831-842.

Amargos-Bosch, M., Lopez-Gil, X., Artigas, F., Adell, A., 2006. Clozapine and olanzapine, but not haloperidol, suppress serotonin efflux in the medial prefrontal cortex elicited by phencyclidine and ketamine. Int J Neuropsychopharmacol 9, 565-573.

Amato, D., Natesan, S., Yavich, L., Kapur, S., Muller, C.P., 2011. Dynamic regulation of dopamine and serotonin responses to salient stimuli during chronic haloperidol treatment. Int J Neuropsychopharmacol 14, 1327-1339.

Andersen, F.L., Ladefoged, C.N., Beyer, T., Keller, S.H., Hansen, A.E., Hojgaard, L., Kjaer, A., Law, I., Holm, S., 2014. Combined PET/MR imaging in neurology: MR-based attenuation correction implies a strong spatial bias when ignoring bone. Neuroimage 84, 206-216.

Antunes, M.L., Johnson, L.L., Seldin, D.W., Bhatia, K., Tresgallo, M.E., Greenspan, R.L., Vaccarino, R.A., Rodney, R.A., 1992. Diagnosis of right ventricular acute myocardial infarction by dual isotope thallium-201 and indium-111 antimyosin SPECT imaging. Am J Cardiol 70, 426-431.

Audenaert, K., Van Laere, K., Dumont, F., Slegers, G., Mertens, J., van Heeringen, C., Dierckx, R.A., 2001. Decreased frontal serotonin 5-HT 2a receptor binding index in deliberate self-harm patients. Eur J Nucl Med 28, 175-182.

Baeken, C., D'Haenen, H., Flamen, P., Mertens, J., Terriere, D., Chavatte, K., Boumon, R., Bossuyt, A., 1998. 123I-5-I-R91150, a new single-photon emission tomography ligand for 5-HT2A receptors:

influence of age and gender in healthy subjects. Eur J Nucl Med 25, 1617-1622.

Bailey, D.L., Townsend, D.W., Valk, P.E., Maisey, M.N., 2006. Positron Emission Tomography: Basic Sciences. Springer London.

Bakshi, V.P., Geyer, M.A., 1998. Multiple limbic regions mediate the disruption of prepulse inhibition produced in rats by the noncompetitive NMDA antagonist dizocilpine. J Neurosci 18, 8394-8401.

Bansal, T., Jaggi, M., Khar, R.K., Talegaonkar, S., 2009. Emerging significance of flavonoids as P-glycoprotein inhibitors in cancer chemotherapy. J Pharm Pharm Sci 12, 46-78.

Barber, D.C., 1980. The use of principal components in the quantitative analysis of gamma camera dynamic studies. Phys Med Biol 25, 283-292.

Bishnoi, M., Chopra, K., Kulkarni, S.K., 2007. Neurochemical changes associated with chronic administration of typical antipsychotics and its relationship with tardive dyskinesia. Methods Find Exp Clin Pharmacol 29, 211-216.

Blanckaert, P., Burvenich, I., Staelens, S., De Bruyne, S., Moerman, L., Wyffels, L., De Vos, F., 2009. Effect of cyclosporin A administration on the biodistribution and multipinhole muSPECT imaging of [123I]R91150 in rodent brain. Eur J Nucl Med Mol Imaging 36, 446-453.

Blasi, G., Selvaggi, P., Fazio, L., Antonucci, L.A., Taurisano, P., Masellis, R., Romano, R., Mancini, M., Zhang, F., Caforio, G., Popolizio, T., Apud, J., Weinberger, D.R., Bertolino, A., 2015. Variation in Dopamine D2 and Serotonin 5-HT2A Receptor Genes is Associated with Working Memory Processing and Response to Treatment with Antipsychotics. Neuropsychopharmacology 40, 1600-1608.

Borroto-Escuela, D.O., Romero-Fernandez, W., Narvaez, M., Oflijan, J., Agnati, L.F., Fuxe, K., 2014. Hallucinogenic 5-HT2AR agonists LSD and DOI enhance dopamine D2R protomer recognition and signaling of D2-5-HT2A heteroreceptor complexes. Biochem Biophys Res Commun 443, 278-284.

Bortolozzi, A., Diaz-Mataix, L., Scorza, M.C., Celada, P., Artigas, F., 2005. The activation of 5-HT2A receptors in prefrontal cortex enhances dopaminergic activity. J Neurochem 95, 1597-1607.

Bortolozzi, A., Masana, M., Diaz-Mataix, L., Cortes, R., Scorza, M.C., Gingrich, J.A., Toth, M., Artigas, F., 2010. Dopamine release induced by atypical antipsychotics in prefrontal cortex requires 5-HT(1A) receptors but not 5-HT(2A) receptors. Int J Neuropsychopharmacol 13, 1299-1314.

Bouvard, S., Costes, N., Bonnefoi, F., Lavenne, F., Mauguiere, F., Delforge, J., Ryvlin, P., 2005. Seizure-related short-term plasticity of benzodiazepine receptors in partial epilepsy: a [11C]flumazenil-PET study. Brain 128, 1330-1343.

Bruce, I.N., Burns, R.J., Gladman, D.D., Urowitz, M.B., 2000. Single photon emission computed tomography dual isotope myocardial perfusion imaging in women with systemic lupus erythematosus. I. Prevalence and distribution of abnormalities. J Rheumatol 27, 2372-2377.

Bruyant, P.P., Sau, J., Mallet, J.J., 1999. Noise removal using factor analysis of dynamic structures: application to cardiac gated studies. J Nucl Med 40, 1676-1682.

Bubenikova, V., Votava, M., Horacek, J., Palenicek, T., Dockery, C., 2005. The effect of zotepine, risperidone, clozapine and olanzapine on MK-801-disrupted sensorimotor gating. Pharmacol Biochem Behav 80, 591-596.

Buiter, H.J., Windhorst, A.D., Huisman, M.C., De Maeyer, J.H., Schuurkes, J.A., Lammertsma, A.A., Leysen, J.E., 2013. Radiosynthesis and preclinical evaluation of [11C]prucalopride as a potential

agonist PET ligand for the 5-HT4 receptor. EJNMMI Res 3, 24.

Burnet, P.W., Chen, C.P., McGowan, S., Franklin, M., Harrison, P.J., 1996. The effects of clozapine and haloperidol on serotonin-1A, -2A and -2C receptor gene expression and serotonin metabolism in the rat forebrain. Neuroscience 73, 531-540.

Buvat, I., Benali, H., Frouin, F., Bazin, J.P., Di Paola, R., 1993. Target apex-seeking in factor analysis of medical image sequences. Phys Med Biol 38, 123-138.

Carbon, M., Hsieh, C.H., Kane, J.M., Correll, C.U., 2017. Tardive Dyskinesia Prevalence in the Period of Second-Generation Antipsychotic Use: A Meta-Analysis. J Clin Psychiatry 78, e264-e278.

Carbon, M., Kane, J.M., Leucht, S., Correll, C.U., 2018. Tardive dyskinesia risk with first- and second-generation antipsychotics in comparative randomized controlled trials: a meta-analysis. World Psychiatry 17, 330-340.

Carson, R.E., 2000. PET physiological measurements using constant infusion. Nucl Med Biol 27, 657-660.

Casey, D.E., 2006. Implications of the CATIE trial on treatment: extrapyramidal symptoms. CNS Spectr 11, 25-31.

Castner, S.A., Williams, G.V., Goldman-Rakic, P.S., 2000. Reversal of antipsychotic-induced working memory deficits by short-term dopamine D1 receptor stimulation. Science 287, 2020-2022.

Catafau, A.M., Bullich, S., Danus, M., Penengo, M.M., Cot, A., Abanades, S., Farre, M., Pavia, J., Ros, D., 2008. Test-retest variability and reliability of 123I-IBZM SPECT measurement of striatal dopamine D2 receptor availability in healthy volunteers and influence of iterative reconstruction algorithms. Synapse 62, 62-69.

Catafau, A.M., Bullich, S., Nucci, G., Burgess, C., Gray, F., Merlo-Pich, E., 2011. Contribution of SPECT Measurements of D2 and 5-HT2A Occupancy to the Clinical Development of the Antipsychotic SB-773812. Journal of Nuclear Medicine 52, 526-534.

Choi, Y.K., Adham, N., Kiss, B., Gyertyan, I., Tarazi, F.I., 2017. Long-term effects of aripiprazole exposure on monoaminergic and glutamatergic receptor subtypes: comparison with cariprazine. CNS Spectr, 1-11.

Choy, K.H., Shackleford, D.M., Malone, D.T., Mistry, S.N., Patil, R.T., Scammells, P.J., Langmead, C.J., Pantelis, C., Sexton, P.M., Lane, J.R., Christopoulos, A., 2016. Positive Allosteric Modulation of the Muscarinic M1 Receptor Improves Efficacy of Antipsychotics in Mouse Glutamatergic Deficit Models of Behavior. J Pharmacol Exp Ther 359, 354-365.

Collin, G., Keshavan, M.S., 2018. Connectome development and a novel extension to the neurodevelopmental model of schizophrenia. Dialogues Clin Neurosci 20, 101-111.

Constantinescu, C.C., Coleman, R.A., Pan, M.L., Mukherjee, J., 2011. Striatal and extrastriatal microPET imaging of D2/D3 dopamine receptors in rat brain with [(1)(8)F]fallypride and [(1)(8)F]desmethoxyfallypride. Synapse 65, 778-787.

Correll, C.U., 2017. Epidemiology and Prevention of Tardive Dyskinesia. J Clin Psychiatry 78, e1426.

Creed-Carson, M., Oraha, A., Nobrega, J.N., 2011. Effects of 5-HT(2A) and 5-HT(2C) receptor antagonists on acute and chronic dyskinetic effects induced by haloperidol in rats. Behav Brain Res 219, 273-279.

Crunelle, C.L., de Wit, T.C., de Bruin, K., Ramakers, R.M., van der Have, F., Beekman, F.J., van den Brink, W., Booij, J., 2012. Varenicline increases in vivo striatal dopamine D(2/3) receptor binding:

an ultra-high-resolution pinhole [(123)I]IBZM SPECT study in rats. Nucl Med Biol.

Cselenyi, Z., Lundberg, J., Halldin, C., Farde, L., Gulyas, B., 2004. Joint explorative analysis of neuroreceptor subsystems in the human brain: application to receptor-transporter correlation using PET data. Neurochem Int 45, 773-781.

Csomor, P.A., Stadler, R.R., Feldon, J., Yee, B.K., Geyer, M.A., Vollenweider, F.X., 2007. Haloperidol Differentially Modulates Prepulse Inhibition and P50 Suppression in Healthy Humans Stratified for Low and High Gating Levels. Neuropsychopharmacology 33, 497-512.

Cunningham, V.J., Gunn, R.N., Matthews, J.C., 2004. Quantification in positron emission tomography for research in pharmacology and drug development. Nucl Med Commun 25, 643-646.

De Bruyne, S., Wyffels, L., Boos, T.L., Staelens, S., Deleye, S., Rice, K.C., De Vos, F., 2010. In vivo evaluation of [123I]-4-(2-(bis(4-fluorophenyl)methoxy)ethyl)-1-(4-iodobenzyl)piperidine, an iodinated SPECT tracer for imaging the P-gp transporter. Nucl Med Biol 37, 469-477.

de Paulis, T., 2003. The discovery of epidepride and its analogs as high-affinity radioligands for imaging extrastriatal dopamine D(2) receptors in human brain. Curr Pharm Des 9, 673-696.

Delforge, J., Spelle, L., Bendriem, B., Samson, Y., Bottlaender, M., Papageorgiou, S., Syrota, A., 1996. Quantitation of benzodiazepine receptors in human brain using the partial saturation method. J Nucl Med 37, 5-11.

Delforge, J., Spelle, L., Bendriem, B., Samson, Y., Syrota, A., 1997. Parametric images of benzodiazepine receptor concentration using a partial-saturation injection. J Cereb Blood Flow Metab 17, 343-355.

Delforge, J., Syrota, A., Bottlaender, M., Varastet, M., Loc'h, C., Bendriem, B., Crouzel, C., Brouillet, E., Maziere, M., 1993. Modeling analysis of [11C]flumazenil kinetics studied by PET: application to a critical study of the equilibrium approaches. J Cereb Blood Flow Metab 13, 454-468.

Delforge, J., Syrota, A., Mazoyer, B.M., 1989. Experimental design optimisation: theory and application to estimation of receptor model parameters using dynamic positron emission tomography. Phys Med Biol 34, 419-435.

Delforge, J., Syrota, A., Mazoyer, B.M., 1990. Identifiability analysis and parameter identification of an in vivo ligand-receptor model from PET data. IEEE Trans Biomed Eng 37, 653-661.

Demjaha, A., Murray, R.M., McGuire, P.K., Kapur, S., Howes, O.D., 2012. Dopamine synthesis capacity in patients with treatment-resistant schizophrenia. Am J Psychiatry 169, 1203-1210.

Desamericq, G., Schurhoff, F., Meary, A., Szoke, A., Macquin-Mavier, I., Bachoud-Levi, A.C., Maison, P., 2014. Long-term neurocognitive effects of antipsychotics in schizophrenia: a network meta-analysis. Eur J Clin Pharmacol 70, 127-134.

Di Giovanni, G., De Deurwaerdere, P., 2016. New therapeutic opportunities for 5-HT2C receptor ligands in neuropsychiatric disorders. Pharmacol Ther 157, 125-162.

Di Paola, R., Bazin, J.P., Aubry, F., Aurengo, A., Cavailloles, F., Herry, J.Y., Kahn, E., 1982. Handling of dynamic sequences in nuclear medicine. IEEE Trans on Nuclear Science NS29, 1310-1321.

Donthamsetti, P., Gallo, E.F., Buck, D.C., Stahl, E.L., Zhu, Y., Lane, J.R., Bohn, L.M., Neve, K.A., Kellendonk, C., Javitch, J.A., 2018. Arrestin recruitment to dopamine D2 receptor mediates locomotion but not incentive motivation. Mol Psychiatry.

Dossenbach, M., Arango-Davila, C., Silva Ibarra, H., Landa, E., Aguilar, J., Caro, O., Leadbetter, J., Assuncao, S., 2005. Response and relapse in patients with schizophrenia treated with

olanzapine, risperidone, quetiapine, or haloperidol: 12-month follow-up of the Intercontinental Schizophrenia Outpatient Health Outcomes (IC-SOHO) study. J Clin Psychiatry 66, 1021-1030.

Doze, P., Van Waarde, A., Elsinga, P.H., Hendrikse, N.H., Vaalburg, W., 2000. Enhanced cerebral uptake of receptor ligands by modulation of P-glycoprotein function in the blood-brain barrier. Synapse 36, 66-74.

Dumas, N., Moulin-Sallanon, M., Fender, P., Tournier, B.B., Ginovart, N., Charnay, Y., Millet, P., 2015. In Vivo Quantification of 5-HT2A Brain Receptors in Mdr1a KO Rats with 123I-R91150 Single-Photon Emission Computed Tomography. Mol Imaging 14.

Dumas, N., Moulin-Sallanon, M., Ginovart, N., Tournier, B.B., Suzanne, P., Cailly, T., Fabis, F., Rault, S., Charnay, Y., Millet, P., 2014. Small-animal single-photon emission computed tomographic imaging of the brain serotoninergic systems in wild-type and mdr1a knockout rats. Mol Imaging 13.

Ebdrup, B.H., Rasmussen, H., Arnt, J., Glenthoj, B., 2011. Serotonin 2A receptor antagonists for treatment of schizophrenia. Expert Opin Investig Drugs 20, 1211-1223.

Egan, M.F., Hyde, T.M., Kleinman, J.E., Wyatt, R.J., 1995. Neuroleptic-induced vacuous chewing movements in rodents: incidence and effects of long-term increases in haloperidol dose. Psychopharmacology (Berl) 117, 74-81.

Egerton, A., Ahmad, R., Hirani, E., Grasby, P.M., 2008. Modulation of striatal dopamine release by 5-HT2A and 5-HT2C receptor antagonists: [11C]raclopride PET studies in the rat. Psychopharmacology (Berl) 200, 487-496.

Egerton, A., Mehta, M.A., Montgomery, A.J., Lappin, J.M., Howes, O.D., Reeves, S.J., Cunningham, V.J., Grasby, P.M., 2009. The dopaminergic basis of human behaviors: A review of molecular imaging studies. Neurosci Biobehav Rev 33, 1109-1132.

El Fakhri, G., Trott, C.M., Sitek, A., Bonab, A., Alpert, N.M., 2013. Dual-tracer PET using generalized factor analysis of dynamic sequences. Mol Imaging Biol 15, 666-674.

Fagerlund, B., Pinborg, L.H., Mortensen, E.L., Friberg, L., Baare, W.F., Gade, A., Svarer, C., Glenthoj, B.Y., 2013. Relationship of frontal D(2/3) binding potentials to cognition: a study of antipsychotic-naive schizophrenia patients. Int J Neuropsychopharmacol 16, 23-36.

Fakhri, G.E., 2012. Ready for prime time? Dual tracer PET and SPECT imaging. Am J Nucl Med Mol Imaging 2, 415-417.

Fdez Espejo, E., Gil, E., 1997. Single restraint stress sensitizes acute chewing movements induced by haloperidol, but not if the 5-HT1A agonist 8-OH-DPAT is given prior to stress. Brain Res 755, 351-355.

Feifel, D., Priebe, K., 1999. The effects of subchronic haloperidol on intact and dizocilpine-disrupted sensorimotor gating. Psychopharmacology (Berl) 146, 175-179.

Feng, B., Bai, B., Smith, A.M., Austin, D.W., Mintzer, R.A., Gregor, J., 2007. Reconstruction of multi-pinhole SPECT data with correction of attenuation, scatter and intrinsic detector resolution. 2007 IEEE Nuclear Science Symposium Conference Record, pp. 3482-3485.

Fijal, K., Popik, P., Nikiforuk, A., 2014. Co-administration of 5-HT6 receptor antagonists with clozapine, risperidone, and a 5-HT2A receptor antagonist: effects on prepulse inhibition in rats. Psychopharmacology (Berl) 231, 269-281.

Fleischhacker, W., Galderisi, S., Laszlovszky, I., Szatmari, B., Barabassy, A., Acsai, K., Szalai, E.,

Harsanyi, J., Earley, W., Patel, M., Nemeth, G., 2019. The efficacy of cariprazine in negative symptoms of schizophrenia: Post hoc analyses of PANSS individual items and PANSS-derived factors. Eur Psychiatry 58, 1-9.

Fox, E., Bates, S.E., 2007. Tariquidar (XR9576): a P-glycoprotein drug efflux pump inhibitor. Expert Rev Anticancer Ther 7, 447-459.

Frankle, W.G., Slifstein, M., Talbot, P.S., Laruelle, M., 2005. Neuroreceptor imaging in psychiatry: theory and applications. Int Rev Neurobiol 67, 385-440.

Freeman, L., Garcia-Lorenzo, D., Bottin, L., Leroy, C., Louapre, C., Bodini, B., Papeix, C., Assouad, R., Granger, B., Tourbah, A., Dolle, F., Lubetzki, C., Bottlaender, M., Stankoff, B., 2015. The neuronal component of gray matter damage in multiple sclerosis: A [(11) C]flumazenil positron emission tomography study. Ann Neurol 78, 554-567.

Froklage, F.E., Syvanen, S., Hendrikse, N.H., Huisman, M.C., Molthoff, C.F., Tagawa, Y., Reijneveld, J.C., Heimans, J.J., Lammertsma, A.A., Eriksson, J., de Lange, E.C., Voskuyl, R.A., 2012. [11C]Flumazenil brain uptake is influenced by the blood-brain barrier efflux transporter P-glycoprotein. EJNMMI Res 2, 12.

Fujita, M., Seibyl, J.P., Verhoeff, N.P., Ichise, M., Baldwin, R.M., Zoghbi, S.S., Burger, C., Staley, J.K., Rajeevan, N., Charney, D.S., Innis, R.B., 1999. Kinetic and equilibrium analyses of [(123)I]epidepride binding to striatal and extrastriatal dopamine D(2) receptors. Synapse 34, 290-304.

Fujita, M., Verhoeff, N.P., Varrone, A., Zoghbi, S.S., Baldwin, R.M., Jatlow, P.A., Anderson, G.M., Seibyl, J.P., Innis, R.B., 2000. Imaging extrastriatal dopamine D(2) receptor occupancy by endogenous dopamine in healthy humans. Eur J Pharmacol 387, 179-188.

Fusar-Poli, P., Meyer-Lindenberg, A., 2013. Striatal presynaptic dopamine in schizophrenia, part II: meta-analysis of [(18)F/(11)C]-DOPA PET studies. Schizophr Bull 39, 33-42.

Gao, J., Huang, Y., Li, M., 2019. Does antagonism at 5-HT2A receptors potentiate D(2) blockade-induced disruption of conditioned avoidance response? Exp Clin Psychopharmacol 27, 103-108.

Geyer, M.A., Krebs-Thomson, K., Braff, D.L., Swerdlow, N.R., 2001. Pharmacological studies of prepulse inhibition models of sensorimotor gating deficits in schizophrenia: a decade in review. Psychopharmacology (Berl) 156, 117-154.

Ginovart, N., 2005. Imaging the dopamine system with in vivo [11C]raclopride displacement studies: understanding the true mechanism. Mol Imaging Biol 7, 45-52.

Ginovart, N., Kapur, S., 2012. Role of dopamine D(2) receptors for antipsychotic activity. Handb Exp Pharmacol, 27-52.

Ginovart, N., Wilson, A.A., Houle, S., Kapur, S., 2004. Amphetamine pretreatment induces a change in both D2-Receptor density and apparent affinity: a [11C]raclopride positron emission tomography study in cats. Biol Psychiatry 55, 1188-1194.

Ginovart, N., Wilson, A.A., Hussey, D., Houle, S., Kapur, S., 2008. D2-Receptor Upregulation is Dependent upon Temporal Course of D2-Occupancy: A Longitudinal [11C]-Raclopride PET Study in Cats. Neuropsychopharmacology 34, 662-671.

Glenthoj, B., 1993. Persistent vacuous chewing in rats following neuroleptic treatment: relationship to dopaminergic and cholinergic function. Psychopharmacology (Berl) 113, 157-166.

González-Maeso, J., Ang, R.L., Yuen, T., Chan, P., Weisstaub, N.V., López-Giménez, J.F., Zhou, M.,

Okawa, Y., Callado, L.F., Milligan, G., Gingrich, J.A., Filizola, M., Meana, J.J., Sealfon, S.C., 2008. Identification of a serotonin/glutamate receptor complex implicated in psychosis. Nature 452, 93-97.

Goozee, R., Reinders, A., Handley, R., Marques, T., Taylor, H., O'Daly, O., McQueen, G., Hubbard, K., Mondelli, V., Pariante, C., Dazzan, P., 2016. Effects of aripiprazole and haloperidol on neural activation during the n-back in healthy individuals: A functional MRI study. Schizophr Res 173, 174-181.

Gregor, J., Black, N., Wall, J., 2007. Monte Carlo study of scatter and attenuation effects in connection with I-125 pinhole imaging of mice. International Meeting on Fully 3D Image Reconstruction in Radiology and Nuclear Medicine, Lindau, Germany.

Gumusoglu, S.B., Stevens, H.E., 2019. Maternal Inflammation and Neurodevelopmental Programming: A Review of Preclinical Outcomes and Implications for Translational Psychiatry. Biol Psychiatry 85, 107-121.

Gunn, R.N., Gunn, S.R., Cunningham, V.J., 2001. Positron emission tomography compartmental models. J Cereb Blood Flow Metab 21, 635-652.

Gunn, R.N., Lammertsma, A.A., Hume, S.P., Cunningham, V.J., 1997. Parametric imaging of ligand-receptor binding in PET using a simplified reference region model. Neuroimage 6, 279-287.

Hartling, L., Abou-Setta, A.M., Dursun, S., Mousavi, S.S., Pasichnyk, D., Newton, A.S., 2012. Antipsychotics in adults with schizophrenia: comparative effectiveness of first-generation versus second-generation medications: a systematic review and meta-analysis. Ann Intern Med 157, 498-511.

Herman, A., El Mansari, M., Adham, N., Kiss, B., Farkas, B., Blier, P., 2018. Involvement of 5-HT1A and 5-HT2A Receptors but Not alpha 2-Adrenoceptors in the Acute Electrophysiological Effects of Cariprazine in the Rat Brain In Vivo. Mol Pharmacol 94, 1363-1370.

Hijnen, N.M., de Vries, A., Nicolay, K., Grull, H., 2012. Dual-isotope 111In/177Lu SPECT imaging as a tool in molecular imaging tracer design. Contrast Media Mol Imaging 7, 214-222.

Hillmer, A.T., Wooten, D.W., Tudorascu, D.L., Barnhart, T.E., Ahlers, E.O., Resch, L.M., Larson, J.A., Converse, A.K., Moore, C.F., Schneider, M.L., Christian, B.T., 2014. The effects of chronic alcohol self-administration on serotonin-1A receptor binding in nonhuman primates. Drug Alcohol Depend 144, 119-126.

Howes, O.D., Egerton, A., Allan, V., McGuire, P., Stokes, P., Kapur, S., 2009. Mechanisms underlying psychosis and antipsychotic treatment response in schizophrenia: insights from PET and SPECT imaging. Curr Pharm Des 15, 2550-2559.

Howes, O.D., Kambeitz, J., Kim, E., Stahl, D., Slifstein, M., Abi-Dargham, A., Kapur, S., 2012. The nature of dopamine dysfunction in schizophrenia and what this means for treatment. Arch Gen Psychiatry 69, 776-786.

Howes, O.D., Kapur, S., 2009. The dopamine hypothesis of schizophrenia: version III--the final common pathway. Schizophr Bull 35, 549-562.

Huang, M., Panos, J.J., Kwon, S., Oyamada, Y., Rajagopal, L., Meltzer, H.Y., 2014. Comparative effect of lurasidone and blonanserin on cortical glutamate, dopamine, and acetylcholine efflux: role of relative serotonin (5-HT)2Aand DA D2antagonism and 5-HT1Apartial agonism. J Neurochem 128, 938-949.

Huang, X.-F., Tan, Y.Y., Huang, X., Wang, Q., 2007. Effect of chronic treatment with clozapine and haloperidol on 5-HT2A and 2C receptor mRNA expression in the rat brain. Neurosci Res 59, 314-321.

Hudson, M.R., Rind, G., O'Brien, T.J., Jones, N.C., 2016. Reversal of evoked gamma oscillation deficits is predictive of antipsychotic activity with a unique profile for clozapine. Transl Psychiatry 6, e784.

Hutchings, E.J., Waller, J.L., Terry, A.V., 2013. Differential Long-Term Effects of Haloperidol and Risperidone on the Acquisition and Performance of Tasks of Spatial Working and Short-Term Memory and Sustained Attention in Rats. Journal of Pharmacology and Experimental Therapeutics 347, 547-556.

Hutton, B.F., Buvat, I., Beekman, F.J., 2011. Review and current status of SPECT scatter correction. Phys Med Biol 56, R85-112.

Ichihara, T., Ogawa, K., Motomura, N., Kubo, A., Hashimoto, S., 1993. Compton Scatter Compensation Using the Triple-Energy Window Method for Single- and Dual-Isotope SPECT. Journal of Nuclear Medecine 34, 2216-2221.

Ichikawa, J., Ishii, H., Bonaccorso, S., Fowler, W.L., O'Laughlin, I.A., Meltzer, H.Y., 2001. 5-HT(2A) and D(2) receptor blockade increases cortical DA release via 5-HT(1A) receptor activation: a possible mechanism of atypical antipsychotic-induced cortical dopamine release. J Neurochem 76, 1521-1531.

Ichikawa, J., Meltzer, H.Y., 1995. DOI, a 5-HT2A/2C receptor agonist, potentiates amphetamine-induced dopamine release in rat striatum. Brain Res 698, 204-208.

Ikeda, H., Adachi, K., Hasegawa, M., Sato, M., Hirose, N., Koshikawa, N., Cools, A.R., 1999. Effects of chronic haloperidol and clozapine on vacuous chewing and dopamine-mediated jaw movements in rats: evaluation of a revised animal model of tardive dyskinesia. J Neural Transm (Vienna) 106, 1205-1216.

Innis, R.B., Cunningham, V.J., Delforge, J., Fujita, M., Gjedde, A., Gunn, R.N., Holden, J., Houle, S., Huang, S.C., Ichise, M., Iida, H., Ito, H., Kimura, Y., Koeppe, R.A., Knudsen, G.M., Knuuti, J., Lammertsma, A.A., Laruelle, M., Logan, J., Maguire, R.P., Mintun, M.A., Morris, E.D., Parsey, R., Price, J.C., Slifstein, M., Sossi, V., Suhara, T., Votaw, J.R., Wong, D.F., Carson, R.E., 2007. Consensus nomenclature for in vivo imaging of reversibly binding radioligands. J Cereb Blood Flow Metab 27, 1533-1539.

Inoue, A., Miki, S., Seto, M., Kikuchi, T., Morita, S., Ueda, H., Misu, Y., Nakata, Y., 1997. Aripiprazole, a novel antipsychotic drug, inhibits quinpirole-evoked GTPase activity but does not up-regulate dopamine D2 receptor following repeated treatment in the rat striatum. Eur J Pharmacol 321, 105-111.

Ishikane, T., Kusumi, I., Matsubara, R., Matsubara, S., Koyama, T., 1997. Effects of serotonergic agents on the up-regulation of dopamine D2 receptors induced by haloperidol in rat striatum. Eur J Pharmacol 321, 163-169.

Ji, B., Chen, C.J., Bando, K., Ashino, H., Shiraishi, H., Sano, H., Kasahara, H., Minamizawa, T., Yamada, K., Ono, M., Zhang, M.R., Seki, C., Farde, L., Suhara, T., Higuchi, M., 2015. Distinct binding of amyloid imaging ligands to unique amyloid-beta deposited in the presubiculum of Alzheimer's disease. J Neurochem 135, 859-866.

Johnson, M., Kozielska, M., Pilla Reddy, V., Vermeulen, A., Barton, H.A., Grimwood, S., de Greef, R.,

Groothuis, G.M., Danhof, M., Proost, J.H., 2014. Dopamine D2 receptor occupancy as a predictor of catalepsy in rats: a pharmacokinetic-pharmacodynamic modeling approach. Pharm Res 31, 2605-2617.

Jones, H.M., Travis, M.J., Mulligan, R., Bressan, R.A., Visvikis, D., Gacinovic, S., Ell, P.J., Pilowsky, L.S., 2001. In vivo 5-HT2A receptor blockade by quetiapine: an R91150 single photon emission tomography study. Psychopharmacology (Berl) 157, 60-66.

Jongen, C., de Bruin, K., Beekman, F., Booij, J., 2008. SPECT imaging of D2 dopamine receptors and endogenous dopamine release in mice. Eur J Nucl Med Mol Imaging 35, 1692-1698.

Joshi, R.S., Quadros, R., Drumm, M., Ain, R., Panicker, M.M., 2017. Sedative effect of Clozapine is a function of 5-HT2A and environmental novelty. Eur Neuropsychopharmacol 27, 70-81.

Joshi, R.S., Singh, S.P., Panicker, M.M., 2019. 5-HT2A deletion protects against Clozapine-induced hyperglycemia. J Pharmacol Sci 139, 133-135.

Kadrmas, D.J., Rust, T.C., Hoffman, J.M., 2013. Single-scan dual-tracer FLT+FDG PET tumor characterization. Phys Med Biol 58, 429-449.

Kambeitz, J., Abi-Dargham, A., Kapur, S., Howes, O.D., 2014. Alterations in cortical and extrastriatal subcortical dopamine function in schizophrenia: systematic review and meta-analysis of imaging studies. Br J Psychiatry 204, 420-429.

Kanno-Nozaki, K., Miura, I., Kaneko, H., Horikoshi, S., Ota, T., Nozaki, M., Ejiri, H., Yahiro, M., Watanabe, K., Hino, M., Yabe, H., 2018. Influences of the T102C polymorphism in the 5-HT2A receptor gene on the five-factor model of Positive and Negative Syndrome Scale and treatment response to aripiprazole in patients with acute schizophrenia. Psychiatry Res 265, 244-245.

Kapur, S., Remington, G., 2001. Dopamine D(2) receptors and their role in atypical antipsychotic action: still necessary and may even be sufficient. Biol Psychiatry 50, 873-883.

Kapur, S., Wadenberg, M.L., Remington, G., 2000. Are animal studies of antipsychotics appropriately dosed? Lessons from the bedside to the bench. Can J Psychiatry 45, 241-246.

Karl, T., Duffy, L., O'Brien, E., Matsumoto, I., Dedova, I., 2006. Behavioural effects of chronic haloperidol and risperidone treatment in rats. Behav Brain Res 171, 286-294.

Kaur, G., Gupta, D., Chavan, B.S., Sinhmar, V., Prasad, R., Tripathi, A., Garg, P.D., Gupta, R., Khurana, H., Gautam, S., Margoob, M.A., Aneja, J., 2017. Identification of genetic correlates of response to Risperidone: Findings of a multicentric schizophrenia study from India. Asian J Psychiatr 29, 174-182.

Kegeles, L.S., Slifstein, M., Frankle, W.G., Xu, X., Hackett, E., Bae, S.A., Gonzales, R., Kim, J.H., Alvarez, B., Gil, R., Laruelle, M., Abi-Dargham, A., 2008. Dose-occupancy study of striatal and extrastriatal dopamine D2 receptors by aripiprazole in schizophrenia with PET and [18F]fallypride. Neuropsychopharmacology 33, 3111-3125.

Kessler, R.M., Ansari, M.S., de Paulis, T., Schmidt, D.E., Clanton, J.A., Smith, H.E., Manning, R.G., Gillespie, D., Ebert, M.H., 1991. High affinity dopamine D2 receptor radioligands. 1. Regional rat brain distribution of iodinated benzamides. J Nucl Med 32, 1593-1600.

Kim, E., Howes, O.D., Turkheimer, F.E., Kim, B.H., Jeong, J.M., Kim, J.W., Lee, J.S., Jang, I.J., Shin, S.G., Kapur, S., Kwon, J.S., 2013. The relationship between antipsychotic D2 occupancy and change in frontal metabolism and working memory : A dual [(11)C]raclopride and [(18) F]FDG imaging study with aripiprazole. Psychopharmacology (Berl) 227, 221-229.

Kim, J., Herrero, P., Sharp, T., Laforest, R., Rowland, D.J., Tai, Y.C., Lewis, J.S., Welch, M.J., 2006. Minimally invasive method of determining blood input function from PET images in rodents. J Nucl Med 47, 330-336.

Kim, K.M., Watabe, H., Kawachi, N., Iida, H., 2003. Extraction of blood pool in dynamic O-15 water PET with slow-infusion using factor analysis. Nuclear Science Symposium Conference Record, 2003 IEEE, pp. 2640-2641 Vol.2644.

Koeppe, R.A., Raffel, D.M., Snyder, S.E., Ficaro, E.P., Kilbourn, M.R., Kuhl, D.E., 2001. Dual-[11C]tracer single-acquisition positron emission tomography studies. J Cereb Blood Flow Metab 21, 1480-1492.

Kroll, T., Elmenhorst, D., Matusch, A., Celik, A.A., Wedekind, F., Weisshaupt, A., Beer, S., Bauer, A., 2014. [(1)(8)F]Altanserin and small animal PET: impact of multidrug efflux transporters on ligand brain uptake and subsequent quantification of 5-HT(2)A receptor densities in the rat brain. Nucl Med Biol 41, 1-9.

Kuehner, J.N., Bruggeman, E.C., Wen, Z., Yao, B., 2019. Epigenetic Regulations in Neuropsychiatric Disorders. Front Genet 10, 268.

Kugaya, A., Fujita, M., Innis, R.B., 2000. Applications of SPECT imaging of dopaminergic neurotransmission in neuropsychiatric disorders. Ann Nucl Med 14, 1-9.

Kung, H.F., Pan, S., Kung, M.P., Billings, J., Kasliwal, R., Reilley, J., Alavi, A., 1989. In vitro and in vivo evaluation of [123I]IBZM: a potential CNS D-2 dopamine receptor imaging agent. J Nucl Med 30, 88-92.

Kurita, M., Holloway, T., Garcia-Bea, A., Kozlenkov, A., Friedman, A.K., Moreno, J.L., Heshmati, M., Golden, S.A., Kennedy, P.J., Takahashi, N., Dietz, D.M., Mocci, G., Gabilondo, A.M., Hanks, J., Umali, A., Callado, L.F., Gallitano, A.L., Neve, R.L., Shen, L., Buxbaum, J.D., Han, M.H., Nestler, E.J., Meana, J.J., Russo, S.J., Gonzalez-Maeso, J., 2012. HDAC2 regulates atypical antipsychotic responses through the modulation of mGlu2 promoter activity. Nat Neurosci 15, 1245-1254.

Kuroki, T., Meltzer, H.Y., Ichikawa, J., 1999. Effects of antipsychotic drugs on extracellular dopamine levels in rat medial prefrontal cortex and nucleus accumbens. J Pharmacol Exp Ther 288, 774-781.

Kusumi, I., Takahashi, Y., Suzuki, K., Kameda, K., Koyama, T., 2000. Differential effects of subchronic treatments with atypical antipsychotic drugs on dopamine D2 and serotonin 5-HT2A receptors in the rat brain. J Neural Transm (Vienna) 107, 295-302.

Kuwabara, H., McCaul, M.E., Wand, G.S., Earley, C.J., Allen, R.P., Weerts, E.M., Dannals, R.F., Wong, D.F., 2012. Dissociative changes in the Bmax and KD of dopamine D2/D3 receptors with aging observed in functional subdivisions of the striatum: a revisit with an improved data analysis method. J Nucl Med 53, 805-812.

la Fougere, C., Boning, G., Bartmann, H., Wangler, B., Nowak, S., Just, T., Wagner, E., Winter, P., Rominger, A., Forster, S., Gildehaus, F.J., Rosa-Neto, P., Minuzzi, L., Bartenstein, P., Potschka, H., Cumming, P., 2010. Uptake and binding of the serotonin 5-HT1A antagonist [18F]-MPPF in brain of rats: effects of the novel P-glycoprotein inhibitor tariquidar. Neuroimage 49, 1406-1415.

Lacan, G., Plenevaux, A., Rubins, D.J., Way, B.M., Defraiteur, C., Lemaire, C., Aerts, J., Luxen, A., Cherry, S.R., Melega, W.P., 2008. Cyclosporine, a P-glycoprotein modulator, increases

[18F]MPPF uptake in rat brain and peripheral tissues: microPET and ex vivo studies. Eur J Nucl Med Mol Imaging 35, 2256-2266.

Lammertsma, A.A., Hume, S.P., 1996. Simplified reference tissue model for PET receptor studies. Neuroimage 4, 153-158.

Laruelle, M., 2000. Imaging synaptic neurotransmission with in vivo binding competition techniques: a critical review. J Cereb Blood Flow Metab 20, 423-451.

Lavoie, S., Polari, A.R., Goldstone, S., Nelson, B., McGorry, P.D., 2019. Staging model in psychiatry: Review of the evolution of electroencephalography abnormalities in major psychiatric disorders. Early Interv Psychiatry.

Lee, S., Gregor, J., Kennel, S.J., Osborne, D.R., Wall, J., 2015. GATE validation of standard dual energy corrections in small animal SPECT-CT. PLoS One 10, e0122780.

Lee, S., Gregor, J., Osborne, D., Wall, J., 2013. Dual isotope SPECT imaging of I-123 and I-125. Nuclear Science Symposium and Medical Imaging Conference (NSS/MIC), 2013 IEEE. IEEE.

Lehto, S.M., Kuikka, J., Tolmunen, T., Hintikka, J., Viinamaki, H., Vanninen, R., Koivumaa-Honkanen, H., Honkalampi, K., Tiihonen, J., 2009. Altered hemispheric balance of temporal cortex dopamine D(2/3) receptor binding in major depressive disorder. Psychiatry Res 172, 251.

Leslie, W.D., Abrams, D.N., Greenberg, C.R., Hobson, D., 1996. Comparison of iodine-123-epidepride and iodine-123-IBZM for dopamine D2 receptor imaging. J Nucl Med 37, 1589-1591.

Leucht, S., Cipriani, A., Spineli, L., Mavridis, D., Örey, D., Richter, F., Samara, M., Barbui, C., Engel, R.R., Geddes, J.R., Kissling, W., Stapf, M.P., Lässig, B., Salanti, G., Davis, J.M., 2013. Comparative efficacy and tolerability of 15 antipsychotic drugs in schizophrenia: a multiple-treatments meta-analysis. The Lancet 382, 951-962.

Lewis, D.A., Lieberman, J.A., 2000. Catching up on schizophrenia: natural history and neurobiology. Neuron 28, 325-334.

Lewis, S., Lieberman, J., 2008. CATIE and CUtLASS: can we handle the truth? The British Journal of Psychiatry 192, 161-163.

Li, C., Tang, Y., Yang, J., Zhang, X., Liu, Y., Tang, A., 2016. Sub-chronic Antipsychotic Drug Administration Reverses the Expression of Neuregulin 1 and ErbB4 in a Cultured MK801-Induced Mouse Primary Hippocampal Neuron or a Neurodevelopmental Schizophrenia Model. Neurochem Res 41, 2049-2064.

Lian, J., Huang, X.-F., Pai, N., Deng, C., 2013. Effects of olanzapine and betahistine co-treatment on serotonin transporter, 5-HT2A and dopamine D2 receptor binding density. Progress in Neuro-Psychopharmacology and Biological Psychiatry 47, 62-68.

Lidow, M.S., Goldman-Rakic, P.S., 1994. A common action of clozapine, haloperidol, and remoxipride on D1- and D2-dopaminergic receptors in the primate cerebral cortex. Proc Natl Acad Sci U S A 91, 4353-4356.

Liegeois, J.F., Ichikawa, J., Meltzer, H.Y., 2002. 5-HT(2A) receptor antagonism potentiates haloperidol-induced dopamine release in rat medial prefrontal cortex and inhibits that in the nucleus accumbens in a dose-dependent manner. Brain Res 947, 157-165.

Liow, J.S., Lu, S., McCarron, J.A., Hong, J., Musachio, J.L., Pike, V.W., Innis, R.B., Zoghbi, S.S., 2007. Effect of a P-glycoprotein inhibitor, Cyclosporin A, on the disposition in rodent brain and blood of the 5-HT1A receptor radioligand, [11C](R)-(-)-RWAY. Synapse 61, 96-105.

Logan, J., Fowler, J.S., Volkow, N.D., Wang, G.J., Ding, Y.S., Alexoff, D.L., 1996. Distribution volume ratios without blood sampling from graphical analysis of PET data. J Cereb Blood Flow Metab 16, 834-840.

Loscher, W., Potschka, H., 2005. Role of drug efflux transporters in the brain for drug disposition and treatment of brain diseases. Prog Neurobiol 76, 22-76.

Lucas, G., De Deurwaerdere, P., Caccia, S., Umberto, S., 2000. The effect of serotonergic agents on haloperidol-induced striatal dopamine release in vivo: opposite role of 5-HT(2A) and 5-HT(2C) receptor subtypes and significance of the haloperidol dose used. Neuropharmacology 39, 1053-1063.

Lukasiewicz, S., Polit, A., Kedracka-Krok, S., Wedzony, K., Mackowiak, M., Dziedzicka-Wasylewska, M., 2010. Hetero-dimerization of serotonin 5-HT(2A) and dopamine D(2) receptors. Biochim Biophys Acta 1803, 1347-1358.

Lustig, C., Meck, W.H., 2005. Chronic treatment with haloperidol induces deficits in working memory and feedback effects of interval timing. Brain Cogn 58, 9-16.

Lyoo, C.H., Ikawa, M., Liow, J.S., Zoghbi, S.S., Morse, C.L., Pike, V.W., Fujita, M., Innis, R.B., Kreisl, W.C., 2015. Cerebellum Can Serve As a Pseudo-Reference Region in Alzheimer Disease to Detect Neuroinflammation Measured with PET Radioligand Binding to Translocator Protein. J Nucl Med 56, 701-706.

Ma, J., Ye, N., Cohen, B.M., 2006. Expression of noradrenergic α1, serotoninergic 5HT2a and dopaminergic D2 receptors on neurons activated by typical and atypical antipsychotic drugs. Progress in Neuro-Psychopharmacology and Biological Psychiatry 30, 647-657.

Maejima, T., Masseck, O.A., Mark, M.D., Herlitze, S., 2013. Modulation of firing and synaptic transmission of serotonergic neurons by intrinsic G protein-coupled receptors and ion channels. Front Integr Neurosci 7, 40.

Mahmoudi, S., Levesque, D., Blanchet, P.J., 2014. Upregulation of dopamine D3, not D2, receptors correlates with tardive dyskinesia in a primate model. Mov Disord 29, 1125-1133.

Marchese, G., Bartholini, F., Casu, M.A., Ruiu, S., Casti, P., Congeddu, E., Tambaro, S., Pani, L., 2004. Haloperidol versus risperidone on rat "early onset" vacuous chewing. Behav Brain Res 149, 9-16.

Marissal, T., Salazar, R.F., Bertollini, C., Mutel, S., De Roo, M., Rodriguez, I., Muller, D., Carleton, A., 2018. Restoring wild-type-like CA1 network dynamics and behavior during adulthood in a mouse model of schizophrenia. Nat Neurosci 21, 1412-1420.

Martinez, D., Saccone, P.A., Liu, F., Slifstein, M., Orlowska, D., Grassetti, A., Cook, S., Broft, A., Van Heertum, R., Comer, S.D., 2012. Deficits in dopamine D(2) receptors and presynaptic dopamine in heroin dependence: commonalities and differences with other types of addiction. Biol Psychiatry 71, 192-198.

Martino, D., Karnik, V., Osland, S., Barnes, T.R.E., Pringsheim, T.M., 2018. Movement Disorders Associated With Antipsychotic Medication in People With Schizophrenia: An Overview of Cochrane Reviews and Meta-Analysis. Can J Psychiatry, 706743718777392.

Mattner, F., Bandin, D.L., Staykova, M., Berghofer, P., Gregoire, M.C., Ballantyne, P., Quinlivan, M., Fordham, S., Pham, T., Willenborg, D.O., Katsifis, A., 2011. Evaluation of [(1)(2)(3)I]-CLINDE as a potent SPECT radiotracer to assess the degree of astroglia activation in cuprizone-induced neuroinflammation. Eur J Nucl Med Mol Imaging 38, 1516-1528.

Mattner, F., Mardon, K., Katsifis, A., 2008. Pharmacological evaluation of [123I]-CLINDE: a radioiodinated imidazopyridine-3-acetamide for the study of peripheral benzodiazepine binding sites (PBBS). Eur J Nucl Med Mol Imaging 35, 779-789.

Mauger, G., Saba, W., Hantraye, P., Dolle, F., Coulon, C., Bramoulle, Y., Chalon, S., Gregoire, M.C., 2005. Multiinjection approach for D2 receptor binding quantification in living rats using [11C]raclopride and the beta-microprobe: crossvalidation with in vitro binding data. J Cereb Blood Flow Metab 25, 1517-1527.

McCormick, P.N., Ginovart, N., Wilson, A.A., 2011. Isoflurane anaesthesia differentially affects the amphetamine sensitivity of agonist and antagonist D2/D3 positron emission tomography radiotracers: implications for in vivo imaging of dopamine release. Mol Imaging Biol 13, 737-746.

McCutcheon, R., Beck, K., Jauhar, S., Howes, O.D., 2018. Defining the Locus of Dopaminergic Dysfunction in Schizophrenia: A Meta-analysis and Test of the Mesolimbic Hypothesis. Schizophr Bull 44, 1301-1311.

McCutcheon, R.A., Abi-Dargham, A., Howes, O.D., 2019. Schizophrenia, Dopamine and the Striatum: From Biology to Symptoms. Trends Neurosci 42, 205-220.

McEvoy, J., Citrome, L., 2016. Brexpiprazole for the Treatment of Schizophrenia: A Review of this Novel Serotonin-Dopamine Activity Modulator. Clin Schizophr Relat Psychoses 9, 177-186.

McOmish, C.E., Lira, A., Hanks, J.B., Gingrich, J.A., 2012. Clozapine-induced locomotor suppression is mediated by 5-HT2A receptors in the forebrain. Neuropsychopharmacology 37, 2747-2755.

Meltzer, H.Y., 2004. What's atypical about atypical antipsychotic drugs? Curr Opin Pharmacol 4, 53-57.

Meltzer, H.Y., Li, Z., Kaneda, Y., Ichikawa, J., 2003. Serotonin receptors: their key role in drugs to treat schizophrenia. Prog Neuropsychopharmacol Biol Psychiatry 27, 1159-1172.

Mendlin, A., Martin, F.J., Jacobs, B.L., 1998. Involvement of dopamine D2 receptors in apomorphine-induced facilitation of forebrain serotonin output. Eur J Pharmacol 351, 291-298.

Mertens, J., Terriere, D., Sipido, V., Gommeren, W., Janssen, P.M.F., Leysen, J.E., 1994. Radiosynthesis of a new radioidinated ligand for serotonin-5Ht2-receptor, a promising tracer for gamma emission tomography. J Labelled Comp Radiopharm 34, 795-806.

Meyer, P.T., Salber, D., Schiefer, J., Cremer, M., Schaefer, W.M., Kosinski, C.M., Langen, K.J., 2008a. Cerebral kinetics of the dopamine D(2) receptor ligand [(123)I]IBZM in mice. Nucl Med Biol 35, 467-473.

Meyer, P.T., Salber, D., Schiefer, J., Cremer, M., Schaefer, W.M., Kosinski, C.M., Langen, K.J., 2008b. Comparison of intravenous and intraperitoneal [123I]IBZM injection for dopamine D2 receptor imaging in mice. Nucl Med Biol 35, 543-548.

Meyer, P.T., Sattler, B., Winz, O.H., Fundke, R., Oehlwein, C., Kendziorra, K., Hesse, S., Schaefer, W.M., Sabri, O., 2008c. Kinetic analyses of [123I]IBZM SPECT for quantification of striatal dopamine D2 receptor binding: a critical evaluation of the single-scan approach. Neuroimage 42, 548-558.

Millet, P., Graf, C., Buck, A., Walder, B., Ibanez, V., 2002a. Evaluation of the reference tissue models for PET and SPECT benzodiazepine binding parameters. Neuroimage 17, 928-942.

Millet, P., Graf, C., Buck, A., Walder, B., Ibáñez, V., 2002b. Evaluation of the Reference Tissue Models for PET and SPECT Benzodiazepine Binding Parameters. Neuroimage 17, 928-942.

Millet, P., Graf, C., Buck, A., Walder, B., Westera, G., Broggini, C., Arigoni, M., Slosman, D., Bouras, C., Ibanez, V., 2000a. Similarity and robustness of PET and SPECT binding parameters for

benzodiazepine receptors. J Cereb Blood Flow Metab 20, 1587-1603.

Millet, P., Graf, C., Moulin, M., Ibanez, V., 2006. SPECT quantification of benzodiazepine receptor concentration using a dual-ligand approach. J Nucl Med 47, 783-792.

Millet, P., Ibanez, V., Delforge, J., Pappata, S., Guimon, J., 2000b. Wavelet analysis of dynamic PET data: application to the parametric imaging of benzodiazepine receptor concentration. Neuroimage 11, 458-472.

Millet, P., Lemoigne, Y., 2008. Pharmacokinetics Application in Biophysics Experiments. In: Lemoigne, Y., Caner, A. (Eds.), Molecular Imaging: Computer Reconstruction and Practice. Springer Netherlands, Dordrecht, pp. 211-228.

Millet, P., Moulin-Sallanon, M., Tournier, B.B., Dumas, N., Charnay, Y., Ibanez, V., Ginovart, N., 2012. Quantification of dopamine D(2/3) receptors in rat brain using factor analysis corrected [18F]Fallypride images. Neuroimage 62, 1455-1468.

Mocci, G., Jiménez-Sánchez, L., Adell, A., Cortés, R., Artigas, F., 2014. Expression of 5-HT2A receptors in prefrontal cortex pyramidal neurons projecting to nucleus accumbens. Potential relevance for atypical antipsychotic action. Neuropharmacology 79, 49-58.

Mombereau, C., Arnt, J., Mork, A., 2017. Involvement of presynaptic 5-HT1A receptors in the low propensity of brexpiprazole to induce extrapyramidal side effects in rats. Pharmacol Biochem Behav 153, 141-146.

Moreno, J.L., Holloway, T., Umali, A., Rayannavar, V., Sealfon, S.C., Gonzalez-Maeso, J., 2013. Persistent effects of chronic clozapine on the cellular and behavioral responses to LSD in mice. Psychopharmacology (Berl) 225, 217-226.

Morris, E.D., Bonab, A.A., Alpert, N.M., Fischman, A.J., Madras, B.K., Christian, B.T., 1999. Concentration of dopamine transporters: to Bmax or not to Bmax? Synapse 32, 136-140.

Morris, E.D., Endres, C.J., Schmidt, K.C., Christian, B.T., Muzic Jr, R.F., Fisher, R.E., 2004. CHAPTER 23 - Kinetic Modeling in Positron Emission Tomography A2 - Wernick, Miles N. In: Aarsvold, J.N. (Ed.), Emission Tomography. Academic Press, San Diego, pp. 499-540.

Morris, E.D., Lucas, M.V., Petrulli, J.R., Cosgrove, K.P., 2014. How to design PET experiments to study neurochemistry: application to alcoholism. Yale J Biol Med 87, 33-54.

Muguruza, C., Moreno, J.L., Umali, A., Callado, L.F., Meana, J.J., González-Maeso, J., 2013. Dysregulated 5-HT2A receptor binding in postmortem frontal cortex of schizophrenic subjects. European Neuropsychopharmacology 23, 852-864.

Murnane, K.S., Howell, L.L., 2011. Neuroimaging and drug taking in primates. Psychopharmacology (Berl) 216, 153-171.

Naef, M., Muller, U., Linssen, A., Clark, L., Robbins, T.W., Eisenegger, C., 2017. Effects of dopamine D2/D3 receptor antagonism on human planning and spatial working memory. Transl Psychiatry 7, e1107.

Naidu, P.S., Kulkarni, S.K., 2001. Effect of 5-HT1A and 5-HT2A/2C receptor modulation on neuroleptic-induced vacuous chewing movements. Eur J Pharmacol 428, 81-86.

Narendran, R., Martinez, D., 2008. Cocaine abuse and sensitization of striatal dopamine transmission: a critical review of the preclinical and clinical imaging literature. Synapse 62, 851-869.

Nasrallah, H.A., Fedora, R., Morton, R., 2019. Successful treatment of clozapine-nonresponsive refractory hallucinations and delusions with pimavanserin, a serotonin 5HT-2A receptor inverse

agonist. Schizophr Res.

Natesan, S., Reckless, G.E., Nobrega, J.N., Fletcher, P.J., Kapur, S., 2005. Dissociation between In Vivo Occupancy and Functional Antagonism of Dopamine D2 Receptors: Comparing Aripiprazole to Other Antipsychotics in Animal Models. Neuropsychopharmacology 31, 1854-1863.

Naumenko, V.S., Bazovkina, D.V., Kondaurova, E.M., Zubkov, E.A., Kulikov, A.V., 2010. The role of 5-HT2A receptor and 5-HT2A/5-HT1A receptor interaction in the suppression of catalepsy. Genes Brain Behav 9, 519-524.

Nielsen, R.E., Levander, S., Kjaersdam Telléus, G., Jensen, S.O.W., Østergaard Christensen, T., Leucht, S., 2015. Second-generation antipsychotic effect on cognition in patients with schizophrenia-a meta-analysis of randomized clinical trials. Acta Psychiatr Scand 131, 185-196.

Nikolaus, S., Antke, C., Beu, M., Kley, K., Wirrwar, A., Huston, J.P., Muller, H.W., 2011. Binding of [123I]iodobenzamide to the rat D2 receptor after challenge with various doses of methylphenidate: an in vivo imaging study with dedicated small animal SPECT. Eur J Nucl Med Mol Imaging 38, 694-701.

Nørbak-Emig, H., Ebdrup, B.H., Fagerlund, B., Svarer, C., Rasmussen, H., Friberg, L., Allerup, P.N., Rostrup, E., Pinborg, L.H., Glenthøj, B.Y., 2016. Frontal D2/3Receptor Availability in Schizophrenia Patients Before and After Their First Antipsychotic Treatment: Relation to Cognitive Functions and Psychopathology. International Journal of Neuropsychopharmacology 19, pyw006.

Norbak-Emig, H., Pinborg, L.H., Raghava, J.M., Svarer, C., Baare, W.F., Allerup, P., Friberg, L., Rostrup, E., Glenthoj, B., Ebdrup, B.H., 2016. Extrastriatal dopamine D2/3 receptors and cortical grey matter volumes in antipsychotic-naive schizophrenia patients before and after initial antipsychotic treatment. World J Biol Psychiatry, 1-11.

Olijslagers, J.E., Perlstein, B., Werkman, T.R., McCreary, A.C., Siarey, R., Kruse, C.G., Wadman, W.J., 2005. The role of 5-HT(2A) receptor antagonism in amphetamine-induced inhibition of A10 dopamine neurons in vitro. Eur J Pharmacol 520, 77-85.

Olten, B., Bloch, M.H., 2018. Meta regression: Relationship between antipsychotic receptor binding profiles and side-effects. Prog Neuropsychopharmacol Biol Psychiatry 84, 272-281.

Ordonez, A.A., Pokkali, S., DeMarco, V.P., Klunk, M., Mease, R.C., Foss, C.A., Pomper, M.G., Jain, S.K., 2015. Radioiodinated DPA-713 imaging correlates with bactericidal activity of tuberculosis treatments in mice. Antimicrob Agents Chemother 59, 642-649.

Osborne, P.G., O'Connor, W.T., Beck, O., Ungerstedt, U., 1994. Acute versus chronic haloperidol: relationship between tolerance to catalepsy and striatal and accumbens dopamine, GABA and acetylcholine release. Brain Res 634, 20-30.

Ott, T., Nieder, A., 2016. Dopamine D2 Receptors Enhance Population Dynamics in Primate Prefrontal Working Memory Circuits. Cerebral Cortex.

Passchier, J., van Waarde, A., Doze, P., Elsinga, P.H., Vaalburg, W., 2000. Influence of P-glycoprotein on brain uptake of [18F]MPPF in rats. Eur J Pharmacol 407, 273-280.

Pellerin, L., Magistretti, P.J., 1994. Glutamate uptake into astrocytes stimulates aerobic glycolysis: a mechanism coupling neuronal activity to glucose utilization. Proc Natl Acad Sci U S A 91, 10625-10629.

Phelps, M.E., 2000. PET: the merging of biology and imaging into molecular imaging. J Nucl Med 41,

661-681.

Pimlott, S.L., Ebmeier, K.P., 2007. SPECT imaging in dementia. Br J Radiol 80 Spec No 2, S153-159.

Pinborg, L.H., Videbaek, C., Ziebell, M., Mackeprang, T., Friberg, L., Rasmussen, H., Knudsen, G.M., Glenthoj, B.Y., 2007. [123I]Epidepride binding to cerebellar dopamine D2/D3 receptors is displaceable: Implications for the use of cerebellum as a reference region. Neuroimage 34, 1450-1453.

Pogorelov, V.M., Rodriguiz, R.M., Cheng, J., Huang, M., Schmerberg, C.M., Meltzer, H.Y., Roth, B.L., Kozikowski, A.P., Wetsel, W.C., 2017. 5-HT2C Agonists Modulate Schizophrenia-Like Behaviors in Mice. Neuropsychopharmacology 42, 2163-2177.

Rasmussen, H., Ebdrup, B.H., Oranje, B., Pinborg, L.H., Knudsen, G.M., Glenthoj, B., 2014. Neocortical serotonin2A receptor binding predicts quetiapine associated weight gain in antipsychotic-naive first-episode schizophrenia patients. Int J Neuropsychopharmacol 17, 1729-1736.

Rasmussen, H., Erritzoe, D., Andersen, R., Ebdrup, B.H., Aggernaes, B., Oranje, B., Kalbitzer, J., Madsen, J., Pinborg, L.H., Baare, W., Svarer, C., Lublin, H., Knudsen, G.M., Glenthoj, B., 2010. Decreased frontal serotonin2A receptor binding in antipsychotic-naive patients with first-episode schizophrenia. Arch Gen Psychiatry 67, 9-16.

Reavill, C., Kettle, A., Holland, V., Riley, G., Blackburn, T.P., 1999. Attenuation of haloperidol-induced catalepsy by a 5-HT2C receptor antagonist. Br J Pharmacol 126, 572-574.

Rosengarten, H., Quartermain, D., 2002. The effect of chronic treatment with typical and atypical antipsychotics on working memory and jaw movements in three- and eighteen-month-old rats. Prog Neuropsychopharmacol Biol Psychiatry 26, 1047-1054.

Sakurai, H., Bies, R.R., Stroup, S.T., Keefe, R.S., Rajji, T.K., Suzuki, T., Mamo, D.C., Pollock, B.G., Watanabe, K., Mimura, M., Uchida, H., 2013. Dopamine D2 receptor occupancy and cognition in schizophrenia: analysis of the CATIE data. Schizophr Bull 39, 564-574.

Santana, N., Bortolozzi, A., Serrats, J., Mengod, G., Artigas, F., 2004. Expression of serotonin1A and serotonin2A receptors in pyramidal and GABAergic neurons of the rat prefrontal cortex. Cereb Cortex 14, 1100-1109.

Scherfler, C., Scholz, S.W., Donnemiller, E., Decristoforo, C., Oberladstatter, M., Stefanova, N., Diederen, E., Virgolini, I., Poewe, W., Wenning, G.K., 2005. Evaluation of [123I]IBZM pinhole SPECT for the detection of striatal dopamine D2 receptor availability in rats. Neuroimage 24, 822-831.

Schmid, C.L., Streicher, J.M., Meltzer, H.Y., Bohn, L.M., 2014. Clozapine Acts as an Agonist at Serotonin 2A Receptors to Counter MK-801-Induced Behaviors through a βArrestin2-Independent Activation of Akt. Neuropsychopharmacology 39, 1902-1913.

Sehlin, D., Fang, X.T., Cato, L., Antoni, G., Lannfelt, L., Syvanen, S., 2016. Antibody-based PET imaging of amyloid beta in mouse models of Alzheimer's disease. Nat Commun 7, 10759.

Selvaraj, S., Arnone, D., Cappai, A., Howes, O., 2014. Alterations in the serotonin system in schizophrenia: a systematic review and meta-analysis of postmortem and molecular imaging studies. Neurosci Biobehav Rev 45, 233-245.

Shin, S., Kim, S., Seo, S., Lee, J.S., Howes, O.D., Kim, E., Kwon, J.S., 2018. The relationship between dopamine receptor blockade and cognitive performance in schizophrenia: a [(11)C]-raclopride PET study with aripiprazole. Transl Psychiatry 8, 87.

Shrestha, S., Hirvonen, J., Hines, C.S., Henter, I.D., Svenningsson, P., Pike, V.W., Innis, R.B., 2012. Serotonin-1A receptors in major depression quantified using PET: Controversies, confounds, and recommendations. Neuroimage 59, 3243-3251.

Silvestri, S., Seeman, M.V., Negrete, J.C., Houle, S., Shammi, C.M., Remington, G.J., Kapur, S., Zipursky, R.B., Wilson, A.A., Christensen, B.K., Seeman, P., 2000. Increased dopamine D2 receptor binding after long-term treatment with antipsychotics in humans: a clinical PET study. Psychopharmacology (Berl) 152, 174-180.

Skene, N.G., Bryois, J., Bakken, T.E., Breen, G., Crowley, J.J., Gaspar, H.A., Giusti-Rodriguez, P., Hodge, R.D., Miller, J.A., Munoz-Manchado, A.B., O'Donovan, M.C., Owen, M.J., Pardinas, A.F., Ryge, J., Walters, J.T.R., Linnarsson, S., Lein, E.S., Major Depressive Disorder Working Group of the Psychiatric Genomics, C., Sullivan, P.F., Hjerling-Leffler, J., 2018. Genetic identification of brain cell types underlying schizophrenia. Nat Genet 50, 825-833.

Skinbjerg, M., Seneca, N., Liow, J.S., Hong, J., Weinshenker, D., Pike, V.W., Halldin, C., Sibley, D.R., Innis, R.B., 2010. Dopamine beta-hydroxylase-deficient mice have normal densities of D(2) dopamine receptors in the high-affinity state based on in vivo PET imaging and in vitro radioligand binding. Synapse 64, 699-703.

Slifstein, M., Laruelle, M., 2001. Models and methods for derivation of in vivo neuroreceptor parameters with PET and SPECT reversible radiotracers. Nucl Med Biol 28, 595-608.

Slifstein, M., Parsey, R.V., Laruelle, M., 2000. Derivation of [(11)C]WAY-100635 binding parameters with reference tissue models: effect of violations of model assumptions. Nucl Med Biol 27, 487-492.

Slifstein, M., van de Giessen, E., Van Snellenberg, J., Thompson, J.L., Narendran, R., Gil, R., Hackett, E., Girgis, R., Ojeil, N., Moore, H., D'Souza, D., Malison, R.T., Huang, Y., Lim, K., Nabulsi, N., Carson, R.E., Lieberman, J.A., Abi-Dargham, A., 2015. Deficits in prefrontal cortical and extrastriatal dopamine release in schizophrenia: a positron emission tomographic functional magnetic resonance imaging study. JAMA Psychiatry 72, 316-324.

Steen, N.E., Aas, M., Simonsen, C., Dieset, I., Tesli, M., Nerhus, M., Gardsjord, E., Mørch, R., Agartz, I., Melle, I., Ueland, T., Spigset, O., Andreassen, O.A., 2016. Serum levels of second generation antipsychotics are associated with cognitive function in psychotic disorders. The World Journal of Biological Psychiatry, 1-33.

Steward, L.J., Kennedy, M.D., Morris, B.J., Pratt, J.A., 2004. The atypical antipsychotic drug clozapine enhances chronic PCP-induced regulation of prefrontal cortex 5-HT2A receptors. Neuropharmacology 47, 527-537.

Sun, W., Ginovart, N., Ko, F., Seeman, P., Kapur, S., 2003. In vivo evidence for dopamine-mediated internalization of D2-receptors after amphetamine: differential findings with [3H]raclopride versus [3H]spiperone. Mol Pharmacol 63, 456-462.

Swerdlow, N.R., Weber, M., Qu, Y., Light, G.A., Braff, D.L., 2008. Realistic expectations of prepulse inhibition in translational models for schizophrenia research. Psychopharmacology (Berl) 199, 331-388.

Szlachta, M., Kusmider, M., Pabian, P., Solich, J., Kolasa, M., Zurawek, D., Dziedzicka-Wasylewska, M., Faron-Gorecka, A., 2018. Repeated Clozapine Increases the Level of Serotonin 5-HT1AR Heterodimerization with 5-HT2A or Dopamine D2 Receptors in the Mouse Cortex. Front Mol Neurosci 11, 40.

Takano, H., 2018. Cognitive Function and Monoamine Neurotransmission in Schizophrenia: Evidence From Positron Emission Tomography Studies. Front Psychiatry 9, 228.

Tarazi, F.I., Florijn, W.J., Creese, I., 1997a. Differential regulation of dopamine receptors after chronic typical and atypical antipsychotic drug treatment. Neuroscience 78, 985-996.

Tarazi, F.I., Yeghiayan, S.K., Baldessarini, R.J., Kula, N.S., Neumeyer, J.L., 1997b. Long-term effects of S(+)N-n-propylnorapomorphine compared with typical and atypical antipsychotics: differential increases of cerebrocortical D2-like and striatolimbic D4-like dopamine receptors. Neuropsychopharmacology 17, 186-196.

Tarazi, F.I., Zhang, K., Baldessarini, R.J., 2002. Long-term effects of olanzapine, risperidone, and quetiapine on serotonin 1A, 2A and 2C receptors in rat forebrain regions. Psychopharmacology (Berl) 161, 263-270.

Tomasi, D., Wang, G.J., Volkow, N.D., 2016. Association between striatal dopamine D2/D3 receptors and brain activation during visual attention: effects of sleep deprivation. Transl Psychiatry 6, e828.

Tsartsalis, S., Dumas, N., Tournier, B.B., Pham, T., Moulin-Sallanon, M., Gregoire, M.C., Charnay, Y., Millet, P., 2015. SPECT imaging of glioma with radioiodinated CLINDE: evidence from a mouse GL26 glioma model. EJNMMI Res 5, 9.

Tsartsalis, S., Moulin-Sallanon, M., Dumas, N., Tournier, B.B., Ghezzi, C., Charnay, Y., Ginovart, N., Millet, P., 2014. Quantification of GABAA receptors in the rat brain with [(123)I]Iomazenil SPECT from factor analysis-denoised images. Nucl Med Biol 41, 186-195.

Tsartsalis, S., Tournier, B.B., Aoun, K., Habiby, S., Pandolfo, D., Dimiziani, A., Ginovart, N., Millet, P., 2017. A single-scan protocol for absolute D2/3 receptor quantification with [123I]IBZM SPECT. Neuroimage 147, 461-472.

Tsartsalis, S., Tournier, B.B., Graf, C.E., Ginovart, N., Ibanez, V., Millet, P., 2018. Dynamic image denoising for voxel-wise quantification with Statistical Parametric Mapping in molecular neuroimaging. PLoS One 13, e0203589.

Tsartsalis, S., Tournier, B.B., Huynh-Gatz, T., Dumas, N., Ginovart, N., Moulin-Sallanon, M., Millet, P., 2016. 5-HT2A receptor SPECT imaging with [(1)(2)(3)I]R91150 under P-gp inhibition with tariquidar: More is better? Nucl Med Biol 43, 81-88.

Tuppurainen, H., Kuikka, J.T., Laakso, M.P., Viinamaki, H., Husso, M., Tiihonen, J., 2006. Midbrain dopamine D2/3 receptor binding in schizophrenia. Eur Arch Psychiatry Clin Neurosci 256, 382-387.

Tuppurainen, H., Kuikka, J.T., Viinamaki, H., Husso, M., Tiihonen, J., 2009. Dopamine D2/3 receptor binding potential and occupancy in midbrain and temporal cortex by haloperidol, olanzapine and clozapine. Psychiatry Clin Neurosci 63, 529-537.

Turrone, P., Remington, G., Kapur, S., Nobrega, J.N., 2003a. Differential effects of within-day continuous vs. transient dopamine D2 receptor occupancy in the development of vacuous chewing movements (VCMs) in rats. Neuropsychopharmacology 28, 1433-1439.

Turrone, P., Remington, G., Kapur, S., Nobrega, J.N., 2003b. The relationship between dopamine D2 receptor occupancy and the vacuous chewing movement syndrome in rats. Psychopharmacology (Berl) 165, 166-171.

Uchida, H., Takeuchi, H., Graff-Guerrero, A., Suzuki, T., Watanabe, K., Mamo, D.C., 2011. Dopamine D2 receptor occupancy and clinical effects: a systematic review and pooled analysis. J Clin

Psychopharmacol 31, 497-502.

Urs, N.M., Gee, S.M., Pack, T.F., McCorvy, J.D., Evron, T., Snyder, J.C., Yang, X., Rodriguiz, R.M., Borrelli, E., Wetsel, W.C., Jin, J., Roth, B.L., O'Donnell, P., Caron, M.G., 2016. Distinct cortical and striatal actions of a beta-arrestin-biased dopamine D2 receptor ligand reveal unique antipsychotic-like properties. Proc Natl Acad Sci U S A 113, E8178-E8186.

Vaessen, T., Hernaus, D., Myin-Germeys, I., van Amelsvoort, T., 2015. The dopaminergic response to acute stress in health and psychopathology: A systematic review. Neurosci Biobehav Rev 56, 241-251.

Vanover, K., Glass, S., Kozauer, S., Saillard, J., Sanchez, J., Weingart, M., Mates, S., Satlin, A., Davis, R., 2019. 30 Lumateperone (ITI-007) for the Treatment of Schizophrenia: Overview of Placebo-Controlled Clinical Trials and an Open-label Safety Switching Study. CNS Spectr 24, 190-191.

Varela, F.A., Der-Ghazarian, T., Lee, R.J., Charntikov, S., Crawford, C.A., McDougall, S.A., 2014. Repeated aripiprazole treatment causes dopamine D2 receptor up-regulation and dopamine supersensitivity in young rats. J Psychopharmacol 28, 376-386.

Varela, M.J., Lage, S., Caruncho, H.J., Cadavid, M.I., Loza, M.I., Brea, J., 2015. Reelin influences the expression and function of dopamine D2 and serotonin 5-HT2A receptors: a comparative study. Neuroscience 290, 165-174.

Varrone, A., Fujita, M., Verhoeff, N.P., Zoghbi, S.S., Baldwin, R.M., Rajeevan, N., Charney, D.S., Seibyl, J.P., Innis, R.B., 2000. Test-retest reproducibility of extrastriatal dopamine D2 receptor imaging with [123I]epidepride SPECT in humans. J Nucl Med 41, 1343-1351.

Varty, G.B., Bakshi, V.P., Geyer, M.A., 1999. M100907, a serotonin 5-HT2A receptor antagonist and putative antipsychotic, blocks dizocilpine-induced prepulse inhibition deficits in Sprague-Dawley and Wistar rats. Neuropsychopharmacology 20, 311-321.

Varty, G.B., Higgins, G.A., 1995. Examination of drug-induced and isolation-induced disruptions of prepulse inhibition as models to screen antipsychotic drugs. Psychopharmacology (Berl) 122, 15-26.

Vazquez-Borsetti, P., Cortes, R., Artigas, F., 2008. Pyramidal Neurons in Rat Prefrontal Cortex Projecting to Ventral Tegmental Area and Dorsal Raphe Nucleus Express 5-HT2A Receptors. Cerebral Cortex 19, 1678-1686.

Verhoeff, N.P., Bobeldijk, M., Feenstra, M.G., Boer, G.J., Maas, M.A., Erdtsieck-Ernste, E., de Bruin, K., van Royen, E.A., 1991. In vitro and in vivo D2-dopamine receptor binding with [123I]S(-) iodobenzamide ([123I]IBZM) in rat and human brain. Int J Rad Appl Instrum B 18, 837-846.

Vivash, L., Gregoire, M.C., Bouilleret, V., Berard, A., Wimberley, C., Binns, D., Roselt, P., Katsifis, A., Myers, D.E., Hicks, R.J., O'Brien, T.J., Dedeurwaerdere, S., 2014. In vivo measurement of hippocampal GABAA/cBZR density with [18F]-flumazenil PET for the study of disease progression in an animal model of temporal lobe epilepsy. PLoS One 9, e86722.

Volkow, N.D., Fowler, J.S., Wang, G.J., Baler, R., Telang, F., 2009a. Imaging dopamine's role in drug abuse and addiction. Neuropharmacology 56 Suppl 1, 3-8.

Volkow, N.D., Fowler, J.S., Wang, G.J., Swanson, J.M., Telang, F., 2007. Dopamine in drug abuse and addiction: results of imaging studies and treatment implications. Arch Neurol 64, 1575-1579.

Volkow, N.D., Tomasi, D., Wang, G.J., Telang, F., Fowler, J.S., Wang, R.L., Logan, J., Wong, C., Jayne, M., Swanson, J.M., 2009b. Hyperstimulation of striatal D2 receptors with sleep deprivation:

Implications for cognitive impairment. Neuroimage 45, 1232-1240.

Volkow, N.D., Wang, G.J., Telang, F., Fowler, J.S., Logan, J., Wong, C., Ma, J., Pradhan, K., Tomasi, D., Thanos, P.K., Ferre, S., Jayne, M., 2008. Sleep deprivation decreases binding of [11C]raclopride to dopamine D2/D3 receptors in the human brain. J Neurosci 28, 8454-8461.

Wadenberg, M.G., Browning, J.L., Young, K.A., Hicks, P.B., 2001a. Antagonism at 5-HT(2A) receptors potentiates the effect of haloperidol in a conditioned avoidance response task in rats. Pharmacol Biochem Behav 68, 363-370.

Wadenberg, M.G., Sills, T.L., Fletcher, P.J., Kapur, S., 2000. Antipsychoticlike effects of amoxapine, without catalepsy, using the prepulse inhibition of the acoustic startle reflex test in rats. Biol Psychiatry 47, 670-676.

Wadenberg, M.L., 2010. Conditioned avoidance response in the development of new antipsychotics. Curr Pharm Des 16, 358-370.

Wadenberg, M.L., Ahlenius, S., 1995. Antagonism by the 5-HT2A/C receptor agonist DOI of raclopride-induced catalepsy in the rat. Eur J Pharmacol 294, 247-251.

Wadenberg, M.L., Hicks, P.B., Richter, J.T., Young, K.A., 1998. Enhancement of antipsychoticlike properties of raclopride in rats using the selective serotonin2A receptor antagonist MDL 100,907. Biol Psychiatry 44, 508-515.

Wadenberg, M.L., Soliman, A., VanderSpek, S.C., Kapur, S., 2001b. Dopamine D(2) receptor occupancy is a common mechanism underlying animal models of antipsychotics and their clinical effects. Neuropsychopharmacology 25, 633-641.

Wagner, C.C., Bauer, M., Karch, R., Feurstein, T., Kopp, S., Chiba, P., Kletter, K., Loscher, W., Muller, M., Zeitlinger, M., Langer, O., 2009. A pilot study to assess the efficacy of tariquidar to inhibit P-glycoprotein at the human blood-brain barrier with (R)-11C-verapamil and PET. J Nucl Med 50, 1954-1961.

Wang, G.J., Volkow, N.D., Fowler, J.S., Logan, J., Abumrad, N.N., Hitzemann, R.J., Pappas, N.S., Pascani, K., 1997. Dopamine D2 receptor availability in opiate-dependent subjects before and after naloxone-precipitated withdrawal. Neuropsychopharmacology 16, 174-182.

Wesolowska, A., Partyka, A., Jastrzebska-Wiesek, M., Kolaczkowski, M., 2018. The preclinical discovery and development of cariprazine for the treatment of schizophrenia. Expert Opin Drug Discov 13, 779-790.

Wiers, C.E., Shumay, E., Cabrera, E., Shokri-Kojori, E., Gladwin, T.E., Skarda, E., Cunningham, S.I., Kim, S.W., Wong, T.C., Tomasi, D., Wang, G.J., Volkow, N.D., 2016. Reduced sleep duration mediates decreases in striatal D2/D3 receptor availability in cocaine abusers. Transl Psychiatry 6, e752.

Williams, G.V., Rao, S.G., Goldman-Rakic, P.S., 2002. The physiological role of 5-HT2A receptors in working memory. J Neurosci 22, 2843-2854.

Wimberley, C., Angelis, G., Boisson, F., Callaghan, P., Fischer, K., Pichler, B.J., Meikle, S.R., Gregoire, M.C., Reilhac, A., 2014a. Simulation-based optimisation of the PET data processing for Partial Saturation Approach protocols. Neuroimage 97c, 29-40.

Wimberley, C.J., Fischer, K., Reilhac, A., Pichler, B.J., Gregoire, M.C., 2014b. A data driven method for estimation of B and appK using a single injection protocol with [C]raclopride in the mouse. Neuroimage.

Winterdahl, M., Audrain, H., Landau, A.M., Smith, D.F., Bonaventure, P., Shoblock, J.R., Carruthers, N., Swanson, D., Bender, D., 2014. PET brain imaging of neuropeptide Y2 receptors using N-11C-methyl-JNJ-31020028 in pigs. J Nucl Med 55, 635-639.

Wooten, D.W., Hillmer, A.T., Moirano, J.M., Ahlers, E.O., Slesarev, M., Barnhart, T.E., Mukherjee, J., Schneider, M.L., Christian, B.T., 2012. Measurement of 5-HT(1A) receptor density and in-vivo binding parameters of [(18)F]mefway in the nonhuman primate. J Cereb Blood Flow Metab 32, 1546-1558.

Wooten, D.W., Hillmer, A.T., Moirano, J.M., Tudorascu, D.L., Ahlers, E.O., Slesarev, M.S., Barnhart, T.E., Mukherjee, J., Schneider, M.L., Christian, B.T., 2013. 5-HT1A sex based differences in Bmax, in vivo KD, and BPND in the nonhuman primate. Neuroimage 77, 125-132.

Wu, H.M., Hoh, C.K., Choi, Y., Schelbert, H.R., Hawkins, R.A., Phelps, M.E., Huang, S.C., 1995. Factor analysis for extraction of blood time-activity curves in dynamic FDG-PET studies. J Nucl Med 36, 1714-1722.

Xu, H., Yang, H.-J., Rose, G.M., 2012. Chronic haloperidol-induced spatial memory deficits accompany the upregulation of D1 and D2 receptors in the caudate putamen of C57BL/6 mouse. Life Sci 91, 322-328.

Yadav, P.N., Kroeze, W.K., Farrell, M.S., Roth, B.L., 2011. Antagonist functional selectivity: 5-HT2A serotonin receptor antagonists differentially regulate 5-HT2A receptor protein level in vivo. J Pharmacol Exp Ther 339, 99-105.

Zangrando, J., Carvalheira, R., Labbate, G., Medeiros, P., Longo, B.M., Melo-Thomas, L., Silva, R.C., 2013. Atypical antipsychotic olanzapine reversed deficit on prepulse inhibition of the acoustic startle reflex produced by microinjection of dizocilpine (MK-801) into the inferior colliculus in rats. Behav Brain Res 257, 77-82.

Zhang, G., Stackman, R.W., 2015. The role of serotonin 5-HT2A receptors in memory and cognition. Front Pharmacol 6.

Zhou, Y., Li, G., Li, D., Cui, H., Ning, Y., 2018. Dose reduction of risperidone and olanzapine can improve cognitive function and negative symptoms in stable schizophrenic patients: A single-blinded, 52-week, randomized controlled study. J Psychopharmacol 32, 524-532.

Zhuo, C., Hou, W., Li, G., Mao, F., Li, S., Lin, X., Jiang, D., Xu, Y., Tian, H., Wang, W., Cheng, L., 2019. The genomics of schizophrenia: Shortcomings and solutions. Prog Neuropsychopharmacol Biol Psychiatry 93, 71-76.

Zoghbi, S.S., Liow, J.S., Yasuno, F., Hong, J., Tuan, E., Lazarova, N., Gladding, R.L., Pike, V.W., Innis, R.B., 2008. 11C-loperamide and its N-desmethyl radiometabolite are avid substrates for brain permeability-glycoprotein efflux. J Nucl Med 49, 649-656.

5. Articles

Article 1

A single-scan protocol for absolute $D_{2/3}$ quantification with [^{123}I]IBZM SPECT.

Tsartsalis S., Tournier B.B., Aoun K., Habiby S., Pandolfo D., Dimiziani A., Ginovart N., Millet P. **Neuroimage**, 2017, 147:461-72

Article 2

A simple protocol for striatal and extra-striatal $D_{2/3}$ receptor quantification using [^{123}I]Epidepride.

Tsartsalis S., Tournier B.B., Millet P. In preparation

Article 3

5-HT_{2A} receptor SPECT imaging with [^{123}I]R91150 under P-gp inhibition with tariquidar: more is better?

Tsartsalis S., Tournier B.B., Huynh-Gatz T., Dumas N., Ginovart N., Moulin-Sallanon M., Millet P**. Nucl Med Biol**, 2016, 43(1);81-8

Article 4

Dual-radiotracer translational SPECT neuroimaging. comparison of three methods for the simultaneous brain imaging of $D_{2/3}$ and 5-HT_{2A} receptors.

Tsartsalis S., Tournier B.B., Habiby S., Barca C., Dimiziani A., Pandolfo D., Ginovart N., Millet P. **Neuroimage,** 2018, 176:528-540

Article 5

Effect of 5-ht_{2A} receptor antagonism on levels of $D_{2/3}$ receptor occupancy and adverse behavioral side-effects induced by haloperidol: a SPECT imaging study in the rat

Tsartsalis S. Tournier B.B., Gloria Y., Millet P., Ginovart N. In preparation

6. Appendix

Involvement in published studies during the present thesis work:

1. Fluorescence activated cell sorting to reveal the cell origin of radioligand binding
Tournier B.B., **Tsartsalis S.,** Ceyzeriat K., Medina Z., Fraser B., Grégoire M.C., Kovari E., Millet P.
J Cereb Blood Flow Metab, In Press

2. TSPO and amyloid deposits in sub-regions of the hippocampus in the 3xtgAD mouse model of Alzheimer's disease
Tournier B.B., **Tsartsalis S.**, Rigaud R., Cailly T., Fabis F., Pham T., Grégoire M.C., Moulin-Sallanon M., Savioz A., Millet P.
Neurobiology of Disease, 2019, 121:95-105

3. Differential involvement of D_2 and D_3 receptors during reinstatement of cocaine-seeking behavior in the Roman high- and low-avoidance rats
Dimiziani A., Bellés Añó L., **Tsartsalis S.,** Millet P., Herrmann F., Ginovart N.
Behavioral Neuroscience, 2019, 133(1):77-85

4. Early Alzheimer-type lesions in cognitively normal subjects
Tsartsalis S., Xekardaki A., Hof P.R., Kovari E., Bouras C.
Neurobiol Aging, 2018, 62:34-44

5. Dynamic image denoising for voxel-wise quantification with statistical parametric mapping in molecular neuroimaging
Tsartsalis S., Tournier B.B., Graf C., Ginovart N., Ibanez V., Millet P.
PLoS One, 2018, 5;13(9):e0203589

6. Differential effect of chronic THC on the neuroadaptive response of dopamine $D_{2/3}$ receptor-mediated signalling in roman high- and low-avoidance rats: relationship to cb1 receptor expression
Tournier B.B., Dimiziani A., **Tsartsalis S.**, Millet P., Ginovart N.
Synapse, 2018, 72(4)

7. Time-dependent effects of repeated THC treatment on $D_{2/3}$-mediated signalling in mesencephalon and striatum

Tournier B.B., **Tsartsalis S.**, Dimiziani A., Millet P., Ginovart N.

Behav Brain Res, 2016, 311;322-9

Article 1

NeuroImage 147 (2017) 461–472

Contents lists available at ScienceDirect

NeuroImage

journal homepage: www.elsevier.com/locate/neuroimage

A single-scan protocol for absolute $D_{2/3}$ receptor quantification with [^{123}I] IBZM SPECT

Stergios Tsartsalis[a,b,c], Benjamin B. Tournier[a], Karl Aoun[a], Selim Habiby[a], Diego Pandolfo[a], Andrea Dimiziani[a], Nathalie Ginovart[a,c], Philippe Millet[a,c,*]

[a] Vulnerability Biomarkers Unit, Division of Adult Psychiatry, Department of Mental Health and Psychiatry, University Hospitals of Geneva, Switzerland
[b] Division of Addictology, Department of Mental Health and Psychiatry, University Hospitals of Geneva, Switzerland
[c] Department of Psychiatry, University of Geneva, Switzerland

ARTICLE INFO

Keywords:
[^{123}I]IBZM
SPECT
$D_{2/3}$ receptor
Rat

ABSTRACT

Purpose: Molecular imaging of the $D_{2/3}$ receptor is widely used in neuropsychiatric research. Non-displaceable binding potential (BP_{ND}) is a very popular quantitative index, defined as the product of the receptor concentration (B_{avail}) and the radiotracer affinity for the receptor ($1/appK_d$). As the $appK_d$ is influenced by parameters such as the endogenous neurotransmitter dynamics, it often constitutes a confounding factor in research studies. A simplified method for absolute quantification of both these parameters would be of great interest in this context. Here, we describe the use of a partial saturation protocol that permits to produce an *in vivo* Scatchard plot and thus estimate B_{avail} and $appK_d$ separately, through a single dynamic SPECT session. To validate this approach, a multi-injection protocol is used for the full kinetic modeling of [^{123}I]IBZM using a 3-tissue compartment, 7-parameter model (3T-7k). Finally, more "classic" BP_{ND} estimation methods are also validated against the results of the 3T-7k.

Methods: Twenty-nine male rats were used. Binding parameters were estimated using the 3T-7k in a multi-injection protocol. A partial saturation protocol was applied at the region- and voxel-level and results were compared to those obtained with the 3T-7k model. The partial saturation protocol was applied after an adenovirus-mediated D_2 receptor striatal overexpression and in an amphetamine-induced dopamine release paradigm. The Simplified Reference Tissue Model (SRTM), the Logan's non-invasive graphical analysis (LNIGA) and a simple standardized uptake ratio (SUR) method were equally applied.

Results: The partial saturation experiments gave similar values as the 3T-7k both at the regional and voxel-level. After adenoviral-mediated D_2-receptor overexpression, an increase in B_{avail} by approximately 18% was observed in the striatum. After amphetamine administration, a 16.93% decrease in B_{avail} ($p < 0.05$) and a 39.12% increase ($p < 0.01$) in $appK_d$ was observed. BP_{ND} derived from SRTM, LNIGA and SUR correlated well with the B_{avail} values from the 3T-7k (r=0.84, r=0.84 and r=0.83, respectively, $p < 0.0001$ for all correlations).

Conclusion: A partial saturation protocol permits the non-invasive and time-efficient estimation of $\mathbf{B_{avail}}$ and $appK_d$ separately. Given the different biological phenomena that underlie these parameters, this method may be applied for the in-depth study of the dopaminergic system in translational molecular imaging studies. It can detect the biological variations in these parameters, dissociating the variations in receptor density (B_{avail}) from affinity ($1/appK_d$), which reflects the interactions of the receptor with its endogenous ligand.

1. Introduction

Molecular imaging of the dopaminergic system has been a particularly useful tool in the study of neurobiological mechanisms of neuropsychiatric disorders. Single photon emission tomography (SPECT) with [^{123}I]IBZM permits the *in vivo* study of striatal $D_{2/3}$ receptors in human and translational studies with a particular interest in psychosis and addiction (Abi-Dargham et al., 2009; Murnane and Howell, 2011). Molecular imaging enables a wide range of functional studies ranging from $D_{2/3}$ receptor quantification, receptor occupancy by medications to the effect of induced endogenous dopamine release across physiological and pathological conditions (Kugaya et al., 2000).

Full pharmacokinetic modeling requires a complex scanning protocol to identify the absolute neuroreceptor density, available for

* Correspondence to: Vulnerability Biomarkers Unit, Division of Adult Psychiatry, Department of Mental Health and Psychiatry, University Hospitals of Geneva, Switzerland, Chemin du Petit-Bel-Air 2, CH1225 Chêne-Bourg, Switzerland.
E-mail address: Philippe.Millet@hcuge.ch (P. Millet).

http://dx.doi.org/10.1016/j.neuroimage.2016.12.050
Received 12 September 2016; Accepted 18 December 2016
Available online 21 December 2016

binding (B_{avail}) and the kinetic constants governing the transfer of the radiotracer between the plasma- and tissue compartments as well as its interaction with the receptor. Furthermore, it is highly invasive. Regarding the radiotracer-receptor interactions, the ratio of radiotracer dissociation (k_{off}) and association constants (k_{on}) provides the equilibrium dissociation constant ($appK_d$), which equals the inverse of radiotracer affinity ($1/appK_d$) (Delforge et al., 1989, 1990). Because of technical limitations inherent to the complexity of scanning protocols and the limited parameter identifiability, pharmacokinetic models are simplified with respect to the number of compartments and parameters to be estimated: thus, B_{avail} and $appK_d$ are jointly estimated as the binding potential ($BP=B_{avail}/appK_d$), perhaps the most popular index of receptor density in *in vivo* imaging studies (Innis et al., 2007). Beyond this simplification, the use of a brain region devoid of the receptor under study as an index of non-displaceable binding abolishes the need for arterial blood sampling and estimation of the model's input function (Gunn et al., 1997; Lammertsma and Hume, 1996; Logan et al., 1996). It is important to note that these simplified approaches may introduce significant bias in biological studies if not properly validated (Shrestha et al., 2012) against the "gold-standard" quantitative neuroreceptor estimates obtained with full pharmacokinetic modeling.

The use of BP as a quantitative measure in *in vivo* molecular neuroimaging may reflect the B_{avail} of the receptor under study only if the radiotracer's affinity for the receptor (thus the $appK_d$) remains stable across subjects of a given population in physiological conditions and disease states. However, there is evidence pointing to variations in a radiotracer's affinity for its target-receptor, violating this assumption. For instance, a radiotracer and the endogenous ligand (e.g. the neurotransmitter) present a competitive binding to the receptor. Baseline neurotransmitter levels in the vicinity of the receptor as well as challenge-induced neurotransmitter changes both vary with respect to physiological parameters and pathological conditions (Kuwabara et al., 2012; Narendran and Martinez, 2008; Vaessen et al., 2015; Volkow et al., 2009a), thereby modifying $appK_d$ while changes in B_{avail} may also occur in the same contexts. Using BP over-simplifies the study of such complex phenomena. In other words, a simplified method of *in vivo* estimation of B_{avail} and $appK_d$ would be of utmost value, particularly in studies of dopamine neurochemistry.

The *in vivo* separate estimation of B_{avail} and $appK_d$ has been described by Delforge et al. (1996, 1997, 1993); Vivash et al. (2014) for the quantification of benzodiazepine receptors in the human brain using [^{11}C]flumazenil positron emission tomography (PET). In this approach, a quantity of unlabeled radiotracer compound is co-injected with the labeled radiotracer to induce a partial saturation of the receptor sites. The pharmacological properties of the radiotracer permit the equilibrium to be rapidly installed. Delforge et al. proposed the saturation of at least 50% of receptor sites in order to permit a rapid decrease in specific binding during the scan duration. Plotting the ratio of specific to non-displaceable binding against specific binding forms a Scatchard plot from which B_{avail} and $appK_d$ can be deduced. Ideally, receptor occupancy should not exceed 70% so that a relatively large number of points are aligned within the regression line. A region devoid of receptor gives an estimate of the non-displaceable binding, further simplifying the quantification.

In this study, we describe a partial saturation approach for the *in vivo* estimation of B_{avail} and $appK_d$ with [^{123}I]IBZM SPECT using a single-scan protocol in the region- and voxel-level. This method is validated against the results of full pharmacokinetic modeling with a multiple-injection protocol that provides the "gold-standard" estimates of all kinetic parameters along with B_{avail} and $appK_d$. Other simplified methods to estimate BP without input function estimation are validated against the aforementioned results.

2. Materials and methods

2.1. Animals and general SPECT scan protocol

Thirty-two male Sprague-Dawley rats (Janvier Laboratories, Le Genet-St-Isle, France), weighing between 380 and 500 g were employed in the study. Of these, three rats were employed in an *in vivo* multi-injection SPECT imaging protocol for absolute $D_{2/3}$ receptor quantification. One rat was employed in a long (180 min) single-injection SPECT scan. Four rats were employed in an arterial plasma analysis for the study of plasma kinetics of the radiotracer and the estimation of the free parent radiotracer fraction. Fourteen rats were employed in an *ex vivo* study to determine the dose-occupancy relationship of the unlabeled IBZM when co-injected with the radiolabeled compound (described in Supplementary Materials and Methods S1.2). Two rats were employed in a presaturation SPECT study (described in detail in Supplementary Materials and Methods S1.3). Seven rats were employed in a SPECT experiment with a partial $D_{2/3}$ receptor saturation design for the determination of B_{avail} and $appK_d$ parameters from an *in vivo* Scatchard plot. Two rats out of seven of the partial saturation experiment were employed in an *in vivo* study of the effect of amphetamine-induced dopamine release on the B_{avail} and $appK_d$ parameters as determined with two SPECT scans with a partial saturation design, one before and one after amphetamine administration. Finally, one rat was employed in an adenoviral-mediated D_2-receptor overexpression experiment. The repartition of rats is summarized in Table 1.

SPECT scans were performed with a U-SPECT-II camera (MiLabs, Utrecht, Netherlands). In rats that underwent SPECT scans with the multi-injection protocol, two polyethylene catheters (i.d.=0.58 mm,

Table 1
Repartition of rats into experimental groups.

Experiment	n	Methods	Model/Outcome measures
Multi-injection protocol	3	SPECT scan and arterial blood sampling	3T-7k/ $\mathbf{B_{avail}}$, $\mathbf{appK_d}$, $\mathbf{K_1}$, $\mathbf{k_{2\text{-}6}}$ SRTM, LNIGA, SUR/$\mathbf{BP_{ND}}$
Single-injection protocol	1	SPECT scan of a long duration (180 min)	SRTM, Full RTM, 2-TRM
Free parent radiotracer fraction estimation	4	Serial arterial blood sampling after radiotracer injection and TLC	Tri-exponential model of free parent radiotracer in arterial plasma
Dose- occupancy curve for unlabeled IBZM	14	*Ex-vivo* whole-tissue radioactivity measurements after administration of various doses of unlabeled IBZM along with labeled radiotracer	Receptor occupancy
Presaturation study	2	A 50-min long SPECT scan after administration of fully-saturating doses of unlabeled IBZM	Relationship between the non-displaceable binding in striatum and cerebellum (r factor)
In vivo Scatchard analysis study	5	SPECT scan after co-injection of a partially saturating dose of unlabeled compound, along with labeled one	Scatchard plot analysis/ $\mathbf{B_{avail}}$, $\mathbf{appK_d}$
	1	SPECT scan as above after AAV-mediated overexpression of D_2 receptors in unilateral striatum	
	2	Two SPECT scans as above, the second preceeded by administration of amphetamine (15 mg/kg, i.v.)	

o.d= 0.96 mm) were inserted in the left femoral vein and artery for radiotracer administration and blood sampling, respectively. SPECT scans were performed under isoflurane anesthesia (3% for induction and 1–2% for maintenance). In rats that underwent SPECT scans for the partial saturation protocol or *ex vivo* imaging, radiotracer injection was performed via a tail vein catheter. Body temperature was monitored during the scans and maintained at 37 ± 1 °C by means of a thermostatically controlled heating blanket.

SPECT image reconstruction was performed using a pixel ordered subsets expectation maximization (P-OSEM, 0.4-mm voxel size, 4 iterations, 6 subsets) algorithm using MiLabs image reconstruction software. Radioactive decay correction was performed while correction for attenuation or scatter was not. Following reconstruction, dynamic images from the partial saturation experiment were denoised with factor analysis (FA) using Pixies software (Apteryx, Issy-les-Moulineaux, France) as previously described (Tsartsalis et al., 2014). FA permits the decomposition of dynamic signal into a few elementary components, termed factors (Di Paola et al., 1982; Millet et al., 2012; Tsartsalis et al., 2014). In this study, four factors were retained and the rest of the signal was discarded as noise.

All experimental procedures were approved by the Ethical Committee on Animal Experimentation of the Canton of Geneva, Switzerland.

2.2. Radiotracer preparation

^{123}I radioiodide was purchased from Heider AG (Schöftland, Switzerland). [^{123}I]IBZM was obtained by incubation, for 15 min at 68 °C, of a mixture containing 5 µl of BZM precursor (24 nmol/µl in ethanol), 2 µl of glacial acetic acid, 1 µl of 30% H_2O_2 and 10 mCi of carrier-free ^{123}I sodium iodide in 0.05 M NaOH. Radiotracer was isolated by a linear gradient HPLC run (from 5% acetonitrile, ACN, to 95% ACN, 10 mM H_3PO_4, in 10 min).

HPLC was equipped with a reverse-phase column (Phenomenex Bonclone C18, Phenomenex, Schlieren, Switzerland) and radiotracer was eluted at a flow of 3 ml/min. Fractions containing [^{123}I]IBZM were diluted in water and loaded on a Sep-Pak cartridge (Sep-Pak C18, Waters, Switzerland). [^{123}I]IBZM was eluted with 0.5 ml of 95% ACN, 10 mM H_3PO_4 and concentrated using a rotary evaporator, and the final product was diluted in saline prior to animal administration.

2.3. SPECT single- and multi-injection imaging and quantification, arterial plasma analysis and free parent radiotracer fraction estimation

A multi-injection protocol for full kinetic modeling of [^{123}I]IBZM was employed (Millet et al., 2006; Millet et al., 2012). The scan protocol began with a first injection of the radiotracer (91.47 ± 2.91 MBq) at a high specific activity (934.04 ± 114.37 GBq/µmol), followed by a second co-injection of [^{123}I]IBZM (93.06 ± 7.11 MBq) and the unlabeled compound (6.2 nmol/kg) at 120 min and a third injection of the unlabeled compound only at 180 min (1.24 µmol/kg). The overall scan protocol included 240 1-minute frames.

During dynamic SPECT acquisitions, forty arterial blood samples (of 25 µl each) were withdrawn after each radiotracer injection at regular time intervals. Radioactivity was measured in a gamma counting system and expressed in kBq/ml after calibration. To estimate the plasma input function in *in vivo* SPECT experiments, only whole-blood radioactivity was measured individually.

Metabolite correction and plasma protein binding analysis for the estimation of radiotracer plasma input function was performed in an independent group of four rats, as previously described (Gandelman et al., 1994; Millet et al., 2008, 2012; Mintun et al., 1984; Tsartsalis et al., 2014, 2015). A detailed description can be found in Supplementary Materials and Methods paragraph S1.1.

To evaluate the pharmacokinetic behavior of [^{123}I]IBZM in scans with a longer duration, a 180-min scan was performed using one rat. The scan protocol began with an injection of the radiotracer (66.6 MBq) at a high specific activity (> 900 GBq/µmol). The overall scan protocol included 80 2-minute frames.

2.4. In vivo Scatchard plot study

A partial saturation imaging experiment was designed to estimate B_{avail} and $appK_d$ as proposed by Delforge et al. (1996, 1997) and optimized by Wimberley et al. (2014a, b). In theory, the original Scatchard plot can be approached with an *in vivo* imaging experiment by plotting the specifically bound fraction of radiotracer activity in a given region (C_S) versus the ratio of specific-to-non-displaceable binding in the same region (C_S/C_{ND}) during the time course of a single imaging experiment. When a dose of unlabeled compound is co-administered with the radiotracer at a concentration to occupy 50–70% of the receptor binding sites, the natural decrease of radiotracer binding over time permits to the different points of the plot to form a straight line when equilibrium has been reached. B_{avail} and $appK_d$ may be estimated from the intercept to the C_s axis and the inverse of the line slope, respectively.

SPECT scans and image reconstruction were performed in the same conditions as in experiment 2.3. A single radiotracer injection (50.8 ± 6.3 MBq) (containing a dose of unlabeled IBZM determined in the *ex vivo* occupancy study, described in supplementary Materials and Methods section S1.2 and leading to specific activities of 8.94 ± 0.33 GBq/µmol) was followed by a scan composed of 90 frames of 1-min. No arterial blood sampling took place and cerebellum was employed as the reference region.

2.5. Simulation study, adenovirus-mediated D_2 receptor overexpression and amphetamine-induced dopamine release experiment

A simulation study was also performed to verify the validity of the Scatchard equilibrium conditions across different B_{avail} and $appK_d$ parameters values: using the results of one multi-injection experiment, we simulated striatal specific- and free-binding TACs corresponding to a 30% higher and lower B_{avail} and $appK_d$ using a partially saturating dose of unlabeled IBZM compound (see results section).

One animal was employed in the D_2-receptor overexpression experiment by a stereotactic viral injection. The D_2R adenovirus was generated using the pENTR directional TOPO cloning kit (Invitrogen) and the pAD/CMV/V5-DEST gateway vectors kit (Invitrogen). Briefly, the full-length cDNA corresponding to the sequence of rattus D_2R was inserted into the pENTR vector. After plasmid purification from transformed Top10 competent cells, the cDNA was transferred into the pAd/CMV/V5-DEST vector by means of the Gateway system using LR Clonase. Following propagation of plasmids in Top10 competent cells, the recombinant adenoviral DNA was digested with PacI (New England Biolabs) and purified (QIAquick nucleotide removal kit, Qiagen). Linear D_2R adenovirus was transfected into subconfluent 293 A cells according to the manufacturer's instructions (ViraPower Adenovirus Expression System, Invitrogen). The 293 A cells were cultured until regions of cytopathic effect are clearly observed (1–2 weeks). Cells and culture medium were centrifuge and freeze-thawed twice (−80 °C overnight; +25 °C, 15 min) to obtain the adenovirus-enriched supernatants. Aliquots of the crude viral stock were used to amplify D_2R adenovirus using fresh 293 A cell cultures. After amplification, D_2R adenovirus were purified using the Vivapure AdenoPack 500 kit (Sartorius) and titered using the QuickTiter Adenovirus Titer Immunoassay Kit (Cell Biolabs). The D_2R adenovirus titer was of 2×10^{10} infectious units per ml (Ifu/ml).

The animal was anesthetized with 2.5% isoflurane in O_2 and preventively treated against postoperative pain with buprenorphine (0.05 mg/kg, s.c.). Gel moisturizer (Lacryvisc) was applied on both eyes

and a 2 mm diameter hole was carefully drilled through the skull at the injection site. Two microliters of the D_2R adenovirus were injected in the left striatum (coordinates from bregma: anteroposterior = −0.5 mm; lateral = +3.0 mm; dorsoventral = −5.0 mm).

In two out of six rats of the partial saturation experiment of paragraph 2.5, a second partial saturation experiment (under the exact same conditions) took place two days after the first SPECT scan, preceded by an amphetamine injection (1.5 mg/kg i.v.) at 30 min before the radiotracer injection. This preliminary study aimed to evaluate the efficacy of this partial saturation paradigm to detect changes on the B_{avail} and $appK_d$ parameters owed to the amphetamine-induced dopamine release in the striatum.

2.6. Data analysis

SPECT images were processed with PMOD software v3.7 (PMOD Technologies Ltd, Zurich, Switzerland). Averaged images corresponding to the first ten frames of acquisition were co-registered to an MRI template integrated in PMOD (Schiffer et al., 2006). Transformation matrices were then applied to dynamic images. Tissue-activity curves (TACs) from the striatum as a whole, from the striatal sub-regions (Caudate-Putamen, CP, and Nucleus Accumbens, NAcc, bilaterally), and cerebellum were extracted from dynamic images using the predefined VOI template integrated in PMOD.

Several model configurations were employed for quantitative analysis of radiotracer kinetics in the multi-injection experiments. The whole multi-injection study TAC data was fitted with a two-tissue compartment five-parameter model (2T-5k), to estimate K_1, k_2, k_{on}, k_{off} and B_{avail} and a three-tissue compartment seven-parameter model (3T-7k) in order to obtain K_1, k_2, k_{on}, k_{off}, k_5, k_6 and B_{avail} and the binding potential ($BP=B_{avail}/appK_d$). Given the number of parameters to estimate with the 3T-7k model and the subsequent low identifiability of model parameters, k_{off} was fixed at a pre-determined value after a preliminary fit of the model on whole-striatum TACs from the three rats, as previously described (Ginovart et al., 2001; Millet et al., 1995, 2006, 2000b). Average k_{off} value was fixed for further application of 3T-7k. The free, non-metabolized radiotracer fraction in the plasma was used as the input function (Delforge et al., 1999). Analysis was performed in Matlab software R2015b (Mathworks, USA). All other models were applied using PMOD software. TAC data corresponding to the first (high specific activity) injection of the multi-injection experiments were fitted with the 1) Simplified reference tissue model (SRTM) and the 2) Logan non-invasive graphical analysis (hereon, LNIGA), using a pre-defined k_2' value estimated with the SRTM, to obtain BP_{ND} images (Innis et al., 2007). Cerebellum was used as the reference region, given that no [^{123}I]IBZM specific binding is observed. Finally, the standardized uptake ratio (SUR) was obtained by normalizing delayed activity images to the activity in the reference region. For all methods of quantification, analysis was performed on TACs from the whole-striatum VOI as well as from the four sub-regions.

For SRTM and LNIGA, we evaluated the minimum duration of scan required to obtain stable binding parameters. BP_{ND} was estimated in whole-striatum TACs of diminishing duration (by 10-min decrements). The mean deviation of the BP_{ND} value, across the three rats, for a given scan duration from the value corresponding to the maximal duration was used as the evaluation criterion. A mean estimation within 5% of the parameter value at maximum duration with a coefficient of variation (CV) $<10\%$ was considered a stable estimate. For SUR, BP_{ND} values were estimated over different fragments of data with a fixed-duration (10 min).

TACs from the long-duration single-injection study were first fitted with SRTM. To explain a misfit in the last time-points (see Results section), the full reference tissue model (Full-RTM) (Lammertsma et al., 1996) and the 2-tissue reference model (2-TRM) (Millet et al., 2002; Watabe et al., 2000) were also employed in PKIN. 2-TRM considers a second compartment in the reference region, corresponding either to specific or non-specific binding. Kinetic constants corresponding to this compartment were fixed with average values extracted from the multi-injection study.

TACs from the partial saturation experiments (whole- and sub-regional striatal VOIs) were processed in a Matlab R2015b code. Data corresponding to the linear part of the Scatchard plot were used for the estimation of B_{avail} and $appK_d$ as previously described (Delforge et al., 1996). Cerebellum TAC was employed as an index of the non-displaceable binding in striatum. As described in Supplementary Materials and Methods section S1.3, the ratio (r) of striatal-to-cerebellar non-displaceable binding was used to correct the cerebellar TAC (C_{cer}) before it was used in the Scatchard plot analysis, so $C_{ND}=r\times C_{cer}$ (Wimberley et al., 2014b). In addition, the Matlab R2015b code was employed to estimate B_{avail} and $appK_d$ at the voxel level in the striatum, after masking the extrastriatal voxels, using the TAC from the cerebellum as the non-displaceable binding index as in the VOI-level estimation. To evaluate the validity of voxel-wise application of the *in vivo* Scatchard analysis, we averaged the B_{avail} and $appK_d$ values in the striatum of each rat and compared it to the VOI-wise estimated value.

2.7. Statistical analysis

B_{avail}, $appK_d$ and BP_{ND} values resulting from fitting the data of the whole duration of the multi-injection protocol were used as the "gold standard" for comparison of estimations with the non-invasive quantification approaches by means of regression analysis. Comparisons of average B_{avail} and $appK_d$ values from the multi-injection study and the partial saturation experiments were performed by means of a two-samples t-test.

3. Results

3.1. Arterial plasma input function estimation

The mean percentage of non-metabolized radiotracer in the plasma was fitted with a triexponential function resulting in the following values: $A_1=0.035$, $B_1=0.0064$, $A_2=0.1097$, $B_2=0.3597$, $A_3=0.8546$, $B_3=42$. Average percentage of radiotracer bound to plasma proteins was 87.3%.

3.2. Full kinetic modeling of [^{123}I]IBZM with the multi-injection approach

Fit of the 3T-7k models is shown in Fig. 1. 3T-7k provides excellent fits, while 2T-5k failed to fit, especially in cerebellar TACs: this is due to a non-negligible amount of non-specific binding, requiring the inclusion of the k_5 and k_6 parameters in the model that are the constants of radiotracer exchange between the free ligand and non-specific binding compartments. We thus only consider the results of 3T-7k fits for further comparisons in our study. Average B_{avail} values (in pmol/ml) were 13.41 ± 2.35 in left and 15.30 ± 1.35 in right NAcc. In the respective CP regions values were 20.28 ± 4.75 and 19.96 ± 1.87. $appK_d$ values (in pmol/ml) were 6.21 ± 0.48 in left NAcc and 5.44 ± 0.45 in right NAcc. In CP, values were 7.20 ± 2.00 and 7.63 ± 2.87, respectively.

Cerebellar TACs from the multi-injection protocol showed no radiotracer displacement with the third injection (unlabeled IBZM). The ratio of non-displaceable binding between the striatum and cerebellum was found equal to $r=1.55\pm0.08$ (Supplementary Materials and Methods S1.3 and Results S2.1). Regarding the non-specific binding, given by the ratio of k_5/k_6 kinetic constants, it took values of 0.56 ± 0.21 in the whole-striatum VOI and 1.83 ± 0.50 in the cerebellum. The respective kinetic parameter values estimates in the individual sub-regions of the striatum are presented in Table 2.

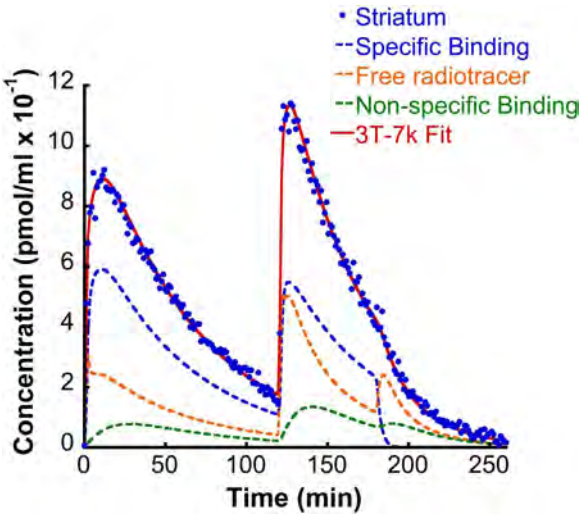

Fig. 1. TACs extracted from the striatum of one multi-injection dynamic SPECT scan, along with 3T-7k model fit and the kinetics specific, free and non-specific binding. Note the remnant striatal radioactivity at the end of the scan and after a displacement with unlabeled IBZM, explained the presence of non-specific binding.

3.3. BP_{ND} estimation using non-invasive approaches

SRTM and LNIGA, using cerebellum as reference region, provided excellent fits to data corresponding to the first injection (120 min) of the multi-injection scanning protocol. Average BP_{ND} values across the three rats are presented in Table 3. Application of both these models on TACs of diminishing duration revealed BP_{ND} values within 5% of the value at 120 min with a SD of < 10% for duration up to 70 min. Average striatal SUR values obtained from time fragments within the time window between 80 and 110 min of acquisition satisfied this stability criterion, thus, SUR values were estimated over data between the 80th and the 110th minute of acquisition for further comparisons in our study. Comparison of the quantitative estimates from all three non-invasive methods gave excellent correlations with B_{avail} values of the multi-injection protocol data (r=0.84 for SRTM, r=0.84 for LNIGA and r=0.83 for SUR, $p < 0.0001$ for all correlations) (Fig. 2).

The application of SRTM on TACs with a long duration (> 120 min) failed to provide an optimal fit (Fig. 3) as did the Full RTM. In contrast, only the 2-TRM provided an excellent fit to the whole range of data.

3.4. Partial saturation experiments

An injected dose between 12 and 24 nmol/kg occupies 50–70% of the receptors in the striatum as demonstrated in the *ex vivo* dose-occupancy study in 14 rats (see supplementary section S1.2 and supplementary Figure S1). 12 nmol/kg was the concentration of unlabeled compound that was co-injected with the radiotracer for the partial saturation scans.

Fig. 4a shows representative TACs obtained from the striatum and the cerebellum of a partial saturation experiment on one rat. The corresponding Scatchard plot is shown in Fig. 4b. The time-points that were employed for the Scatchard analysis, for all rats were found between then 10th and the 45th minute post radiotracer injection. They provided a sufficiently high number of points to be used for tracing the regression line. Average B_{avail} values (pmol/ml) were 11.99 ± 8.47 in left and 16.36 ± 7.89 in right NAcc. In the respective CP regions values were 30.44 ± 7.57 and 28.77 ± 7.49. $appK_d$ values (pmol/ml) were 8.38 ± 4.18 in left NAcc and 9.84 ± 3.16 in right NAcc. In CP, values were 10.57 ± 1.63 and 9.67 ± 1.60, respectively (Table 4). B_{avail} and $appK_d$ values from the partial saturation experiment were in accordance with the respective values from the multi-injection study ($p > 0.05$ in two-sample t test). Fig. 5 shows a parametric image of B_{avail}, as estimated at the voxel level. Averaged voxel values correlated with VOI-wise estimates in an excellent manner (r=0.96, $p < 0.0001$).

Table 3
Mean and standard deviations of binding parameter estimates obtained from 3 rats.

VOI	$BP_{ND-SRTM}$	± SD	$BP_{ND-LNIGA}$	± SD	SUR	± SD
Acb L	1.52	0.16	1.53	0.15	3.46	0.76
Acb R	1.39	0.20	1.39	0.19	3.17	0.34
CP L	2.63	0.28	2.61	0.29	6.04	0.89
CP R	2.58	0.24	2.57	0.26	5.83	0.58

Acb: nucleus accumbens, **CP**: caudate-putamen, BP_{ND} values are unitless

3.5. Simulation study and application of the partial saturation protocol in adenoviral-mediated D_2-receptor increase and amphetamine-induced dopamine release

The results of the simulation study are shown in Fig. 6a. Both a 30% increase and decrease in B_{avail} and $appK_d$ did not alter the validity of the Scatchard equilibrium conditions thereby permitting the extraction of unbiased parameter values from the Scatchard plot. The results of the partial saturation study in the rat that participated in the adenovirus-mediated D_2-receptor overexpression experiment are shown in Fig. 6b. The ipsilateral striatum has a B_{avail} of 19.56 pmol/ml versus 16.58 pmol/ml in the contralateral striatum (an increase of 18%). $appK_d$ values were 5.40 pmol/ml and 5.56 pmol/ml, respectively. Finally, a coronal section of the parametric B_{avail} image of this rat is shown in Fig. 6c. In two of the six rats that were employed in the partial saturation study, a second SPECT scan under the same conditions was performed two days after the first one. Amphetamine (0.15 mg/kg) pretreatment led to an average 16.93% decrease in B_{avail} ($p < 0.05$ in a paired t-test comparison) and a 39.12% increase in $appK_d$ ($p < 0.01$), as shown in Figs. 7a and 7b, respectively.

4. Discussion

4.1. Full quantitative modeling of [^{123}I]IBZM and validation of non-invasive approaches

The present study presents and validates a wide range of applications of molecular imaging of the $D_{2/3}$ receptor in fundamental and –potentially- clinical research. To the best of our knowledge, this is the first description of full pharmacokinetic modeling of [^{123}I]IBZM *in*

Table 2
Mean and standard deviations of binding parameter estimates Obtained from 3 rats.

VOI	B_{avail}	± SD	$appK_D$	± SD	K_1	± SD	k_2	± SD	k_{on}	± SD	k_{off}	± SD	k_5	± SD	k_6	± SD
Acb L	13.41	2.35	6.21	0.48	1.09	0.32	0.09	0.02	0.06	0.005	0.4	–	0.04	0.02	0.04	0.02
Acb R	15.30	1.35	5.44	0.45	1.00	0.31	0.10	0.03	0.07	0.01	0.4	–	0.04	0.03	0.04	0.02
CP L	20.28	4.75	7.20	2.00	1.20	0.34	0.06	0.01	0.06	0.01	0.4	–	0.013	0.01	0.07	0.04
CP R	19.96	1.87	7.63	2.87	1.21	0.35	0.06	0.02	0.06	0.02	0.4	–	0.02	0.02	0.10	0.04
Cer	–	–	–	–	1.06	0.29	0.23	0.03	0.06	0.03	0.4	–	0.02	0.01	0.01	0.00

Acb: nucleus accumbens, **CP**: caudate-putamen, **Cer:** cerebellum, B_{avail} and $appK_d$ are in pmol/ml, K_1 in mL.cm^{-3}.min^{-1}, k_2, k_3, k_{off}, k_5 and k_6 in min^{-1}

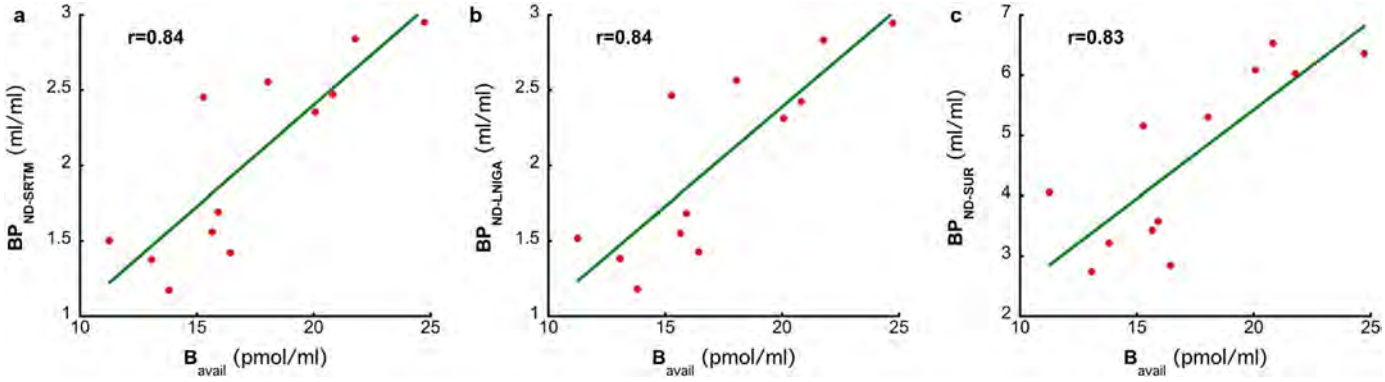

Fig. 2. Linear regression plots of comparisons between B_{avail} and BP_{ND} estimated with (a) SRTM, (b) LNIGA and (c) SUR.

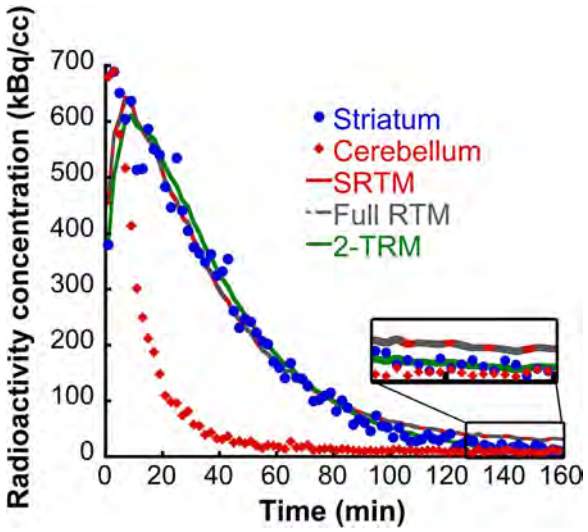

Fig. 3. TACs extracted from the striatum and cerebellum of data from the 180-min long single injection study. SRTM, Full-RTM and 2-TRM fits to the striatum. Note that SRTM and Full-RTM produce a misfit, especially during the latest time-points. 2-TRM fits well to the whole duration of data. In the magnified field, note the fits of the different models in detail.

vivo. B_{avail} values in Caudate-Putamen and Nucleus accumbens are in accordance with values previously described by our group Millet et al. (2012) and others (Mauger et al., 2005; Wimberley et al., 2014b), despite an apparent underestimation, probably due to a different delineation of VOIs in the two studies. $appK_d$ values of this size range correspond to the modest affinity of [^{123}I]IBZM and are comparable for respective estimations for [^{11}C]raclopride in small animals (Mauger et al., 2005; Wimberley et al., 2014b). As expected, no displaceable binding was observed in regions other than the striatum. The cerebellum was an exception, given that radioactivity binding in this "reference" region is used as an estimate of non-displaceable binding in striatum.

Table 4
Mean and standard deviations of B_{avail} and $appK_d$ estimates obtained from the partial saturation protocol in 7 rats.

VOI	B_{avail}	± SD	$appK_D$	± SD
Acb L	11.99	8.47	8.38	4.18
Acb R	16.37	7.89	9.85	3.17
CP L	30.44	7.57	10.58	1.64
CP R	28.77	7.49	9.67	1.61

Acb: nucleus accumbens, **CP**: caudate-putamen, B_{avail} and $appK_d$ are in pmol/ml

The mutli-injection approach can be considered a "gold-standard" in modeling radiotracer kinetics in the brain, permitting an in-depth decomposition of the radioactive signal and full quantification of kinetic parameters, to our knowledge more than any other approach. Its use to validate simpler quantitative methods is invaluable (Dumas et al., 2015; Millet et al., 2002, 2000a, 2006, 2012). However, the estimation of a high number of parameters through a very complex protocol naturally comes at a cost. Indeed, the full quantification of the kinetic parameters may sometimes be difficult and some assumptions

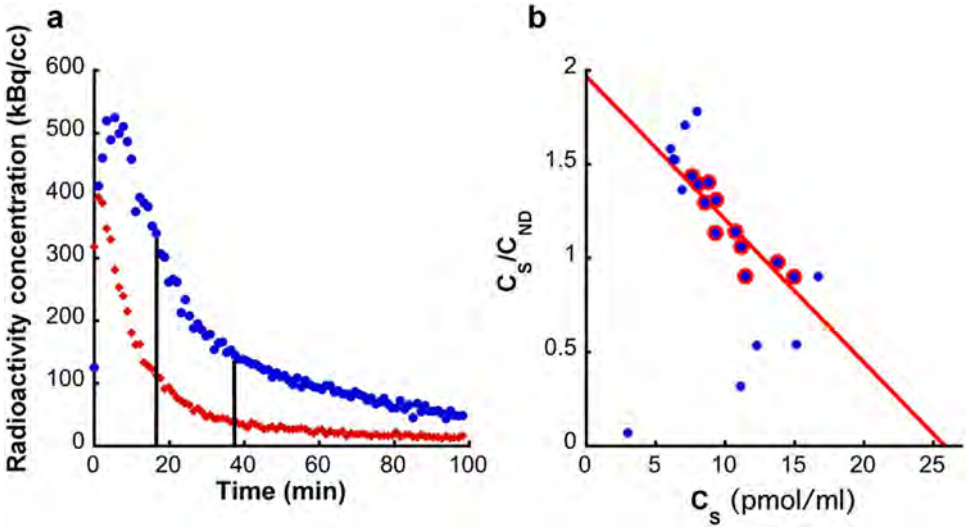

Fig. 4. (a) TACs extracted from the striatum and cerebellum of a partial saturation dynamic SPECT scan in one rat. (b) Corresponding Scatchard plots along with linear fit.

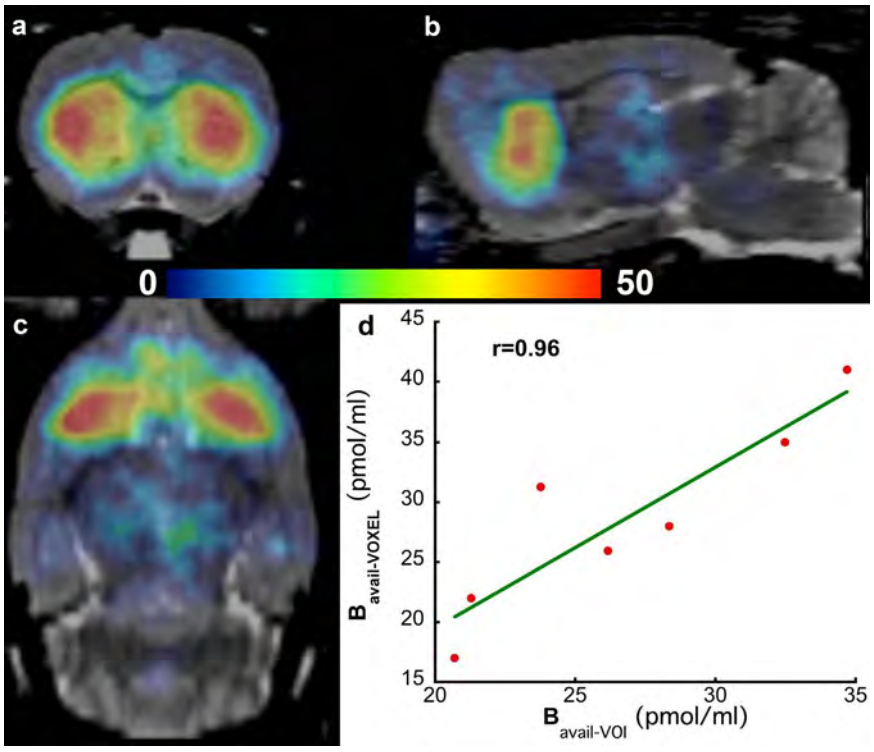

Fig. 5. (a) Coronal, (b) sagittal and (c) axial planes of a parametric B_{avail} images (the image presented here is the average image of 6 rats that underwent the partial saturation protocol and is filtered with a Gaussian kernel with a FWHM of 0.6×0.6×0.6 mm^3). (d) After extraction of the average B_{avail} values in each of the four sub-striatal VOIs, they were compared to the VOI-wise estimated B_{avail} values by means of linear regressions.

and simplifications may need to be applied: a fundamental assumption is that the kinetics of the unlabeled ligand are identical to this of the labeled one (Delforge et al., 1990). Fixing k_{off} to reduce uncertainty in parameter estimations is also necessary for this radiotracer, which, nevertheless, as described elsewhere, does not induce bias in B_{avail} or $appK_d$ estimates (Millet et al., 1995). Measuring the arterial plasma input function also is an invasive and technically difficult procedure, especially in small-animal SPECT and an overestimation of K_1 values may occur, as is the case in the present study (this does not influence B_{avail} and appKd values, as discussed elsewhere (Dumas et al., 2015)). Despite criticism, the interest of accurately estimating B_{avail} and $appK_d$ is well accepted (Morris et al., 1999). In this context, the partial saturation method is much more interesting for routine research application given its simplicity and robustness, especially for voxel-wise estimations, as discussed in Section 4.3, especially compared to the multi-injection protocol.

Using cerebellum as reference region for the estimation of BP_{ND} with all three methods (SRTM, LNIGA and SUR) gave excellent correlations with B_{avail} values estimated from full kinetic modeling, the "gold-standard" of kinetic parameters in molecular neuroimaging, thus validating the use of these non-invasive methods. Despite other studies having employed non-invasive approaches before and mainly the SUR with inconsistent time-windows (Crunelle et al., 2012; Meyer et al., 2008a, b, c; Nikolaus et al., 2011; Scherfler et al., 2005; Verhoeff et al., 1991), the present is the only one validating these results against B_{avail}. SRTM and LNIGA applied on scans as short as 70-min long and

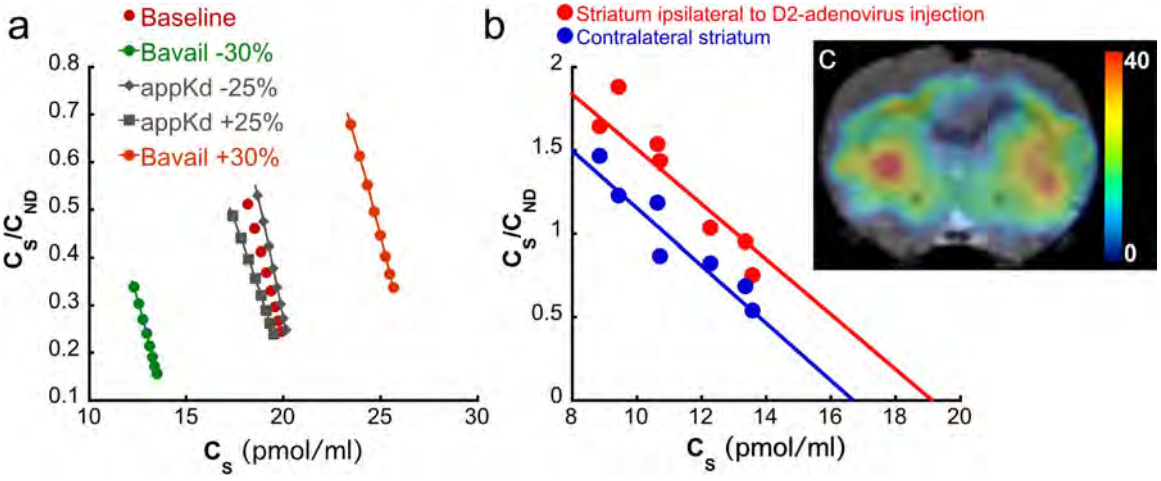

Fig. 6. (a) Scatchard plots corresponding to simulated specific and non-displaceable binding from striatum. Note that the Scatchard equilibrium condition is satisfied in all simulated variations of B_{avail} and $appK_d$, permitting accurate estimation of these parameters. (b) Scatchard plots from a partial saturation experiment in the rat that participated in the adenovirus-mediated D_2-receptor overexpression experiment. Red points correspond to the left striatum, ipsilateral to adenovirus injection, while the blue points correspond to the contralateral striatum. Note the augmentation of B_{avail} whilst $appK_d$ remains virtually stable. (c) Parametric image of B_{avail} (pmol/ml), the injection point is on the left side of the image.

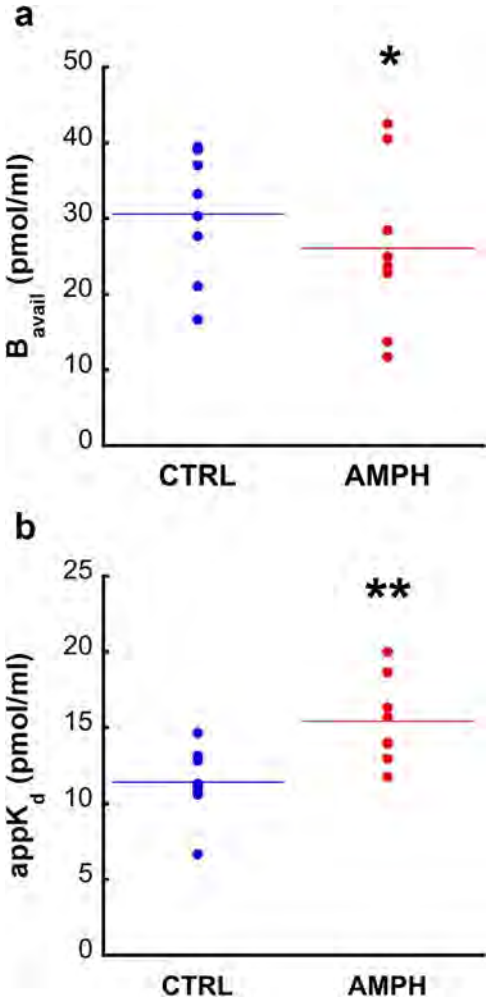

Fig. 7. (a) B_{avail} and (b) $appK_d$ of partial saturation experiments in all four sub-striatal VOIs in two rats. CTRL (in blue color) describes baseline values and AMPH (red), the corresponding values from a second partial saturation study in the same rats, two days after the first and 30 min post-amphetamine administration. Statistically significant differences in B_{avail} and $appK_d$ values after the amphetamine challenge are marked (*, $p < 0.05$ and **, $p < 0.01$).

the SUR, estimated at 80–110 min post radiotracer injection, accurately reflect B_{avail} in rat imaging.

4.2. Impact of non-specific binding on BP_{ND}

An apparent bias in the absolute values of BP_{ND}, when compared to BP values of the 3T-7k likely originates from the difference in non-displaceable binding between striatum and cerebellum. In addition, BP values obtained from the 3T-7k model are quite homogenous across the four striatal subregions, an observation that differs from BP_{ND} values. BP_{ND} values present a difference between CP and NAcc, the latter having consistently lower BP_{ND}. The kinetic pattern of non-specific binding was identified in the multi-injection data using the 3T-7k model (Fig. 1). Non-specific binding is more important in late time-points, in terms of proportion of the total tissue-radioactivity. Thus, the impact of this difference between striatum and cerebellum is only observable in late time-points. This may be clearly observed in the quality of SRTM fits in striatum as a function of the duration of SPECT acquisition: the SRTM fits are excellent and BP_{ND} values are stable when applied on data corresponding to 70–120 min of acquisition. For a scan-duration of more than 120 min, the SRTM model fails to fit the natural decrease in radioactivity in striatum (Fig. 3). To confirm that this misfit derives from the difference in non-specific binding between striatum and cerebellum, we fitted the data with reference tissue models other than the SRTM, that do not depend on the assumption that the target and reference region present a one tissue-compartment kinetics: the Full-RTM includes a two tissue-compartment model in the target region and a one tissue-compartment in the reference region. Thus, if the misfit were due to the striatal kinetics, Full-RTM would correct it, which is clearly not the case. On the other hand, the 2-TRM, which assumes a two tissue-compartment model kinetics in the reference region, perfectly fits the data for the whole duration of the scan and gives BP_{ND} values that are virtually identical to SRTM-derived values extracted from TACs shorter than 120-min long. As the presence of a specific binding in the cerebellum is excluded by the multi-injection, the second compartment in the cerebellum may conclusively be considered as non-specific binding and the misfit in striatum with SRTM on data longer that 120 min are most probably due to the non-negligible difference in non-specific binding between this region and the cerebellum.

This difference in non-displaceable binding between striatum and cerebellum and within the striatal subregions does not impede the use of these simplified methods, provided that it is stable across different subjects of a given population and independent of the experimental conditions of a biological study. Indeed, the striatal-to-cerebellar non-displaceable distribution volumes (V_{ND}) ratios (1.55 ± 0.08) present a minimal variability, thus supporting this argument for [^{123}I]IBZM. The excellent correlation of BP_{ND} values with B_{avail} further confirms that BP_{ND} values reflect the absolute receptor concentration. Simplified quantification models generally provide robust kinetic parameters with a lower variability than invasive models that use the plasma-derived input function (Lyoo et al., 2015; Tsartsalis et al., 2016b). BP_{ND} values obtained with the SRTM, LNIGA and SUR present a reasonable variability and may thus be employed as an index of $D_{2/3}$ receptor expression in preclinical biological studies.

4.3. Non-invasive estimation of B_{avail} and $appK_d$ using a partial saturation experiment

A simple method for the estimation of both parameters would be of great interest in the context of translational and clinical molecular imaging. To date, only few biological studies have considered both parameters because their separate estimation is very complicated. This is frequently cited as a limitation of imaging studies of brain physiology and pathology. For instance, regarding normal brain function, Wooten et al. (2012, 2013), after having showed a lack of correlation between B_{avail} and BP_{ND} for the 5-HT_{1A} PET radiotracer [^{18}F]mefway (Wooten et al., 2012), demonstrated that sex-based differences in BP_{ND} in rhesus monkeys, that could have otherwise been attributed to differences in 5-HT_{1A} receptor concentration (B_{avail}), were actually due to differences in $appK_d$ (Wooten et al., 2013), probably reflecting the endogenous serotonin level. Modifications both in the absolute receptor concentration and endogenous neurotransmitter levels are probably implicated in addiction (Hillmer et al., 2014; Martinez et al., 2012; Wang et al., 1997). Similarly, Vivash et al. (2014) demonstrated that both [^{18}F]flumazenil-measured $GABA_A$ receptor density and affinity are diminished in epileptic rats. In this case, a reduced $appK_d$ could be attributed, according to the authors, to differences in endogenous ligand concentration (GABA) or into a modified composition of $GABA_A$ receptor subunits. In other words, if $appK_d$ can be robustly dissociated from B_{avail}, valuable information is extracted, which is otherwise only subject to speculation when only BP is estimated. A robust $appK_d$ measurement may permit a more direct study of endogenous ligand level and the detection of more subtle variations across the spectrum of normal and pathological brain function. This is probably not the case in the way the study of endogenous neurotransmitter level is actually performed, that is by evaluating the impact of pharmacologically induced ligand release (e.g. using amphetamine in the case of dopamine) on BP_{ND}. Interestingly, a recent study associated person-

ality traits with endogenous serotonin levels as reflected on 5-HT_4 receptor BP_{ND} (da Cunha-Bang et al., 2016). In this type of studies, using the partial saturation protocol described here could potentially significantly enhance precision when simultaneously estimating serotonin levels (using $appK_d$) and B_{avail} that is clearly a confounding parameter in BP_{ND} because it may as well vary according to study conditions.

In this paper, we present and validate such a simplified method that employs a partial saturation protocol. This method has been developed by Delforge et al., for the estimation of B_{avail} and $appK_d$ of [^{11}C] flumazenil (Delforge et al., 1996, 1997) and has been employed in clinical research ever since (Bouvard et al., 2005; Freeman et al., 2015). It requires no blood sampling as it relies on cerebellar kinetics for the estimation of the non-displaceable radioactivity fraction in the striatum. Another advantage is that Scatchard equilibrium is rapidly established after injection of a partially saturating dose of unlabeled radiotracer with the radiolabeled one, thus requiring only short scans of a maximum duration of less than 60 min. A preliminary *ex vivo* study demonstrated that a dose between 12 and 24 nmol/kg of unlabeled IBZM, when injected with labeled radiotracer, occupies between 50 and 70% of striatal $D_{2/3}$ receptors. We chose to use the lowest concentration of the spectrum (i.e. 12 nmol/kg) because we considered that saturation of a higher percentage of receptors would lead to very few data-points in the Scatchard equilibrium, given that [^{123}I]IBZM has already a rapid kinetic behavior. Such a dose of unlabeled IBZM induces a rapid decrease in specific binding (Fig. 4a) for a sufficient period of time in order to trace the Scatchard plot.

The results of the partial saturation experiments are in accordance with the B_{avail} and $appK_d$ values obtained with the 3T-7k model on the multi-injection data. B_{avail} values in CP present an apparent overestimation compared to the respective values from the 3T-7k on multi-injection data. Applying the partial saturation method is based on the assumption that the free binding in the region of interest is described by the kinetics of radioactivity in the reference region after proper correction (Delforge et al., 1996; Wimberley et al., 2014b). As with all simplified methods that use the kinetics in a reference region as an input to the pharmacokinetic model (Slifstein et al., 2000), such a bias in the absolute values is acceptable, as for all other simplified methods of quantification. Regarding the estimation of the r factor that scales the TAC from the cerebellum to better represent the striatal non-displaceable binding, two approaches were employed: in the first one the r value was estimated by the ratio of the V_{ND} values between the striatum and cerebellum (in this case r=1.55), as estimated with the multi-injection approach. The ratio of V_{ND} is in fact not identical to the actual ratio of the C_{ND} in the striatum to the C_{ND} in cerebellum, which is not even perfectly stable during the scan. However, in equilibrium and even in a pseudo-equilibrium condition (that is approached by the Scatchard equilibrium during the partial saturation scan) the ratio of V_{ND} is the best approximation of the striatal-to-cerebellar C_{ND}. The second method that we employed, a presaturation study (Wimberley et al., 2014b) gave an average r value (r=1.68) very close to those estimated with the first method. As discussed by Delforge et al., the presaturation experiment may lead to biased estimates of the non-displaceable binding kinetics (Delforge et al., 1996, 1993) given the fact that the totality of specific binding sites is occupied by the unlabeled ligand, whereas in the partial saturation experiment the occupation is between 50% and 70%. In any case, the simulation study (Supplementary Figure S2) demonstrates that 1) as with all simplified "reference-tissue" methods (Salinas et al., 2015), a difference in the non-displaceable binding leads to biases in the binding parameter values (in this case mainly in B_{avail}) and 2) this bias is virtually identical for a range of simulated B_{avail} values meaning that an existing difference in B_{avail} or $appK_d$ will still be detected regardless of this bias.

To demonstrate the feasibility of performing biological studies of the dopaminergic system with [^{123}I]IBZM with this partial saturation protocol we first performed a simulation study. 30% variations in B_{avail} and $appK_d$ that are comparable, if not superior, to any biological variation expected in the context of a molecular imaging study were simulated. As the objective of the simulation study was to verify the validity of the Scatchard equilibrium condition, free ligand kinetics was directly extracted from the striatum and not from cerebellum. The results of a partial saturation experiment, considering a fixed dose of unlabeled compound (12 nmol/kg), demonstrated that virtually no bias is introduced in B_{avail} or $appK_d$. The only considerable parameter that changed in this study was the duration of the Scatchard equilibrium condition. The number of time points that form the Scatchard plot is diminished for lower B_{avail} values.

As a preliminary evaluation of the sensitivity of the partial saturation approach, we induced a unilateral overexpression of D_2 receptors in the striatum of one rat. This permitted a direct comparison of the Scatchard plots from the two regions (shown in Fig. 6b). D_2-receptor overexpression induced an increase in B_{avail} of about 18%, while $appK_d$ remained stable. This finding seems justifiable, as the overexpression of the receptor should increase its concentration. Of course, this experiment is a mere demonstration of the sensitivity of the partial saturation approach. A statistical analysis in a sufficiently large groups of rats should examine the changes in B_{avail} and $appK_d$ after adenovirus injection, to answer in two important questions: 1) whether an overexpression of the receptor actually translates into an increase in the receptor concentration in the brain (so this increase in B_{avail} found here may be confirmed) and 2) whether the increase in receptor concentration follows the cellular and sub-cellular distribution of the receptor at baseline conditions. In this case, no modification of $appK_d$ should be detected (Laruelle, 2000).

Next, we evaluated the feasibility of studying amphetamine-induced dopamine release in striatal sub-regions. This paradigm is widely employed to assess the function of presynaptic dopaminergic terminals (Ginovart, 2005; Laruelle, 2000). Dopamine is thought to act on [^{123}I] IBZM binding by direct competitive antagonistic binding to the $D_{2/3}$ receptor (thereby augmenting the $appK_d$) as well as by provoking receptors' endocytosis, thereby diminishing receptor concentration that is available for binding (Ginovart et al., 2004; Jongen et al., 2008; Skinbjerg et al., 2010; Sun et al., 2003). Given the complexity of this phenomenon and the potential biological implications, the partial saturation protocol could provide a simple method to assess the impact of the amphetamine challenge on both B_{avail} and $appK_d$. Our results demonstrate that the partial saturation study is robust enough to detect such changes even at the sub-striatal level. Moreover, they are in accordance with previously reported effects of amphetamine on [^{11}C] raclopride *in vivo* binding in cats, where a 28% decrease in B_{avail} and a 36% increase in $appK_d$ were found (Ginovart et al., 2004). The partial saturation approach permits perhaps a more efficient study of this phenomenon, especially in the light of the results of microdialysis studies that have assessed the kinetics of amphetamine-induced dopamine release (using equivalent administration schemes). Indeed, dopamine concentrations peak rapidly (> 1000-fold) after amphetamine administration and return to baseline, very rapidly at early and more slowly at late time-points (Breier et al., 1997; Butcher et al., 1988; Kuczenski and Segal, 1989; Laruelle et al., 1997; Shoblock et al., 2003; Tsukada et al., 1999). The time-window in which our experiments are performed (that is roughly at 40–75 min after amphetamine administration) falls within a period during which dopamine concentrations decrease relatively slowly and are certainly still significantly higher than baseline. Based on current literature and quantification methods, the partial saturation method seems to be one of the most appropriate for this purpose, at least in terms of simplicity and timing. Previous studies of this phenomenon that dissociated B_{avail} from $appK_d$ estimates have employed complex and long scan protocols composed of three or four scans overall (because of the need to perform scans with different specific activities) with a total duration well beyond the temporal window in which the dopamine release can be captured (Ginovart et al., 2004) while an important effect of timing of scans after

induction of dopamine release has been demonstrated (Doudet and Holden, 2003a, b; Doudet et al., 2003; Doudet et al., 2006).

The partial saturation method in [^{123}I]IBZM imaging has potential applications in clinical SPECT imaging. The arguments exposed in previous paragraphs, in favor of the separate study of B_{avail} and $appK_d$ are even more prominent in clinical imaging studies of the dopaminergic system. The complexity of the human brain may not be diminished to the study of animal models that only approach some of the aspects of brain physiology and disease while others remain totally out of reach (to cite only few of them; higher cognitive processes and pathological conditions such as perception and thought disorders). In addition, brain neurochemistry underlies a plexus of functional and pathological properties that compose the clinical picture: for instance, psychiatric pathologies are often present in several dimensions going from acute "diseases" to permanent traits of personality that potentially interact with both the quantity of a neurotransmitter receptor and the endogenous neurotransmitter concentration that may not be assessed with the BP. That said, the development of clinical molecular imaging has been a capital step towards a better understanding of how the brain functions and dysfunctions. The possibility for a more in-depth study with the partial saturation protocol, which is as technically feasible as currently employed methods to estimate BP_{ND} is highly promising to alleviate the confounding effect of $appK_d$ on B_{avail} and vice versa. To date, variations BP may not be conclusively attributed to differences in actual receptor concentration or in endogenous dopamine quantity and this confounding effect (to cite only a few relevant studies; (Egerton et al., 2009; Howes et al., 2009, 2012; Tomasi et al., 2016; Vaessen et al., 2015; Volkow et al., 2007, 2009b, 2008; Wiers et al., 2016)) is only approached theoretically. Assessing $appK_d$ may also permit the (indirect) evaluation of the level of endogenous dopamine without relying on the stimulant-induced dopamine release paradigm that not only involves the administration of the stimulant agent but also presents an important biological complexity *per se* (Laruelle, 2000). Currently employed methods to separately estimate B_{avail} and $appK_d$ are very difficult to employ in routine clinical research and are practically limited to animal and very rarely in human studies (Delforge et al., 1993; Doudet et al., 2003; Ginovart et al., 2004; Millet et al., 2000a, 2006). Regarding the feasibility of applying the partial saturation protocol in clinical [^{123}I]IBZM SPECT, it should not be problematic, in theory. Indeed, occupying 50–70% of striatal $D_{2/3}$ receptors for the application of the partial saturation approach induces little, if any, adverse effects. Indeed, this level of blockade is identical to the one induced by antipsychotic agents at therapeutic doses and it is accepted that adverse events appear when blockade is higher that 80–85% (Ginovart and Kapur, 2012). Proper validation of safety of administering partially saturating doses of unlabeled IBZM through animal and clinical studies could thus permit the application of this protocol in clinical imaging where its impact in the understanding of brain function and disease would be invaluable.

4.4. Denoising of [^{123}I]IBZM SPECT images with FA

SPECT images are particularly noised. Employing raw images for analysis was in fact particularly difficult, even when TACs extracted from the whole-striatal VOI were considered. Indeed, the variability of 3T-7k-derived parameters from the multi-injection study was high in raw images (data not shown). In the case of partial saturation scans, noise induced important deviations from linearity in Scatchard plots and a high uncertainty in estimations as linear fits were of poor quality (data not shown). We thus employed FA, as previously described (Di Paola et al., 1982; Millet et al., 2012; Tsartsalis et al., 2016a), retaining four prevalent factors that efficiently removes noise while inducing negligible bias (if any), given that is a relatively "conservative" configuration, compared to a two- (Tsartsalis et al., 2016a) or three-factor analysis applied before (Tsartsalis et al., 2014). FA notably permits to construct valid parametric images of B_{avail} using the partial saturation method, as demonstrated by the quality of parametric images and the excellent correlation of the voxel-wise estimated results with their VOI-estimated counterparts. It is important to note that FA application may also correct for the contamination of brain structures under study with radioactivity from adjacent structures due to partial volume effects (Millet et al., 2012).

5. Conclusion

In conclusion, we validate here the use of simplified methods for the estimation of either BP_{ND} or B_{avail} and $appK_d$. SRTM and LNIGA applied on 70-minute long scans and SUR applied on data corresponding to a static scan between 80 and 110 minutes after radiotracer injection may robustly provide BP_{ND} estimates that accurately reflect the B_{avail} estimation after full kinetic modeling of [^{123}I]IBZM. We also describe here a simplified and robust method for the separate estimation of B_{avail} and $appK_d$, at both the VOI- and the voxel-level for a more in-depth study of the absolute receptor quantity in striatum and the interactions between receptor and endogenous ligand. This method may thus be used for more technically demanding studies of the dopaminergic system, such as the amphetamine-induced dopamine release effect in translational and, potentially, in clinical imaging studies.

Acknowledgements

This work was supported by the Swiss National Science Foundation (grant no. 310030_156829), by the Geneva Neuroscience Center and by the Maria Zaousi Memorial Foundation (Greece) through a scholarship of the Hellenic State Scholarship Foundation (ST) and by the " Swiss Association for Alzheimer's Research " which was created in 2009 to finance Swiss fundamental and clinical research programs on Alzheimer's disease. Authors are grateful to Mrs Maria Surini-Demiri for excellent technical assistance and declare that they have no conflict of interest.

Appendix A. Supplementary material

Supplementary data associated with this article can be found in the online version at http://dx.doi.org/10.1016/j.neuroimage.2016.12.050.

References

Abi-Dargham, A., van de Giessen, E., Slifstein, M., Kegeles, L.S., Laruelle, M., 2009. Baseline and amphetamine-stimulated dopamine activity are related in drug-naive schizophrenic subjects. Biol. Psychiatry 65, 1091–1093.

Bouvard, S., Costes, N., Bonnefoi, F., Lavenne, F., Mauguiere, F., Delforge, J., Ryvlin, P., 2005. Seizure-related short-term plasticity of benzodiazepine receptors in partial epilepsy: a [11C]flumazenil-PET study. Brain 128, 1330–1343.

Breier, A., Su, T.P., Saunders, R., Carson, R.E., Kolachana, B.S., de Bartolomeis, A., Weinberger, D.R., Weisenfeld, N., Malhotra, A.K., Eckelman, W.C., Pickar, D., 1997. Schizophrenia is associated with elevated amphetamine-induced synaptic dopamine concentrations: evidence from a novel positron emission tomography method. Proc. Natl. Acad. Sci. USA 94, 2569–2574.

Butcher, S.P., Fairbrother, I.S., Kelly, J.S., Arbuthnott, G.W., 1988. Amphetamine-induced dopamine release in the rat striatum: an in vivo microdialysis study. J. Neurochem. 50, 346–355.

Crunelle, C.L., de Wit, T.C., de Bruin, K., Ramakers, R.M., van der Have, F., Beekman, F.J., van den Brink, W., Booij, J., 2012. Varenicline increases in vivo striatal dopamine D(2/3) receptor binding: an ultra-high-resolution pinhole [(123)I]IBZM SPECT study in rats. Nucl. Med. Biol..

da Cunha-Bang, S., Mc Mahon, B., MacDonald Fisher, P., Jensen, P.S., Svarer, C., Moos Knudsen, G., 2016. High trait aggression in men is associated with low 5-HT levels, as indexed by 5-HT4 receptor binding. Soc. Cogn. Affect. Neurosci. 11, 548–555.

Delforge, J., Bottlaender, M., Loc'h, C., Guenther, I., Fuseau, C., Bendriem, B., Syrota, A., Maziere, B., 1999. Quantitation of extrastriatal D2 receptors using a very high-affinity ligand (FLB 457) and the multi-injection approach. J. Cereb. Blood Flow. Metab. 19, 533–546.

Delforge, J., Spelle, L., Bendriem, B., Samson, Y., Bottlaender, M., Papageorgiou, S., Syrota, A., 1996. Quantitation of benzodiazepine receptors in human brain using the partial saturation method. J. Nucl. Med. 37, 5–11.

Delforge, J., Spelle, L., Bendriem, B., Samson, Y., Syrota, A., 1997. Parametric images of benzodiazepine receptor concentration using a partial-saturation injection. J. Cereb. Blood Flow. Metab. 17, 343–355.
Delforge, J., Syrota, A., Bottlaender, M., Varastet, M., Loc'h, C., Bendriem, B., Crouzel, C., Brouillet, E., Maziere, M., 1993. Modeling analysis of [11C]flumazenil kinetics studied by PET: application to a critical study of the equilibrium approaches. J. Cereb. Blood Flow. Metab. 13, 454–468.
Delforge, J., Syrota, A., Mazoyer, B.M., 1989. Experimental design optimisation: theory and application to estimation of receptor model parameters using dynamic positron emission tomography. Phys. Med. Biol. 34, 419–435.
Delforge, J., Syrota, A., Mazoyer, B.M., 1990. Identifiability analysis and parameter identification of an in vivo ligand-receptor model from PET data. IEEE Trans. Biomed. Eng. 37, 653–661.
Di Paola, R., Bazin, J.P., Aubry, F., Aurengo, A., Cavailloles, F., Herry, J.Y., Kahn, E., 1982. Handling of dynamic sequences in nuclear medicine. IEEE Trans. Nucl. Sci. NS29, 1310–1321.
Doudet, D.J., Holden, J.E., 2003a. Raclopride studies of dopamine release: dependence on presynaptic integrity. Biol. Psychiatry 54, 1193–1199.
Doudet, D.J., Holden, J.E., 2003b. Sequential versus nonsequential measurement of density and affinity of dopamine D2 receptors with [11C]raclopride: effect of methamphetamine. J. Cereb. Blood Flow. Metab. 23, 1489–1494.
Doudet, D.J., Jivan, S., Holden, J.E., 2003. In vivo measurement of receptor density and affinity: comparison of the routine sequential method with a nonsequential method in studies of dopamine D2 receptors with [11C]raclopride. J. Cereb. Blood Flow. Metab. 23, 280–284.
Doudet, D.J., Ruth, T.J., Holden, J.E., 2006. Sequential versus nonsequential measurement of density and affinity of dopamine D2 receptors with [11C]raclopride: 2: effects of DAT inhibitors. J. Cereb. Blood Flow. Metab. 26, 28–37.
Dumas, N., Moulin-Sallanon, M., Fender, P., Tournier, B.B., Ginovart, N., Charnay, Y., Millet, P., 2015. In Vivo Quantification of 5-HT2A Brain Receptors in Mdr1a KO Rats with 123I-R91150 Single-Photon Emission Computed Tomography. Mol. Imaging, 14.
Egerton, A., Mehta, M.A., Montgomery, A.J., Lappin, J.M., Howes, O.D., Reeves, S.J., Cunningham, V.J., Grasby, P.M., 2009. The dopaminergic basis of human behaviors: a review of molecular imaging studies. Neurosci. Biobehav. Rev. 33, 1109–1132.
Freeman, L., Garcia-Lorenzo, D., Bottin, L., Leroy, C., Louapre, C., Bodini, B., Papeix, C., Assouad, R., Granger, B., Tourbah, A., Dolle, F., Lubetzki, C., Bottlaender, M., Stankoff, B., 2015. The neuronal component of gray matter damage in multiple sclerosis: a [(11) C]flumazenil positron emission tomography study. Ann. Neurol. 78, 554–567.
Gandelman, M.S., Baldwin, R.M., Zoghbi, S.S., Zea-Ponce, Y., Innis, R.B., 1994. Evaluation of ultrafiltration for the free-fraction determination of single photon emission computed tomography (SPECT) radiotracers: beta-cit, IBF, and iomazenil. J. Pharm. Sci. 83, 1014–1019.
Ginovart, N., 2005. Imaging the dopamine system with in vivo [11C]raclopride displacement studies: understanding the true mechanism. Mol. Imaging Biol. 7, 45–52.
Ginovart, N., Kapur, S., 2012. Role of dopamine D(2) receptors for antipsychotic activity. Handb. Exp. Pharmacol., 27–52.
Ginovart, N., Wilson, A.A., Houle, S., Kapur, S., 2004. Amphetamine pretreatment induces a change in both D2-Receptor density and apparent affinity: a [11C] raclopride positron emission tomography study in cats. Biol. Psychiatry 55, 1188–1194.
Ginovart, N., Wilson, A.A., Meyer, J.H., Hussey, D., Houle, S., 2001. Positron emission tomography quantification of [(11)C]-DASB binding to the human serotonin transporter: modeling strategies. J. Cereb. Blood Flow. Metab. 21, 1342–1353.
Gunn, R.N., Lammertsma, A.A., Hume, S.P., Cunningham, V.J., 1997. Parametric imaging of ligand-receptor binding in PET using a simplified reference region model. Neuroimage 6, 279–287.
Hillmer, A.T., Wooten, D.W., Tudorascu, D.L., Barnhart, T.E., Ahlers, E.O., Resch, L.M., Larson, J.A., Converse, A.K., Moore, C.F., Schneider, M.L., Christian, B.T., 2014. The effects of chronic alcohol self-administration on serotonin-1A receptor binding in nonhuman primates. Drug Alcohol Depend. 144, 119–126.
Howes, O.D., Egerton, A., Allan, V., McGuire, P., Stokes, P., Kapur, S., 2009. Mechanisms underlying psychosis and antipsychotic treatment response in schizophrenia: insights from PET and SPECT imaging. Curr. Pharm. Des. 15, 2550–2559.
Howes, O.D., Kambeitz, J., Kim, E., Stahl, D., Slifstein, M., Abi-Dargham, A., Kapur, S., 2012. The nature of dopamine dysfunction in schizophrenia and what this means for treatment. Arch. Gen. Psychiatry 69, 776–786.
Innis, R.B., Cunningham, V.J., Delforge, J., Fujita, M., Gjedde, A., Gunn, R.N., Holden, J., Houle, S., Huang, S.C., Ichise, M., Iida, H., Ito, H., Kimura, Y., Koeppe, R.A., Knudsen, G.M., Knuuti, J., Lammertsma, A.A., Laruelle, M., Logan, J., Maguire, R.P., Mintun, M.A., Morris, E.D., Parsey, R., Price, J.C., Slifstein, M., Sossi, V., Suhara, T., Votaw, J.R., Wong, D.F., Carson, R.E., 2007. Consensus nomenclature for in vivo imaging of reversibly binding radioligands. J Cereb. Blood Flow. Metab. 27, 1533–1539.
Jongen, C., de Bruin, K., Beekman, F., Booij, J., 2008. SPECT imaging of D2 dopamine receptors and endogenous dopamine release in mice. Eur. J. Nucl. Med. Mol. Imaging 35, 1692–1698.
Kuczenski, R., Segal, D., 1989. Concomitant characterization of behavioral and striatal neurotransmitter response to amphetamine using in vivo microdialysis. J. Neurosci. 9, 2051–2065.
Kugaya, A., Fujita, M., Innis, R.B., 2000. Applications of SPECT imaging of dopaminergic neurotransmission in neuropsychiatric disorders. Ann. Nucl. Med. 14, 1–9.
Kuwabara, H., McCaul, M.E., Wand, G.S., Earley, C.J., Allen, R.P., Weerts, E.M., Dannals, R.F., Wong, D.F., 2012. Dissociative changes in the Bmax and KD of dopamine D2/D3 receptors with aging observed in functional subdivisions of the striatum: a revisit with an improved data analysis method. J. Nucl. Med. 53, 805–812.
Lammertsma, A.A., Bench, C.J., Hume, S.P., Osman, S., Gunn, K., Brooks, D.J., Frackowiak, R.S., 1996. Comparison of methods for analysis of clinical [11C] raclopride studies. J. Cereb. Blood Flow. Metab. 16, 42–52.
Lammertsma, A.A., Hume, S.P., 1996. Simplified reference tissue model for PET receptor studies. Neuroimage 4, 153–158.
Laruelle, M., 2000. Imaging synaptic neurotransmission with in vivo binding competition techniques: a critical review. J. Cereb. Blood Flow. Metab. 20, 423–451.
Laruelle, M., Iyer, R.N., al-Tikriti, M.S., Zea-Ponce, Y., Malison, R., Zoghbi, S.S., Baldwin, R.M., Kung, H.F., Charney, D.S., Hoffer, P.B., Innis, R.B., Bradberry, C.W., 1997. Microdialysis and SPECT measurements of amphetamine-induced dopamine release in nonhuman primates. Synapse 25, 1–14.
Logan, J., Fowler, J.S., Volkow, N.D., Wang, G.J., Ding, Y.S., Alexoff, D.L., 1996. Distribution volume ratios without blood sampling from graphical analysis of PET data. J. Cereb. Blood Flow. Metab. 16, 834–840.
Lyoo, C.H., Ikawa, M., Liow, J.S., Zoghbi, S.S., Morse, C.L., Pike, V.W., Fujita, M., Innis, R.B., Kreisl, W.C., 2015. Cerebellum Can Serve As a Pseudo-Reference Region in Alzheimer Disease to Detect Neuroinflammation Measured with PET Radioligand Binding to Translocator Protein. J. Nucl. Med. 56, 701–706.
Martinez, D., Saccone, P.A., Liu, F., Slifstein, M., Orlowska, D., Grassetti, A., Cook, S., Broft, A., Van Heertum, R., Comer, S.D., 2012. Deficits in dopamine D(2) receptors and presynaptic dopamine in heroin dependence: commonalities and differences with other types of addiction. Biol. Psychiatry 71, 192–198.
Mauger, G., Saba, W., Hantraye, P., Dolle, F., Coulon, C., Bramoulle, Y., Chalon, S., Gregoire, M.C., 2005. Multiinjection approach for D2 receptor binding quantification in living rats using [11C]raclopride and the beta-microprobe: crossvalidation with in vitro binding data. J. Cereb. Blood Flow. Metab. 25, 1517–1527.
Meyer, P.T., Salber, D., Schiefer, J., Cremer, M., Schaefer, W.M., Kosinski, C.M., Langen, K.J., 2008a. Cerebral kinetics of the dopamine D(2) receptor ligand [(123)I]IBZM in mice. Nucl. Med. Biol. 35, 467–473.
Meyer, P.T., Salber, D., Schiefer, J., Cremer, M., Schaefer, W.M., Kosinski, C.M., Langen, K.J., 2008b. Comparison of intravenous and intraperitoneal [123I]IBZM injection for dopamine D2 receptor imaging in mice. Nucl. Med. Biol. 35, 543–548.
Meyer, P.T., Sattler, B., Winz, O.H., Fundke, R., Oehlwein, C., Kendziorra, K., Hesse, S., Schaefer, W.M., Sabri, O., 2008c. Kinetic analyses of [123I]IBZM SPECT for quantification of striatal dopamine D2 receptor binding: a critical evaluation of the single-scan approach. Neuroimage 42, 548–558.
Millet, P., Delforge, J., Mauguiere, F., Pappata, S., Cinotti, L., Frouin, V., Samson, Y., Bendriem, B., Syrota, A., 1995. Parameter and index images of benzodiazepine receptor concentration in the brain. J. Nucl. Med. 36, 1462–1471.
Millet, P., Graf, C., Buck, A., Walder, B., Ibanez, V., 2002. Evaluation of the reference tissue models for PET and SPECT benzodiazepine binding parameters. Neuroimage 17, 928–942.
Millet, P., Graf, C., Buck, A., Walder, B., Westera, G., Broggini, C., Arigoni, M., Slosman, D., Bouras, C., Ibanez, V., 2000a. Similarity and robustness of PET and SPECT binding parameters for benzodiazepine receptors. J. Cereb. Blood Flow. Metab. 20, 1587–1603.
Millet, P., Graf, C., Moulin, M., Ibanez, V., 2006. SPECT quantification of benzodiazepine receptor concentration using a dual-ligand approach. J Nucl. Med. 47, 783–792.
Millet, P., Ibanez, V., Delforge, J., Pappata, S., Guimon, J., 2000b. Wavelet analysis of dynamic PET data: application to the parametric imaging of benzodiazepine receptor concentration. Neuroimage 11, 458–472.
Millet, P., Moulin, M., Bartoli, A., Del Guerra, A., Ginovart, N., Lemoucheux, L., Buono, S., Fagret, D., Charnay, Y., Ibanez, V., 2008. In vivo quantification of 5-HT1A-[18F] MPPF interactions in rats using the YAP-(S)PET scanner and a beta-microprobe. Neuroimage 41, 823–834.
Millet, P., Moulin-Sallanon, M., Tournier, B.B., Dumas, N., Charnay, Y., Ibanez, V., Ginovart, N., 2012. Quantification of dopamine D(2/3) receptors in rat brain using factor analysis corrected [18F]Fallypride images. Neuroimage 62, 1455–1468.
Mintun, M.A., Raichle, M.E., Kilbourn, M.R., Wooten, G.F., Welch, M.J., 1984. A quantitative model for the in vivo assessment of drug binding sites with positron emission tomography. Ann. Neurol. 15, 217–227.
Morris, E.D., Bonab, A.A., Alpert, N.M., Fischman, A.J., Madras, B.K., Christian, B.T., 1999. Concentration of dopamine transporters: to Bmax or not to Bmax? Synapse 32, 136–140.
Murnane, K.S., Howell, L.L., 2011. Neuroimaging and drug taking in primates. Psychopharmacol. (Berl.) 216, 153–171.
Narendran, R., Martinez, D., 2008. Cocaine abuse and sensitization of striatal dopamine transmission: a critical review of the preclinical and clinical imaging literature. Synapse 62, 851–869.
Nikolaus, S., Antke, C., Beu, M., Kley, K., Wirrwar, A., Huston, J.P., Muller, H.W., 2011. Binding of [123I]iodobenzamide to the rat D2 receptor after challenge with various doses of methylphenidate: an in vivo imaging study with dedicated small animal SPECT. Eur. J. Nucl. Med. Mol. Imaging 38, 694–701.
Salinas, C.A., Searle, G.E., Gunn, R.N., 2015. The simplified reference tissue model: model assumption violations and their impact on binding potential. J. Cereb. Blood Flow. Metab. 35, 304–311.
Scherfler, C., Scholz, S.W., Donnemiller, E., Decristoforo, C., Oberladstatter, M., Stefanova, N., Diederen, E., Virgolini, I., Poewe, W., Wenning, G.K., 2005. Evaluation of [123I]IBZM pinhole SPECT for the detection of striatal dopamine D2 receptor availability in rats. Neuroimage 24, 822–831.
Schiffer, W.K., Mirrione, M.M., Biegon, A., Alexoff, D.L., Patel, V., Dewey, S.L., 2006. Serial microPET measures of the metabolic reaction to a microdialysis probe implant. J. Neurosci. Method. 155, 272–284.

Shoblock, J.R., Sullivan, E.B., Maisonneuve, I.M., Glick, S.D., 2003. Neurochemical and behavioral differences between d-methamphetamine and d-amphetamine in rats. Psychopharmacol. (Berl.) 165, 359–369.
Shrestha, S., Hirvonen, J., Hines, C.S., Henter, I.D., Svenningsson, P., Pike, V.W., Innis, R.B., 2012. Serotonin-1A receptors in major depression quantified using PET: controversies, confounds, and recommendations. Neuroimage 59, 3243–3251.
Skinbjerg, M., Seneca, N., Liow, J.S., Hong, J., Weinshenker, D., Pike, V.W., Halldin, C., Sibley, D.R., Innis, R.B., 2010. Dopamine beta-hydroxylase-deficient mice have normal densities of D(2) dopamine receptors in the high-affinity state based on in vivo PET imaging and in vitro radioligand binding. Synapse 64, 699–703.
Slifstein, M., Parsey, R.V., Laruelle, M., 2000. Derivation of [(11)C]WAY-100635 binding parameters with reference tissue models: effect of violations of model assumptions. Nucl. Med. Biol. 27, 487–492.
Sun, W., Ginovart, N., Ko, F., Seeman, P., Kapur, S., 2003. In vivo evidence for dopamine-mediated internalization of D2-receptors after amphetamine: differential findings with [3H]raclopride versus [3H]spiperone. Mol. Pharmacol. 63, 456–462.
Tomasi, D., Wang, G.J., Volkow, N.D., 2016. Association between striatal dopamine D2/D3 receptors and brain activation during visual attention: effects of sleep deprivation. Transl. Psychiatry 6, e828.
Tsartsalis, S., Moulin-Sallanon, M., Dumas, N., Tournier, B.B., Ghezzi, C., Charnay, Y., Ginovart, N., Millet, P., 2014. Quantification of GABAA receptors in the rat brain with [(123)I]Iomazenil SPECT from factor analysis-denoised images. Nucl. Med. Biol. 41, 186–195.
Tsartsalis, S., Tournier, B.B., Ginovart, N., Ibanez, V., Millet, P., 2016a. Exploring the full potential of factor analysis for the optimization of voxel-wise parameter estimation and inference analysis with Statistical Parametric Mapping in molecular neuroimaging.Submitted.
Tsartsalis, S., Tournier, B.B., Huynh-Gatz, T., Dumas, N., Ginovart, N., Moulin-Sallanon, M., Millet, P., 2015. 5-HT2A receptor SPECT imaging with [I]R91150 under P-gp inhibition with tariquidar: More is better?Nucl Med Biol.
Tsartsalis, S., Tournier, B.B., Huynh-Gatz, T., Dumas, N., Ginovart, N., Moulin-Sallanon, M., Millet, P., 2016b. 5-HT2A receptor SPECT imaging with [(1)(2)(3)I]R91150 under P-gp inhibition with tariquidar: more is better? Nucl. Med. Biol. 43, 81–88.
Tsukada, H., Nishiyama, S., Kakiuchi, T., Ohba, H., Sato, K., Harada, N., 1999. Is synaptic dopamine concentration the exclusive factor which alters the in vivo binding of [11C]raclopride?: pet studies combined with microdialysis in conscious monkeys. Brain Res 841, 160–169.
Vaessen, T., Hernaus, D., Myin-Germeys, I., van Amelsvoort, T., 2015. The dopaminergic response to acute stress in health and psychopathology: a systematic review. Neurosci. Biobehav. Rev. 56, 241–251.
Verhoeff, N.P., Bobeldijk, M., Feenstra, M.G., Boer, G.J., Maas, M.A., Erdtsieck-Ernste, E., de Bruin, K., van Royen, E.A., 1991. In vitro and in vivo D2-dopamine receptor binding with [123I]S(-) iodobenzamide ([123I]IBZM) in rat and human brain. Int. J. Rad. Appl. Instrum. B 18, 837–846.
Vivash, L., Gregoire, M.C., Bouilleret, V., Berard, A., Wimberley, C., Binns, D., Roselt, P., Katsifis, A., Myers, D.E., Hicks, R.J., O'Brien, T.J., Dedeurwaerdere, S., 2014. In vivo measurement of hippocampal GABAA/cBZR density with [18F]-flumazenil PET for the study of disease progression in an animal model of temporal lobe epilepsy. PLoS One 9, e86722.
Volkow, N.D., Fowler, J.S., Wang, G.J., Baler, R., Telang, F., 2009a. Imaging dopamine's role in drug abuse and addiction. Neuropharmacology 56 (Suppl 1), 3–8.
Volkow, N.D., Fowler, J.S., Wang, G.J., Swanson, J.M., Telang, F., 2007. Dopamine in drug abuse and addiction: results of imaging studies and treatment implications. Arch. Neurol. 64, 1575–1579.
Volkow, N.D., Tomasi, D., Wang, G.J., Telang, F., Fowler, J.S., Wang, R.L., Logan, J., Wong, C., Jayne, M., Swanson, J.M., 2009b. Hyperstimulation of striatal D2 receptors with sleep deprivation: implications for cognitive impairment. Neuroimage 45, 1232–1240.
Volkow, N.D., Wang, G.J., Telang, F., Fowler, J.S., Logan, J., Wong, C., Ma, J., Pradhan, K., Tomasi, D., Thanos, P.K., Ferre, S., Jayne, M., 2008. Sleep deprivation decreases binding of [11C]raclopride to dopamine D2/D3 receptors in the human brain. J. Neurosci. 28, 8454–8461.
Wang, G.J., Volkow, N.D., Fowler, J.S., Logan, J., Abumrad, N.N., Hitzemann, R.J., Pappas, N.S., Pascani, K., 1997. Dopamine D2 receptor availability in opiate-dependent subjects before and after naloxone-precipitated withdrawal. Neuropsychopharmacology 16, 174–182.
Watabe, H., Carson, R.E., Iida, H., 2000. The reference tissue model: three compartments for the reference region. Neuroimage, 11.
Wiers, C.E., Shumay, E., Cabrera, E., Shokri-Kojori, E., Gladwin, T.E., Skarda, E., Cunningham, S.I., Kim, S.W., Wong, T.C., Tomasi, D., Wang, G.J., Volkow, N.D., 2016. Reduced sleep duration mediates decreases in striatal D2/D3 receptor availability in cocaine abusers. Transl. Psychiatry 6, e752.
Wimberley, C., Angelis, G., Boisson, F., Callaghan, P., Fischer, K., Pichler, B.J., Meikle, S.R., Gregoire, M.C., Reilhac, A., 2014a. Simulation-based optimisation of the PET data processing for Partial Saturation Approach protocols. Neuroimage 97c, 29–40.
Wimberley, C.J., Fischer, K., Reilhac, A., Pichler, B.J., Gregoire, M.C., 2014b. A data driven method for estimation of B and appK using a single injection protocol with [C] raclopride in the mouse. Neuroimage.
Wooten, D.W., Hillmer, A.T., Moirano, J.M., Ahlers, E.O., Slesarev, M., Barnhart, T.E., Mukherjee, J., Schneider, M.L., Christian, B.T., 2012. Measurement of 5-HT(1A) receptor density and in-vivo binding parameters of [(18)F]mefway in the nonhuman primate. J. Cereb. Blood Flow. Metab. 32, 1546–1558.
Wooten, D.W., Hillmer, A.T., Moirano, J.M., Tudorascu, D.L., Ahlers, E.O., Slesarev, M.S., Barnhart, T.E., Mukherjee, J., Schneider, M.L., Christian, B.T., 2013. 5-HT1A sex based differences in Bmax, in vivo KD, and BPND in the nonhuman primate. Neuroimage 77, 125–132.

Supplementary Materials and Methods

S1.1 SPECT single- and multi-injection imaging and quantification, arterial plasma analysis and free parent radiotracer fraction estimation

A multi-injection protocol for full kinetic modeling of [^{123}I]IBZM was employed (Millet et al., 2006; Millet et al., 2012). The scan protocol began with a first injection of the radiotracer (91.47±2.91 MBq) at a high specific activity (934.04±114.37 GBq/μmol), followed by a second co-injection of [^{123}I]IBZM (93.06±7.11 MBq) and the unlabeled compound (6.2 nmol/kg) at 120 min and a third injection of the unlabeled compound only at 180 min (1.24 μmol/kg). The overall scan protocol included 240 1-minute frames.

During dynamic SPECT acquisitions, forty arterial blood samples (of 25 μl each) were withdrawn after each radiotracer injection at regular time intervals and immediately centrifuged for 5 min. Radioactivity was measures in a gamma counting system and expressed in kBq/ml after calibration. To estimate the plasma input function in *in vivo* SPECT experiments, only whole-blood radioactivity was measured individually.

Metabolite correction was performed in an independent group of four rats, as previously described (Millet et al., 2012; Tsartsalis et al., 2014; Tsartsalis et al., 2015) using acetonitrile extraction of serial arterial blood samples and Thin Layer Chromatography (TLC) for separation of radioactive molecules. The distribution of radioactivity on the TLC sheet was detected using a phosphor imaging plate (BAS-IP MS2325; Fuji Photo Film Co, Ltd.) and the Fujifilm BAS-1800 II phosphor imager system and Image Reader v2.02 software (Raytest, Straubenhardt, Germany). Quantitative analysis was performed with the Aida Mac Software v4.06 (Raytest Isotopenmessgerate GmbH).

The mean percentage of non-metabolized radiotracer was fitted with a triexponential model as follows: $P_{nm}(t) = A_1e^{-B_1t} + A_2e^{-B_2t} + A_3e^{-B_3t}$, while the metabolite-corrected plasma input function (C_p) was calculated using $C_p(t) = f_1 * P_{nm}(t) * C_{Total\ plasma}(t)$ with f_1, defined as the free fraction of plasma parent compound (Mintun et al., 1984). These parameters were adjusted with a coupled-fitting over the four (bilateral) striatal sub-regions in the four rats used in this experiment, as previously described (Millet et al., 2008; Millet et al., 2012). The percentage of parent compound that is bound to plasma proteins was also estimated as previously described and was considered constant over the duration of the SPECT scan (Gandelman et al., 1994; Mintun et al., 1984).

To evaluate the pharmacokinetic behavior of [^{123}I]IBZM in scans with a longer duration, a 180-min scan was performed using one rat. The scan protocol began with an injection of the radiotracer (66.6 MBq) at a high specific activity (>900 GBq/μmol). The overall scan protocol included 80 2-minute frames.

S1.2 Ex vivo study of the unlabeled compound dose-occupancy curve

Fourteen rats were employed in this study to establish the dose-$D_{2/3}$ receptor occupancy curve for the unlabeled IBZM. Rats were injected with 12.42±1.37 MBq of [^{123}I]IBZM at a high specific activity (>900 GBq/μmol) through a tail vein catheter under isoflurane anesthesia (as described above). A quantity of non-radiolabeled compound was co-injected with the radiolabeled tracer at concentrations ranging from 0 to 10 μmol/kg of rat body weight. 120 minutes post-injection, bilateral striatal regions and cerebellum were excised and radioactivity was measured using a gamma counting system. Radiotracer binding (Specific Binding Ratio) was estimated as follows: SBR=(Activity in striatum)/(Activity in cerebellum)-1. The receptor occupancy at a given dose of unlabeled compound was expressed as the percentage of SBR value (corrected for the non-saturable radioactive concentration), when radiolabeled [^{123}I]IBZM is injected at a high specific activity. The dose-occupancy plot was fitted with a sigmoid curve using the Prism software (GraphPad).

S1.3 Estimation of the ratio (r) of striatal-to-cerebellar non-displaceable binding and simulation of its effect on B_{avail} and appK_d values of the partial saturation approach

The non-displaceable binding in the cerebellum is employed as an index of the non-displaceable binding in the striatum. A difference between the target and reference-regions is possible and may induce a bias in the estimates. For this reason, as Wimberley et al., (Wimberley et al., 2014) have proposed, we corrected the cerebellar TAC by a scaling factor (r) that represents the ratio of non-displaceable binding between the striatal subregions and the difference in the non-displaceable binding ratio (r) of striatal-to-cerebellar non-displaceable binding was used to correct the cerebellar TAC (C_{cer}) before it was used in the Scatchard plot analysis, so C_{ND} = r x $C_{cer.}$ To estimate and validate the r value we employed several different methods:

Method 1: given that a full quantification of the radiotracer kinetics was performed using the multi-injection protocol, we used the precise estimation of the non-displaceable distribution volumes (V_{ND}) in striatum and cerebellum as an index of the relationship of the non-displaceable binding during the scans.

Method 2: we performed a presaturation SPECT study in two rats in which a fully-saturating dose of unlabeled IBZM (1.24 μmol/kg) was administered five minutes before the injection of a high-specific activity (>900 GBq/μmol) [^{123}I]IBZM injection (at radioactive doses of 60.79 and 72.91 MBq, respectively). A dynamic SPECT scan composed of 60 1-minute long frames was initiated right after radiotracer injection. SPECT acquisition and image processing was performed as described in section 2.1. The ratio of non-displaceable binding between target and reference regions was estimated as the ratio of the average radioactive concentration between the four striatal subregions to the one of the cerebellum. This was estimated over time-frames between the 10th and the 45th minute of scan, during which the

Scatchard equilibrium is observed and estimations are performed (see section 3.4) (Wimberley et al., 2014).

In order to study the impact of the choice of r factor and any possible deviation from its true value in B_{avail} and appK_d estimates with the partial saturation approach, the simulated curves of the specific and free binding in the striatum that were generated as described in paragraph 2.5 were processed using a +20% and a -20% deviation from the true value (r=1, given that the true free binding in striatum is simulated). Furthermore, to determine if any possible bias due to the deviation from the true r value is stable across experimental conditions, the same simulation study was performed on simulated specific and free binding curves corresponding to a +30% higher B_{avail} (as in section 2.5).

Supplementary Results

S2.1 Estimation of the ratio (r) of striatal-to-cerebellar non-displaceable binding and simulation of its effect on B_{avail} and appK_d values of the partial saturation approach

Using Method 1, the r value was found r=1.55±0.08. Method two gave similar results with the ratio of non-displaceable binding between the striatum and cerebellum being 1.68 for rat one and 1.69 in rat two over the period between the 10^{th} and 45^{th} minute post radiotracer injection.

The results of the simulated study are presented in Supplementary Figure S2. Using a r value that deviates from the true one induces a bias in the B_{avail} estimates that takes values roughly up to +20% and -20%, while appK_d estimates are much less affected and present a negligible bias. Interestingly, the bias induced by the deviation in the applied r value is virtually identical when applied to simulated curves corresponding to the baseline condition and to the +30% simulated B_{avail} value.

Supplementary Figures

Figure S1. Unlabeled IBZM dose and $D_{2/3}$ receptor occupancy curve. Note that dose window covering 60-70% of receptors (ideal occupancy for the partial saturation study) is between 12 and 24 nmol/kg.

Figure S2. Bias introduced in B_{avail} and appK_d values estimated with the partial saturation approach when the applied r value deviates from the true by +20% and -20%. The simulation is performed on a set of curves corresponding to a baseline B_{avail} value and a simulated +30% increase in B_{avail}.

References

Gandelman, M.S., Baldwin, R.M., Zoghbi, S.S., Zea-Ponce, Y., Innis, R.B., 1994. Evaluation of ultrafiltration for the free-fraction determination of single photon emission computed tomography (SPECT) radiotracers: beta-CIT, IBF, and iomazenil. J Pharm Sci 83, 1014-1019.

Millet, P., Graf, C., Moulin, M., Ibanez, V., 2006. SPECT quantification of benzodiazepine receptor concentration using a dual-ligand approach. J Nucl Med 47, 783-792.

Millet, P., Moulin, M., Bartoli, A., Del Guerra, A., Ginovart, N., Lemoucheux, L., Buono, S., Fagret, D., Charnay, Y., Ibanez, V., 2008. In vivo quantification of 5-HT1A-[18F]MPPF interactions in rats using the YAP-(S)PET scanner and a beta-microprobe. Neuroimage 41, 823-834.

Millet, P., Moulin-Sallanon, M., Tournier, B.B., Dumas, N., Charnay, Y., Ibanez, V., Ginovart, N., 2012. Quantification of dopamine D(2/3) receptors in rat brain using factor analysis corrected [18F]Fallypride images. Neuroimage 62, 1455-1468.

Mintun, M.A., Raichle, M.E., Kilbourn, M.R., Wooten, G.F., Welch, M.J., 1984. A quantitative model for the in vivo assessment of drug binding sites with positron emission tomography. Ann Neurol 15, 217-227.

Tsartsalis, S., Moulin-Sallanon, M., Dumas, N., Tournier, B.B., Ghezzi, C., Charnay, Y., Ginovart, N., Millet, P., 2014. Quantification of GABAA receptors in the rat brain with [(123)I]Iomazenil SPECT from factor analysis-denoised images. Nucl Med Biol 41, 186-195.

Tsartsalis, S., Tournier, B.B., Huynh-Gatz, T., Dumas, N., Ginovart, N., Moulin-Sallanon, M., Millet, P., 2015. 5-HT2A receptor SPECT imaging with [I]R91150 under P-gp inhibition with tariquidar: More is better? Nucl Med Biol.

Wimberley, C.J., Fischer, K., Reilhac, A., Pichler, B.J., Gregoire, M.C., 2014. A data driven method for estimation of B and appK using a single injection protocol with [C]raclopride in the mouse. Neuroimage.

Article 2

In vivo absolute quantification of striatal and extrastriatal $D_{2/3}$ receptors with [^{123}I]epidepride SPECT

Stergios Tsartsalis[1,2], Benjamin B. Tournier[1], Philippe Millet[1,3]

[1]Division of Adult Psychiatry, Department of Psychiatry, University Hospitals of Geneva, Switzerland
[2]Division of Psychiatric Specialties, Department of Psychiatry, University Hospitals of Geneva, Switzerland
[3]Department of Psychiatry, University of Geneva, Switzerland

Corresponding Author
Prof. Philippe Millet
Division of Adult Psychiatry, Department of Psychiatry, University Hospitals of Geneva, Switzerland
Chemin du Petit-Bel-Air 2,
CH1226, Thônex, Switzerland
Tel: +41 22 305 5376, Fax: +41 22 305 5375
e-mail: Philippe.Millet@hcuge.ch

Abstract

Purpose [^{123}I]epidepride is a high-affinity radiotracer used in Single Photon Emission Computed Tomography (SPECT) imaging of the $D_{2/3}$ receptors. It has the ability to bind with high affinity to both striatal and extrastriatal receptors. Nevertheless, its particularly slow kinetics in the striatum impedes the quantification in this region. In this context, a quantification approach that would permit a simultaneous quantification of both striatal and extrastriatal $D_{2/3}$ receptors would be of great interest for preclinical and clinical SPECT neuroimaging. Here, we describe the use of a partial saturation protocol that permits to produce an *in vivo* Scatchard plot and thus estimate B_{avail} and $appK_d$ separately in both striatal and extrastriatal regions,, through a single dynamic SPECT session. To validate this approach, a multi-injection protocol is used for the full kinetic modelling of [^{123}I]epidepride using a 2-tissue compartment, 5-parameter model (2T-5k).

Methods 18 male rats were used. Binding parameters were estimated using the 2T-5k multi-injection protocol. A set of simulation studies was performed to estimate the optimal conditions for the application of the partial saturation protocol and to assess the impact of the presence of specific binding in the cerebellum (reference region) on the quantification. A partial saturation protocol was applied at the region- and pixel-level. In the extrastriatal regions, the separate estimation of B_{avail} and $appK_d$ led to values that were highly variable, so the $appK_d$ value was fixed at an average value extracted from the multi-injection study. The results of the partial saturation study were compared to those obtained with the 2T-5k model. To illustrate the interest of the partial saturation approach, we performed a preliminary study of the effect of a chronic, subcutaneous administration of haloperidol (1 mg/kg/day), a D_2 receptor antagonist, on the B_{avail} of [^{123}I]epidepride in the rat striatum.

Results A series of simulations demonstrated that a mass of 3 ug/kg of unlabelled epidepride allows the formation of an *in vivo* Scatchard plot. The partial saturation study led to robust estimations of B_{avail} in all brain regions that highly correlated (r=0.99) with the corresponding values from the multi-injection study. If the specific binding in the reference region (cerebellum) varies, a bias is induced in the B_{avail} values from the extrastriatal regions, as well as in the $appK_d$ value estimations. A chronic haloperidol treatment resulted in a 17.9% increase in the B_{avail} values in the left Caudate Putamen nucleus (CP) (p=0.07) and a 13.8% increase in the right CP (p=0.12).

Conclusion A partial saturation method allowed the robust quantification of $D_{2/3}$ receptors in striatal and extrastriatal $D_{2/3}$ receptors in the rat brain with a single-scan approach. This approach may be applied in the whole-brain mapping of the $D_{2/3}$ receptor in translational biological studies and potentially, in clinical SPECT imaging.

Key words: [^{123}I]epidepride, $D_{2/3}$ receptor, dopamine, molecular imaging, SPECT, rat

1. Introduction

Molecular imaging of the dopaminergic system with Positron Emission Tomography (PET) and Single Photon Emission Tomography (SPECT) is a powerful tool for the non-invasive study of the living brain in clinical and translational settings. Molecular imaging of the $D_{2/3}$ receptor in particular has provided insight into the pathophysiology of a wide spectrum of neuropsychiatric disorders, ranging from mood and psychotic disorders to addiction and neurodegeneration (Abi-Dargham et al., 2009; Murnane and Howell, 2011). Imaging of the $D_{2/3}$ receptor provides information on the receptor density and, after appropriate experimental manipulation, such as the administration of amphetamine or the performance of a neurocognitive test, its interaction with the endogenous ligand, thus allowing an indirect measure of the endogenous dopamine availability (Kugaya et al., 2000).

Several $D_{2/3}$-binding radiotracers have been developed and routinely used in research settings. Among them, [^{11}C]raclopride and [^{123}I]IBZM are perhaps the most widely employed in PET and SPECT imaging of the dopaminergic system, respectively. These radioligands have the disadvantage of a relatively low affinity for the $D_{2/3}$ receptor, limiting their use to imaging of the striatal receptors with a relatively low signal-to-noise binding ratio (de Paulis, 2003; Laruelle, 2000). For this reason, high-affinity radiotracers have been developed, allowing extrastriatal receptor imaging (de Paulis, 2003). Nevertheless, the high-affinity of the radiotracer is a serious impediment for the quantification of striatal $D_{2/3}$ receptors. In this region, the kinetics of these radiotracers is particularly slow, meaning that a quantitative approach with standard pharmacokinetic modeling would require an impractical scan duration, both for preclinical and, especially, for clinical imaging (Ichise et al., 1999).

One prominent example of such radiotracers is [^{123}I]epidepride (Kessler et al., 1991; Leslie et al., 1996). Because of its very high affinity for the $D_{2/3}$ receptor, [^{123}I]epidepride is only used for imaging of extrastriatal receptors in human SPECT imaging (Fagerlund et al., 2013; Fujita et al., 1999; Fujita et al., 2000; Kegeles et al., 2008; Lehto et al., 2009; Nørbak-Emig et al., 2016; Norbak-Emig et al., 2016; Tuppurainen et al., 2006; Tuppurainen et al., 2009; Varrone et al., 2000). However, a quantification approach permitting the use of [^{123}I]epidepride SPECT for whole-brain imaging would be highly advantageous: on one hand, its high-affinity and thus the high signal-to-noise ratio allow a better sensitivity for the quantification of biological changes compared to lower-affinity radiotracers. On the other hand, compared to PET imaging, SPECT has the advantage of being more accessible to clinical or experimental use, given that it requires no in-house cyclotron (as is the case for PET imaging). ^{123}I has a considerably longer half-life (~13h) than positron-emitting radioisotopes, which is a crucial feature for these high-affinity radiotracers, for which imaging over sufficiently long periods is required to accurately quantify receptor binding. In addition, the development of novel SPECT cameras, in the preclinical and very recently in the clinical level, has led to SPECT imaging with a high spatial resolution, comparable to that PET (Meikle et al., 2005). Interestingly, the use of ^{124}I, a positron-emitting radioisotope has been employed to label epidepride, allowing the use of this radiotracer in PET and providing another argument for the development of epidepride imaging for both SPECT and PET (Pandey et al., 2014).

In this context, a methodology that would allow to quantify [$^{123/124}$I]epidepride in both the striatum and the extrastriatal regions would be of great interest. Given that the main obstacle in [^{123}I]epidepride imaging is its very slow kinetics in the striatum, we proposed to employ the partial saturation approach, which, in principle, implies an alteration of the radiotracer's kinetics. The partial saturation approach has been originally developed for [^{11}C]flumazenil imaging of $GABA_A$ receptors (Delforge et al., 1996; Delforge et al., 1997). In this approach, a dose of unlabeled ligand is co-injected with the labeled radiotracer. The resulting kinetics of the radiotracer allow an *in vivo* Scatchard plot to be formed and the B_{avail} and $appK_d$ to be separately estimated. This protocol has been recently employed by our group (Tsartsalis et al., 2017) and others (Wimberley et al., 2014a; Wimberley et al., 2014b) for $D_{2/3}$ imaging using [^{123}I]IBZM and [^{11}C]raclopride in small animals. Overall, this approach has been used to quantify radiotracers with rapid kinetics and this paper presents that first application for a radiotracer with such slow kinetics as [^{123}I]epidepride.

In this paper, we firstly perform a full-quantification of [^{123}I]epidepride kinetics using a multi-injection imaging protocol (Delforge et al., 1990; Millet et al., 2012; Tsartsalis et al., 2014; Tsartsalis et al., 2017), which separately identifies B_{avail} and $appK_d$. The results of the multi-injection protocol serve as a "gold-standard" for the validation of the partial saturation approach, which is applied at the region- and at the voxel-level.

2. Materials and Methods

2.1 Animals and general SPECT scan protocol

18 male Mdr1a knock-out (KO) rats (Janvier Laboratories, Le Genet-St-Isle, France), weighing between 380 and 500 g were employed in the study. Of these, 3 rats were employed in an *in vivo* multi-injection SPECT imaging protocol for absolute $D_{2/3}$ receptor quantification (SPECT-MI in Table 1). 4 rats were employed in an arterial plasma analysis for the study of plasma kinetics of the radiotracer and the estimation of the free parent radiotracer fraction (TLC in Table 1) (Tsartsalis et al., 2017). 4 rats were employed in a SPECT experiment with a partial $D_{2/3}$ receptor saturation design for the determination of B_{avail} and $appK_d$ parameters from an *in vivo* Scatchard plot (SPECT-PSA in Table 1) (Tsartsalis et al., 2017). Finally, 7 rats were employed in a proof-of-concept study of the effect of a chronic haloperidol treatment on the B_{avail} and $appK_d$ of the $D_{2/3}$ receptors in rats (SPECT_PSA_HAL for haloperidol-treated and SPECT_PSA_CON for control rats in Table 1, see Supplement 1).

SPECT scans were performed with a U-SPECT-II camera (MiLabs, Utrecht, Netherlands). In rats that underwent SPECT scans with the multi-injection protocol, two polyethylene catheters (i.d.=0.58 mm, o.d= 0.96 mm) were inserted in the left femoral vein and artery for radiotracer administration and blood sampling, respectively. SPECT scans were performed under isoflurane anaesthesia (3% for induction and 1-2 % for maintenance). In rats that underwent SPECT scans for the partial saturation protocol, radiotracer injection was performed via a tail vein catheter. Body temperature was monitored during the scans and maintained at 37±1 °C by means of a thermostatically controlled heating blanket.

SPECT image reconstruction was performed using a pixel ordered subsets expectation maximization (P-OSEM, 0.4-mm voxel size, 4 iterations, 6 subsets) algorithm using MiLabs image reconstruction software. Radioactive decay correction was performed, while correction for attenuation or scatter was not. Following reconstruction, dynamic images from the partial saturation experiment were denoised with factor analysis (FA) using Pixies software (Apteryx, Issy-les-Moulineaux, France) as previously described (Tsartsalis et al., 2014; Tsartsalis et al., 2017; Tsartsalis et al., 2018). FA permits the decomposition of dynamic signal into a few elementary components, termed factors (Di Paola et al., 1982; Millet et al., 2012; Tsartsalis et al., 2014). In this study, 3 factors were retained and the rest of the signal was discarded as noise (Tsartsalis et al., 2014; Tsartsalis et al., 2017). SPECT images were processed with PMOD software v3.7 (PMOD Technologies Ltd, Zurich, Switzerland). Averaged images corresponding to the ten first frames of acquisition were co-registered to an MRI template integrated in PMOD (Schiffer et al., 2006). Transformation matrices were then applied to dynamic images. Tissue-activity curves (TACs) from the following regions were extracted: caudate-putamen (CP), nucleus accumbens (NAc), ventral tegmental area (VTA), frontal cortex (FC), amygdala (Amy), hypothalamus (Hyp), superior colliculus (SupC), inferior colliculus (InfC) and cerebellum.

All experimental procedures were approved by the Ethical Committee on Animal Experimentation of the Canton of Geneva, Switzerland.

2.2 Radiotracer preparation

[^{123}I]epidepride was prepared as previously described (Kessler et al., 1991), using a commercially available precursor (ABX, Radenberg, Germany). Radiochemical purity was >99%. The specific activities in the experiments are shown in Table 1.

2.3 SPECT multi-injection imaging protocol and quantification, arterial plasma analysis and free parent radiotracer fraction estimation

A multi-injection protocol for full kinetic modelling of [^{123}I]Epidepride was employed (Millet et al., 2006; Millet et al., 2012; Tsartsalis et al., 2017). The scan protocol began with a first injection of the radiotracer at a high specific activity, followed by a second co-injection of [^{123}I]Epidepride and the unlabeled compound at 180 min and a third injection of the unlabeled compound alone at 240 min. The overall scan protocol included 360 1-minute frames (Figure 1). The specific activities and radioactive doses of each experiment are presented in Table 1.

The whole multi-injection study TAC data was fitted in with a two-tissue compartment five-parameter model (2T-5k), to estimate K_1, k_2, k_{on}, k_{off} and B_{avail} as previously described (Ginovart et al., 2001; Millet et al., 1995; Millet et al., 2006; Millet et al., 2000). The free, non-metabolized radiotracer fraction in the plasma was used as the input function (Delforge et al., 1999). During dynamic SPECT acquisitions, 40 arterial blood samples (of 25 μl each) were withdrawn after each radiotracer injection at regular time intervals. Radioactivity was measured in a gamma counting system and expressed in kBq/ml after calibration. To estimate the plasma input function in *in vivo* SPECT experiments, only whole-blood radioactivity was measured individually. Metabolite correction and plasma protein binding analysis for the estimation of radiotracer plasma input function was performed in an independent group of 4 rats, as previously described (Gandelman et al., 1994; Millet et al., 2008; Millet et al., 2012; Mintun et al., 1984; Tsartsalis et al., 2015; Tsartsalis et al., 2014) (the radioactive doses employed in this experiment are presented in Table 1). Analysis was performed in Matlab software R2015b (Mathworks, USA).

2.4 Simulations and in vivo partial saturation study

2.4.1 The partial saturation protocol

A partial saturation protocol was employed to estimate B_{avail} and appK_d as recently described for another $D_{2/3}$ radiotracer (Tsartsalis et al., 2017) based on the original description by Delforge et al (Delforge et al., 1996; Delforge et al., 1997), as optimized by Wimberley et al (Wimberley et al., 2014a; Wimberley et al., 2014b). Briefly, co-injection of a dose of unlabeled compound at doses that occupy 50-70% of the receptors permits to form a Scatchard plot when the specifically bound fraction of radiotracer (C_S) is plotted against the ratio of C_S to the non-displaceable binding at the same region (C_S/C_{ND}). The intercept to the C_S axis provides the B_{avail} and the inverse of the slope the appK_d.

2.4.2 Simulation study 1: estimation of the dose of the unlabeled epidepride for the partial saturation study

A first simulation study was performed to estimate the dose of the unlabeled compound that is needed to produce an *in vivo* Scatchard plot. This simulation study was based on the results of the full quantification from one of the multi-injection experiments. This full-quantification approach allows the complete discrimination of the different components of the radiotracer's kinetics, namely the free and the specific binding in each VOI. As a consequence, in Simulation study 1, single injection experiments using variable doses of unlabeled Epidepride were simulated and *in vivo* Scatchard plots were delineated using the free and the specific binding from the CP (a high-binding) and VTA (a low-binding VOI). B_{avail} and $appK_d$ were estimated and compared to the results of the full-quantification using the multi-injection study, to estimate the % bias in the parameter values as a function of the dose of unlabeled epidepride. The dose of the unlabeled epidepride that allows an optimal estimation of B_{avail} and $appK_d$ using the partial saturation method was thus determined.

2.4.3 Estimation of the r parameter for the correction of the cerebellar TAC

In the partial saturation approach, the cerebellar TAC is employed as an approximation of the non-displaceable binding in the target brain VOIs. Given the differences in the concentration of this binding between the cerebellum and the target VOIs, as well as the presence of a non-negligible specific binding in the cerebellum with [^{123}I]epidepride, the cerebellar TAC has to be corrected. As originally proposed by Delforge et al. (Delforge et al., 1996; Delforge et al., 1997) and more recently by Wimberley et al. (Wimberley et al., 2014b) the concentration of the non-displaceable binding in a given brain VOI (C_{ND}) is approximated by the corrected concentration of the total (measured) cerebellar binding (C_{cer}) using an estimated r parameter, so that $C_{ND} = r \times C_{cer}$.

The estimation of r was based on Simulation study 1 using the optimal concentration of unlabeled compound as determined in section 2.4.2. Average radioactivity data corresponding to the time points between the 30th and the 180th minutes from the simulated TACs of the non-displaceable binding in the CP ($C_{ND\text{-}CP}$), representing the high-binding, striatal VOIs and the VTA ($C_{ND\text{-}VTA}$), representing the low-binding, extrastriatal VOIs and the total binding in the cerebellum (C_{cer}) were used. The r parameter was determined using the ratio $r = C_{ND\text{-}CP}/C_{cer}$ for the striatal VOI and $r = C_{ND\text{-}VTA}/C_{cer}$ for extrastriatal VOIs.

2.4.4 Simulation study 2: evaluation of the bias induced by the presence of specific binding in the cerebellum

[^{123}I]epidepride has a non-negligible specific binding in the cerebellum, a region which is used as an approximation of the non-displaceable binding in the whole brain ("reference" region). The presence of specific binding may induce a bias in the estimation of the quantitative parameters. To evaluate this phenomenon, we employed the results of the full-quantification from one of the multi-injection

experiments, as in Simulation study 1. Various levels of specific binding in the cerebellum were simulated. A partial saturation experiment, using the optimal dose of unlabeled epidepride as determined in Simulation study 1, was simulated. The results of the quantification of B_{avail} and $appK_d$ were compared to the results of the full-quantification of the multi-injection study and the % bias in these parameters was estimated as a function of the specific binding in the cerebellum.

2.4.5 In vivo partial saturation study

In vivo partial saturation SPECT scans and image reconstruction were performed in the same conditions as described in section 2.3. A single radiotracer injection (containing a dose of unlabeled Epidepride determined in the simulation study) was followed by a scan composed of 180 frames of 1-min. No arterial blood sampling took place and the cerebellum was employed as the reference region. The radioactive doses of each experiment are presented in Table 1. TACs were processed in PMOD (PKIN module), in which the model for the analysis of data from partial saturation experiments, as optimized by Wimberley et al (Wimberley et al., 2014a; Wimberley et al., 2014b), is implemented.

2.4.6 In vivo partial saturation study with a fixed $appK_d$ in extrastriatal regions

Given the low binding of [^{123}I]epidepride in extrastriatal regions, the estimation of both B_{avail} and $appK_d$ may be suboptimal, suffering from high inter-subject variability. For this reason, we performed the same *in vivo* partial saturation protocol as described in section 2.4.5 by fixing the $appK_d$ value in PMOD and thus only fitting B_{avail}. This fixed $appK_d$ value was determined as the average $appK_d$ across the extrastriatal VOIs of the three multi-injection experiments (section 2.3).

2.4.7 Simulation study 3: impact of fixing the $appK_d$ value on the estimation of B_{avail}

The $appK_d$ parameter may be altered across experimental conditions, notably with respect to the concentration of the endogenous ligand in the vicinity of the receptor under study. As a consequence, if the fixed $appK_d$ value in the partial saturation experiments (as in section 2.4.6) differs from the real $appK_d$ value, a bias in the estimation of B_{avail} may be induced. To study this phenomenon, we performed a simulation study based on Simulation study 1. Using the optimal dose of unlabeled compound, as determined in 2.4.2, a series of partial saturation experiments was performed, in which varying $appK_d$ values were simulated. *In vivo* Scatchard plots were delineated and B_{avail} was estimated using the same fixed $appK_d$ value as determined in section 2.4.6. The % bias in the B_{avail} estimates, compared to the simulated B_{avail} values, was calculated.

2.6 Parametric images of B_{avail} using [^{123}I]epidepride

B_{avail} values may also be estimated with the partial saturation approach at the voxel-level to produce parametric images (Tsartsalis et al., 2017). Nevertheless, the partial saturation quantification

method that we employed in this study, included in the PKIN module for VOI-wise estimations, has not been included in the PXMOD module of the PMOD software yet, in which parametric estimations are performed. For this reason, to produce parametric images of B_{avail}, we applied the partial saturation protocol on a coronal section including the CP and the NAc and another one including the VTA. TACs were extracted from each pixel and processed in PKIN, exactly as described in section 2.4.6. The resulting pixel-wise B_{avail} values were used to create parametric images in Matlab.

2.7 Statistical Analysis

B_{avail} and $appK_d$ values resulting from fitting the data of the whole duration of the multi-injection protocol were used as the “gold standard” for comparison of estimations with the partial saturation approach by means of regression analysis. Comparisons of average B_{avail} and $appK_d$ values from the multi-injection study and the partial saturation experiments were also performed by means of a two-samples t-test.

3. Results

3.1 Quantitative parameters from the multi-injection study

The parameters of the bi-exponential function describing the kinetics of the mean percent non-metabolized plasma radiotracer were: A_1=0.61, B_1=-0.20, A_2=0.27, B_2=-0.006. Average percentage of radiotracer bound to plasma proteins was 22%. The 2T-5k model provided satisfactory fits to the TACs of the multi-injection study, as shown in Figure 1. Parameter estimates are provided in Table 2. A non-negligible amount of displaceable binding in Cer is observed (data not shown).

3.2 Simulation studies

3.2.1 A simulation study to determine the dose of unlabeled Epidepride that needs to be injected for the partial saturation protocol

As shown in Figure 2, a dose of unlabeled Epidepride of 3 μg/kg or higher produces a Scatchard plot in both high- and low-binding VOI (Figure 2A and 2B, respectively). We chose to employ this dose of 3 μg/kg, as it produces a Scatchard plot with the highest range of C_S/C_{ND} values. In this case, the impact of noise in the *in vivo* experiments should be the lowest.

3.2.2 A simulation study to determine the r value for the correction of the cerebellar TAC

In addition, according to the simulation study (Figure 3), the r value for the correction of the cerebellar TAC was found to be equal to 1 for CP and NAc and equal to 0.4 for the extrastriatal VOI and this value presents an adequate temporal stability in time points beyond 70 min after the injection of the radiotracer, i.e. the time points that are employed in the Scatchard plot. In addition, small variations in the mass of the unlabeled epidepride do not remarkably modify the r value.

3.2.3 A simulation study to assess the impact of variations in the specific binding in the cerebellum on B_{avail} and appK_d values

The results of the simulation study, in which the impact of varying specific binding levels in the Cer on B_{avail} and appK_d are evaluated, are presented in Figure 4. The B_{avail} values estimated with the partial saturation method from high-binding VOI (the CP) are minimally influenced by this variation in cerebellar specific binding. However, the B_{avail} values from the low-binding VOI (such as the VTA in this simulation) and the appK_d values from both high- and low-binding VOI may be biased, depending on the variation in the specific binding in Cer. Indeed, a variation of ±30% in the specific binding in the Cer will lead to ±20% bias in the appK_d at the striatum, a ±18% bias in the B_{avail} in the VTA and a ±7% bias in the appK_d in the VTA.

3.2.4 Assessing the impact of fixing appK$_d$ in extrastriatal B$_{avail}$ value estimations

In the last simulation study, the impact of fixing appK$_d$ values in extrastiatal B$_{avail}$ value estimations was evaluated. A fixed appK$_d$ led to a percent bias in the estimation of the B$_{avail}$ value in the VTA that is almost linear as a function of the percent difference between the "true"-simulated and the fixed appK$_d$ (Figure 5). In detail, a fixed appK$_d$ which is higher than the simulated value by 60% leads to an underestimation of the B$_{avail}$ value by 16%. On the contrary, a fixed appK$_d$ which is lower than the simulated value by 60% leads to an overestimation of the B$_{avail}$ by 25%.

3.3 Quantitative parameters from the in vivo partial saturation study at the VOI and pixel level

B$_{avail}$ and appK$_d$ values estimated from the *in vivo* partial saturation experiments are also provided in Table 2. These values are comparable and highly correlated to the corresponding values from the multi-injection experiments, as the linear regression analysis demonstrates ($r= 0.99$, $p<0.01$ for B$_{avail}$ Figure 6). In addition, no significant difference in the average B$_{avail}$ or appK$_d$ values from the multi-injection and the partial saturation studies was found ($p>0.05$). The parametric images of B$_{avail}$ in the section including the CP and VTA and in the section including the VTA are shown in Figure 7.

3.4 Preliminary study of the effect of chronic haloperidol treatment on the striatal D$_{2/3}$ B$_{avail}$ values

A chronic (28 days) haloperidol treatment (1 mg/kg/day), as described in the supplemental materials and methods (S1), resulted in an increase in the B$_{avail}$ values (Figure 8): 25.67±2.30 pmol/ml in the haloperidol-treated group vs 21.76±2.20 pmol/ml in the vehicle-treated group in the left CP ($p=0.07$ using two-samples t test) and 25.33±2.52 pmol/ml vs 22.25±3.40 pmol/ml in the right CP ($p=0.12$).

4. Discussion

4.1 Validation of B_{avail} and appK_d values

In this study, we applied a partial saturation approach in nuclear neuroimaging for the separate quantification of $D_{2/3}$ B_{avail} and appK_d. The multi-injection approach, the "gold-standard" for the validation of the results of the partial saturation method was also applied in a group of rats. The results of the multi-injection experiment are in accordance with previous studies of absolute $D_{2/3}$ receptor quantification from our group (Tsartsalis et al., 2017), using the same protocol: using [^{123}I]IBZM and a multi-injection protocol, B_{avail} values in the CP were found in the range between 19 and 20 pmol/ml. At the level of NAc, the B_{avail} values were found in the range between 13 and 15 pmol/ml, slightly higher than those found in the present study. Considering the extrastriatal VOI, B_{avail} values were roughly between 2 and 4 pmol/ml. In a previous study from our group using [^{18}F]fallypride, B_{avail} values were found in the range between 2 and 9 pmol/ml (Millet et al., 2012). This difference may be explained by the different delineation of the VOI in the two studies. In the [^{18}F]fallypride study, VOI were spherical structures placed in the middle of the corresponding anatomical structure of the brain, whereas in the present study the Schiffer atlas (Schiffer et al., 2006) was employed to delineate VOI that correspond to the entire size of the anatomical structure.

For the partial saturation study, we first estimated the r parameter that is necessary for the correction of the cerebellar TAC and its use as an index of the non-specific binding of a given VOI in the partial saturation studies. The r parameter was estimated using a simulation study in which the total PET signal was decomposed and the non-displaceable binding in striatal and extrastriatal VOI was extracted. The ratio of this non-displaceable binding of the target VOI to the total binding in the Cer gave the r parameter. We did not use a pre-saturation *in vivo* study as described previously from our group (Tsartsalis et al., 2017) and others (Wimberley et al., 2014a; Wimberley et al., 2014b). This was impossible, because a pre-saturation study would not be able to take the specific binding in the Cer into account in the estimation of r. This is because In that case, the specific binding in this region would have been displaced. Taking the specific binding in the reference region into account has already been described for the application of the partial saturation approach with [^{11}C]flumazenil (Delforge et al., 1996). In this way, the correction of the TAC of the reference region more accurately represents the ratio of the non-specific binding in the target VOI. Another finding considering the use of the Cer as a reference region in [^{123}I]epidepride imaging is illustrated in the simulation study described in 2.4.4. The results of this study suggest that should the specific binding in the Cer vary, the B_{avail} values in the low-binding, extrastriatal regions will vary accordingly. B_{avail} values in high-binding regions remain virtually unbiased even with large variations of the specific binding in the Cer. Similarly, appK_d estimations in both striatal and extrastriatal regions will vary considerably as a function of the variation in the specific binding in the Cer in a given experimental context (e.g. a brain pathology). [^{123}I]epidepride has been employed in multiple studies (discussed in more detail in the following section) of different psychiatric conditions, in which the cerebellar specific binding of the radiotracer is considered unchanged. As demonstrated by Pinborg et al (Pinborg et al., 2007), this issue may be particularly problematic when

extrastriatal occupancy of $D_{2/3}$ receptors by pharmaceutical agents is estimated. Possible variations in the specific binding in the Cer have to be taken into account in the design of biological studies using [^{123}I]epidepride and the stability of this specific binding across the experimental conditions has to be verified in order to obtain unbiased results.

The partial saturation approach using [^{123}I]epidepride gave highly similar values with previous studies of the $D_{2/3}$ receptor using the same method (Tsartsalis et al., 2017; Wimberley et al., 2014b) in the striatum. All B_{avail} values obtained with the partial saturation approach highly correlated with the corresponding B_{avail} values from the multi-injection experiment. However, the appK_d values obtained using the partial saturation method in the striatal VOI differ considerably from the corresponding values obtained using the multi-injection approach (Table 2). This is could possibly be due to inter-individual variations in the specific binding in the reference region and in the overall correction of the cerebellar TAC with the r parameter. As predicted in the simulation study (Figure 4), a variation in the specific binding in the Cer induces a considerable bias in the appK_d in such high-binding VOI, whereas the B_{avail} values are minimally impacted and this is observed in the estimated parameter values here. Regarding the extrastriatal VOI, the appK_d values were fixed in a value obtained from the multi-injection experiment, as attempting to fit both B_{avail} and appK_d led to highly variable estimations (data not shown). Fixing appK_d in these VOI permitted estimation of B_{avail} with acceptable variability (Table 2). In this case, as the simulation study suggests (Figure 5), if the "true" appK_d varies, the B_{avail} estimations vary accordingly. This means that, by fixing the appK_d parameter value, the B_{avail} becomes a composite parameter which integrates information on both the absolute concentration of the target protein (i.e. the B_{avail} *per se*) and the affinity of the radiotracer for the target protein (i.e. 1/appK_d). In this case, in a molecular neuroimaging study involving [^{123}I]epidepride, a variation in the B_{avail} value in the extrastriatal VOI in a given experimental condition may be interpreted as either an true elevation of the quantity of the $D_{2/3}$ receptor or a modification of the affinity of the radiotracer for the receptor, which could be linked to alterations in the concentration of dopamine in the synapse. This is essentially similar to the information provided by the binding potential ($BP=B_{avail}/appK_d$), a composite measure that is most widely employed in molecular neuroimaging (Innis et al., 2007).

4.2 Potential applications of [^{123}I]epidepride imaging using the partial saturation approach

The method proposed here is the first approach that allows the quantification of the striatal binding of [^{123}I]epidepride. The high-affinity of this radiotracer allows to obtain excellent quality images. Figure 9 illustrates the superiority of the quality of a [^{123}I]epidepride SPECT image compared to an image obtained with another SPECT $D_{2/3}$ radiotracer, the low-affinity [^{123}I]IBZM. The binding of [^{123}I]epidepride is considerably higher that the binding of [^{123}I]IBZM (note the difference in the range of radioactive concentrations, 0-10 KBq/ml and 0-2.5 KBq/ml, respectively). The high binding of [^{123}I]epidepride also allows for an adequate anatomical delineation of the striatal substructures and notably the distinction of the NAc from the CP, which is not possible with [^{123}I]IBZM.

The quality of the radioactive signal and the robustness of the quantitative parameters that are obtained with the partial saturation approach are supported by the low standard deviations and the

percent coefficients of variance (CV) of the B_{avail} values (Table 2): indeed, the CV of these values obtained with [^{123}I]epidepride in the CP is 5.87% and in the NAc is 24.14%. In the extrastriatal regions, CV values range from 10 to 35%. In comparison, the same approach with [^{123}I]IBZM yielded B_{avail} values with a CV of 25.43% in the CP and 58% in the NAc in rats (Tsartsalis et al., 2017). Using the same approach and the low-affinity PET radiotracer [^{11}C]raclopride, Wimberley et al found B_{avail} values with a CV around 40% in mice (as roughly depicted in Figure 8 of the aforementioned paper) (Wimberley et al., 2014b). In rat PET imaging with [^{18}F]fallypride (Millet et al., 2012), CV of BP values estimated with the Logan graphical analysis approach (38.31% in CP and 30% in the NAc and from 38 to 58% in the extrastriatal VOI) were also higher than the CV of B_{avail} values presented here. Overall, the robustness of the quantitative parameters obtained with the partial saturation approach in [^{123}I]epidepride SPECT suggests that biological studies using this radiotracer may provide high statistical power compared to other available PET and SPECT imaging modalities of the dopaminergic system.

To illustrate the potential application of the partial saturation approach, we performed a preliminary study of the effect of a chronic, high-dose haloperidol treatment (Turrone et al., 2003) on the absolute quantity of $D_{2/3}$ receptors in the striatum. We found an up-regulation of the $D_{2/3}$ receptor in the CP, as suggested by previous studies in the literature (Ginovart et al., 2008). Chronic haloperidol treatment led to an increase in the B_{avail} of [^{123}I]epidepride of 17.97% in the left CP and of 13.84% in the right CP. Associated p values with respect to a comparison by means of a two-samples t test were 0.07 and 0.12, respectively, i.e. the differences are not statistically significant using a conventional two-tailed threshold of p=0.05. Indeed, the small sample size (4 rats in the control and 3 in the haloperidol treatment group) suggests that this study was underpowered. However, if a one-tailed significance threshold is considered, the difference in B_{avail} values in the left CP achieves statistical significance. Given the purely illustrative purpose of this experiment, we chose to maintain its preliminary character in the context of the present study. It is for the same reason that we only studied the effect of haloperidol in high-binding VOIs and not in extrastriatal VOIs. Another prominent experimental paradigm where [^{123}I]epidepride imaging with the partial saturation protocol is the study of endogenous dopamine alterations in physiological and pathological conditions. It has been experimentally and theoretically established (Morris and Yoder, 2007) that [^{123}I]epidepride binding is not sensitive to “rapid” changes in endogenous dopamine binding in the $D_{2/3}$ receptor, as in the case of amphetamine induced dopamine release. Nevertheless, using the partial saturation protocol described here, one may gain access into enduring alterations of baseline receptor occupancy by endogenous dopamine in experimental models and pathological conditions, such as in schizophrenia (Caravaggio et al., 2019; Kegeles et al., 2010).

The high affinity of the binding of [^{123}I]epidepride allowed it to be employed in clinical studies of the extrastriatal $D_{2/3}$ receptors in various psychiatric conditions, such as in major depressive disorder (Lehto et al., 2008) and schizophrenia (Glenthoj et al., 2006; Tuppurainen et al., 2003; Tuppurainen et al., 2009). Using the partial saturation approach presented here, striatal and extrastriatal $D_{2/3}$ receptor binding can be studied simultaneously. The interest of dissociating B_{avail} and appK_d estimations in PET studies has been discussed extensively in a previous study from our group (Tsartsalis et al., 2017). The application of the partial saturation protocol in translational [^{123}I]epidepride imaging may further potentialize the preclinical studies of the dopaminergic system, well beyond the mesostriatal circuit.

The partial saturation protocol described here for preclinical imaging is potentially applicable in clinical PET studies of the dopaminergic system. Indeed, occupying 50-70% of striatal $D_{2/3}$ receptors for the application of the partial saturation approach induces little, if any, adverse effects. Indeed, this level of blockade is identical to the one induced by antipsychotic agents at therapeutic doses and it is accepted that adverse events appear when blockade is higher that 80-85% (Ginovart and Kapur, 2012). After the safety of administering pharmacological doses of epidepride is confirmed, the application of this protocol in clinical imaging will be feasible and its impact in the understanding of brain function and disease can be invaluable.

5. Conclusions

In conclusion, we propose here, for the first time, a method that allows a simultaneous quantification of striatal and extrastriatal $D_{2/3}$ receptors using [^{123}I]epidepride. A whole-brain cartography of the $D_{2/3}$ receptor is now feasible using this radiotracer. The robustness of the radioactive signal (especially compared to low-affinity $D_{2/3}$ radiotracers) and the stability of the resulting quantitative parameters, which highlight the potential of conducting studies with high statistical power, have been demonstrated. In addition, this approach is relatively simple to apply and already integrated in a commercial image-analysis software. Overall, this study highlights an innovative tool of preclinical brain SPECT imaging in the study of dopamine neurochemistry in physiology and animal models of disease with an approach that is validated for rat SPECT studies but is potentially applicable in clinical brain SPECT.

6. Acknowledgments

This work was supported by the Swiss National Science Foundation (grant no. 310030_156829), by the Geneva Neuroscience Centre, the Jean and Madeleine Vachoux Foundation, by the Maria Zaousi Memorial Foundation (Greece) through a scholarship of the Hellenic State Scholarship Foundation (ST) and by the “Swiss Association for Alzheimer’s Research" which was created in 2009 to finance Swiss fundamental and clinical research programs on Alzheimer’s disease. The authors are grateful to Mrs Maria Surini-Demiri for excellent technical assistance and declare that they have no conflict of interest.

TABLE 1: Numerical values of the SPECT and metabolite protocol parameters corresponding to the 18 experiments.

			Injection 1 (T = 0 min)		Injection 2			Injection 3	
Rats	Modality/tracer	Duration (min)	SA† (GBq/μmol)	J_1^* (MBq/μg)	Time (min)	J_2^* (MBq/μg)	J_2 (μg)	Time (min)	J_3 (μg)
1	TLC/[^{123}I]Epidepride	180	>1000	89.6/<0.05	-	-	-	-	-
2	TLC/[^{123}I]Epidepride	180	>1000	98.2/<0.05	-	-	-	-	-
3	TLC/[^{123}I]Epidepride	180	>1000	96.9/<0.05	-	-	-	-	-
4	TLC/[^{123}I]Epidepride	180	>1000	77.4/<0.05	-	-	-	-	-
5	SPECT-MI/[^{123}I]Epidepride	360	1065.86	95.4/0.043	180	103.4/0.047	1.07	240	214.00
6	SPECT-MI/[^{123}I]Epidepride	360	967.71	87.4/0.043	180	93.5/0.046	2.35	240	234.50
7	SPECT-MI/[^{123}I]Epidepride	360	955.45	87.6/0.044	180	97.5/0.049	1.10	240	221.00
8	SPECT-PSA/[^{123}I]Epidepride	180	19.50	52.7/1.30	-	-	-	-	-
9	SPECT-PSA/[^{123}I]Epidepride	180	23.74	58.6/1.19	-	-	-	-	-
10	SPECT-PSA/[^{123}I]Epidepride	180	40.67	113.06/1.34	-	-	-	-	-
11	SPECT-PSA/[^{123}I]Epidepride	180	29.51	75.24/1.23	-	-	-	-	-
12	SPECT-PSA_CON/[^{123}I]Epidepride	180	18.85	49.35/1.26	-	-	-	-	-
13	SPECT-PSA_CON/[^{123}I]Epidepride	180	16.98	43.48/1.23	-	-	-	-	-
14	SPECT-PSA_CON/[^{123}I]Epidepride	180	22.74	45.65/0.97	-	-	-	-	-
15	SPECT-PSA_CON/[^{123}I]Epidepride	180	17.10	41.15/1.16	-	-	-	-	-
16	SPECT-PSA_HSPE/[^{123}I]Epidepride	180	18.81	46.09/1.18	-	-	-	-	-
17	SPECT-PSA_HSPE/[^{123}I]Epidepride	180	16.72	40.7/1.17	-	-	-	-	-
18	SPECT-PSA_HSPE/[^{123}I]Epidepride	180	16.95	38.47/1.09	-	-	-	-	-

J_i* and J_i correspond respectively to [^{123}I]Epidepride activity (activity/mass) and unlabeled Epidepride mass, injected during the i^{th} injection. †Specific activity at the beginning of the experiment.

Table 2 Mean and Standard Deviations of Binding Parameter Estimates Obtained from 3 Rats of the Multi-injection Study and from 4 rats of the Partial Saturation Study.

	Multi-injection study												Partial saturation			
VOI	**B_{avail}**	**±SD**	**appK_D**	**±SD**	**K_1**	**±SD**	**k_2**	**±SD**	**k_{on}**	**±SD**	**k_{off}**	**±SD**	**B_{avail}**	**±SD**	**appK_D**	**±SD**
NAc	10.18	1.72	0.15	0.04	0.53	0.14	0.10	0.02	0.26	0.06	0.04	0.00	11.75	2.84	0.27	0.22
CP	24.22	2.62	0.22	0.06	0.69	0.16	0.10	0.04	0.21	0.06	0.04	0.01	21.25	1.25	0.08	0.03
VTA	3.77	1.86	0.34	0.21	0.57	0.07	0.14	0.04	0.28	0.36	0.04	0.02	4.01	1.40	-	-
FC	20.67	22.60	4.50	5.25	0.40	0.15	0.09	0.03	0.01	0.01	0.03	0.01	5.15	2.05	-	-
Amy	2.71	1.53	0.36	0.12	0.38	0.11	0.16	0.10	0.09	0.02	0.03	0.00	2.77	0.72	-	-
Hyp	3.64	1.10	0.37	0.09	0.50	0.21	0.13	0.03	0.15	0.03	0.05	0.01	3.85	0.90	-	-
SupC	3.86	1.65	0.28	0.18	0.70	0.19	0.16	0.04	0.26	0.20	0.05	0.02	3.97	0.93	-	-
InfC	3.03	0.40	0.18	0.02	0.80	0.26	0.17	0.03	0.23	0.02	0.04	0.00	4.46	0.45	-	-
Cer	2.02	1.09	0.65	0.27	0.66	0.18	0.20	0.02	0.04	0.03	0.02	0.01	-	-	-	-

NAc: nucleus accumbens, **CP**: caudate-putamen, **VTA:** ventral tegmental area, **FC:** frontal cortex, **Amy:** amygdala, **Hyp:** hypothalamus, **SupC:** superior colliculus, **InfC:** inferior colliculus, **Cer:** cerebellum, B_{avail} and appK_d are in pmol/ml, K_1 in mL.cm^{-3}.min^{-1}, k_2, k_3, k_{off}, in min^{-1}

Figure legends

Figure 1 TACs extracted from the CP of one multi-injection dynamic SPECT scan, along with 2T-5k model fit and the decomposition of the radioactive signal into the specific and the free binding.

Figure 2 Scatchard plots of the simulation study in the (A) CP (a high-binding VOI) and (B) VTA (a low-binding VOI) for various masses of injected unlabelled ligand. Note that a dose of unlabelled ligand of 3 ng/kg or higher produces a Scatchard plot in both VOI. The dose of 3 ng/kg produces a Scatchard plot with the highest range of C_S/C_{ND} values.

Figure 3 The ratio of radioactivity in the CP (a high-binding VOI) or VTA (a low-binding VOI) to the radioactivity in the Cer (the reference region), as estimated on the basis of a simulated partial saturation experiment. At time-points beyond 70 min post radiotracer injection, this ratio is around 1 in the CP and 0.4 in the VTA. This ratio is relatively temporally stable at the time points employed in the Scatchard plot quantification with the partial saturation approach.

Figure 4 The bias (%), in the B_{avail} and $appK_d$ values in the CP and the VTA, induced by a simulated variation (%) in the specific binding in the Cer (reference region), expressed as a variation in the B_{avail} of this VOI. The B_{avail} estimations in the VTA and the $appK_d$ estimations in both CP and VTA may be considerably biased in case of a variation in the specific binding in the Cer. The B_{avail} in the CP remains virtually unbiased and independent of any variation in the specific binding in the Cer.

Figure 5 The potential impact of fixing the $appK_d$ value in low-binding regions (here the VTA was employed in the simulation study) for the partial saturation quantification. If the “true” $appK_d$ of the VOI differs from the fixed value, a bias is introduced in the B_{avail} value estimation. This bias is virtually linearly proportional to the bias in the fixed $appK_d$ value.

Figure 6 Correlation between the B_{avail} values estimated with the multi-injection approach (horizontal axis) in three rats and the corresponding values estimated with the partial saturation approach (vertical axis).

Figure 7 Parametric images of B_{avail} values, estimated with the partial saturation method on a coronal section including (A) the CP and NAc and a section including (B) midbrain structures, notably the VTA. Color bars describe the B_{avail} values in pmol/ml.

Figure 8 Result of the preliminary study of the effect of a chronic haloperidol treatment on the B_{avail} values in the rat left and right CP.

Figure 9 A SPECT image (coronal, sagittal and axial planes) obtained with (A) [^{123}I]epidepride and (B) [^{123}I]IBZM. The colour scale is in KBq/ml. Note the superior quality of the image obtained from the

[^{123}I]epidepride experiment in terms of a better anatomical delineation of the striatum and the highest binding of the radiotracer (the colour scale of the [^{123}I]epidepride image ranges from 0-10 KBq/ml, while the [^{123}I]IBZM image ranges has a much lower binding, ranging from 0-2.5 KBq/ml).

7. References

Abi-Dargham, A., van de Giessen, E., Slifstein, M., Kegeles, L.S., Laruelle, M., 2009. Baseline and amphetamine-stimulated dopamine activity are related in drug-naive schizophrenic subjects. Biol Psychiatry 65, 1091-1093.

Caravaggio, F., Iwata, Y., Kim, J., Shah, P., Gerretsen, P., Remington, G., Graff-Guerrero, A., 2019. What proportion of striatal D2 receptors are occupied by endogenous dopamine at baseline? A meta-analysis with implications for understanding antipsychotic occupancy. Neuropharmacology.

de Paulis, T., 2003. The discovery of epidepride and its analogs as high-affinity radioligands for imaging extrastriatal dopamine D(2) receptors in human brain. Curr Pharm Des 9, 673-696.

Delforge, J., Bottlaender, M., Loc'h, C., Guenther, I., Fuseau, C., Bendriem, B., Syrota, A., Maziere, B., 1999. Quantitation of extrastriatal D2 receptors using a very high-affinity ligand (FLB 457) and the multi-injection approach. J Cereb Blood Flow Metab 19, 533-546.

Delforge, J., Spelle, L., Bendriem, B., Samson, Y., Bottlaender, M., Papageorgiou, S., Syrota, A., 1996. Quantitation of benzodiazepine receptors in human brain using the partial saturation method. J Nucl Med 37, 5-11.

Delforge, J., Spelle, L., Bendriem, B., Samson, Y., Syrota, A., 1997. Parametric images of benzodiazepine receptor concentration using a partial-saturation injection. J Cereb Blood Flow Metab 17, 343-355.

Delforge, J., Syrota, A., Mazoyer, B.M., 1990. Identifiability analysis and parameter identification of an in vivo ligand-receptor model from PET data. IEEE Trans Biomed Eng 37, 653-661.

Di Paola, R., Bazin, J.P., Aubry, F., Aurengo, A., Cavailloles, F., Herry, J.Y., Kahn, E., 1982. Handling of dynamic sequences in nuclear medicine. IEEE Trans on Nuclear Science NS29, 1310-1321.

Fagerlund, B., Pinborg, L.H., Mortensen, E.L., Friberg, L., Baare, W.F., Gade, A., Svarer, C., Glenthoj, B.Y., 2013. Relationship of frontal D(2/3) binding potentials to cognition: a study of antipsychotic-naive schizophrenia patients. Int J Neuropsychopharmacol 16, 23-36.

Fujita, M., Seibyl, J.P., Verhoeff, N.P., Ichise, M., Baldwin, R.M., Zoghbi, S.S., Burger, C., Staley, J.K., Rajeevan, N., Charney, D.S., Innis, R.B., 1999. Kinetic and equilibrium analyses of [(123)I]epidepride binding to striatal and extrastriatal dopamine D(2) receptors. Synapse 34, 290-304.

Fujita, M., Verhoeff, N.P., Varrone, A., Zoghbi, S.S., Baldwin, R.M., Jatlow, P.A., Anderson, G.M., Seibyl, J.P., Innis, R.B., 2000. Imaging extrastriatal dopamine D(2) receptor occupancy by endogenous dopamine in healthy humans. Eur J Pharmacol 387, 179-188.

Gandelman, M.S., Baldwin, R.M., Zoghbi, S.S., Zea-Ponce, Y., Innis, R.B., 1994. Evaluation of ultrafiltration for the free-fraction determination of single photon emission computed tomography (SPECT) radiotracers: beta-CIT, IBF, and iomazenil. J Pharm Sci 83, 1014-1019.

Ginovart, N., Kapur, S., 2012. Role of dopamine D(2) receptors for antipsychotic activity. Handb Exp Pharmacol, 27-52.

Ginovart, N., Wilson, A.A., Hussey, D., Houle, S., Kapur, S., 2008. D2-Receptor Upregulation is Dependent upon Temporal Course of D2-Occupancy: A Longitudinal [11C]-Raclopride PET Study in Cats. Neuropsychopharmacology 34, 662-671.

Ginovart, N., Wilson, A.A., Meyer, J.H., Hussey, D., Houle, S., 2001. Positron emission tomography quantification of [(11)C]-DASB binding to the human serotonin transporter: modeling strategies. J Cereb Blood Flow Metab 21, 1342-1353.

Glenthoj, B.Y., Mackeprang, T., Svarer, C., Rasmussen, H., Pinborg, L.H., Friberg, L., Baare, W., Hemmingsen, R., Videbaek, C., 2006. Frontal dopamine D(2/3) receptor binding in drug-naive first-episode schizophrenic patients correlates with positive psychotic symptoms and gender. Biol Psychiatry 60, 621-629.

Ichise, M., Fujita, M., Seibyl, J.P., Verhoeff, N.P., Baldwin, R.M., Zoghbi, S.S., Rajeevan, N., Charney, D.S., Innis, R.B., 1999. Graphical analysis and simplified quantification of striatal and extrastriatal dopamine D2 receptor binding with [123I]epidepride SPECT. J Nucl Med 40, 1902-1912.

Innis, R.B., Cunningham, V.J., Delforge, J., Fujita, M., Gjedde, A., Gunn, R.N., Holden, J., Houle, S., Huang, S.C., Ichise, M., Iida, H., Ito, H., Kimura, Y., Koeppe, R.A., Knudsen, G.M., Knuuti, J., Lammertsma, A.A., Laruelle, M., Logan, J., Maguire, R.P., Mintun, M.A., Morris, E.D., Parsey, R., Price, J.C., Slifstein, M., Sossi, V., Suhara, T., Votaw, J.R., Wong, D.F., Carson, R.E., 2007. Consensus nomenclature for in vivo imaging of reversibly binding radioligands. J Cereb Blood Flow Metab 27, 1533-1539.

Kegeles, L.S., Abi-Dargham, A., Frankle, W.G., Gil, R., Cooper, T.B., Slifstein, M., Hwang, D.R., Huang, Y., Haber, S.N., Laruelle, M., 2010. Increased synaptic dopamine function in associative regions of the striatum in schizophrenia. Arch Gen Psychiatry 67, 231-239.
Kegeles, L.S., Slifstein, M., Frankle, W.G., Xu, X., Hackett, E., Bae, S.A., Gonzales, R., Kim, J.H., Alvarez, B., Gil, R., Laruelle, M., Abi-Dargham, A., 2008. Dose-occupancy study of striatal and extrastriatal dopamine D2 receptors by aripiprazole in schizophrenia with PET and [18F]fallypride. Neuropsychopharmacology 33, 3111-3125.
Kessler, R.M., Ansari, M.S., de Paulis, T., Schmidt, D.E., Clanton, J.A., Smith, H.E., Manning, R.G., Gillespie, D., Ebert, M.H., 1991. High affinity dopamine D2 receptor radioligands. 1. Regional rat brain distribution of iodinated benzamides. J Nucl Med 32, 1593-1600.
Kugaya, A., Fujita, M., Innis, R.B., 2000. Applications of SPECT imaging of dopaminergic neurotransmission in neuropsychiatric disorders. Ann Nucl Med 14, 1-9.
Laruelle, M., 2000. Imaging synaptic neurotransmission with in vivo binding competition techniques: a critical review. J Cereb Blood Flow Metab 20, 423-451.
Lehto, S.M., Kuikka, J., Tolmunen, T., Hintikka, J., Viinamaki, H., Vanninen, R., Haatainen, K., Koivumaa-Honkanen, H., Honkalampi, K., Tiihonen, J., 2008. Temporal cortex dopamine D2/3 receptor binding in major depression. Psychiatry Clin Neurosci 62, 345-348.
Lehto, S.M., Kuikka, J., Tolmunen, T., Hintikka, J., Viinamaki, H., Vanninen, R., Koivumaa-Honkanen, H., Honkalampi, K., Tiihonen, J., 2009. Altered hemispheric balance of temporal cortex dopamine D(2/3) receptor binding in major depressive disorder. Psychiatry Res 172, 251.
Leslie, W.D., Abrams, D.N., Greenberg, C.R., Hobson, D., 1996. Comparison of iodine-123-epidepride and iodine-123-IBZM for dopamine D2 receptor imaging. J Nucl Med 37, 1589-1591.
Meikle, S.R., Kench, P., Kassiou, M., Banati, R.B., 2005. Small animal SPECT and its place in the matrix of molecular imaging technologies. Phys Med Biol 50, R45-61.
Millet, P., Delforge, J., Mauguiere, F., Pappata, S., Cinotti, L., Frouin, V., Samson, Y., Bendriem, B., Syrota, A., 1995. Parameter and index images of benzodiazepine receptor concentration in the brain. J Nucl Med 36, 1462-1471.
Millet, P., Graf, C., Moulin, M., Ibanez, V., 2006. SPECT quantification of benzodiazepine receptor concentration using a dual-ligand approach. J Nucl Med 47, 783-792.
Millet, P., Ibanez, V., Delforge, J., Pappata, S., Guimon, J., 2000. Wavelet analysis of dynamic PET data: application to the parametric imaging of benzodiazepine receptor concentration. Neuroimage 11, 458-472.
Millet, P., Moulin, M., Bartoli, A., Del Guerra, A., Ginovart, N., Lemoucheux, L., Buono, S., Fagret, D., Charnay, Y., Ibanez, V., 2008. In vivo quantification of 5-HT1A-[18F]MPPF interactions in rats using the YAP-(S)PET scanner and a beta-microprobe. Neuroimage 41, 823-834.
Millet, P., Moulin-Sallanon, M., Tournier, B.B., Dumas, N., Charnay, Y., Ibanez, V., Ginovart, N., 2012. Quantification of dopamine D(2/3) receptors in rat brain using factor analysis corrected [18F]Fallypride images. Neuroimage 62, 1455-1468.
Mintun, M.A., Raichle, M.E., Kilbourn, M.R., Wooten, G.F., Welch, M.J., 1984. A quantitative model for the in vivo assessment of drug binding sites with positron emission tomography. Ann Neurol 15, 217-227.
Morris, E.D., Yoder, K.K., 2007. Positron emission tomography displacement sensitivity: predicting binding potential change for positron emission tomography tracers based on their kinetic characteristics. J Cereb Blood Flow Metab 27, 606-617.
Murnane, K.S., Howell, L.L., 2011. Neuroimaging and drug taking in primates. Psychopharmacology (Berl) 216, 153-171.
Nørbak-Emig, H., Ebdrup, B.H., Fagerlund, B., Svarer, C., Rasmussen, H., Friberg, L., Allerup, P.N., Rostrup, E., Pinborg, L.H., Glenthøj, B.Y., 2016. Frontal D2/3Receptor Availability in Schizophrenia Patients Before and After Their First Antipsychotic Treatment: Relation to Cognitive Functions and Psychopathology. International Journal of Neuropsychopharmacology 19, pyw006.
Norbak-Emig, H., Pinborg, L.H., Raghava, J.M., Svarer, C., Baare, W.F., Allerup, P., Friberg, L., Rostrup, E., Glenthoj, B., Ebdrup, B.H., 2016. Extrastriatal dopamine D2/3 receptors and cortical grey matter volumes in antipsychotic-naive schizophrenia patients before and after initial antipsychotic treatment. World J Biol Psychiatry, 1-11.
Pandey, S., Venugopal, A., Kant, R., Coleman, R., Mukherjee, J., 2014. (1)(2)(4)I-Epidepride: a PET radiotracer for extended imaging of dopamine D2/D3 receptors. Nucl Med Biol 41, 426-431.
Pinborg, L.H., Videbaek, C., Ziebell, M., Mackeprang, T., Friberg, L., Rasmussen, H., Knudsen, G.M., Glenthoj, B.Y., 2007. [123I]Epidepride binding to cerebellar dopamine D2/D3 receptors is displaceable: Implications for the use of cerebellum as a reference region. Neuroimage 34, 1450-1453.

Schiffer, W.K., Mirrione, M.M., Biegon, A., Alexoff, D.L., Patel, V., Dewey, S.L., 2006. Serial microPET measures of the metabolic reaction to a microdialysis probe implant. J Neurosci Methods 155, 272-284.
Tsartsalis, S., Dumas, N., Tournier, B.B., Pham, T., Moulin-Sallanon, M., Gregoire, M.C., Charnay, Y., Millet, P., 2015. SPECT imaging of glioma with radioiodinated CLINDE: evidence from a mouse GL26 glioma model. EJNMMI Res 5, 9.
Tsartsalis, S., Moulin-Sallanon, M., Dumas, N., Tournier, B.B., Ghezzi, C., Charnay, Y., Ginovart, N., Millet, P., 2014. Quantification of GABAA receptors in the rat brain with [(123)I]Iomazenil SPECT from factor analysis-denoised images. Nucl Med Biol 41, 186-195.
Tsartsalis, S., Tournier, B.B., Aoun, K., Habiby, S., Pandolfo, D., Dimiziani, A., Ginovart, N., Millet, P., 2017. A single-scan protocol for absolute D2/3 receptor quantification with [123I]IBZM SPECT. Neuroimage 147, 461-472.
Tsartsalis, S., Tournier, B.B., Graf, C.E., Ginovart, N., Ibanez, V., Millet, P., 2018. Dynamic image denoising for voxel-wise quantification with Statistical Parametric Mapping in molecular neuroimaging. PLoS One 13, e0203589.
Tuppurainen, H., Kuikka, J., Viinamaki, H., Husso-Saastamoinen, M., Bergstrom, K., Tiihonen, J., 2003. Extrastriatal dopamine D 2/3 receptor density and distribution in drug-naive schizophrenic patients. Mol Psychiatry 8, 453-455.
Tuppurainen, H., Kuikka, J.T., Laakso, M.P., Viinamaki, H., Husso, M., Tiihonen, J., 2006. Midbrain dopamine D2/3 receptor binding in schizophrenia. Eur Arch Psychiatry Clin Neurosci 256, 382-387.
Tuppurainen, H., Kuikka, J.T., Viinamaki, H., Husso, M., Tiihonen, J., 2009. Dopamine D2/3 receptor binding potential and occupancy in midbrain and temporal cortex by haloperidol, olanzapine and clozapine. Psychiatry Clin Neurosci 63, 529-537.
Turrone, P., Remington, G., Kapur, S., Nobrega, J.N., 2003. Differential effects of within-day continuous vs. transient dopamine D2 receptor occupancy in the development of vacuous chewing movements (VCMs) in rats. Neuropsychopharmacology 28, 1433-1439.
Varrone, A., Fujita, M., Verhoeff, N.P., Zoghbi, S.S., Baldwin, R.M., Rajeevan, N., Charney, D.S., Seibyl, J.P., Innis, R.B., 2000. Test-retest reproducibility of extrastriatal dopamine D2 receptor imaging with [123I]epidepride SPECT in humans. J Nucl Med 41, 1343-1351.
Wimberley, C., Angelis, G., Boisson, F., Callaghan, P., Fischer, K., Pichler, B.J., Meikle, S.R., Gregoire, M.C., Reilhac, A., 2014a. Simulation-based optimisation of the PET data processing for Partial Saturation Approach protocols. Neuroimage 97c, 29-40.
Wimberley, C.J., Fischer, K., Reilhac, A., Pichler, B.J., Gregoire, M.C., 2014b. A data driven method for estimation of B and appK using a single injection protocol with [C]raclopride in the mouse. Neuroimage.

Figure 1

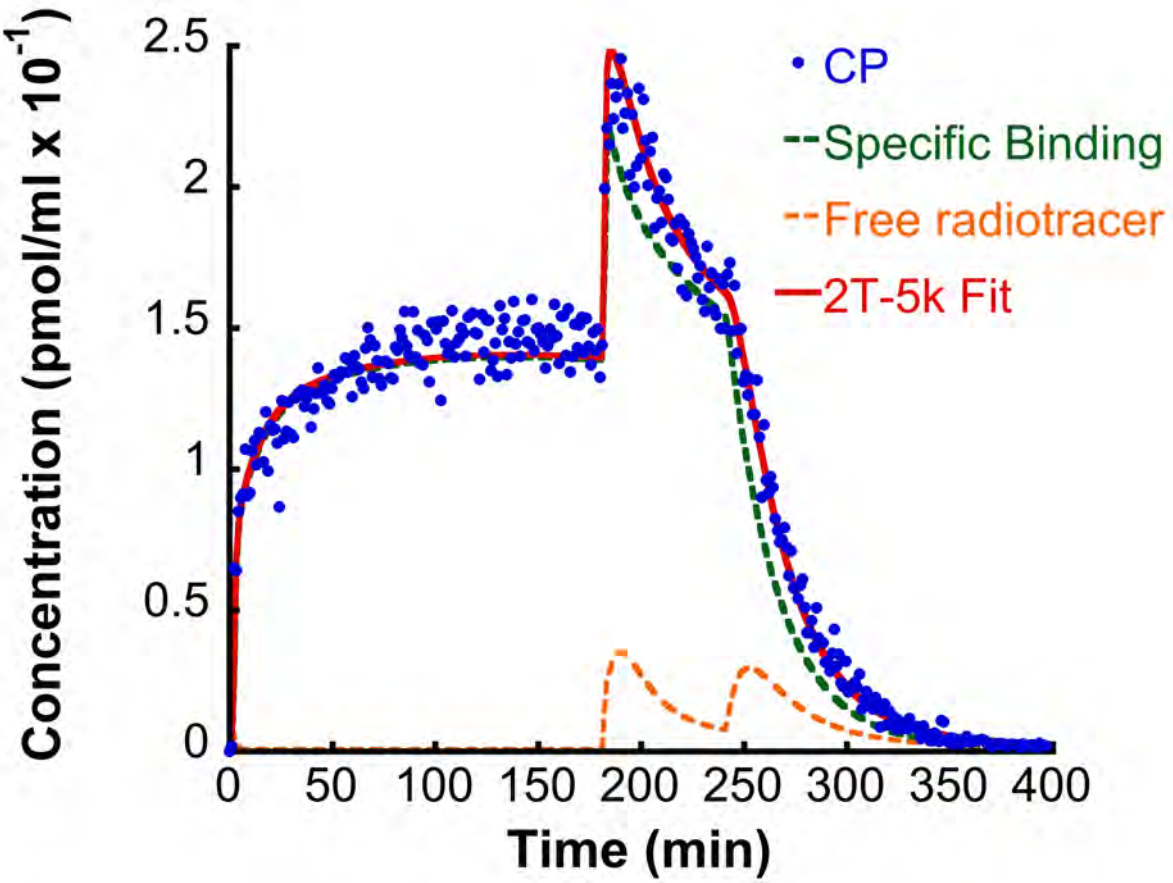
Concentration (pmol/ml x 10^{-1})
2.5
2
1.5
1
0.5
0
0
50
100
150
200
250
300
350
400
Time (min)
CP
Specific Binding
Free radiotracer
2T-5k Fit

Figure 2

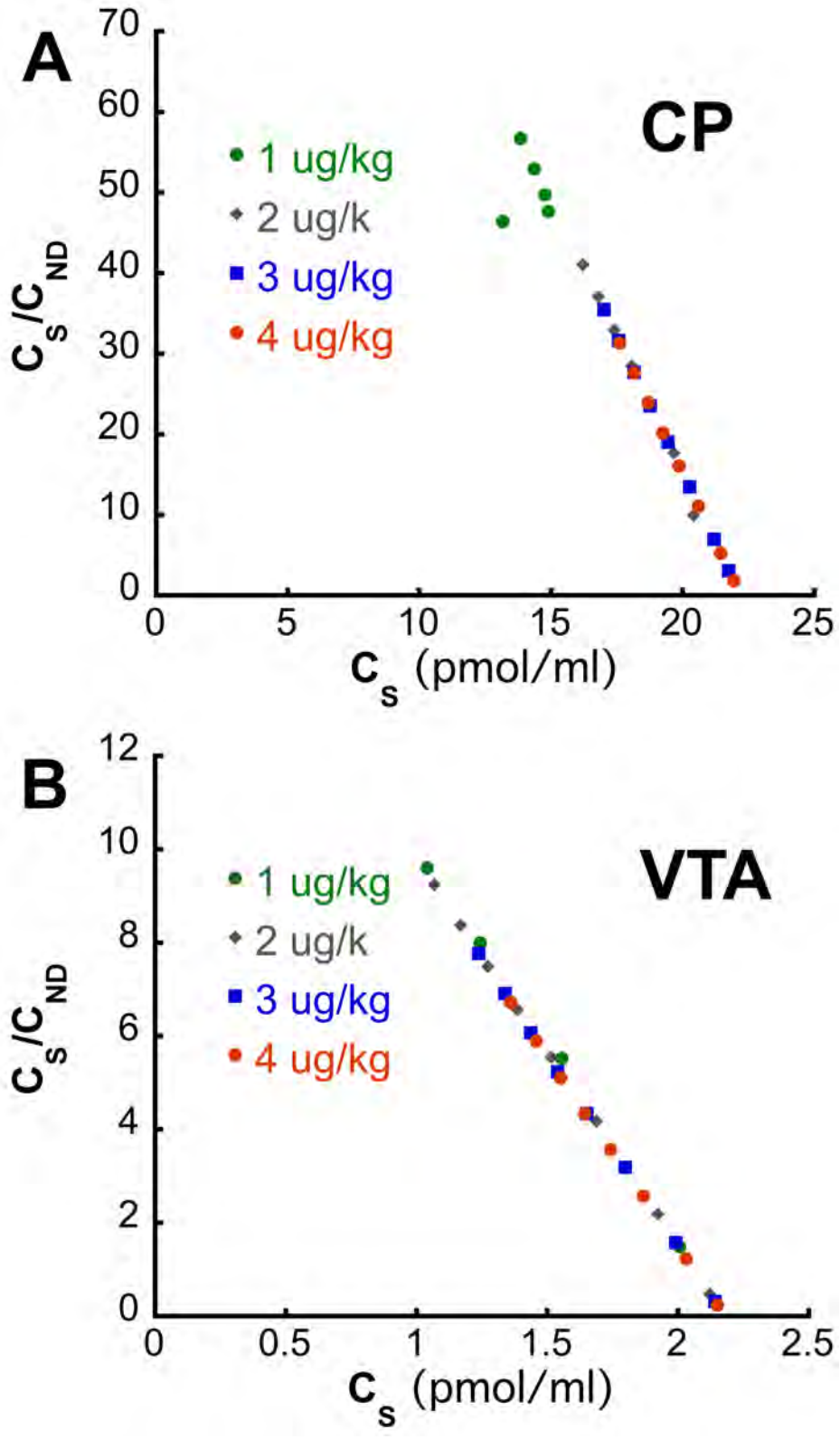
A
CP
1 ug/kg
2 ug/k
3 ug/kg
4 ug/kg
C_s/C_{ND}
C_s (pmol/ml)
0
10
20
30
40
50
60
70
0
5
10
15
20
25
B
VTA
1 ug/kg
2 ug/k
3 ug/kg
4 ug/kg
C_s/C_{ND}
C_s (pmol/ml)
0
2
4
6
8
10
12
0
0.5
1
1.5
2
2.5

Figure 3

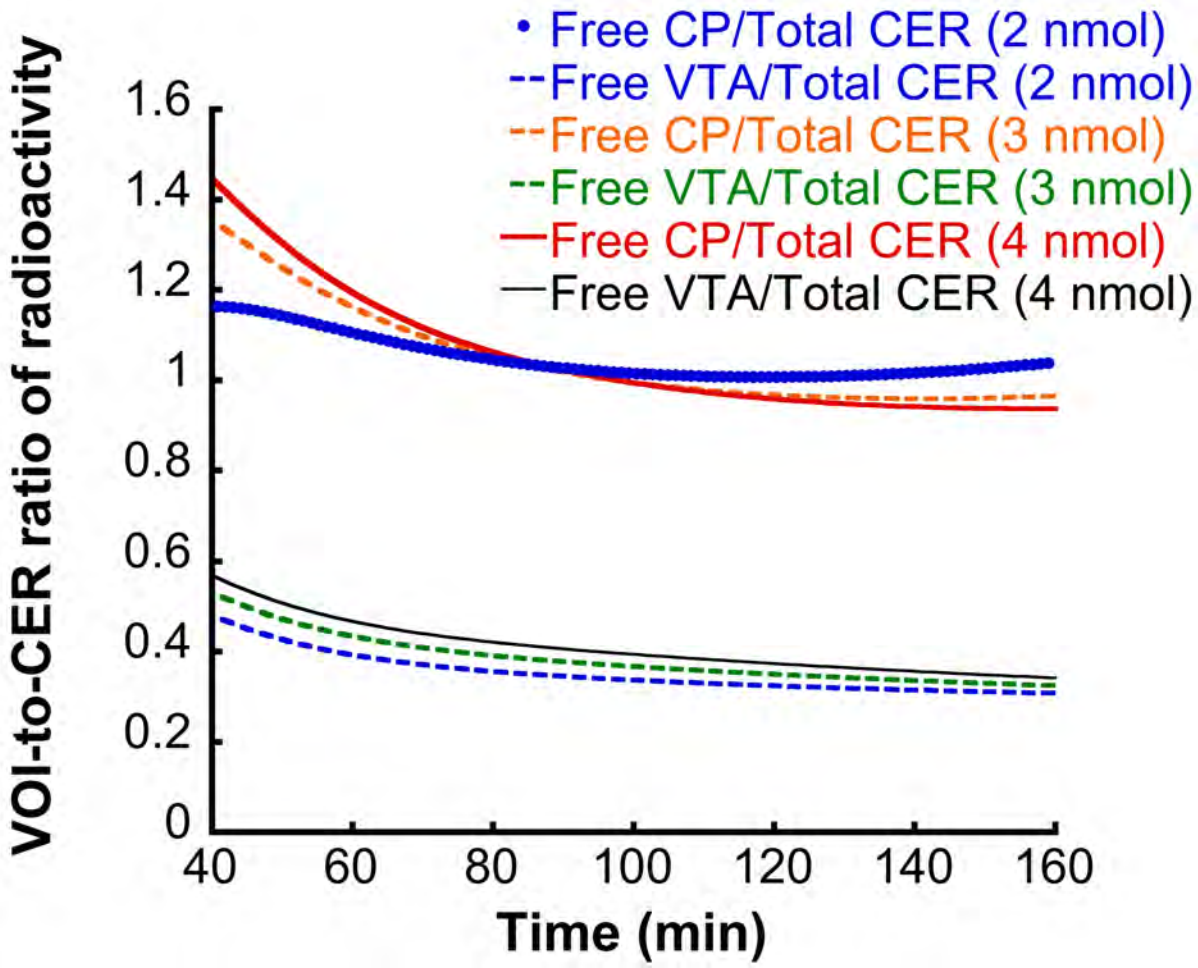
• Free CP/Total CER (2 nmol)
--Free VTA/Total CER (2 nmol)
--Free CP/Total CER (3 nmol)
--Free VTA/Total CER (3 nmol)
—Free CP/Total CER (4 nmol)
—Free VTA/Total CER (4 nmol)
VOI-to-CER ratio of radioactivity
1.6
1.4
1.2
1
0.8
0.6
0.4
0.2
0
40
60
80
100
120
140
160
Time (min)

Figure 4

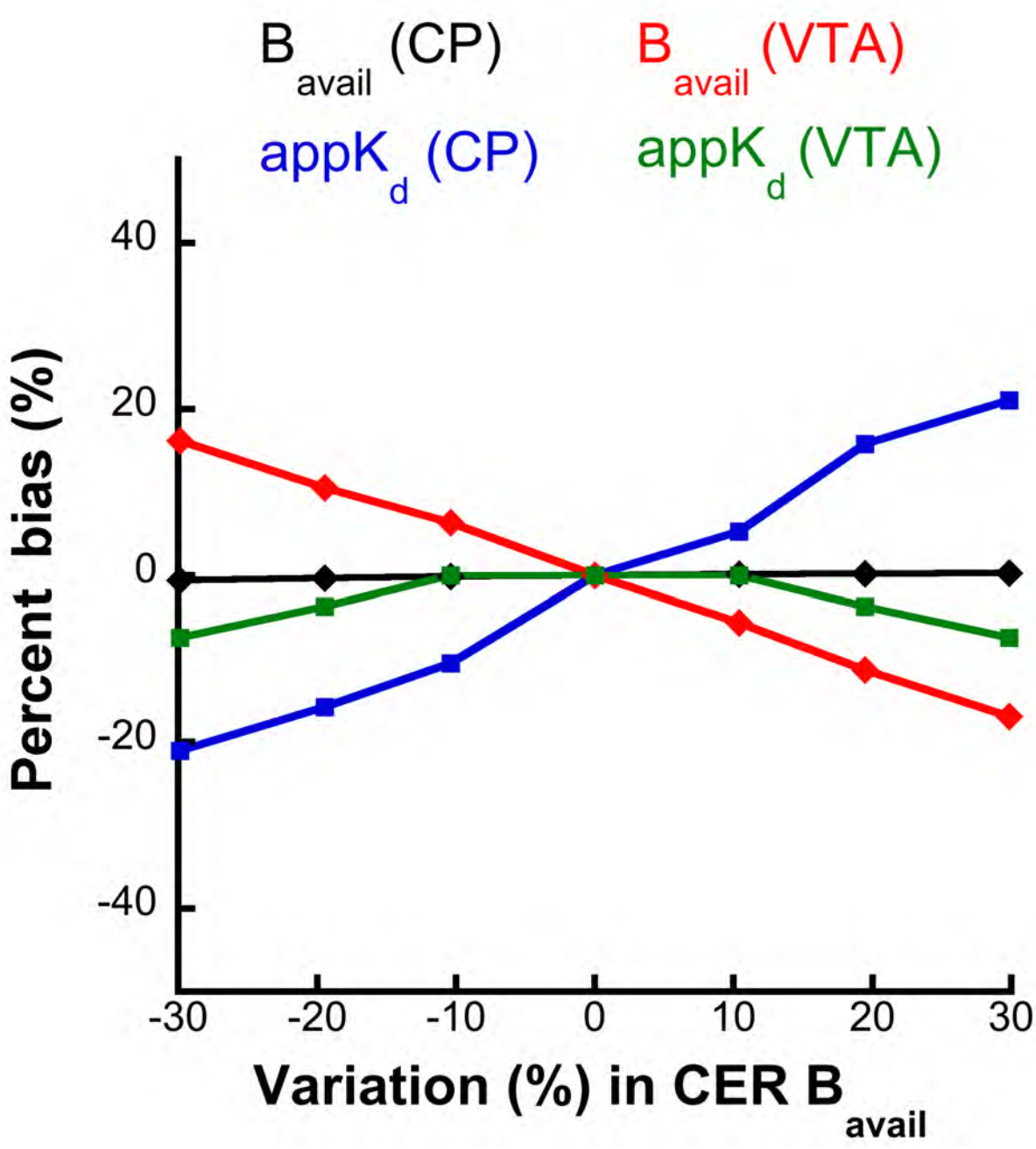
B avail (CP)
B avail (VTA)
appK d (CP)
appK d (VTA)
Percent bias (%)
40
20
0
-20
-40
-30
-20
-10
0
10
20
30
Variation (%) in CER B avail

Figure 5

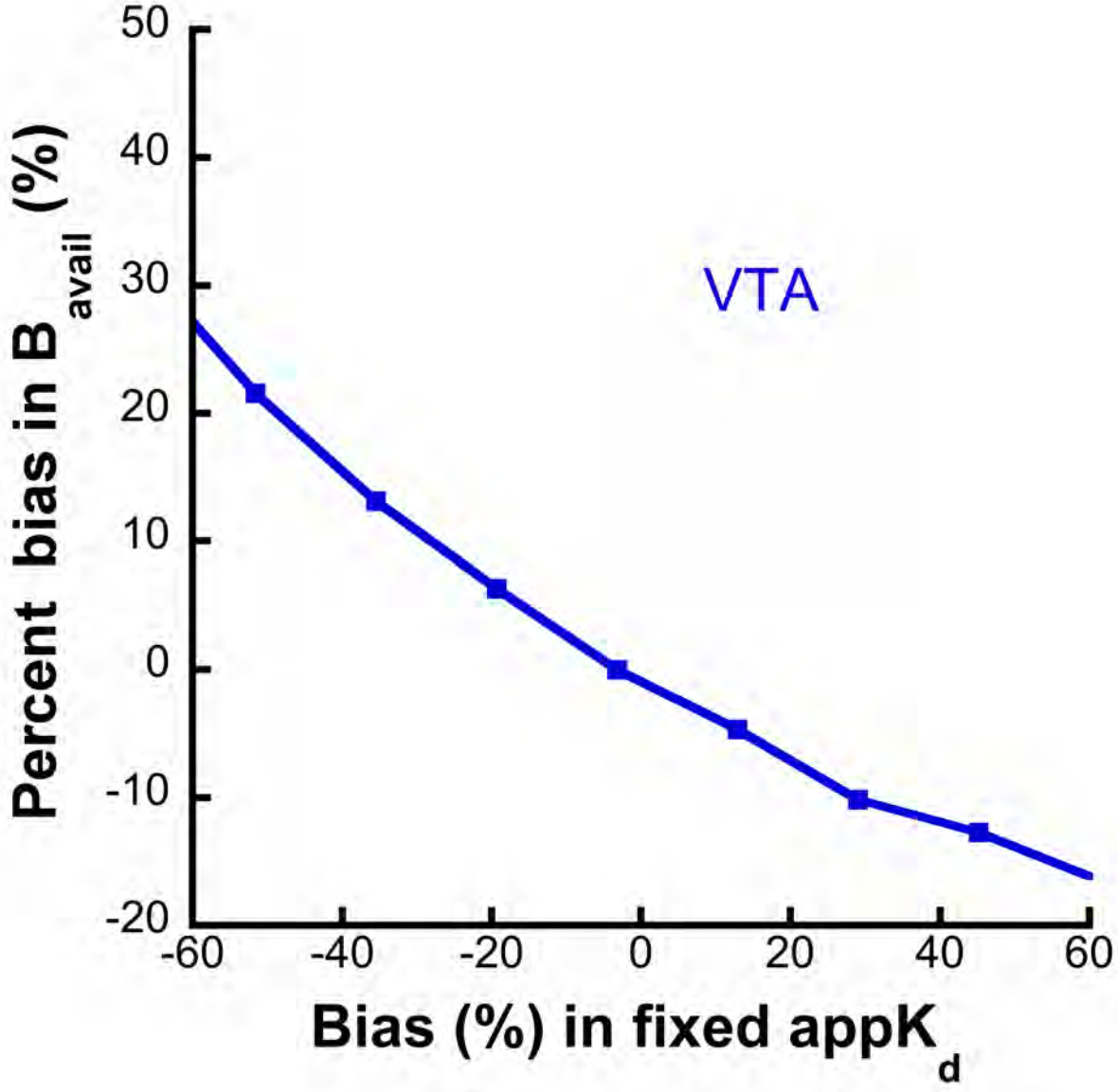
50
40
30
20
10
0
-10
-20
-60
-40
-20
0
20
40
60
Percent bias in B avail (%)
Bias (%) in fixed appK d
VTA

Figure 6

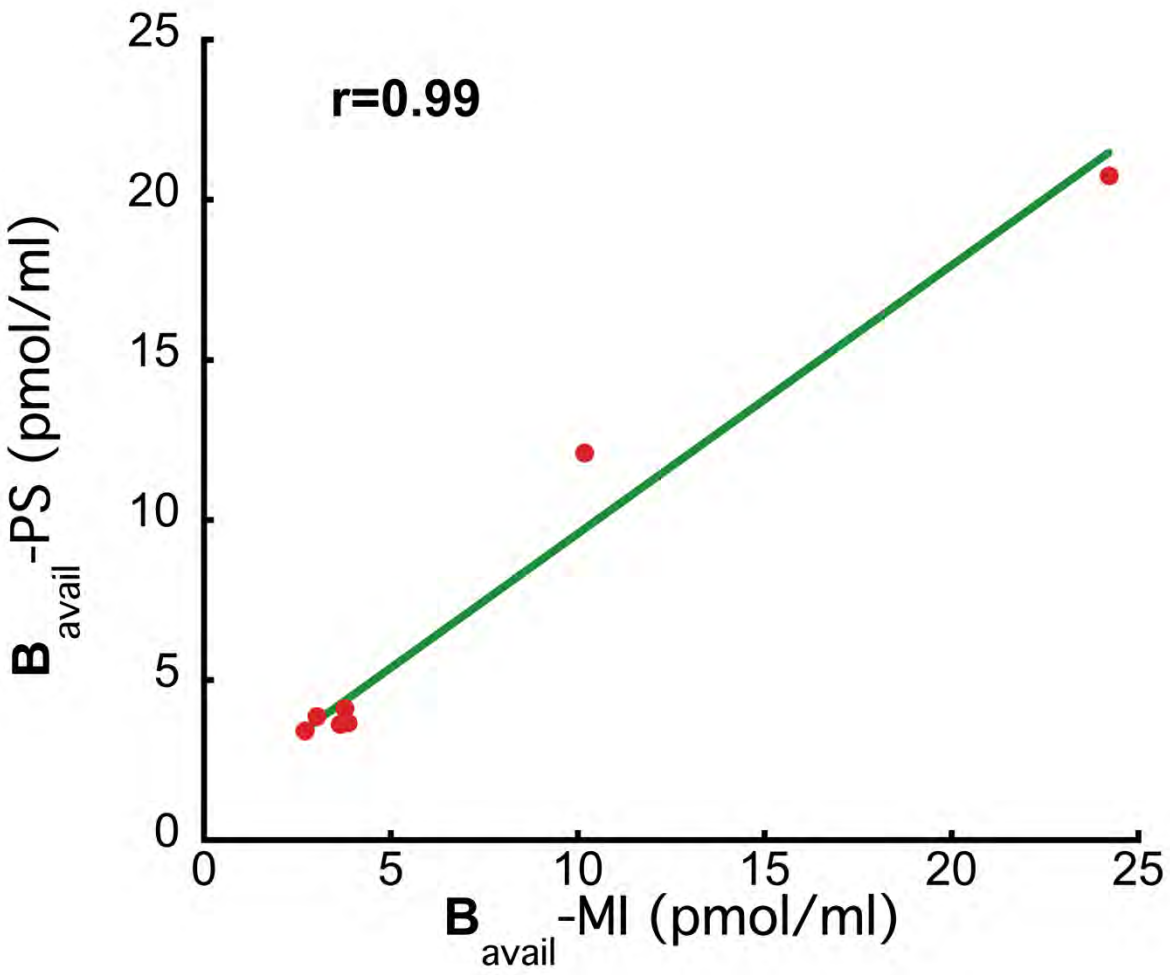

Figure 7

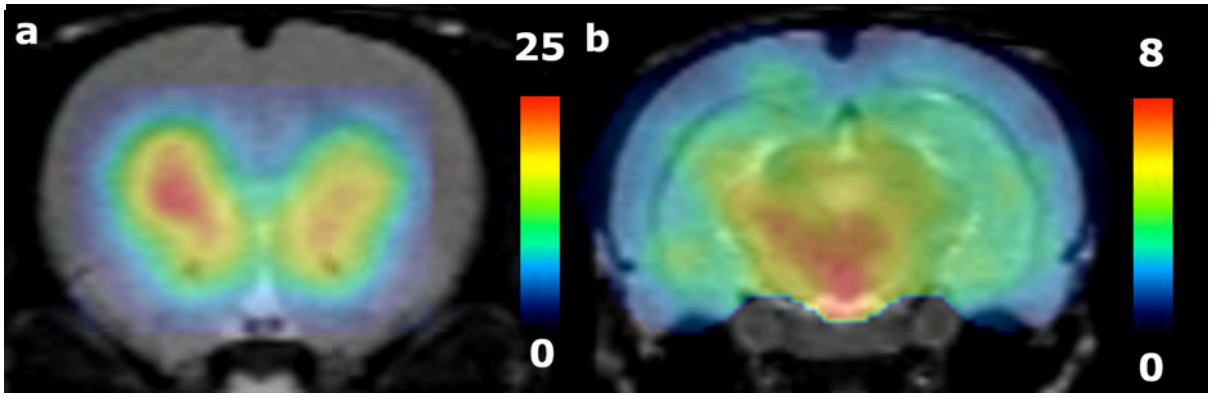

Figure 8

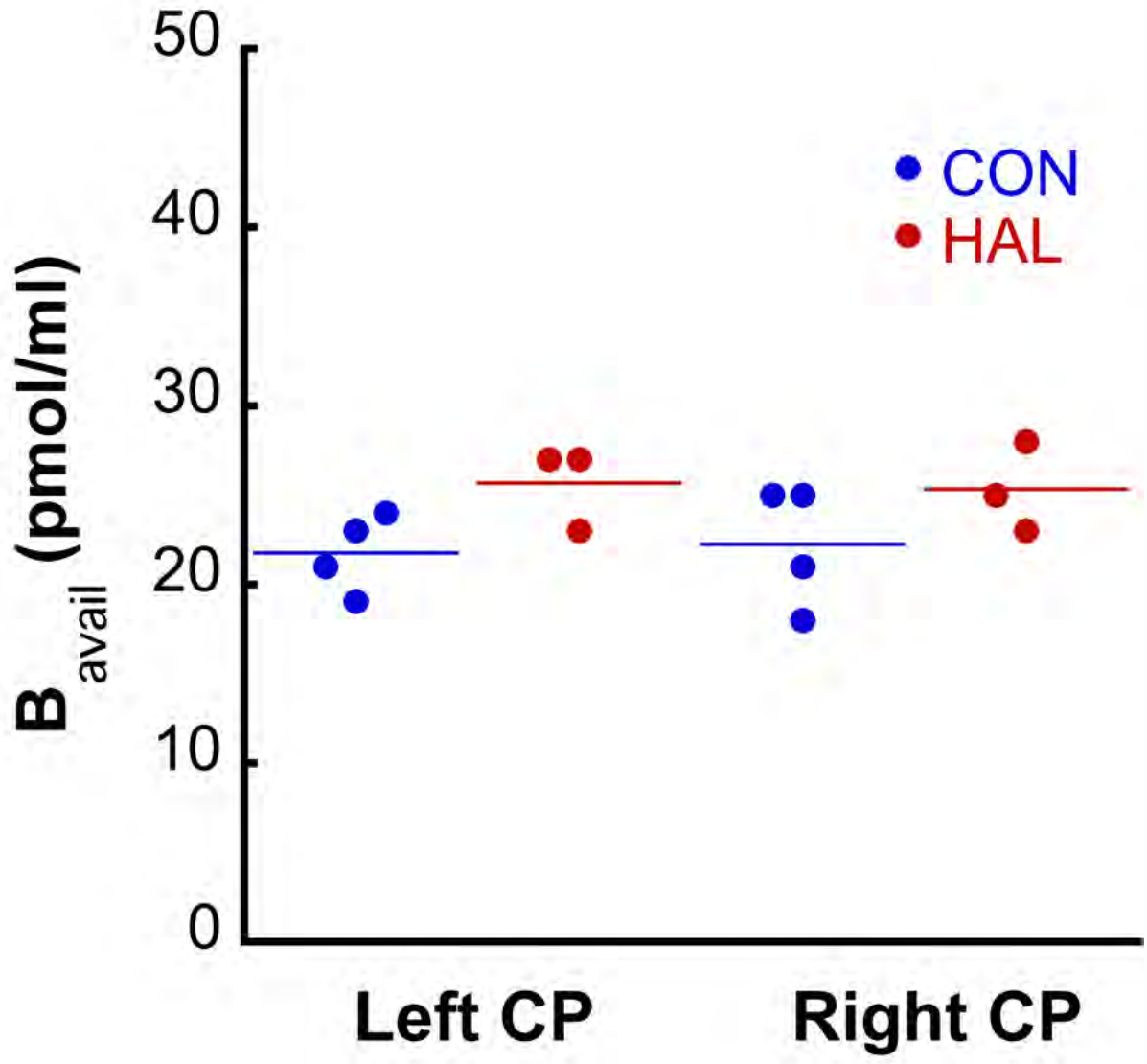

Figure 9

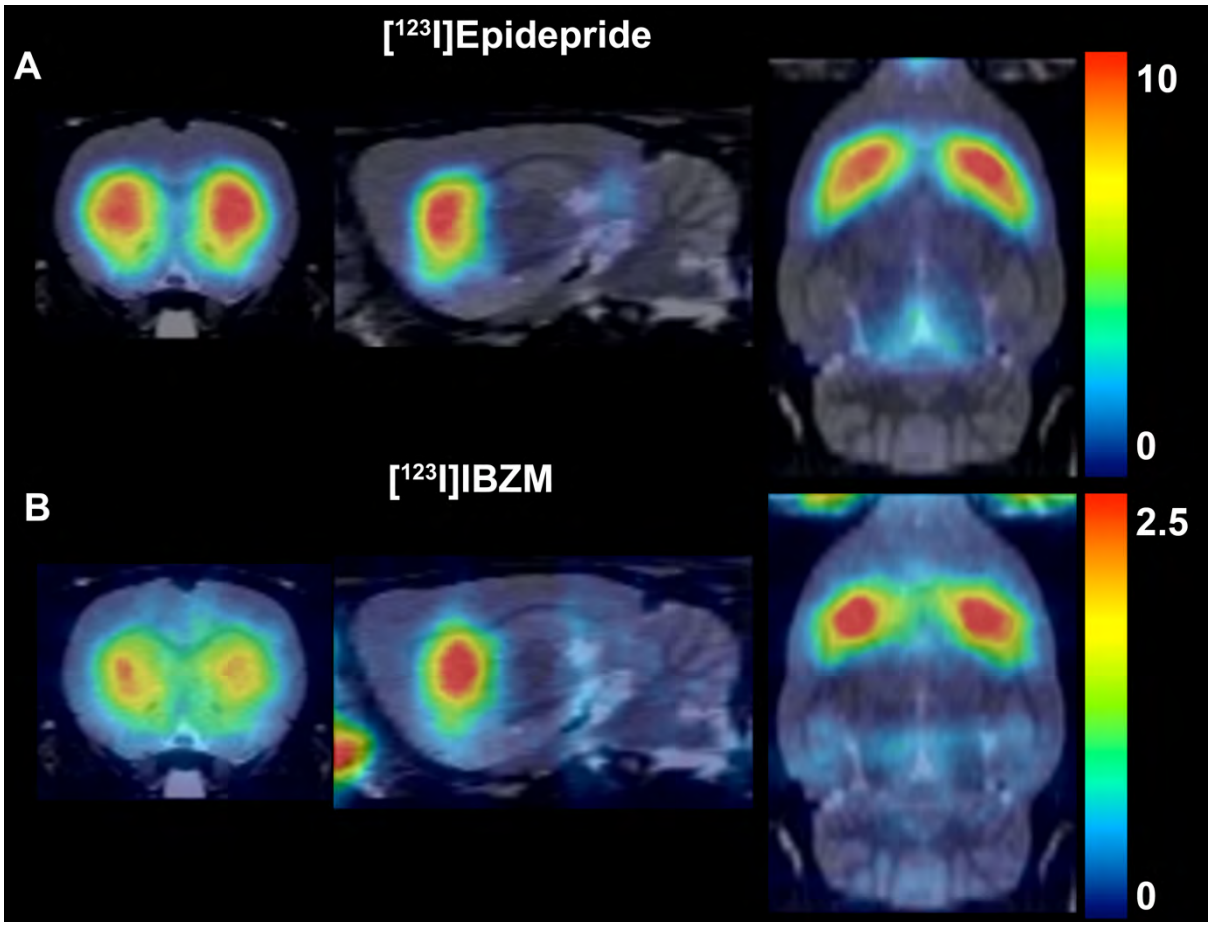

Supplement 1

S1 Supplemental Materials and Methods

S1.1 A preliminary study of the effect of a chronic haloperidol treatment on $D_{2/3}$ B_{avail} and appK_d

To demonstrate the potential of the partial saturation method proposed here, we performed a preliminary, proof-of-concept study of the effect of a chronic haloperidol treatment on the B_{avail} and the appK_d of $D_{2/3}$ receptors in the rat brain. For this purpose, two groups of rats were treated with either haloperidol (1 mg/kg/day, n=4) or vehicle (n=3) for 28 days. A [^{123}I]epidepride SPECT scan using the partial saturation protocol was performed 7 days (a sufficient period for the complete elimination of haloperidol) after the end of the treatment period to assess neurochemical changes with respect to the $D_{2/3}$ receptor. The radioactivity doses that were employed are presented in Table 1 (SPECT_PSA_HAL for haloperidol-treated and SPECT_PSA_CON for control rats). Statistical analysis of the difference in the quantitative parameter values between the groups was performed by means of a two-sample t test.

S1.2 Osmotic minipump preparation and surgery

Haloperidol was purchased from Sigma-Aldrich (Buchs, Switzerland). It was dissolved in dimethyl-sulfoxide (DMSO) 50% v/v in water. Osmotic pumps (Alzet, Durect, Cupertino, CA, USA) were employed to continuously deliver the treatment at a dose of 1 mg/kg/day over 28 days. For the pump implantation, rats were anesthetized with isoflurane (3% for induction and 1-2 % for maintenance). Body temperature was monitored during the scans and maintained at 37±1 °C by means of a thermostatically controlled heating blanket. An incision was performed in the lateral abdominal wall and a pump was subcutaneously implanted. Subcutaneous analgesia (0.02 mg/kg/8h sc; Temgesic, Reckitt Benckiser Pharmaceuticals Inc) was administered right before surgery and was continued *per os* in the drinking water for 48h. For the removal of the osmotic pumps, the same surgical procedure was performed after the end of the treatment period (28 days).

Article 3

Nuclear Medicine and Biology 43 (2016) 81–88

Contents lists available at ScienceDirect

Nuclear Medicine and Biology

journal homepage: www.elsevier.com/locate/nucmedbio

5-HT2A receptor SPECT imaging with [^{123}I]R91150 under P-gp inhibition with tariquidar: More is better?

Stergios Tsartsalis [a,b], Benjamin B. Tournier [a], Trinh Huynh-Gatz [a], Noé Dumas [a], Nathalie Ginovart [a,b], Marcelle Moulin-Sallanon [a,c], Philippe Millet [a,*]

[a] Vulnerability Biomarkers Unit, Division of General Psychiatry, Department of Psychiatry, University Hospitals of Geneva, Switzerland
[b] Department of Psychiatry, University of Geneva, Switzerland
[c] INSERM Unit 1039, J. Fourier University, La Tronche, France

ARTICLE INFO

Article history:
Received 24 June 2015
Received in revised form 18 August 2015
Accepted 5 September 2015

Keywords:
5-HT2A receptors
R91150
Tariquidar
Multi-drug resistance protein
P-glycoprotein
SPECT

ABSTRACT

Introduction: Pharmacological P-glycoprotein (P-gp) inhibition with tariquidar (TQD) is considered a promising strategy for the augmentation of radiotracer brain uptake. However, a region-dependent effect may compromise the robustness of quantitative studies. For this reason, we studied the effect of a TQD pretreatment on 5-HT2A imaging with [^{123}I]R91150 and compared results with those obtained in Mdr1a knock-out (KO) rats.
Methods: Ex vivo autoradiography was performed in TQD (15 mg/kg) pretreated wild-type (WT-TQD), Mdr1a knock-out (KO) and untreated WT rats for Specific Binding Ratio (SBR) estimation. *In vivo* dynamic SPECT imaging with serial arterial blood sampling was performed in the former two groups of rats and kinetic analysis was performed with a one tissue-compartment (1TC) model and the Specific Uptake Ratio (SUR). Results were analyzed statistically using repeated measures ANOVA.
Results: SBR values differed between WT-TQD, Mdr1a KO and WT rats in a region-dependent manner ($p < 0.0001$). *In vivo* brain uptake of radiotracer did not differ between groups. Similarly, kinetic analysis provided distribution volume (V_T) values that did not differ significantly between groups. SUR binding potential (BP_{ND}) values from both groups highly correlated with corresponding V_T ($r = 0.970$, $p < 0.0001$ and $r = 0.962$, $p < 0.0001$, respectively). However, SUR measured over averaged images between 100 and 120 min, using cerebellum as reference region, demonstrated values that were, by average, 2.99 ± 0.53 times higher in the WT-TQD group, with the difference between groups being region-dependent ($p < 0.001$). In addition, coefficient of variation of the SUR BP_{ND} values across brain regions was significantly higher in the WT-TQD rats ($41.25\% \pm 9.63\%$ versus $11.13\% \pm 5.59\%$, $p < 0.0001$).
Conclusion: P-gp inhibition with TQD leads to region-dependent effect in the rat brain, with probably sub-optimal effect in cerebellum. This warrants attention when it is used as a reference region for quantitative studies.

1. Introduction

Nuclear and molecular imaging techniques, namely Positron Emission Tomography (PET) and Single Photon Emission Tomography (SPECT) provide an excellent means of study of functional aspects of the Central Nervous System (CNS) in both physiological and disease states. In these approaches, a molecule that binds to a particular target-receptor in the brain is labeled with a radioactive isotope and injected intravenously. Then, transport across the blood–brain barrier (BBB), mainly by passive diffusion of the radiotracer, permits interaction with the receptor. However, passive diffusion is, in several cases, not the only process governing uptake of molecules by the brain. A family of proteins is involved in active transport of molecules out of the brain, thus hampering nuclear imaging by lowering the concentration of tracer that is available for binding to its target [1,2]. The most prominent member of this protein family, concerning radiotracer kinetics, is the P-glycoprotein (P-gp, or Multi-drug resistance protein, Mdr1). In humans, Mdr1 is expressed in brain capillary endothelium, whereas in rodents two isoforms exist, Mdr1a and Mdr1b, of which only the former is present in brain capillary endothelium, the latter being expressed in brain parenchyma [1].

P-gp activity constitutes a considerable limitation for brain imaging with radiotracers that are its substrates. A multitude of molecules that show promising characteristics when evaluated by preclinical *in vitro* or *ex vivo* imaging show a less-than-optimal pharmacokinetic profile *in vivo* that can range from a low signal-to-noise ratio to a nearly non-detectable radioactivity concentration [3,4]. Furthermore, P-gp activity may vary with respect to disease states (e.g. in epilepsy) and thus, apparent variations of radiotracer binding may actually not reflect brain neurochemistry but merely this modified brain uptake [5]. This has led to the development of strategies to overcome the impact of P-gp

* Corresponding author at: Vulnerability Biomarkers Unit, Division of General Psychiatry, Department of Psychiatry, University Hospitals of Geneva, Chemin du Petit-Bel-Air 2, CH1225, Chêne-Bourg, Switzerland. Tel.: +41 22 305 5376; fax: +41 22 305 5375.
E-mail address: Philippe.Millet@hcuge.ch (P. Millet).

http://dx.doi.org/10.1016/j.nucmedbio.2015.09.003
0969-8051/

activity on PET and SPECT preclinical and clinical imaging with pharmacological inhibition of P-gp. In this context, previous studies have demonstrated the potential of two P-gp inhibitors, cyclosporine A (CsA) [2,6–8] and tariquidar (TQD) [5,9,10] to augment brain uptake of radiotracers and signal-to-noise ratio.

However, translating the aforementioned effects to an amelioration of quantitative measures is not straightforward. Indeed, a number of studies have raised important concerns about the robustness of quantitative measures under P-gp inhibition mainly because the effect of inhibitors is not homogeneous across brain regions, as it has been shown with small animal PET imaging [7,11]. This lack of homogeneity may have an even greater impact when simplified quantification methods are employed, in which radiotracer kinetics in a brain region with negligible specific binding ("reference" region) is used to model the kinetics of radiotracer in arterial plasma [7]. With these simplified methods having gained great popularity, the impact of this heterogeneity could be an obstacle to the widespread use of P-gp inhibition in nuclear neuroimaging.

To date, no study has evaluated the applicability of different quantification approaches after P-gp pretreatment with TQD, a potent P-gp inhibitor [12]. This agent is proposed as an alternative to CsA in neuroreceptor PET and SPECT studies, assuming that a more efficient P-gp inhibition should be homogeneous across brain regions. As a result, an unbiased brain receptor quantification could be performed, in normal as well as in disease states where P-gp activity is already regionally modified [5].

To address this hypothesis, we evaluated the effect of TQD pretreatment on [^{123}I]R91150 *ex vivo* and *in vivo* imaging of 5-HT2A receptors in the rat brain. [^{123}I]R91150 has been employed in human and small-animal SPECT studies, related to schizophrenia and the atypical antipsychotic mechanism of action [3,13–16]. Previous rodent SPECT studies have established the impact of P-gp on the brain kinetics of this particular tracer, which is an almost complete inhibition of its uptake to virtually non-quantifiable concentrations and its reversal by genetic absence of P-gp or pharmacological inhibition with CsA [3,8,17]. In order to have an in-depth evaluation of the effect of TQD, we used full-kinetic modeling and a simplified tissue ratio method to extract quantitative measurements [17]. As the objective of TQD pretreatment is supposed to be a complete inhibition of P-gp, we also employed Mdr1a knock out (Mdr1a KO) as a measure of comparison of inhibition efficiency.

2. Materials and methods

2.1. Animal preparation

Thirteen male Sprague–Dawley rats, (Janvier Laboratories, Le Genet-St-Isle, France) and eight Mdr1a KO rats, weighing 370 to 400 g were used. The repartition of rats into groups is presented in Table 1. Of the Sprague–Dawley rats, four were employed in [^{123}I]R91150 U-SPECT-II scans (miLabs, Utrecht, Netherlands) and four in *ex vivo* autoradiography under prior TQD treatment (hereof, WT-TQD group). Four rats did not receive any prior treatment (WT group) and were employed in *ex vivo* autoradiography. Given the absence of any quantifiable SPECT signal (see Results section) in untreated WT rats, only one rat of this group was employed in a [^{123}I]R91150 SPECT experiment for demonstrative reasons. Of the Mdr1a KO rats, four were employed in SPECT scan experiments and four in *ex vivo* autoradiography. In the rats that underwent SPECT scans (n = 9), one polyethylene catheter (i.d. = 0.58 mm, o.d = 0.96 mm) was inserted into the left femoral vein for radiotracer injection and one in the left femoral artery for blood sampling. SPECT scans were performed under isoflurane anesthesia (4% for induction, 2,5% for maintenance). Body temperature was maintained at 37 ± 1 °C by means of a thermostatically controlled heating blanket. In rats that only underwent autoradiography experiments (n = 12), a 24G catheter was inserted in the tail vein for radiotracer injection.

All experimental procedures were performed in accordance with the Swiss Federal Law on animal care under a protocol approved by the Ethical Committee on Animal Experimentation of the Canton of Geneva, Switzerland.

2.2. Radiotracer preparation

^{123}I radioiodide was purchased from GE Healthcare (Eindhoven, the Netherlands). TQD was purchased from Toronto Research Chemicals (Toronto, Canada). All other chemicals were purchased from Sigma-Aldrich (Buchs, Switzerland) with the highest purity available. R91150 precursor preparation was described elsewhere [3]. For radiolabeling, 300 μg of R91150 precursor in 3 μL ethanol was mixed with 3 μL of glacial acetic acid, 15 μL of carrier-free ^{123}I sodium iodide (10 mCi) in 0.05 M NaOH, and 3 μL of 30% H_2O_2. [^{123}I]R91150 was isolated by an isocratic HPLC run (ACN/water 50/50, 10 mM acetic acid buffer pH 5) with a reversed-phase column (Bondclone C18 10 μm 300 × 7.8 mm, Phenomenex, Schlieren, Switzerland) at a flow rate of 3 mL/min. The radiotracer retention time was 11.0 min. Radiochemical purity, assessed by HPLC, was above 98% [3].

2.3. SPECT imaging, arterial plasma analysis and free parent radiotracer fraction estimation

Four WT-TQD, four Mdr1a KO and one WT rat were employed in this experiment. WT-TQD rats were pre-treated with TQD (15 mg/kg, i.v.), 30 min before radiotracer injection. SPECT scanning experimental protocol included a bolus injection of radiotracer at a volume of 0.6 ml over a 1-min period using an infusion pump. Specific activity of radiotracer at the time of injection was 94.79 ± 26.61 GBq/μmol. A 120 × 1-min frame acquisition was initiated upon radiotracer injection. SPECT image reconstruction was performed using a pixel ordered subsets expectation maximization (P-OSEM, 0.4 mm voxels, 4 iterations, 6 subsets) algorithm using miLabs image reconstruction software. Radioactive decay correction was performed while correction for attenuation or scatter was not.

During SPECT acquisitions, 15 arterial blood samples (corresponding to a plasma volume of 25 μl each) were withdrawn at regular time intervals and immediately centrifuged for 5 min. Radioactivity was measures by means of a gamma counting system and expressed in kBq/ml after calibration. For kinetic analysis of *in vivo* SPECT experiments, only whole-blood radioactivity was measured individually.

For the metabolite and protein-bound fraction correction, the results of a previous work of our group were employed [17]. The mean percentage of non-metabolized [^{123}I]R91150 in plasma (P_{nm}) was fitted using a tri-exponential model to obtain the following A_n and B_n parameters: $P_{nm}(t) = A_1.e^{-B1.t} + A_2.e^{-B2.t} + A_3.e^{-B3.t}$. In order to estimate jointly the model parameters and the metabolite correction model, a coupled fitting procedure was used to adjust the mean metabolite parameters,

Table 1
Repartition of rats into experimental groups.

Rat group	Treatment	n	Experiment	Outcome measures
WT	–	4	*Ex-vivo autoradiography*	SBR
		1	SPECT scan	–
WT-TQD	TQD, 15 mg/kg, i.v.	4	*Ex-vivo autoradiography*	SBR
		4	SPECT scan	Brain and plasma radioactivity AUC, V_T, K_1, k_2, BP_{ND}
Mdr1a KO	–	4	*Ex-vivo autoradiography*	SBR
		4	SPECT scan	Brain and plasma radioactivity AUC, V_T, K_1, k_2, BP_{ND}

as described by Millet et al. [18]. Mean parameter estimates were: $A_1 = 0.4002$; $B_1 = 1.049$; $A_2 = 0.2529$; $B_2 = 0.2135$; $A_3 = 0.4131$; $B_3 = 0.0003295$. The free tracer plasmatic fraction (f_p) was 97% ± 3%. The free and metabolite-corrected plasmatic input function (C_p) was obtained by multiplying the total plasmatic activity (C_{Total}) with the non-metabolized fraction (P_{nm}) and the free fraction (f_p).

2.4. Ex vivo autoradiography

Four WT-TQD, four Mdr1a KO and four WT rats were employed in this experiment. As in the *in vivo* SPECT imaging experiments, WT-TQD rats were pre-treated with TQD (15 mg/kg), 30 min before radiotracer injection. Under isoflurane anesthesia, rats were injected with 11.45 ± 0.48 MBq of radiotracer and sacrificed by decapitation 120 min later. Brains were removed and frozen in precooled isopentane at −20 °C and cut into 20 μm-thick sections that were exposed – along with a standard of a range of radioactivity concentrations – to phosphor imaging plates overnight (Fuji Photo Film Co., Tokyo, Japan). Finally, the plates were scanned with a Fuji Bio-Imaging Analyzer BAS 1800II scanner (Fuji Photo Film Co.), at 50 μm resolution, to obtain the *ex vivo* autoradiograms. Acetylcholinesterase immunohistochemistry of brain sections was performed to better delineate regions-of-interest (ROIs) [19]. Regional quantification of specific binding ratios (SBRs) was performed using AIDA software as follows: (Activity in ROIs)/(Activity in Cerebellum) − 1.

2.5. Data analysis

SPECT images were processed using PMOD software (version 3.6, 2014, PMOD Technologies Ltd, Zurich, Switzerland). Manual co-registration to a rat MRI and volume-of-interest (VOI) template, incorporated in PMOD [20], was performed using averaged images of frames corresponding to the last 60 min of SPECT scan data. Co-registration parameters were then applied to dynamic images and time–activity curves (TACs) were generated. Area under the curve (AUC) for time points corresponding to the first 60 min of SPECT experiments was calculated on injected dose-normalized TACs and metabolite-corrected plasma radioactivity curves, using Matlab (R2011a, Mathworks Inc, USA). The ratio of brain-to-plasma AUC for each VOI was employed as an index of brain uptake of radioactivity. PMOD was employed for regional analysis under different pharmacokinetic model configurations for distribution volume (V_T) estimation [21]: (1) a one and two tissue-compartment model (1TC), (2) a specific uptake ratio (SUR) method, previously validated for analysis in Mdr1a KO rats [17]. BP_{ND} is obtained by dividing the averaged activity in each VOI, between the 100th and 120th min of SPECT scan with the corresponding activity in cerebellum minus one [17]. To validate the employment of this particular time window for SUR analysis in WT-TQD rats we estimated the parameter over different time windows (20 min long each) and compared to V_T parameter values deriving from the same animal by means of regression analysis.

2.6. Statistical analysis

Statistical analysis was performed with Statistica software v.12 (Statsoft, Inc., USA). Linear regression analysis, Student's t-test and repeated measures ANOVA (rmANOVA, using "group" as between-subject independent variable and "ROI" or "VOI" as within-subject independent variable) were employed to compare SBR values obtained from autoradiography and kinetic parameters (V_T, K_1, k_2, BP_{ND} and coefficients of variation, COVs) obtained from *in vivo* experiments over the different groups of rats. Significance level was set at $p < 0.05$.

3. Results

Representative SPECT images, averaged over frames corresponding to the last 60 min of the scans, from a WT-TQD, an Mdr1a KO and a WT rat are presented in Fig. 1. [^{123}I]R91150 brain binding follows the same pattern in WT-TQD and Mdr1a KO rats: frontal cortical regions present the highest binding while posterior cortical and subcortical regions the lowest. An example of %ID/cc TACs for two VOIs (orbitofrontal cortex and cerebellum) is presented in Fig. 2. Radiotracer uptake, in terms of brain-to-plasma radioactivity AUC did not differ between groups ($p > 0.05$).

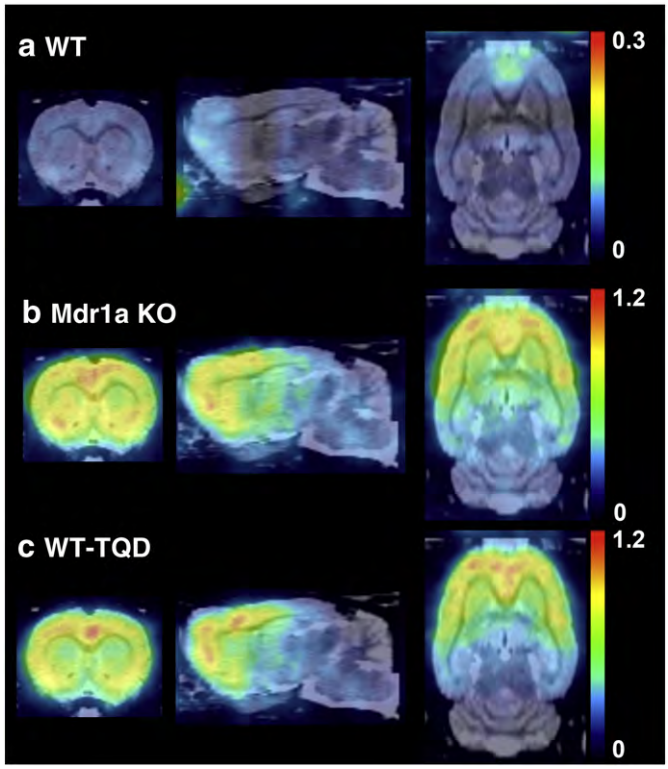

Fig. 1. Averaged frames of SPECT images (coronal, sagittal and axial planes), corresponding to 60–120 min post radiotracer injection from: (a) an untreated WT, (b) an Mdr1a KO and (c) a TQD-treated WT rat. Color bars represent % ID/cc values.

The 1TC provided excellent fits to the data. Results of kinetic analysis of dynamic SPECT scans are presented in detail in Table 2. Average V_T values were found between 167.11 ± 76.29 in orbitofrontal cortex and 17.90 ± 5.30 in cerebellum for WT-TQD rats, while in Mdr1a KO it ranged from 239.91 ± 132.54 to 36.17 ± 9.35, respectively. rmANOVA failed to demonstrate any significant difference between WT-TQD and Mdr1a KO rats. Regarding K_1, they were found between 1.58 ± 1.02 in thalamus and 0.71 ± 0.43 in visual cortex for WT-TQD rats and between 1.58 ± 0.13 in superior colliculus and 1.02 ± 0.08 in auditory cortex for Mdr1a KO. A brain region-dependent difference between the values of the two groups was indicated by rmANOVA ($p < 0.01$), but there was no VOI-wise difference. Similarly, k_2 values were found between 0.071 ± 0.025 in cerebellum and 0.005 ± 0.002 in motor and orbitofrontal cortex for WT-TQD rats and between 0.037 ± 0.009 in cerebellum and 0.006 ± 0.002 in orbitofrontal cortex for Mdr1a KO. They differed between WT-TQD and Mdr1a KO rats in a region-dependent manner ($p < 0.001$). *Post hoc* analysis shows a highly significant difference notably with respect to the k_2 value in the cerebellum ($p < 0.0001$) that was 1.92-fold higher in the former group of rats. A marginally significant difference was also observed in thalamus ($p < 0.05$), in which values were 0.027 ± 0.006 and 0.019 ± 0.003, respectively. Concerning the 2TC model, it failed to provide better fits to the data than the 1TC. In addition, it was associated to remarkably high standard errors (thus, low identifiability) of kinetic parameters reaching, or often exceeding 100% of the parameter value. As a result, 2TC was not further employed in our study.

The SUR method (Fig. 3) resulted in BP_{ND} values that vary from 11.46 ± 3.33 in the motor cortex to 2.16 ± 0.66 in the Superior

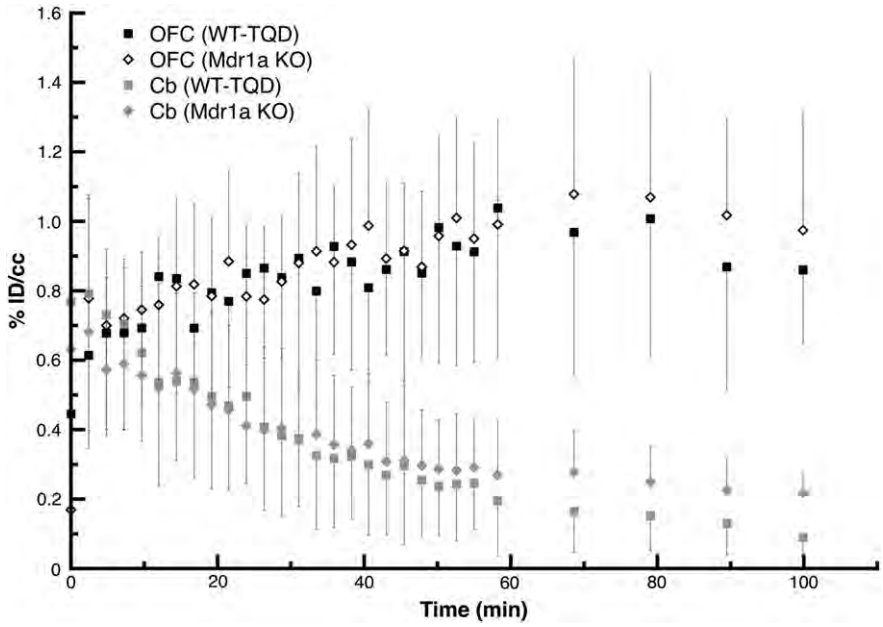

Fig. 2. Average (and standard deviations) TACs (in %ID/cc) extracted from the orbitofrontal cortex (OFC) and the cerebellum (Cb), from Mdr1a KO and WT-TQD rats.

Colliculus in the WT-TQD group. Their Mdr1a KO rat-derived counterparts ranged from 3.66 ± 0.33 to 0.99 ± 0.02, respectively. These values from both groups of rats almost perfectly correlate with the respective V_T values obtained with the 1TC ($r = 0.970$, $p < 0.0001$ and $r = 0.962$, $p < 0.0001$, respectively). However, differences in rmANOVA analysis proved to be highly significant with respect not only to main effect of factors "group" ($p < 0.01$) and "VOI" ($p < 0.0001$) but also to their interaction ($p < 0.0001$), meaning that differences between WT-TQD and Mdr1a KO rats are not homogeneous across VOI. A pattern of diminishing magnitude of BP_{ND} between the two groups of rats from high- to low-binding areas was observed, as shown in Fig. 3. *Post hoc* analysis supported the existence of this pattern as it demonstrated that differences between the two groups of rats are more marked in VOI corresponding to frontal cerebral regions (orbitofrontal, auditory, cingulate, motor and somatosensory cortex as well as in nucleus accumbens and caudate nucleus-putamen, $p < 0.001$ for all comparisons), being on average 3.43 ± 0.36 times higher in WT-TQD rats, with differences in more posterior VOI (visual cortex, hippocampi, hypothalamus, thalamus) not attaining significance. Nevertheless, SUR BP_{ND} values correlated highly between the two groups ($r = 0.964$, $p < 0.0001$).

We also compared the percent COV of average V_T and BP_{ND} values across the different rats by means of Student's t-test. COV of V_T values varied from 19.93% to 45.29% across VOI in the WT-TQD group while, in the Mdr1a KO rats, they were found between 19.15% and 55.25%. The average values were 35.32% ± 8.86% in the former and 29.92% ± 9.81% for the latter group, a difference that failed to show statistical significance in the t-test. Concerning SUR BP_{ND} values, the associated COVs were between 29.08% and 54.40% in the WT-TQD group and between 2.57% and 20.43% in the Mdr1a KO group. Here, the average values were significantly higher; 41.25% ± 9.63% in the WT-TQD group compared with the average COV values in the Mdr1a KO rats that were 11.13% ± 5.59% ($p < 0.0001$).

SBR values obtained from the quantitative analysis of *ex vivo* autoradiography experiments from the three groups of rats (WT, WT-TQD and Mdr1a KO) are included in Fig. 4. rmANOVA analysis revealed a region-dependent difference between the three groups ($p < 0.0001$). VOI-wise *post hoc* analysis of the effects of the different levels of the main factor "group" showed that average SBR values obtained from Mdr1a KO rats are significantly higher than the corresponding values from WT rats ($p < 0.05$) in the nucleus accumbens, orbitofrontal, motor, somatosensory

Table 2
Mean and standard deviations of 1TC parameter estimates obtained from 8 experimental subjects.

VOI[a]	WT-TQD-treated rats						Mdr1a KO rats					
	$V_{T\text{-}1TC}$	±SD	K_1	±SD	k_2	±SD	$V_{T\text{-}1TC}$	±SD	K1	±SD	k_2	±SD
Acb	120	26	1.15	0.50	0.009	0.002	134	49	1.35	0.15	0.011	0.002
CPu	104	37	1.35	0.71	0.013	0.003	127	39	1.36	0.14	0.011	0.002
OFC	167	76	0.84	0.49	0.005	0.002	240	133	1.30	0.14	0.006	0.002
AudC	64	33	0.82	0.50	0.013	0.002	78	17	0.96	0.07	0.013	0.002
CgC	159	43	1.13	0.56	0.007	0.002	179	71	1.34	0.16	0.008	0.002
MC	150	39	0.81	0.50	0.005	0.002	171	70	1.20	0.05	0.008	0.002
SSC	126	63	1.01	0.69	0.008	0.002	128	40	1.16	0.11	0.010	0.002
VsC	44	21	0.71	0.43	0.016	0.002	68	19	1.02	0.08	0.016	0.002
dHip	55	24	0.97	0.55	0.020	0.004	82	17	1.24	0.17	0.016	0.002
vHip	51	27	1.05	0.64	0.019	0.005	80	20	1.31	0.20	0.016	0.003
Hyp	57	28	1.26	0.73	0.022	0.004	81	21	1.49	0.19	0.019	0.003
ColSup	38	17	1.26	0.73	0.032	0.005	66	18	1.58	0.13	0.025	0.006
VTA	44	19	1.18	0.65	0.026	0.006	71	14	1.43	0.18	0.021	0.003
Thal	56	28	1.58	1.02	0.027	0.006	81	16	1.53	0.17	0.019	0.003
Cb	18	5	1.35	0.87	0.071	0.025	36	9	1.26	0.12	0.037	0.009

Acb: nucleus accumbens, CPu: caudate-putamen, OFC: orbitofrontal cortex, AudC: auditory cortex, CgC: cingulate gyrus, MC: motor cortex, SSC: somatosensory cortex, VsC: visual cortex, dHip: dorsal hippocampus, vHip: ventral hippocampus, Hyp: hypothalamus, ColSup: superior colliculus, VTA: ventral tegmental area, Thal: thalamus, Cb: cerebellum.

[a] Values refer to the mean of both left and right VOIs.

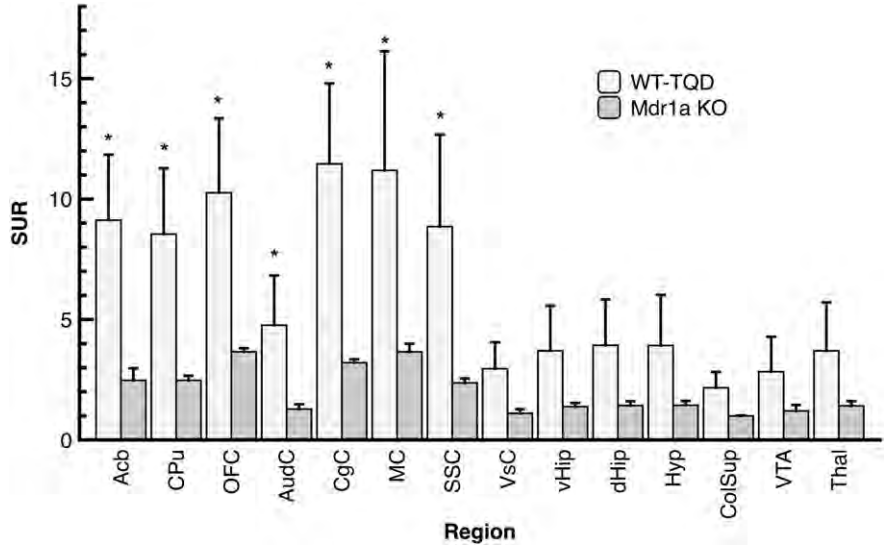

Fig. 3. Histogram (mean and standard deviations) of regional variation of SUR BP_{ND} values from WT-TQD and Mdr1a KO rats. *$p < 0.001$ compared to Mdr1a KO.

and visual cortex, as presented in Fig. 4. SBR of WT-TQD rats is significantly higher than that of WT rats ($p < 0.01$) in all aforementioned regions, as well as in the auditory and cingulate cortex. In these two particular regions, the SBR values of WT-TQD rats are significantly higher than those of Mdr1a KO rats ($p < 0.05$). Correlations between results in these three groups are high ($r = 0.962$ and 0.979, respectively, $p < 0.0001$ for both comparisons), as presented in Fig. 5.

4. Discussion

A wide number of radiotracers show compromised brain uptake because of P-gp-mediated tracer efflux. Therefore, the incorporation of P-gp inhibition in *in vivo* imaging protocols has been proposed. Human and small animal studies have demonstrated the benefits of this approach in terms of amelioration of signal-to-noise ratio that renders signal quantification more feasible with potential benefits on kinetic parameter identifiability and statistical analysis of data [2,7,10,11,22]. This is of particular importance, especially for small animal imaging, given that P-gp has a higher impact on rodent brain pharmacokinetics, compared to human [23]. In fact, with the development of high-resolution dedicated rodent PET and SPECT scanners, preclinical studies have gained popularity for the initial evaluation of novel radiotracers and as a powerful tool in translational biomedical research [24]. So, a radiotracer may show excellent *in vitro* affinity profile, with highly specific receptor binding while *in vivo* imaging results are disappointing, because of a minimal brain uptake, a limitation that could be reversed with P-gp inhibition [3]. Another benefit from P-gp inhibition would be the neutralization of the effect of P-gp activity variations in disease states, such as epilepsy and Alzheimer's disease [1,5], this being very important from a biological point of view. Indeed, in radiotracer kinetic modeling, plasma-to-brain transport kinetics, are in close relationship with the receptor binding parameters, which, when systematically biased due to variations of brain uptake of a radiotracer could falsely be interpreted as modifications of a biological system. In addition, the magnitude of brain uptake augmentation after inhibition has been proposed as a means of assessment of P-gp activity, which may be of particular interest in oncology and neuropsychiatry. This is the case for radiotracers that are markedly affected by this enzyme, such as [^{11}C]verapamil and [^{11}C]-N-desmethyl-loperamide [23,25–30].

Ideally, an inhibitor should have a complete and homogeneous – spatially and temporally – inhibition of efflux proteins, rendering passive diffusion the only determinant of plasma-to-brain transport. Thereby, an estimation of binding parameters, as an index of an underlying biological phenomenon would be feasible, especially with the use of non-invasive quantification approaches, the overall goal being to establish high-throughput and cost-effective study designs. Thus, the benefits

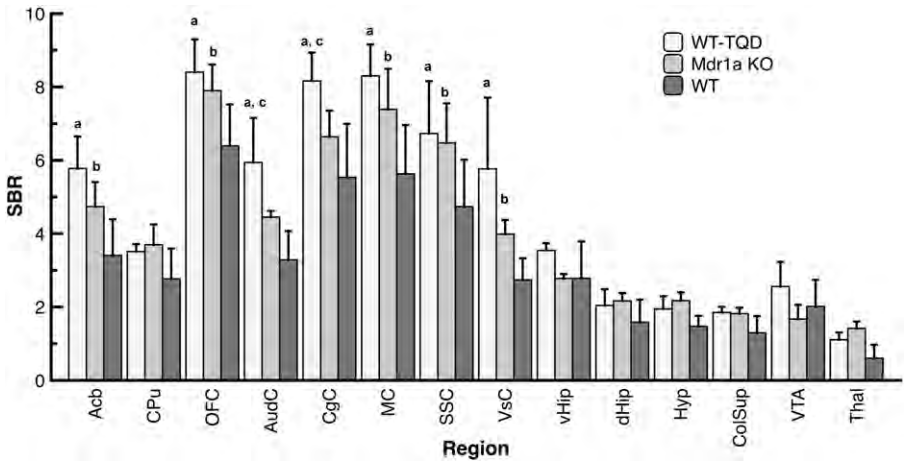

Fig. 4. Histogram (mean and standard deviations) of regional variation of SBR values from WT, WT-TQD and Mdr1a KO rats. (a) $p < 0.001$ compared to WT value. (b) $p < 0.05$ compared to WT value. (c) $p < 0.05$ compared to Mdr1a KO value.

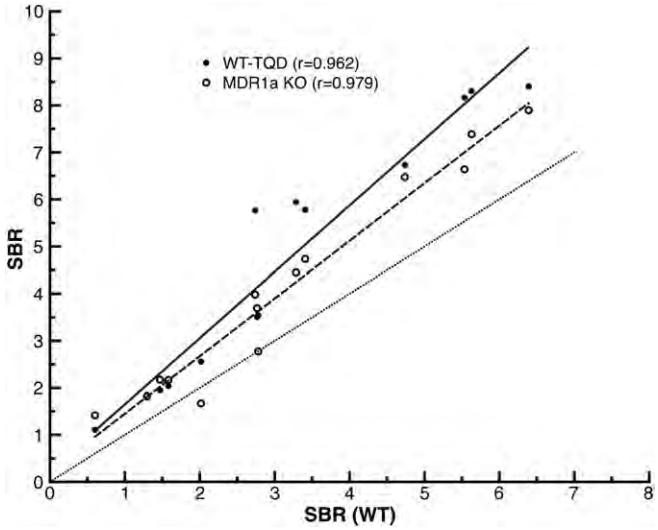

Fig. 5. Correlation of SBR values from WT rats (*x*-axis) with WT-TQD (black dots) and Mdr1a KO rats (white dots) (both in *y*-axis). Dotted line represents line of equality.

of *in vivo* PET and SPECT under conditions of P-gp inhibition in terms of counting statistics have been demonstrated in human and small-animal studies using ciclosporin A (CsA) [2,7,10,11,27,31] and TQD [5,25,32,33]. However, the implementation of this strategy in quantitative protocols is not straightforward: Kroll et al., [7] have recently demonstrated that [^{18}F]altanserin, a 5-HT2A-binding radiotracer is a substrate of P-gp. CsA pretreatment (50 mg/kg) significantly augmented the radiotracer uptake in all brain regions (two- to three-fold), after P-gp inhibition. However, BP_{ND} values, as estimated with several different reference-tissue models showed a region-dependent increase with pretreatment, thus questioning the concept of pharmacological inhibition as a mere "neutralization" of P-gp activity. For this reason, we studied the effect of TQD-mediated inhibition of P-gp activity and compared the resulting brain kinetics with those from Mdr1a KO rats, in which there is a complete absence of the transporter. Consequently, any region-dependent effect of TQD would be more readily observed.

TQD, compared to CsA, is characterized by higher selectivity and inhibitory potential and a clearly more favorable side effect and pharmacokinetic interactions profile. Overall, it is considered to have a superior efficacy as a P-gp inhibitor regarding PET and SPECT radiotracer pharmacokinetics [34]. We thus employed a TQD pretreatment protocol to study the kinetics of [^{123}I]R91150, a 5-HT2A-binding radiotracer, that shows nearly non-detectable brain uptake in WT rats, as measured with SPECT [3,8,17]. Previously, we have shown that this uptake is markedly enhanced in Mdr1a KO rats [3,17] and similarly, Blanckaert et al. [8] demonstrated a comparable augmentation in CsA-treated animals. In the present study, we show that a pretreatment of WT rats with TQD led to an uptake that did not differ from that in Mdr1a KO rats. A dose of 15 mg/kg, injected 30 min before radiotracer injection, has been shown to produce the maximal inhibitory effect elsewhere in the literature [29].

In the present study, we employed partial P-gp KO, as our rat strain presents a normal expression of the Mdr1b isoform. This could be a potential limitation to the interpretation of the differences in the kinetic parameters in our data: TQD pretreatment inhibits both isoforms while Mdr1b remains functional in the Mdr1a KO rats [12,35]. However, its effect should be limited in the hippocampus as the expression of Mdr1b in the brain is mostly localized in this structure [36]. Moreover, Mdr1b as well as the other efflux proteins, such as Breast cancer resistance protein (BCRP) [12,35], seemingly has no considerable effect on [^{123}I]R91150 whatsoever. If the opposite was true, WT-TQD rats should have a higher uptake than Mdr1a KO for two reasons: because TQD also inhibits BCRP and Mdr1b and thus uptake should be augmented in WT-TQD rats, while compensatory augmentations in these proteins' expression in Mdr1a KO rats would diminish uptake in this group, ultimately augmenting the difference between the two groups even more [37].

Regarding plasma pharmacokinetics of [^{123}I]R91150, free parent tracer plasma radioactivity did not significantly differ with respect to the main effect of "group" of rats and not surprisingly, no differences were observed in terms of brain-to-plasma AUC ratio. Nevertheless, it should be noted that correction for radiolabeled metabolites of [^{123}I]R91150 was based on a previous work of our group, where it was performed on treatment-naïve Mdr1a KO rats [17]. As a result, we may not eliminate a possible confounding effect of tariquidar-induced P-gp inhibition on the metabolism of [^{123}I]R91150 and thus on free parent tracer radioactivity in plasma, brain-to-plasma AUC ratio and results of full kinetic modeling with the 1TC model in the WT-TQD. But even if this was the case, quantitative results using the SUR, which present the most significant finding of this study, would not be modified at all in the WT-TQD group, as no plasma input is required for their estimation. Furthermore, concerning P-gp inhibition *per se*, it has been shown not to interfere with [^{123}I]R91150 metabolism [8].

We performed kinetic analysis of dynamic SPECT imaging using the 1TC model, the reason being that it provided excellent fits to TACs, while the 2TC model did not ameliorate fits and provided kinetic parameters associated with high standard errors (data not shown). Our kinetic analysis with the 1TC demonstrated that no significant differences in V_T are observed, a finding that supports the argument that 5-HT2A receptor level does not differ between the two groups of rats. Furthermore, mean K_1 and k_2 values across VOI were not significantly different between the two groups. The fact that both values are significantly influenced by the interaction of the factors "group" and "VOI" points to a non-homogeneous impact, particularly on k_2 parameter. Interestingly, the *post hoc* analysis of k_2 estimate differences with respect to the rat group and VOI demonstrated a marked difference in cerebellum, in which k_2 for TQD-treated WT rats is nearly double than that observed in Mdr1a KO rats (0.071 ± 0.025 in WT-TQD rats and 0.037 ± 0.009 in Mdr1a KO). In this particular brain region, where negligible specific binding is observed, 1TC-derived k_2 parameter is indicative of radiotracer efflux, thus suggesting a higher rate in cerebellum for WT-TQD rats.

This finding has a particular significance for the interpretation of the markedly increased SUR BP_{ND} values in WT-TQD rats with this augmentation being region-dependent, as the interaction of main factors "group" and "VOI" is significant in rmANOVA. In the absence of *in vivo* quantitative binding estimates from WT rats in order to validate the results from WT-TQD and Mdr1a KO rats, we used *ex vivo* autoradiography that has greater sensitivity than *in vivo* SPECT imaging for this purpose. SBR values from *ex vivo* imaging follow a similar pattern with *in vivo* SUR BP_{ND} estimations: average SBR values across all VOIs are higher in the WT-TQD group compared to the WT group, with this effect being region-dependent (significant differences in VOI-wise comparisons are illustrated in Fig. 4). On the contrary, SBR values from Mdr1a KO rats more closely corresponded to values from WT rats, but region-dependent differences may still be found.

Given the aforementioned difference in k_2 estimates, this discrepancy may be, at least partially, explained by a more rapid efflux of radiotracer from cerebellum in WT-TQD rats. This suggests that TQD-mediated P-gp inhibition might be suboptimal in the cerebellum region, an argument supported by the results of Kroll et al. [7] with CsA-mediated inhibition. Importantly, the doses that were employed in their study (50 mg/kg for CsA) and in the present one (15 mg/kg for TQD) produce the maximal effect in rats, as no additional inhibition was observed after administration of higher doses [7,29]. A possible explanation for this distinct level of inhibition in the cerebellum could be that, in this region, P-gp expression is the highest in the brain [11]. A region-dependent effect of TQD is more readily observed in other brain regions when it is administered in lower doses: at 3 mg/kg, the augmentation of V_T of [^{11}C]verapamil, an indicator of P-gp inhibition differs across regions of the rat brain [32]. Consequently, it could be assumed that, despite the high dose employed in our study, the effect was

still suboptimal, notably in the cerebellum. Another possible explanation of this phenomenon could lie on the pharmacokinetics of TQD itself: its effect probably starts to decline at 2 h post injection [38], which could explain the brain kinetics of [^{123}I]R91150.

These results on TQD pretreatment for 5-HT2A receptor SPECT imaging warrant attention when quantification studies are performed. This concerns quantitative approaches in which a reference tissue, devoid of specific binding (here, the cerebellum) is employed to estimate the BP_{ND} [17,39]. If disproportionate inhibition of P-gp is induced in this reference tissue, all estimates are biased. Full kinetic modeling with arterial sampling for input function estimation and estimation of V_T may be more robust. On the other hand, in small-animal molecular imaging, development of a high-throughput, cost-effective experimental design is critical, which implies that the full kinetic modeling with arterial plasma sampling may not be readily employed. Quantitative studies in molecular imaging are, in fact, a trade-off between precision and parsimony. Reference-tissue methods are much less invasive (no arterial sampling) and, in the case of SUR, based on short image acquisitions.

In the present study, WT-TQD rats had higher SUR BP_{ND} estimates, compared to Mdr1a KO rats, but correlations between these groups of values and the respective V_T values were excellent, suggesting that the SUR method is applicable. Correlations between *ex vivo* SBR values from WT-TQD and Mdr1a KO with WT rats are excellent, suggesting that P-gp inhibition is still a viable option for 5-HT2A SPECT imaging with [^{123}I]R91150. However, the marked region-dependent effect of TQD on BP_{ND} estimates, as well as their much higher variability (in terms of % COV), suggests that this approach might not be optimal in experiments where high statistical power is required, i.e. when small biological differences need to be precisely detected. On the other hand, TQD-inhibition of P-gp may be of particular use when novel potential radiotracers are evaluated [4,40–42,44–46].

Alternatively, the use of P-gp KO rats in translational biological studies could rule out the deficient brain penetration of radiotracers and permit extraction of robust quantitative estimates with reference-tissue approaches, provided that neuroreceptor systems of focus are not for any reason perturbed by the absence of P-gp expression. The present and previous studies of our group [3,17] have not provided evidence for the opposite. Concerning human imaging, it is worthy to note that brain region-wise differences in P-gp expression and function seem to be less pronounced than in rat [43]. The results of our study suggest that a careful evaluation of the applicability of the quantification methods must be verified before the employment of TQD inhibition in human imaging. A more sophisticated TQD administration design may be necessary, i.e. a continuous intravenous infusion of TQD throughout the scan. This was studied with [^{11}C]verapamil human PET imaging and demonstrated a superior efficacy of P-gp inhibition, as it resulted in an increase of V_T to a level comparable to that in pituitary, a structure lacking BBB [28].

Taken together, the results of the present study illustrate the advantages and limitations of pharmacological P-gp inhibition. We employed Mdr1a KO rats to "get a glimpse" of complete Mdr1a inhibition and compare to the effect of TQD pretreatment on 5-HT2A SPECT imaging. Region-dependent effects, more pronounced in the cerebellum produced a positive bias in binding potential estimations in TQD-treated rats, which still remained highly correlated with these obtained in Mdr1a KO rats.

Conflict of interest

The authors declare that they have no conflict of interest.

Acknowledgments

This work was supported by the Swiss National Science Foundation (grant no. 310030_156829). The authors are grateful for the contribution of the "Association IFRAD Suisse", which was created in 2009 at the initiative of the "Fondation pour la Recherche sur Alzheimer" (formerly IFRAD France) and the Geneva Neuroscience Center.

References

[1] Loscher W, Potschka H. Role of drug efflux transporters in the brain for drug disposition and treatment of brain diseases. Prog Neurobiol 2005;76:22–76.
[2] Doze P, Van Waarde A, Elsinga PH, Hendrikse NH, Vaalburg W. Enhanced cerebral uptake of receptor ligands by modulation of P-glycoprotein function in the blood–brain barrier. Synapse 2000;36:66–74.
[3] Dumas N, Moulin-Sallanon M, Ginovart N, Tournier BB, Suzanne P, Cailly T, et al. Small-animal single-photon emission computed tomographic imaging of the brain serotoninergic systems in wild-type and mdr1a knockout rats. Mol Imaging 2014; 13.
[4] Buiter HJ, Windhorst AD, Huisman MC, De Maeyer JH, Schuurkes JA, Lammertsma AA, et al. Radiosynthesis and preclinical evaluation of [11C]prucalopride as a potential agonist PET ligand for the 5-HT4 receptor. EJNMMI Res 2013;3:24.
[5] Froklage FE, Syvanen S, Hendrikse NH, Huisman MC, Molthoff CF, Tagawa Y, et al. [11C]Flumazenil brain uptake is influenced by the blood–brain barrier efflux transporter P-glycoprotein. EJNMMI Res 2012;2:12.
[6] Passchier J, van Waarde A, Doze P, Elsinga PH, Vaalburg W. Influence of P-glycoprotein on brain uptake of [18 F]MPPF in rats. Eur J Pharmacol 2000;407: 273–80.
[7] Kroll T, Elmenhorst D, Matusch A, Celik AA, Wedekind F, Weisshaupt A, et al. [(1)(8)F]Altanserin and small animal PET: impact of multidrug efflux transporters on ligand brain uptake and subsequent quantification of 5-HT(2)A receptor densities in the rat brain. Nucl Med Biol 2014;41:1–9.
[8] Blanckaert P, Burvenich I, Staelens S, De Bruyne S, Moerman L, Wyffels L, et al. Effect of cyclosporin A administration on the biodistribution and multipinhole muSPECT imaging of [123I]R91150 in rodent brain. Eur J Nucl Med Mol Imaging 2009;36: 446–53.
[9] Zoghbi SS, Liow JS, Yasuno F, Hong J, Tuan E, Lazarova N, et al. 11C-loperamide and its N-desmethyl radiometabolite are avid substrates for brain permeability-glycoprotein efflux. J Nucl Med 2008;49:649–56.
[10] la Fougere C, Boning G, Bartmann H, Wangler B, Nowak S, Just T, et al. Uptake and binding of the serotonin 5-HT1A antagonist [18 F]-MPPF in brain of rats: effects of the novel P-glycoprotein inhibitor tariquidar. Neuroimage 2010;49:1406–15.
[11] Lacan G, Plenevaux A, Rubins DJ, Way BM, Defraiteur C, Lemaire C, et al. Cyclosporine, a P-glycoprotein modulator, increases [18 F]MPPF uptake in rat brain and peripheral tissues: microPET and ex vivo studies. Eur J Nucl Med Mol Imaging 2008;35:2256–66.
[12] Fox E, Bates SE. Tariquidar (XR9576): a P-glycoprotein drug efflux pump inhibitor. Expert Rev Anticancer Ther 2007;7:447–59.
[13] Mertens J, Terriere D, Sipido V, Gommeren W, Janssen PMF, Leysen JE. Radiosynthesis of a new radioidinated ligand for serotonin-5Ht2-receptor, a promising tracer for gamma-emission tomography. J Labelled Comp Radiopharm 1994;34:795–806.
[14] Jones HM, Travis MJ, Mulligan R, Bressan RA, Visvikis D, Gacinovic S, et al. In vivo 5-HT2A receptor blockade by quetiapine: an R91150 single photon emission tomography study. Psychopharmacology 2001;157:60–6.
[15] Audenaert K, Van Laere K, Dumont F, Slegers G, Mertens J, van Heeringen C, et al. Decreased frontal serotonin 5-HT 2a receptor binding index in deliberate self-harm patients. Eur J Nucl Med 2001;28:175–82.
[16] Catafau AM, Bullich S, Nucci G, Burgess C, Gray F, Merlo-Pich E, et al. Contribution of SPECT measurements of D2 and 5-HT2A occupancy to the clinical development of the antipsychotic SB-773812. J Nucl Med 2011;52:526–34.
[17] Dumas N, Moulin-Sallanon M, Fender P, Tournier BB, Ginovart N, Charnay Y, et al. In vivo quantification of 5-HT2A brain receptors in Mdr1a KO rats with 123I-R91150 single photon emission computed tomography. Mol Imaging 2015;14 [accepted].
[18] Millet P, Moulin M, Bartoli A, Del Guerra A, Ginovart N, Lemoucheux L, et al. In vivo quantification of 5-HT1A-[18 F]MPPF interactions in rats using the YAP-(S)PET scanner and a beta-microprobe. Neuroimage 2008;41:823–34.
[19] Paxinos G, Watson C. The rat brain in stereotaxic coordinates. 2nd ed., Sydney. Orlando: Academic Press; 1986.
[20] Schiffer WK, Mirrione MM, Biegon A, Alexoff DL, Patel V, Dewey SL. Serial microPET measures of the metabolic reaction to a microdialysis probe implant. J Neurosci Methods 2006;155:272–84.
[21] Innis RB, Cunningham VJ, Delforge J, Fujita M, Gjedde A, Gunn RN, et al. Consensus nomenclature for in vivo imaging of reversibly binding radioligands. J Cereb Blood Flow Metab 2007;27:1533–9.
[22] Liow JS, Lu S, McCarron JA, Hong J, Musachio JL, Pike VW, et al. Effect of a P-glycoprotein inhibitor, Cyclosporin A, on the disposition in rodent brain and blood of the 5-HT1A receptor radioligand, [11C](R)-(−)-RWAY. Synapse 2007;61:96–105.
[23] Bauer M, Zeitlinger M, Karch R, Matzneller P, Stanek J, Jager W, et al. Pgp-mediated interaction between (R)-[11C]verapamil and tariquidar at the human blood–brain barrier: a comparison with rat data. Clin Pharmacol Ther 2012;91:227–33.
[24] Meikle SR, Kench P, Kassiou M, Banati RB. Small animal SPECT and its place in the matrix of molecular imaging technologies. Phys Med Biol 2005;50:R45–61.
[25] Bankstahl JP, Kuntner C, Abrahim A, Karch R, Stanek J, Wanek T, et al. Tariquidar-induced P-glycoprotein inhibition at the rat blood–brain barrier studied with (R)-11C-verapamil and PET. J Nucl Med 2008;49:1328–35.
[26] Hendrikse NH, Schinkel AH, de Vries EG, Fluks E, Van der Graaf WT, Willemsen AT, et al. Complete in vivo reversal of P-glycoprotein pump function in the blood–brain barrier visualized with positron emission tomography. Br J Pharmacol 1998;124:1413–8.
[27] Elsinga PH, Hendrikse NH, Bart J, van Waarde A, Vaalburg W. Positron emission tomography studies on binding of central nervous system drugs and P-glycoprotein function in the rodent brain. Mol Imaging Biol 2005;7:37–44.

[28] Bauer M, Karch R, Zeitlinger M, Philippe C, Romermann K, Stanek J, et al. Approaching complete inhibition of P-glycoprotein at the human blood–brain barrier: an (R)-[C]verapamil PET study. J Cereb Blood Flow Metab 2015;35(5):743–6.
[29] Wagner CC, Bauer M, Karch R, Feurstein T, Kopp S, Chiba P, et al. A pilot study to assess the efficacy of tariquidar to inhibit P-glycoprotein at the human blood–brain barrier with (R)-11C-verapamil and PET. J Nucl Med 2009;50:1954–61.
[30] Kreisl WC, Liow JS, Kimura N, Seneca N, Zoghbi SS, Morse CL, et al. P-glycoprotein function at the blood–brain barrier in humans can be quantified with the substrate radiotracer 11C-N-desmethyl-loperamide. J Nucl Med 2010;51:559–66.
[31] Risgaard R, Ettrup A, Balle T, Dyssegaard A, Hansen HD, Lehel S, et al. Radiolabelling and PET brain imaging of the alpha(1)-adrenoceptor antagonist Lu AE43936. Nucl Med Biol 2013;40:135–40.
[32] Kuntner C, Bankstahl JP, Bankstahl M, Stanek J, Wanek T, Stundner G, et al. Dose–response assessment of tariquidar and elacridar and regional quantification of P-glycoprotein inhibition at the rat blood–brain barrier using (R)-[(11)C]verapamil PET. Eur J Nucl Med Mol Imaging 2010;37:942–53.
[33] Romermann K, Wanek T, Bankstahl M, Bankstahl JP, Fedrowitz M, Muller M, et al. (R)-[(11)C]verapamil is selectively transported by murine and human P-glycoprotein at the blood–brain barrier, and not by MRP1 and BCRP. Nucl Med Biol 2013;40:873–8.
[34] Bansal T, Jaggi M, Khar RK, Talegaonkar S. Emerging significance of flavonoids as P-glycoprotein inhibitors in cancer chemotherapy. J Pharm Pharm Sci 2009;12:46–78.
[35] Kannan P, Telu S, Shukla S, Ambudkar SV, Pike VW, Halldin C, et al. The "specific" P-glycoprotein inhibitor Tariquidar is also a substrate and an inhibitor for breast cancer resistance protein (BCRP/ABCG2). ACS Chem Neurosci 2011;2:82–9.
[36] Kwan P, Sills GJ, Butler E, Gant TW, Brodie MJ. Differential expression of multidrug resistance genes in naive rat brain. Neurosci Lett 2003;339:33–6.
[37] Lagas JS, Vlaming ML, Schinkel AH. Pharmacokinetic assessment of multiple ATP-binding cassette transporters: the power of combination knockout mice. Mol Interv 2009;9:136–45.
[38] Mullauer J, Kuntner C, Bauer M, Bankstahl JP, Muller M, Voskuyl RA, et al. Pharmacokinetic modeling of P-glycoprotein function at the rat and human blood–brain barriers studied with (R)-[11C]verapamil positron emission tomography. EJNMMI Res 2012;2:58.
[39] Tsartsalis S, Moulin-Sallanon M, Dumas N, Tournier BB, Ghezzi C, Charnay Y, et al. Quantification of GABAA receptors in the rat brain with [(123)I]lomazenil SPECT from factor analysis-denoised images. Nucl Med Biol 2014;41:186–95.
[40] Haeusler D, Kuntner C, Nics L, Savli M, Zeilinger M, Wanek T, et al. [18 F]FE@SUPPY: a suitable PET tracer for the adenosine A3 receptor? An in vivo study in rodents. Eur J Nucl Med Mol Imaging 2015;42:741–9.
[41] Becker G, Colomb J, Sgambato-Faure V, Tremblay L, Billard T, Zimmer L. Preclinical evaluation of [18 F]2FNQ1P as the first fluorinated serotonin 5-HT6 radioligand for PET imaging. Eur J Nucl Med Mol Imaging 2015;42:495–502.
[42] Winterdahl M, Audrain H, Landau AM, Smith DF, Bonaventure P, Shoblock JR, et al. PET brain imaging of neuropeptide Y2 receptors using N-11C-methyl-JNJ-31020028 in pigs. J Nucl Med 2014;55:635–9.
[43] Bauer M, Karch R, Neumann F, Wagner CC, Kletter K, Muller M, et al. Assessment of regional differences in tariquidar-induced P-glycoprotein modulation at the human blood–brain barrier. J Cereb Blood Flow Metab 2010;30:510–5.
[44] Verbeek J, Syvanen S, Schuit RC, Eriksson J, de Lange EC, Windhorst AD, et al. Synthesis and preclinical evaluation of [11C]D617, a metabolite of (R)-[11C]verapamil. Nucl Med Biol 2012;39:530–9.
[45] Slobbe P, Windhorst AD, Stigter-van Walsum M, Smit EF, Niessen HG, Solca F, et al. A comparative PET imaging study with the reversible and irreversible EGFR tyrosine kinase inhibitors [(11)C]erlotinib and [(18)F]afatinib in lung cancer-bearing mice. EJNMMI Res 2015;5:14.
[46] Mairinger S, Wanek T, Kuntner C, Doenmez Y, Strommer S, Stanek J, et al. Synthesis and preclinical evaluation of the radiolabeled P-glycoprotein inhibitor [(11)C]MC113. Nucl Med Biol 2012;39:1219–25.

Article 4

NeuroImage 176 (2018) 528–540

Contents lists available at ScienceDirect

NeuroImage

journal homepage: www.elsevier.com/locate/neuroimage

Dual-radiotracer translational SPECT neuroimaging. Comparison of three methods for the simultaneous brain imaging of $D_{2/3}$ and 5-HT_{2A} receptors

Stergios Tsartsalis [a,b], Benjamin B. Tournier [a], Selim Habiby [a], Meriem Ben Hamadi [a], Cristina Barca [a], Nathalie Ginovart [a,c], Philippe Millet [a,c,*]

[a] Division of Adult Psychiatry, Department of Mental Health and Psychiatry, University Hospitals of Geneva, Switzerland
[b] Division of Addictology, Department of Mental Health and Psychiatry, University Hospitals of Geneva, Switzerland
[c] Department of Psychiatry, University of Geneva, Switzerland

ARTICLE INFO

Keywords:
IBZM
SPECT
$D_{2/3}$ receptor
5-HT_{2A} receptor
Dual-radiotracer
Simultaneous SPECT

ABSTRACT

Purpose: SPECT imaging with two radiotracers at the same time is feasible if two different radioisotopes are employed, given their distinct energy emission spectra. In the case of ^{123}I and ^{125}I, dual SPECT imaging is not straightforward: ^{123}I emits photons at a principal energy emission spectrum of 143.1–179.9 keV. However, it also emits at a secondary energy spectrum (15–45 keV) that overlaps with the one of ^{125}I and the resulting cross-talk of emissions impedes the accurate quantification of ^{125}I. In this paper, we describe three different methods for the correction of this cross-talk and the simultaneous *in vivo* [^{123}I]IBZM and [^{125}I]R91150 imaging of $D_{2/3}$ and 5-HT_{2A} receptors in the rat brain.

Methods: Three methods were evaluated for the correction of the effect of cross-talk in a series of simultaneous, [^{123}I]IBZM and [^{125}I]R91150 *in vivo* and phantom SPECT scans. Method 1 employs a dual-energy window (DEW) approach, in which the cross-talk on ^{125}I is considered a stable fraction of the energy emitted from ^{123}I at the principal emission spectrum. The coefficient describing the relationship between the emission of ^{123}I at the principal and the secondary spectrum was estimated from a series of single-radiotracer [^{123}I]IBZM SPECT studies. In Method 2, spectral factor analysis (FA) is applied to separate the radioactivity from ^{123}I and ^{125}I on the basis of their distinct emission patterns across the energy spectrum. Method 3 uses a modified simplified reference tissue model ($SRTM_C$) to describe the kinetics of [^{125}I]R91150. It includes the coefficient describing the cross-talk on ^{125}I from ^{123}I in the model parameters. The results of the correction of cross-talk on [^{125}I]R91150 binding potential (BP_{ND}) with each of the three methods, using cerebellum as the reference region, were validated against the results of a series of single-radiotracer [^{123}I]R91150 SPECT studies. In addition, the DEW approach (Method 1), considered to be the most straightforward to apply of the three, was further applied in a dual-radiotracer SPECT study of the relationship between $D_{2/3}$ and 5-HT_{2A} receptor binding in the striatum, both at the voxel and at the regional level.

Results: Average regional BP_{ND} values of [^{125}I]R91150, estimated on the cross-talk corrected dual-radiotracer SPECT studies provided satisfactory correlations with the BP_{ND} values for [^{123}I]R91150 from single-radiotracer studies: $r = 0.92$, $p < 0.001$ for Method 1, $r = 0.92$, $p < 0.001$ for Method 2, $r = 0.92$, $p < 0.001$, for Method 3. The coefficient describing the ratio of the ^{123}I-emitted radioactivity at the ^{125}I-emission spectrum to the radioactivity that it emits at its principal emission spectrum was 0.34 *in vivo*. Dual-radiotracer *in vivo* SPECT studies corrected with Method 1 demonstrated a positive correlation between $D_{2/3}$ and 5-HT_{2A} receptor binding in the rat nucleus accumbens at the voxel level. At the VOI-level, a positive correlation was confirmed in the same region ($r = 0.78$, $p < 0.01$).

Conclusion: Dual-radiotracer SPECT imaging using ^{123}I and ^{125}I-labeled radiotracers is feasible if the cross-talk of ^{123}I on the ^{125}I emission spectrum is properly corrected. The most straightforward approach is Method 1, in which a fraction (34%) of the radioactivity emitted from ^{123}I at its principal energy spectrum is subtracted from the measured radioactivity at the spectrum of ^{125}I. With this method, a positive correlation between the binding of [^{123}I]IBZM and [^{125}I]R91150 was demonstrated in the rat nucleus accumbens. This result highlights the interest

* Corresponding author. Division of Adult Psychiatry, Department of Psychiatry, University Hospitals of Geneva Switzerland, Chemin du Petit-Bel-Air 2, CH1225, Chêne-Bourg, Switzerland.
E-mail address: Philippe.Millet@hcuge.ch (P. Millet).

https://doi.org/10.1016/j.neuroimage.2018.04.063
Received 30 October 2017; Received in revised form 11 March 2018; Accepted 27 April 2018
Available online 30 April 2018

of dual-radiotracer SPECT imaging to study multiple neurotransmitter systems at the same time and under the same biological conditions.

Introduction

Molecular neuroimaging permits the study of brain function in health and disease. Radiotracers targeting a wide panel of neurobiological processes have been developed: regarding the neurotransmitter systems, single-photon emission computed tomography (SPECT) and positron emission tomography (PET) studies provide knowledge on neuroreceptor levels, receptor-neurotransmitter-interactions, endogenous neurotransmitter levels etc. (Frankle et al., 2005; Laruelle, 2000). With the advent of modern small-animal scanners, molecular imaging is now employed in the study of animal models of neuropsychiatric diseases. The advantage of using the same techniques in fundamental as in clinical research lies on the fact that animal models may provide insight into mechanistic aspects of human disease while the knowledge obtained from small-animal imaging may be more directly implemented in human research (Cunha et al., 2014; Frankle and Laruelle, 2002; Meikle et al., 2005; Nestler and Hyman, 2010; Xi et al., 2011).

Given the arsenal of radiotracers available in molecular neuroimaging, multiple biological targets may be studied on the same subject and permit a more thorough evaluation of brain physiology and pathology (Cselenyi et al., 2004; Fakhri, 2012). For example, a joint evaluation of $D_{2/3}$ and 5-HT_{2A} receptors would be of interest for the study of schizophrenia as both receptors are implicated in the pathophysiology of the disease and a target for multiple antipsychotic agents (Ginovart and Kapur, 2012; Howes et al., 2012; Selvaraj et al., 2014). Another highly interesting example of joint exploration of multiple biomarkers would be in dementia imaging (Jack et al., 2013). However, studying multiple targets on the same animal is technically difficult. Multiple scan sessions are time-consuming as they may need to be separated by various amounts of time for the radioisotope of the first scan to decay before the second scan and thus prevent bias in the radioactivity measurements. However, studying two or more biological phenomena using scan sessions that are separated by hours or even days may induce variability and bias due to the dynamic nature of most of biological phenomena that may rapidly evolve or even depend on each other (Fakhri, 2012). For instance, results from neuroreceptor studies may be subject to the effect of endogenous ligand binding to the receptors (Laruelle, 2000), which is a dynamic phenomenon, subject to physiological variations. Other parameters, such as the effect of anesthetic agents may alter the radiotracers' binding (McCormick et al., 2011) and thus hamper the joint interpretation of two phenomena under study unless they are studied at the exact same time, thus under the exact same conditions. Furthermore, multiple scan sessions may reduce the throughput of small animal imaging studies. Given the limitations described above, the development of simultaneous, dual-radiotracer molecular imaging could optimize biological studies both in terms of technical feasibility and of biological understanding of brain function (Fakhri, 2012).

Simultaneous, dual-radiotracer molecular imaging is theoretically feasible in SPECT. Each radioisotope used in SPECT emits photons in a particular energy spectrum. Two (or more) radioisotopes may thus be simultaneously employed in a single scan session and their respective radioactive signals be distinguished based on their emission spectra (Akutsu et al., 2009; Antunes et al., 1992; Bruce et al., 2000; Ichihara et al., 1993). This is the case for two iodine isotopes used in SPECT. ^{123}I has a principal energy emission spectrum of 143.1–179.9 keV and ^{125}I an energy spectrum of 15–45 keV. The majority of radiotracers used in SPECT studies of the central nervous system (CNS) is radioiodinated (Baeken et al., 1998; De Bruyne et al., 2010; Dumas et al., 2014, 2015; Ji et al., 2015; Kessler et al., 1991; Kung et al., 1989; Mattner et al., 2008, 2011; Ordonez et al., 2015; Pimlott and Ebmeier, 2007; Sehlin et al., 2016; Tsartsalis et al., 2014a, 2015) and the possibility to perform dual-radiotracer SPECT using ^{123}I and ^{125}I would thus be of interest for a wide spectrum of *in vivo* studies in animal models of neuropsychiatric conditions. Nevertheless, distinction of ^{123}I- and ^{125}I-emitted photons is not straightforward: ^{123}I emits at a secondary energy spectrum that overlaps with the one of ^{125}I and the resulting cross-talk of emissions impedes the accurate quantification of ^{125}I.

In this paper, we compare three different methods for the correction of cross-talk between ^{123}I and ^{125}I and apply them to the simultaneous quantification of $D_{2/3}$ and 5-HT_{2A} receptors, using the [^{123}I]IBZM and [^{125}I]R91150, respectively. Furthermore, we apply this methodology to study the relationship between the [^{123}I]IBZM and [^{125}I]R91150 binding in the rat striatum and thus illustrate the potential of dual-radiotracer imaging for *in vivo* biological studies of brain function and pathology.

Materials and methods

^{123}I and ^{125}I phantom SPECT studies

Eighteen groups of three cylindrical phantoms each (2 ml Eppendorf® tubes) were prepared. In each group, one tube was filled with a solution containing ^{123}I (GE Healthcare, Eindhoven, Netherlands), one with the same radioactive concentration of ^{125}I (Perkinelmer, Schwerzenbach, Suisse) and a third tube with a mixture of equal concentrations of both radioisotopes (each radioisotope at half the quantity of radioactivity in the adjacent single radioisotope-containing tube). Attention was paid for the tubes to be filled with the exact same radioactive concentration so that the measurement in the single-radioisotope containing tubes to be exactly twice the radioactivity of the same radioisotope in the tubes containing both. In this way, the measurements in the single radioisotope-containing tubes could serve as controls for the measurement in the dual-radioisotope containing tubes after correction for cross-talk. Radioactive concentrations varied from 0.9 to 3.5 MBq/ml. The tubes of each group were positioned along the longitudinal axis of the U-SCAN-II SPECT camera (MiLabs, Utrecht, Netherlands) on a rectangular polystyrene scaffold. A 10-min static SPECT acquisition was performed.

Radiotracer preparation

All chemicals were purchased from Sigma-Aldrich (Buchs, Switzerland) with the highest purity available, unless otherwise specified. [^{123}I]IBZM was obtained by incubation, for 15 min at 68 °C, of a mixture containing 5 μL of BZM precursor (ABX, Germany, 24 nmol/μl in ethanol), 2 μL of glacial acetic acid, 1 μL of 30% H_2O_2 and 10 mCi of carrier-free ^{123}I sodium iodide in 0.05 M NaOH (GE Healthcare, Eindhoven, Netherlands). The radiotracer was isolated by a linear gradient HPLC run (from 5% acetonitrile, ACN, to 95% ACN, 10 mM H_3PO_4, in 10 min).

For R91150 radiolabeling, 300 μg of R91150 precursor in 3 μL ethanol was mixed with 3 μL of glacial acetic acid, 15 μL of carrier-free ^{123}I or ^{125}I (Perkin Elmer) sodium iodide (10 mCi) in 0.05 M NaOH, and 3 μL of 30% H_2O_2. [^{123}I]R91150/[^{125}I]R91150 was isolated by an isocratic HPLC run (ACN/water 50/50, 10 mM acetic acid buffer) with a reversed-phase column (Bondclone C18 10 μm 300 × 7.8 mm, Phenomenex, Schlieren, Switzerland) at a flow rate of 3 ml/min. Radiochemical purity, assessed by HPLC, was above 98% (Dumas et al., 2014).

In vivo SPECT studies and scan procedures

Thirty-two male *Mdr1a* KO rats (SD-Abcba1tm1sage, Sigma Advance Genetic Engineering Labs, USA), weighing 370–573 g were used. Their repartition was as follows: 1) Three rats were used in a single-radiotracer

[^{123}I]IBZM SPECT study. This study allowed the estimation of the α coefficient describing the relationship between the emission of [^{123}I]IBZM at the 15–45 keV spectrum and the emission of the same radiotracer at the 143,1–179,9 keV spectrum (see section 2.5.1 for more detail). 2) Four rats were used in a single-radiotracer [^{123}I]R91150 study and the results of the quantification were used as "ground truth" for the validation of the results of cross-talk correction in dual-radiotracer SPECT studies. 3) Three rats were employed in a simultaneous, dual-radiotracer SPECT study to validate the three different methods of correction of the cross-talk between [^{123}I]IBZM and [^{125}I]R91150 by comparing the results of quantification with the results of study 2. 4) Ten rats were used in a dual-radiotracer [^{123}I]IBZM and [^{125}I]R91150 study to evaluate the test-retest reliability of the quantification of $D_{2/3}$ and 5-HT_{2A} receptors with this protocol. In addition, with these ten rats, the correlation between these two receptors in the nucleus accumbens (NAcc) was studied. 5) In a supplemental study, one rat was employed in a dual-radiotracer study in which [^{123}I]R91150 was labeled with ^{123}I and [^{125}I]IBZM with ^{125}I. 6) Finally, eight rats were used in a supplemental *in vitro* study of $D_{2/3}$ and 5-HT_{2A} quantification in the NAcc to validate the results of the *in vivo* study. Table 1 summarizes the above description. All experimental procedures were performed in accordance with the Swiss Federal Law on animal care under a protocol approved by the Ethical Committee on Animal Experimentation of the Canton of Geneva, Switzerland.

SPECT scans were performed under isoflurane anesthesia (4% for induction, 2.5% for maintenance). Body temperature was maintained at 37 ± 1 °C by means of a thermostatically controlled heating blanket. A polyethylene catheter (22G) was inserted in the tail vein for radiotracer injection, at a volume of 0.6 ml over a 1-min period using an infusion pump. The scan protocol, regarding the number of image-frames is presented for each study in Table 1.

Table 1
Repartition of rats into experimental groups.

Experiment	n	SPECT protocol	Objective/Outcome measures
1. Single-radiotracer [^{123}I]IBZM study	3	120 x 1-min frames	Estimation of α coefficient Estimation of BP_{ND} (SUR)
2. Single-radiotracer [^{123}I]R91150 study	4	120 x 1-min frames	Estimation of BP_{ND} (SUR)
3. Dual-radiotracer [^{123}I]IBZM/[^{125}I]R91150 validation study	3	240 x 1-min frames, ([^{125}I]R91150 injected at t = 0 and [^{123}I]IBZM injected at t = 20 min)	Validation of BP_{ND} estimation with SUR after cross-talk correction with DEW/Spectral FA/$SRTM_C$
4. Study of the $D_{2/3}$-5-HT_{2A} binding in striatum and test-retest variability assessment	10	4 × 10-min frames scan, initiated at t = 80 min after the simultaneous injection of [^{123}I]IBZM/[^{125}I]R91150	Estimation of BP_{ND} (SUR) after DEW-correction for cross-talk/Test-retest variability/correlation between $D_{2/3}$-5-HT_{2A}
5. Supplemental experiment Dual-radiotracer [^{123}I]R91150/[^{125}I]IBZM validation study	1	240 x 1-min frames, ([^{125}I]IBZM injected at t = 0 and [^{123}I]R91150 injected at t = 20 min)	Evaluation of a possible bias of [^{123}I]R91150 on [^{125}I]IBZM
6. Supplemental experiment Single-radiotracer [^{125}I]R91150 study	3	1 × 20-min frame, (initiated at t = 100 min after [^{125}I]R91150 injection)	Evaluation of a possible bias in BP_{ND} due to the use of ^{125}I
7. Supplemental experiment *In vitro* autoradiography study of $D_{2/3}$ and 5-HT_{2A} binding	8	–	Estimation of 1) $D_{2/3}$ binding in brain slices from frontal cortical and striatal regions and 2) 5-HT_{2A} binding onto immediately adjacent slices

SPECT image reconstruction, co-registration and regional radioactivity measurement extraction

SPECT image reconstruction from phantom and *in vivo* rat studies (single- and dual-radiotracer) was performed using a pixel ordered subsets expectation maximization (P-OSEM, 0.4 mm voxels, 4 iterations, 6 subsets) algorithm using MiLabs image reconstruction software. Reconstruction of dynamic SPECT images was performed using the radioactivity measured at each radioisotope's principal energy spectrum, that is at 143,1–179,9 keV for ^{123}I and at 15–45 keV for ^{125}I. Reconstruction of static SPECT images was performed at the aforementioned energy spectra but also over the whole energy spectrum from 0 to 200 keV, with 5 keV-wide windows (in this case, image-volumes containing the reconstructions of a static SPECT image over the whole spectrum are termed "spectral images"). In this way, the pattern of emission of each radioisotope over the whole energy spectrum is studied. Radioactive decay correction was performed while correction for attenuation or scatter was not.

SPECT images were processed using PMOD software (version 3.8, 2014, PMOD Technologies Ltd, Zurich, Switzerland). Radioactivity from the phantom study (section 2.1) was extracted from the SPECT image by means of an ellipsoid volume-of-interest (VOI) manually placed at the center of the tube (2 cm^3). *In vivo* SPECT scans were manually co-registered to a rat MRI and a VOI template (including 57 VOIs), incorporated in PMOD (Schiffer et al., 2006). In the case of dynamic SPECT images, manual co-registration was performed on images of average radioactivity over many frames of acquisition, to enhance the visualization of the brain. Co-registration parameters of these averaged images were then applied to individual frames of the dynamic images and time-activity-curves (TACs) were generated.

Simultaneous dual-radiotracer SPECT signal separation

For the dual-radiotracer study, a 240 x 1-min frame SPECT acquisition started immediately after a [^{125}I]R91150 injection at t = 0 (62.88 ± 19.14 MBq), while [^{123}I]IBZM was injected at t = 20 min (66.33 ± 26.02 MBq). The protocol for the dual-radiotracer studies is presented in Fig. 1. For the single radiotracer studies, a 120 x 1-min frame SPECT acquisition was initiated upon radiotracer injection. Radioactive concentration at the time of injection was 100.45 ± 34.15 MBq for the single-radiotracer [^{123}I]R91150 study and 90.45 ± 3.27 MBq for the single-radiotracer [^{123}I]IBZM study. Three different methods of signal separation in dual-radiotracer SPECT were employed in this paper:

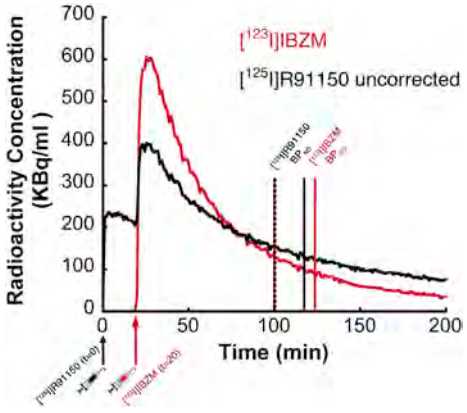

Fig. 1. The protocol employed in the dual-radiotracer experiments (as described in section 2.3). The SPECT scan starts with an injection of [^{125}I]R91150, followed by the injection of [^{123}I]IBZM, 20 min later. The [^{125}I]R91150 TAC is unbiased until the moment of [^{123}I]IBZM injection. The time-windows on which the BP_{ND} values for the two radiotracers is estimated, are indicated with the vertical lines.

Method 1: correction of the cross-talk between ^{123}I and ^{125}I by subtracting the ^{123}I-derived contamination from the ^{125}I radioactive signal (hereon, dual energy window method)

Lee and colleagues (Lee et al., 2013, 2015) proposed a dual energy window (DEW) method, exploiting the fact that the emission of ^{123}I at the principal (high) energy spectrum at 143,1–179,9 keV and the emission at the secondary (low) energy spectrum at 15–45 keV (this one producing the cross-talk with ^{125}I) have a linear relationship, described by the following equation:

$$^{123}I_{low} = \alpha^{*\ 123}I_{high} \quad (1)$$

where $^{123}I_{low}$ and $^{123}I_{high}$ denote the radioactivity of the low and high-energy emission spectra, respectively and α is an unknown coefficient. The α coefficient was estimated from the ^{123}I phantom study (section 2.1) and the *in vivo* single-radiotracer [^{123}I]IBZM SPECT study (section 2.5). It was given by fitting equation (1) to the scatter plot of the radioactivity measured at the high-energy spectrum and the corresponding measurement at the low-energy spectrum, across ^{123}I phantoms. For the *in vivo* imaging study, the α coefficient was estimated by fitting equation (1) to the radioactivity measured at the high-energy spectrum and the corresponding measurement at the low-energy spectrum, in each of the 57 VOIs over the three rats of the single-radiotracer [^{123}I]IBZM study (section 2.3).

Knowing the α coefficient permits to correct the total radioactivity measured at the low-energy window ($^{125/123}I$), where the cross-talk between ^{123}I and ^{125}I is observed. Indeed, in this case, the radioactivity emitted by ^{125}I only (^{125}I) will be given by the following equation:

$$^{125}I = {}^{125/123}I - \alpha\ ^{*\ 123}I_{high} \quad (2)$$

all other parameters are known, including the radioactivity measured at the high-energy spectrum ($^{123}I_{high}$), which is not influenced by cross-talk and directly quantified. After application of the DEW method, the non-displaceable binding potential (BP_{ND}) (Innis et al., 2007) was estimated on static images corresponding to acquisitions between the 80th and the 110th min after injection for the [^{123}I]IBZM studies and between the 100th and the 120th min after injection for [^{125}I]R91150. These time-windows correspond to pseudo-equilibrium conditions and permit a simple specific uptake ratio method (SUR) to be used for BP_{ND} estimation, as previously demonstrated (BP_{ND}=Radioactivity in target region/Radioactivity in reference region-1) (Dumas et al., 2015; Tsartsalis et al., 2017). These time-windows where employed whenever the estimation of BP_{ND} was performed over static SPECT images with the SUR method in this paper.

Method 2: spectral factor analysis (FA)

As described in section 2.4, static images from phantom and *in vivo* experiments were reconstructed across the energy spectrum in 5 keV-wide energy windows and all these reconstructed images were combined in a single volume, termed a spectral image, one for each phantom or rat. Spectral images were processed in the Pixies software (Apteryx, Issy-les-Moulineaux, France) as previously described (Di Paola et al., 1982; Millet et al., 2012; Tsartsalis et al., 2014a). In this paper, FA is used for the decomposition of spectral images into a few elementary component-images, each one of them representing the emission pattern of one radioisotope over the emission spectrum. The decomposition is based on the distinct spectral pattern of each component-image and is performed at the voxel level. The objective is to distinguish the radioactive signal with respect to the radioisotope (^{123}I or ^{125}I) that emitted it. Thus, the emission pattern of radioactivity in each voxel (i) of an original (raw) spectral image, $V_i^{raw}(r)$ (where r is the energy window at which reconstruction was performed), is expressed as a function of a finite number (k) of curves called factors f_k, each one corresponding to a distinct radioactivity emission pattern across the energy spectrum and a set of factor-images M_k that represent the spatial distribution of the factors. Overall, the decomposition of the radioactive signal may be expressed using the following equation:

$$V_i^{raw}(r) = \sum_{k=1}^{K} M_k(i) f_k(r) + e_i(r) \quad (3)$$

where $e_i(r)$ represents the error term for each voxel (i) at energy (r) including both noise and modeling errors. In the present study, K = 3, given that we know *a priori* that the whole radioactive signal is emitted by two radioisotopes and the third factor corresponds to the data that is not attributed to either ^{123}I- or ^{125}I-emitted signal. In addition, the distinct pattern of emission from each radiotracer over the energy spectrum is known from the reconstruction of the single-radiotracer images (section 2.1) that contained only one of the radioisotopes at a time. This *a priori* known pattern of emission was employed as a constraint of similitude in FA, i.e. obliging the software to extract factors similar to the known patterns of emission of ^{123}I and ^{125}I. For a more detailed description of FA and the application of a constraint of similitude, please see (Millet et al., 2012). After FA, the images corresponding to the factor representing ^{125}I and more precisely its emission spectrum at 15–45 keV were extracted and considered cross-talk-corrected. BP_{ND} was estimated over [^{123}I]IBZM and [^{125}I]R91150 SPECT images with the SUR method.

Method 3: inclusion of the effect of cross-talk in the compartmental analysis

Correction of the effect of cross-talk was also performed by including it in the equation of the simplified reference-tissue model (SRTM) (Lammertsma and Hume, 1996; Wu and Carson, 2002), as previously described (Carson et al., 2003; Tsartsalis et al., 2014b). The SRTM equation is the following:

$$C_{VOI}(t) = R_1 C_{REF}(t) + (k_2 - R_1 k_2/(1 + BP_{ND}))C_{REF}(t) \otimes e^{-k_2/(1+BP_{ND})t} \quad (4)$$

where $C_{VOI}(t)$ and $C_{REF}(t)$ are the TACs in the VOI and the reference region, respectively, R_1 is the relative delivery of the radiotracer in the VOI with respect to the reference region ($K_1/K_1^{'}$), k_2 are tissue efflux constants in the VOI.

In the present study, the radioactive signal measured at 15–45 keV corresponds to [^{125}I]R91150 and a part of the [^{123}I]IBZM signal as a result of cross-talk. Taken equation (2) into account, at any time point

$$C_{VOI}^{125}(t) = C_{VOI}^{total}(t) - \alpha\ C_{VOI}^{123}(t) \quad (5)$$

and

$$C_{REF}^{125}(t) = C_{REF}^{total}(t) - \alpha'\ C_{REF}^{123}(t) \quad (6)$$

where $C_{VOI}^{125}(t)$ and $C_{REF}^{125}(t)$ are the true TACs corresponding to [^{125}I]R91150 in the VOI and reference region, $C_{VOI}^{total}(t)$ and $C_{REF}^{total}(t)$ correspond to the measured TAC, that includes the cross-talk from [^{123}I]IBZM, $C_{VOI}^{123}(t)$ and $C_{REF}^{123}(t)$ are measured radioactivities at the ^{123}I principal emission spectrum in the VOI and reference region, respectively. The α parameter, corresponding to the VOIs, is fitted. On the other hand, considering the reference region (α') it is fixed with the value estimated as described in section 2.5.1.

Combining equations (4)–(6) gives the operational equation of the "corrected" SRTM or $SRTM_C$:

$$C_{VOI}^{total}(t) = R_1\left(C_{REF}^{total}(t) - \alpha'\ C_{REF}^{123}(t)\right) + (k_2 - R_1 k_2/(1 + BP_{ND}))\left(C_{REF}^{total}(t) - \alpha'\ C_{REF}^{123}(t)\right) \otimes e^{-\frac{k_2}{(1+BP_{ND})t}} + \alpha\ C_{VOI}^{123}(t) \quad (7)$$

that was implemented in PMOD software, as previously described (Tsartsalis et al., 2014b). Thus, the number of parameters to fit with $SRTM_C$ is one more than in the SRTM, which is the α coefficient for every VOI (given that for the reference region it is fixed (Tsartsalis et al., 2014b)).

Statistical analysis

In phantom experiments, radioactivity measurements from cross-talk corrected images of phantoms that contained both radioisotopes were compared to measurements from the respective adjacent phantoms containing a single radioisotope. In rat experiments, regional BP_{ND} values resulting from the quantification of cross-talk-corrected dual-radiotracer images, were compared with corresponding values from single-radiotracer images of *in vivo* experiments. Comparisons in both cases were performed by means of linear regression analysis and paired-sampled *t*-test. Statistical significance was set to $p < 0.05$.

Evaluation of the relationship between striatal $D_{2/3}$ and 5-HT_{2A}-receptor binding at the voxel and VOI level

The relationship between $D_{2/3}$ and 5-HT_{2A} binding in the striatum has been evaluated in an independent group of ten Mdr1a KO rats, weighing 370–520 g. SPECT scans and image reconstruction were performed as described in sections 2.3 and 2.4, respectively, with the difference that a shorter scanning protocol was employed: a scan composed of four, 10 min-long frames was initiated at t = 80 after a concurrent injection of 30.42 ± 8.92 MBq of [^{123}I]IBZM and 24.6 ± 5.63 MBq of [^{125}I]R91150. In this experiment, no time interval was left between the injections of the two radiotracers, contrary to the dual-radiotracer studies described in section 2.3. In that case, the interval served in the dynamic SPECT protocol and the $SRTM_C$ method, to demonstrate the effect of cross-talk on the radiotracer's kinetics. Dual-radiotracer imaging was performed using the DEW method (Method 1 in section 2.5.1) and BP_{ND} was estimated as in section 2.5.1 with the SUR over frames corresponding to 80–110 min post radiotracer injection for [^{123}I]IBZM and 100–120 min for [^{125}I]R91150. A test-retest analysis of BP_{ND} estimations using this approach is described in the supplemental material. To perform voxel-wise linear regression analysis between $D_{2/3}$ and 5-HT_{2A} receptor binding across the group of six rats, static SPECT images corresponding to 80–110 min post radiotracer injection for [^{123}I]IBZM and 100–120 min for [^{125}I]R91150 were spatially normalized as follows: at first, a [^{125}I]R91150 template-image was created with the Small Animal Molecular Imaging Toolbox (Vallez Garcia et al., 2015) (SAMIT, Groningen, Netherlands) using the static [^{125}I]R91150 SPECT scans mentioned above, in Matlab (R2016, Mathworks Inc, USA). Then, spatial normalization of the [^{125}I]R91150 SPECT images of each rat was performed in PMOD, which implements methods according to SPM5 software (Wellcome Trust Center for Neuroimaging, UCL, London, UK). The resulting transformation matrix was applied to the corresponding [^{123}I]IBZM images. Then, voxel-wise regression analysis of [^{123}I]IBZM and [^{125}I]R91150 binding was performed in Matlab (estimated using the SUR) and images of the Pearson's r coefficient and associated p-values were produced. Linear regression analysis was also performed at the VOI level (in the NAcc and the caudate/putamen nucleus, CPu, bilaterally) on these same parametric images of BP_{ND}. An experimental and simulation study to validate that the observed correlation between $D_{2/3}$ and 5-HT_{2A} binding is not due to any residual cross-talk activity from [^{123}I]IBZM on [^{125}I]R91150 images is described in the supplemental material.

Results

In Fig. 1, the protocol used in the dual-radiotracer experiments (see section 2.3) is presented. The [^{125}I]R91150 TAC is unbiased until the 20th min, when [^{123}I]IBZM is injected. From this moment on, the [^{125}I]R91150 TAC is considerably biased for the whole duration of the experiment. The effect of cross-talk on the radioactivity measurements at the low-energy spectrum is also presented in Fig. 2. Indeed, in Fig. 2A, the SPECT image of the three phantoms was reconstructed at the low-energy window, in which both ^{123}I and ^{125}I are visualized. The emission from the ^{123}I-containing phantom shows that ^{123}I emits a considerable radioactive signal at this energy spectrum thus producing the cross-talk phenomenon with the ^{125}I-derived radioactivity.

Correction of the cross-talk between ^{123}I and ^{125}I with the DEW method

Fig. 3 A depicts the radioactivity measured in a ^{123}I-phantom SPECT experiment across the energy spectrum. The radioactive counts measured from the ^{123}I phantoms at the high- ($^{123}I_{high}$) and the low-energy spectra ($^{123}I_{low}$) highly correlated with each other (Fig. 3B, $r = 0.99$, $p < 0.001$). The α coefficient was found to be 0.58 in the phantom experiments. Fig. 3C depicts an image of three of the dual-radiotracer phantoms reconstructed at the low-energy spectrum before the correction for cross talk. In Fig. 3D, the images have been reconstructed at the high-energy

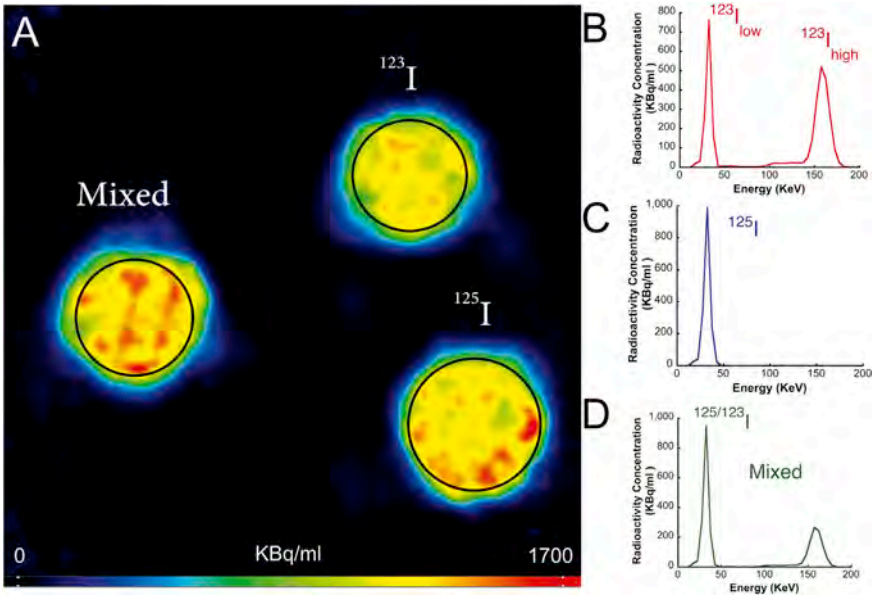

Fig. 2. (A) A static SPECT image from three phantoms filled with ^{123}I, ^{125}I and both ("Mixed") radioisotopes, reconstructed at the low energy spectrum. The respective radioactive emissions across the energy spectrum are shown in (B–D). The double emission of ^{123}I, at the high and low spectra, the latter one overlaps with the ^{125}I spectrum and is at the origin of the cross-talk.

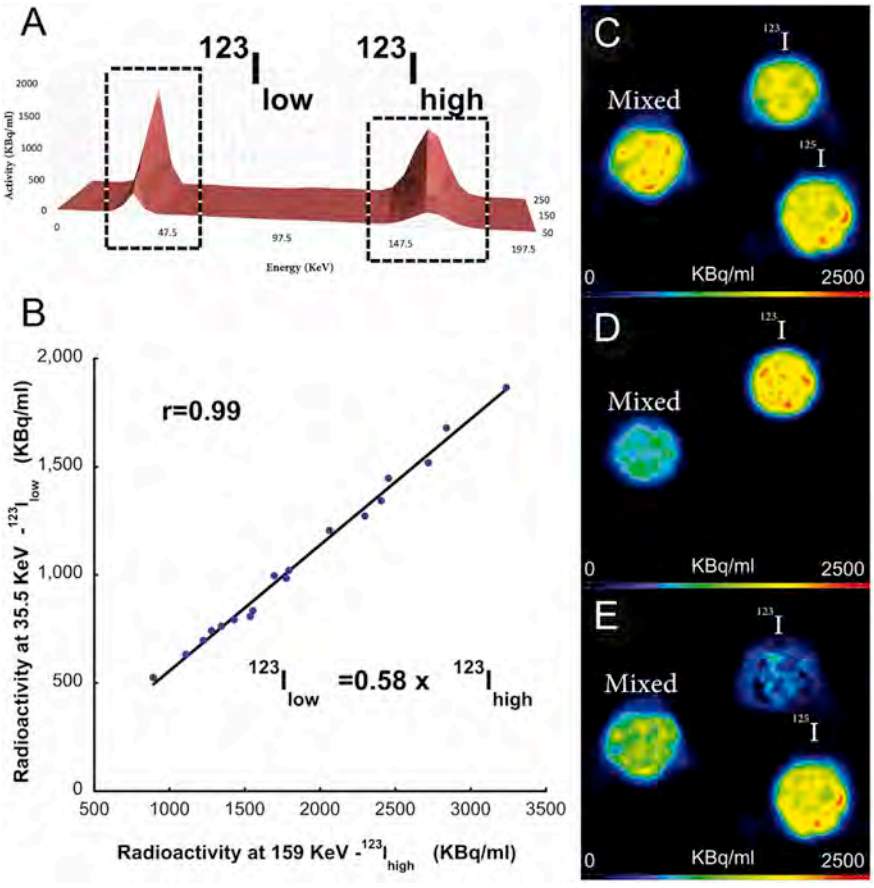

Fig. 3. (A) The radioactivity emission of ^{123}I, across the energy spectrum. The radioactivity measured at the high ($^{123}I_{high}$) and the low energy spectrum ($^{123}I_{low}$) is noted on the plot. (B) linear regression between $^{123}I_{high}$ and $^{123}I_{low}$ for all the phantoms and estimation of the α coefficient from the slope of the regression line (0.58). (C) An image of three phantoms reconstructed at the low energy window. (D) the same image reconstructed at the high energy window. (E) the same image reconstructed at the low energy window, corrected for cross-talk with the DEW method.

window, clearly demonstrating the disappearance of the ^{125}I-containing phantom and the diminution in the activity in the mixed-radioactivity tube that contains both radioisotopes. In Fig. 3E, the image has been corrected for cross-talk with the DEW method. This led to an almost-disappearance of the ^{123}I-containing phantom and a similar decrease in the radioactivity measured in the phantom containing both radioisotopes.

Fig. 4 A presents the corrected [^{125}I]R91150 image from an *in vivo* dual-radiotracer experiment. The images acquired correspond to the window between the 100th and the 120th minute post-injection. The predominance of binding in frontal cortical areas with respect to subcortical structures is observed, along with a fronto-caudal gradient in binding, a pattern typical of 5-HT_{2A} distribution (Tsartsalis et al., 2016a). In Fig. 4B, the good correlation between the radioactive counts emitted

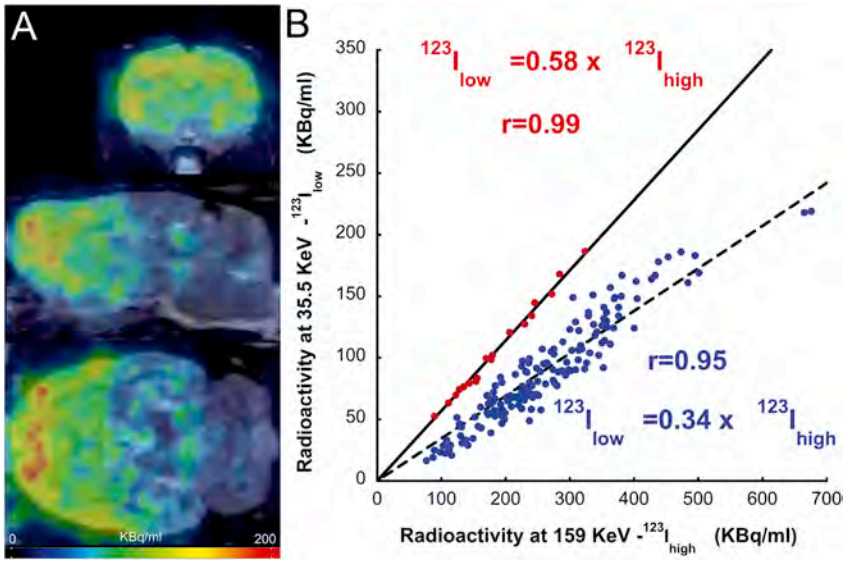

Fig. 4. (A) Coronal, sagittal and axial planes of a DEW-corrected *in vivo* [^{125}I]R91150 SPECT image. (B) The correlation between the radioactivity emitted from [^{123}I] IBZM at the high and the low energy spectra is plotted in blue dots. Each one of them corresponds to the measurements in one of the 57 brain VOIs in three rats *in vivo*. The correlation between the high and low energy emission of ^{123}I as measured in phantom experiments (shown in Fig. 3B) is also shown in red dots.

by [^{123}I]IBZM *in vivo* at the high- and the low-energy spectrum across the brain VOIs is presented ($r = 0.95$, $p < 0.001$). The same correlation from the phantom experiments is included for comparison. The α coefficient was 0.34 ± 0.057 *in vivo* for all VOI and across the three rats. The variability of the α coefficient values was mainly due to some low-binding VOI. On the contrary, high binding VOI, striatal VOI and the CER, had less variable α coefficient values (0.33 ± 0.04 in the motor cortex, MC, 0.36 ± 0.04 in the medial prefrontal cortex, MPFC, 0.30 ± 0.02 in the orbitofrontal cortex, OFC, 0.35 ± 0.04 in the somatosensory cortex, SSC, $0.31 \pm .04$ in the cingulate cortex, CC, 0.35 ± 0.03 in the NAcc, 0.33 ± 0.02 in the Caudate/Putamen, CPu and $0.34 \pm .03$ in the CER).

Correction of the cross-talk between ^{123}I and ^{125}I using spectral FA

Fig. 5 shows the result of the application of spectral FA to correct for the effect of cross-talk on ^{125}I signal in a phantom dual-radiotracer experiment. The factor-images corresponding to the ^{123}I- and ^{125}I-emitted radioactive signal and the third factor (Fig. 5A, C and 5E, respectively) are presented along with their respective factor-curves (Fig. 5B, D and 5F). In Fig. 5A, in which the ^{123}I-emitted signal is retained, the ^{125}I-containing phantom virtually disappears and the opposite is observed in Fig. 5C, where ^{125}I-emitted signal is retained. The third factor-image (Fig. 5E–F, respectively) and the associated curve presents a negligible amount of radioactivity compared to the first two factors. The magnitude of the associated radioactivity concentration is hundreds of times lower than the radioactivity of the first two factors.

Fig. 6 shows the result of the application of FA for cross-talk correction in one *in vivo* dual-radiotracer experiment ([^{123}I]IBZM in Fig. 6A and [^{125}I]R91150 in Fig. 6B) and the three factor curves (Fig. 6C). The images acquired *in vivo* correspond to the window between the 80th and the 110th minute post radiotracer injection for [^{123}I]IBZM and between the 100th and the 120th minute post-injection for [^{125}I]R91150. The corrected *in vivo* brain images present a predominant binding in striatum, compatible with the known spatial distribution of the [^{123}I]IBZM. The spatial distribution of [^{125}I]R91150 binding is as described in section 3.1. The third factor curve represents the rest of the radioactive signal that is negligible compared to the factor-images described above, as was the case for the phantom experiments. Both in the phantom and *in vivo* experiments, the two predominant factors have a visually similar spectral distribution pattern as the spectral patterns of energy emission extracted from single-radiotracer experiments (Fig. 2).

Correction of the cross-talk between ^{123}I and ^{125}I using the $SRTM_C$

Fig. 7 shows the TACs extracted from a dynamic dual-radiotracer *in vivo* SPECT experiment using a VOI corresponding to the OFC (average of bilateral VOIs), a high 5-HT_{2A} binding region. The TAC extracted from the image reconstructed at the high-energy spectrum is shown in red

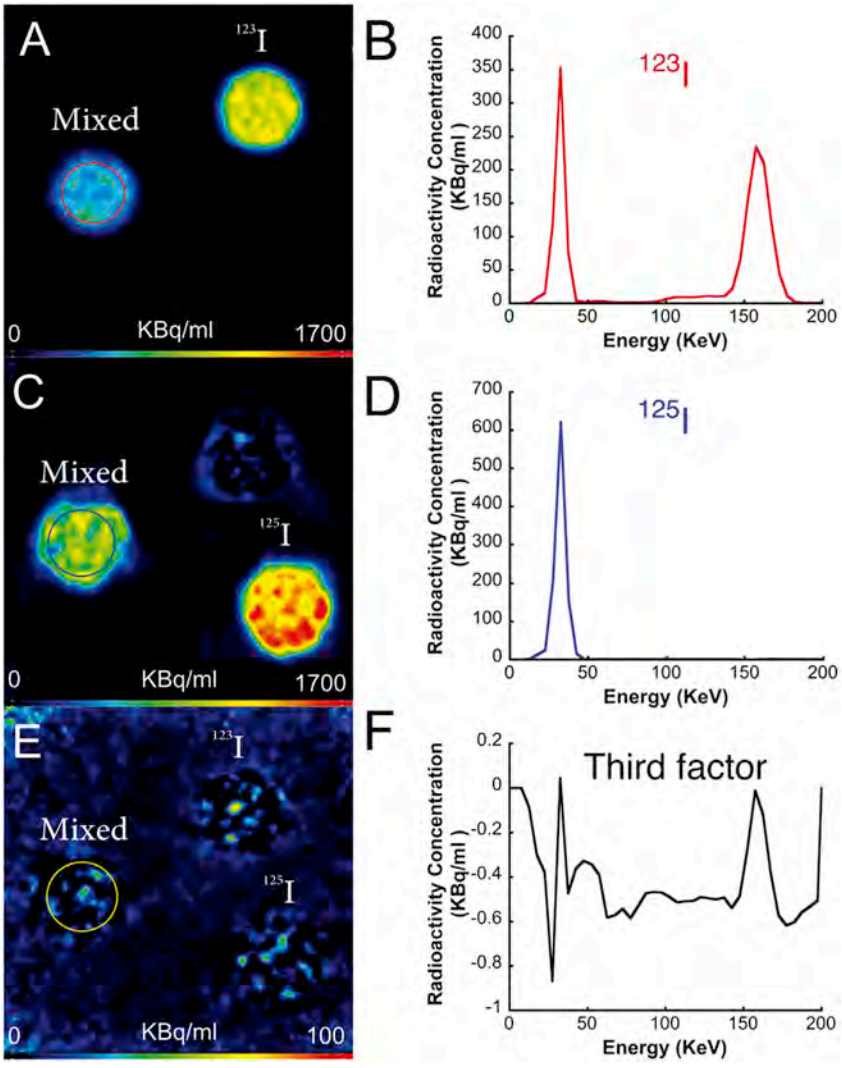

Fig. 5. Image-factors (A, C, E) and associated factor-curves (B, D, E) corresponding to ^{123}I, ^{125}I and the third factor, obtained from FA application in phantom experiments. Note the minimal radioactivity attributed to the third factor (E and F) as opposed to the radioactivity from the first two factors.

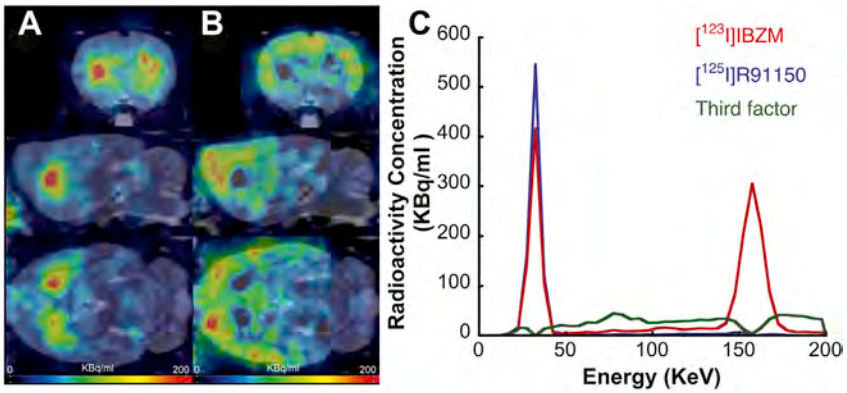

Fig. 6. Coronal, sagittal and axial planes of a FA-corrected *in vivo* [^{125}I]R91150 (A) and [^{123}I]IBZM (B) SPECT image. (C) the associated factor-curves.

color. This TAC corresponds to $D_{2/3}$ binding and is unaffected by any cross-talk effect. In black color is the uncorrected TAC extracted from the image reconstructed at the low-energy spectrum. It is important to note that the initial part of the TAC (first 20 min) that corresponds to the scan duration before the injection of [^{123}I]IBZM overlaps completely with the blue TAC, which is the corrected TAC with the $SRTM_C$ method. The injection of [^{123}I]IBZM at the 20th minute induces a steep increase in the radioactive signal of [^{125}I]R91150 and produces an important deviation from the normal kinetic pattern of this radiotracer. The $SRTM_C$ fitted the [^{125}I]R91150-derived TACs in an excellent manner (data not shown). The α' coefficient in CER, the reference region, was fixed at 0.34, the average value estimated in the series of rats that received only [^{123}I]IBZM, as described in 2.5.1. The coefficient values for the brain VOIs, which were fitted with $SRTM_C$ had an average value of 0.29 ± 0.07, which was close to the average value of the α coefficients estimated in the series of rats that received only [^{123}I]IBZM, as described in 2.5.1.

Comparison of the methods for cross-talk correction

The radioactive concentrations obtained after cross-talk correction of the images of the phantoms containing both ^{123}I and ^{125}I were compared with the values obtained from the corresponding adjacent single-radioisotope containing tubes, which served as controls. For the DEW method, the linear regression for ^{125}I provided an excellent correlation ($r = 0.998$, $p < 0.001$, with a slope of the regression line of 0.96). Similarly, the ^{125}I measurements after FA correction of cross-talk were excellent ($r = 0.998$, $p < 0.001$, with a slope of 0.916). The ^{123}I measurement after FA correction of cross-talk gave equally good results ($r = 0.999$, $p < 0.001$, with a slope of 1.03).

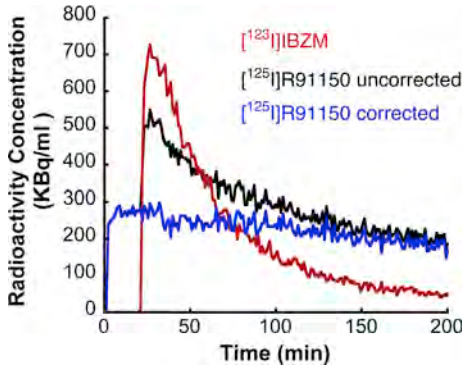

Fig. 7. TACs extracted from a dynamic dual-radiotracer *in vivo* SPECT experiment using a VOI corresponding to the OFC. The TAC extracted from the image reconstructed at the high-energy spectrum is shown in red color. In black color is the uncorrected TAC extracted from the image reconstructed at the low-energy spectrum. The blue TAC corresponds to the corrected [^{125}I]R91150 TAC with the $SRTM_C$ method.

Table 2 presents BP_{ND} values extracted from *in vivo* experiments. Examples of high- and low-binding VOIs for 5-HT_{2A} (MC, MPFC, OFC) and $D_{2/3}$ receptors (NAcc and CPu) are included. The SUR approach was applied over static dual-radiotracer images corrected with the DEW method and FA. The same approach was applied to single-radiotracer SPECT images for comparison. BP_{ND} values extracted from dynamic dual-radiotracer images using the cross-talk correction in the $SRTM_C$ are also included. BP_{ND} values from frontal cortical regions estimated from DEW-corrected dual-radiotracer images ranged from 3.86 ± 0.24 in the MC to 4.75 ± 0.96 in the OFC. FA-corrected images provided similar values ranging from 3.77 ± 0.29 to 4.77 ± 0.93, respectively. $SRTM_C$-derived BP_{ND} values were found in a similar range, i.e. from 3.78 ± 0.11 in the MC to 5.18 ± 1.73 in the OFC. Regarding the high-5-HT_{2A} binding VOIs, all correction methods provide overestimated values, compared to values estimated using the same methods from single-radiotracer experiments and in the case of the DEW- and FA-derived BP_{ND} values reached statistical significance (as evaluated by means of paired-samples *t*-test). The extraction of [^{123}I]IBZM images from dual-radiotracer experiments using FA provides average BP_{ND} values which are very close to the values estimated from [^{123}I]IBZM images that were directly reconstructed at the high energy window (shown in the last column of Table 2).

Furthermore, an evaluation of the cross-talk correction methods was performed. BP_{ND} estimations from the dual-radiotracer experiments, corrected with each one of the three methods were compared to the estimations from single-radiotracer [^{123}I]R91150 experiments by means of linear regression analysis. BP_{ND} values were averaged in every VOI across the rats of the same group and regression analysis was performed using average these VOI values. Average BP_{ND} values estimated in cross-talk corrected [^{125}I]R91150 images using the DEW method correlated well with average BP_{ND} values from single-radiotracer [^{123}I]R91150 experiments ($r = 0.92$, $p < 0.001$, Fig. 8A). Similarly, BP_{ND} values from [^{125}I]R91150 images corrected with FA correlated equally well ($r = 0.92$, $p < 0.001$, Fig. 8B). BP_{ND} values from the spectral FA-extracted [^{123}I]IBZM images from dual-radiotracer experiments were compared to BP_{ND} values from the exact same images that were reconstructed at the high-energy spectrum, where only unbiased ^{123}I-emitted radioactivity is detected ($r = 0.99$, $p < 0.001$, Fig. 8C). A similar same level of agreement was observed using the $SRTM_C$ to account for the impact of cross-talk on [^{125}I]R91150 kinetics ($r = 0.92$, $p < 0.001$, Fig. 8D).

Evaluation of the relationship between striatal $D_{2/3}$ and 5-HT_{2A}-receptor binding at the voxel and VOI level

Fig. 9 A presents a coronal section of a parametric image of Pearson's r coefficients. Linear regression analysis was performed to compare $D_{2/3}$ and 5-HT_{2A} binding across the six rats of the experiment at the voxel level. Parametric images of associated p values of statistical significance reveal that two small clusters of voxels (<20 voxels) in each NAcc reach

Table 2
BP_{ND} (ml/ml) values extracted from dual- and single-radiotracer studies. Values are presented as mean ± standard deviation. The unbiased (control) values were obtained from a single-radiotracer [^{123}I]R91150 experiment (4 rats) while the unbiased [^{123}I]IBZM values were obtained after the reconstruction of the images of the dual-radiotracer experiments at the high energy window, which is not affected by any cross-talk. No BP_{ND} values outside the striatum are presented for [^{123}I]IBZM.

VOI	Dual radiotracer-experiments				Unbiased (control) experiments	
	[^{125}I]R91150			[^{123}I]IBZM	[^{123}I]R91150	[^{123}I]IBZM
	DEW (SUR)	FA (SUR)	$SRTM_C$	FA (SUR)	SUR	SUR
MC	3.86 ± 0.24	3.77 ± 0.29	3.78 ± 0.11	–	2.85 ± 0.21	–
MPFC	4.20 ± 1.13	4.76 ± 0.87	4.28 ± 0.74	–	3.48 ± 0.48	–
OFC	4.75 ± 0.96	4.77 ± 0.93	5.18 ± 1.73	–	3.34 ± 0.24	–
NAcc	1.94 ± 0.66	2.26 ± 0.64	2.04 ± 0.45	2.61 ± 0.29	2.55 ± 0.43	2.59 ± 0.6
CPu	2.51 ± 0.54	2.66 ± 0.57	2.94 ± 0.42	5.12 ± 0.59	2.53 ± 0.34	4.93 ± 0.92

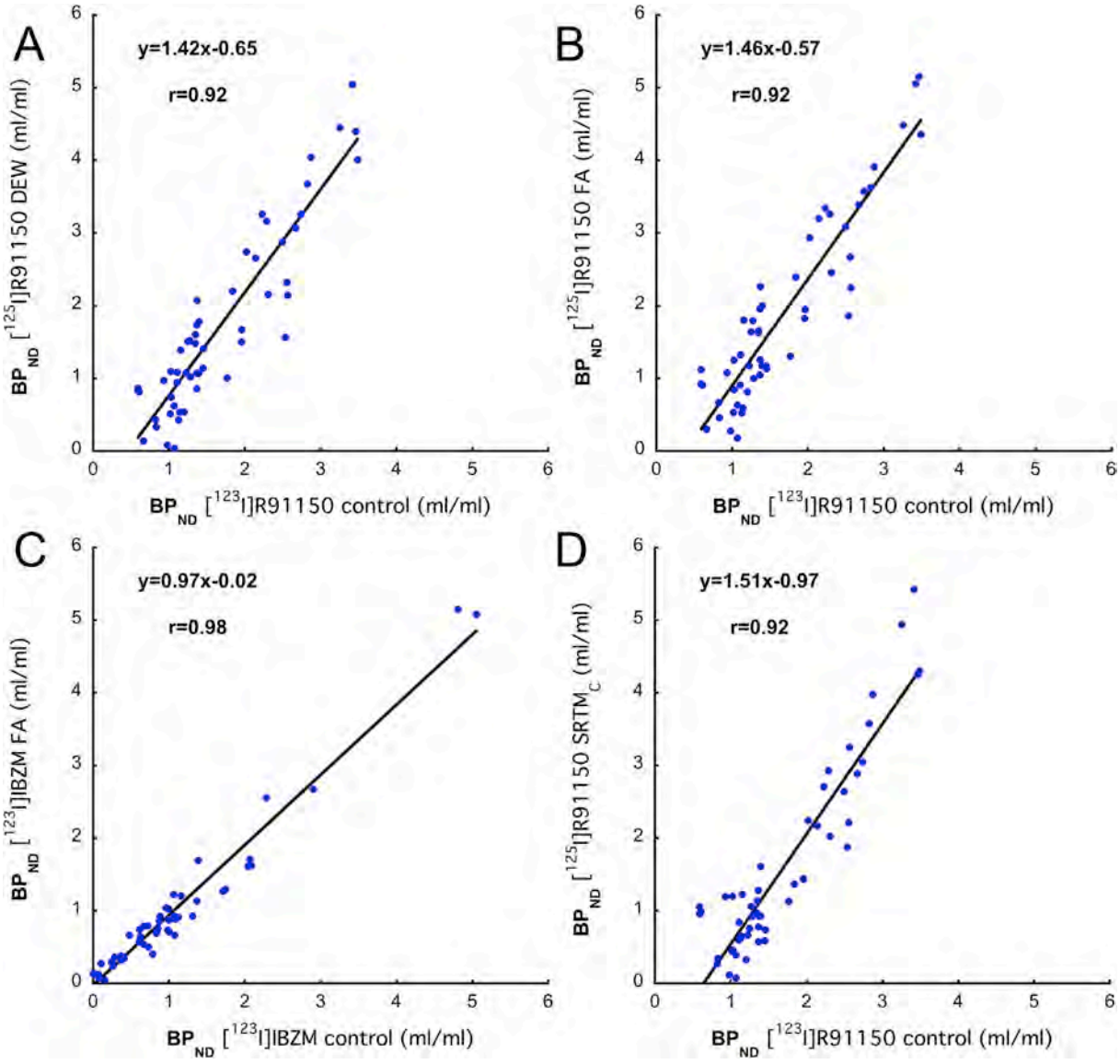

Fig. 8. Scatterplot of average (across rats) regional [^{125}I]R91150 BP_{ND} values (vertical axis) from the dual-radiotracer *in vivo* experiments corrected with the (A) DEW (Method 1) and (B) spectral FA (Method 2). They are plotted against average [^{123}I]R91150 BP_{ND} values from the single-radiotracer experiments (horizontal axis). (C) Correlation between average [^{123}I]IBZM BP_{ND} values obtained after the application of FA (vertical axis) and the average BP_{ND} values from the direct reconstruction of [^{123}I]IBZM at the high-energy spectrum (which is unbiased) from the same experiments (horizontal axis). $SRTM_C$ (Method 3). (D) Scatterplot of average [^{125}I]R91150 BP_{ND} values (vertical axis) obtained with the $SRTM_C$ method plotted against the average [^{123}I]R91150 BP_{ND} values from the single-radiotracer experiments (horizontal axis).

significance at $p < 0.05$. Linear regression analysis was also performed for the comparison of $D_{2/3}$ and 5-HT_{2A} binding across these six rats at the VOI level in bilateral CPu and NAcc. A statistically significant correlation is observed ($r = 0.78$, $p < 0.01$, Fig. 9B) in NAcc, but not in CPu (data not shown).

Discussion

BP_{ND} estimation from dual-radiotracer SPECT studies

The present paper evaluates three different methods for the simultaneous, dual-radiotracer imaging using a ^{123}I- and a ^{125}I-labeled molecule. These methods correct the effect of cross-talk on radioactivity measurements of ^{125}I. All three methods provide BP_{ND} values of [^{125}I]R91150 that correlate highly with values obtained from single-radiotracer [^{123}I]R91150 experiments and are similar to values from the literature (Dumas et al., 2015; Tsartsalis et al., 2016b, 2017). Using one of the proposed methods (DEW), we also demonstrated that BP_{ND} values from dual-radiotracer experiments have an acceptable test-retest variability, which is 14% for [^{123}I]IBZM and 14.10% for [^{125}I]R91150 (see section S2.1). Indeed, in SPECT, [^{123}I]R91150 BP_{ND} values' test-retest variability ranges between 10 and 20% (Catafau et al., 2008). In small animal imaging in general, a variability of 15–20% is considered acceptable (Constantinescu et al., 2011), as is the case for the BP_{ND} values presented here.

The DEW method (Method 1) provides the most straightforward means of correction of the cross-talk between ^{123}I- and ^{125}I-labeled molecules. It exploits the linear relationship between the ^{123}I-emitted activity on the ^{125}I spectrum and thus its use has no statistical noise. To our knowledge, the present paper is the first to employ this method in brain imaging (Lee et al., 2013, 2015). The validity of this methods is supported by the excellent correlation between BP_{ND} values from DEW-corrected, dual-radiotracer and from single-radiotracer SPECT studies. One disadvantage of this method is the variability of the α coefficient values across the brain regions, due to the interaction of photons with matter. Indeed, this interaction is illustrated by the difference in the value of the α coefficient as estimated in phantoms (where there is a minimal interaction with matter) and *in vivo*. This is not surprising and has been described for another pair of SPECT-employed radioisotopes, ^{111}In^{111} and ^{177}Lu (Hijnen et al., 2012). Importantly, in our experiments, the effect of the interaction with matter is quite homogeneous across the brain VOI and across rats with a coefficient of variation of α at 17%. This variation in the α parameter values, albeit non-negligible *per se*, probably has a little impact in the context of this study. Indeed, looking into the value of this parameter in individual VOI across rats shows that in cortical, receptor-rich regions, as well as in the striatum and the CER, α values are less variable (with a coefficient of variation <10% as described in section 3.1 and close to the average value that was used in the application of the DEW method.

Using FA (Method 2) for the correction of the cross-talk resulted in BP_{ND} values that correlated similarly well with the [^{123}I]R91150 values from the single-radiotracer group. As a further validation step, the BP_{ND} values of [^{123}I]IBZM extracted with FA was directly compared to the corresponding values from [^{123}I]IBZM images that were directly reconstructed at the principal (hence cross-talk-free) emission spectrum of ^{123}I. The highly significant correlation proposes that FA does not considerably bias the radioactivity measurements. The use of extra-striatal BP_{ND} values in the linear regression analysis of ^{123}I binding may appear odd, given the lack of specific binding of [^{123}I]IBZM out of the striatum. However, the objective of this comparison was to assess the correction of a physical phenomenon (cross-talk) that is little affected, if at all, by the kind of binding (specific, free or non-specific). The application of FA is not limited to dual ^{123}I and ^{125}I experiments but extends to dual ^{123}I and ^{99m}Tc imaging, which may equally be applied in clinical neuroimaging. Indeed, correction of cross-talk between ^{123}I and ^{99m}Tc with independent component analysis has been described in the literature (Chang et al., 2006). In the same paper, this method proved superior to a simple reconstruction using an energy spectrum at 15% around the ^{99m}Tc photopeak. Model-based correction methods have also been proposed for this correction (Du and Frey, 2009; El Fakhri et al., 2001). Another advantage of FA is that it may potentially be used for triple-radiotracer SPECT using ^{123}I, ^{125}I and ^{99m}Tc and preliminary studies of our group on phantoms show promising results (data not shown). FA is not as straightforward as the DEW method and presents a statistical noise. In addition, in voxels that have the highest binding of the ^{123}I-labeled radiotracer and a moderate or low binding of the ^{125}I-labeled radiotracer, FA tends to attribute all the radioactivity to the ^{123}I, thus underestimate the ^{125}I-associated binding. This seems to be the case for some striatal voxels, as illustrated in Fig. 6B. This could be of little importance when BP_{ND} values are studied in whole VOIs but could be a considerable limitation in voxel-wise quantification.

Method 3, which implements the cross-talk correction in the kinetic analysis with SRTM, provides a valuable alternative to the previous two methods when kinetic modeling in dynamic images is required for quantification. Indeed, using the first two methods, FA in particular, in dynamic studies would be computationally challenging. One disadvantage of the $SRTM_C$ method is the need for an interval between the injections of each radiotracer. In addition, $SRTM_C$ necessitates an *a priori* determination of the α coefficient in the reference region to optimize the identifiability of the model's parameters. Nevertheless, an interesting finding is that the estimates of the α coefficient with Method 3 have comparable values to the ones found with Method 1 and this consistency is, to our view, an argument in favor of the validity of the proposed methods.

Given the fact that Method 1 (DEW) is the most straightforward and computationally feasible to apply, while it has no statistical noise, it was the method of choice for the study of the relationship of $D_{2/3}$ and 5-HT_{2A} receptor binding in the striatum, as discussed further in this paper.

Dual-radiotracer imaging in PET and SPECT

Dual SPECT imaging is feasible when radiotracers are labeled with radioisotopes with non-overlapping emission spectra (Akutsu et al., 2009; Antunes et al., 1992; Bruce et al., 2000; Ichihara et al., 1993). Dual [^{99m}Tc]pyrophosphate/^{201}Tl SPECT has been proposed in cardiac nuclear imaging to assess the viability of the myocardium and its irrigation, respectively. Similarly, ^{201}Tl/[^{123}I]β-methyl-iodophenyl pentadecanoic acid (BMIPP) dual-radiotracer SPECT has been described for a simultaneous assessment of cardiac perfusion (^{201}Tl) and fatty acid metabolism ([^{123}I]BMIPP) (Akutsu et al., 2004). In both cases, the energy emission spectra of the combined radioisotopes had no considerable overlap, thus no cross-talk correction was required. ^{111}In/^{177}Lu dual-radioisotope SPECT has also been described, given the minimal overlap of their respective emission spectra, with a DEW method to account for this overlap (Hijnen et al., 2012).

Recently, a PET system that proposes dual (or higher) simultaneous radiotracer imaging using pure positron and positron-γ emitters, has been described (Fukuchi et al., 2017). In addition, discrimination of positron-emitting radioisotopes based on their unique decay rate has been described for ^{18}F and ^{13}N (Figueiras et al., 2011). Dual-radiotracer PET has also been described in the case of brain tumor studies in which tumor metabolism and proliferative activity are assessed with [^{18}F]FDG and [^{18}F]FLT, respectively. In that paper, a joint-radiotracer pharmacokinetic model was considered and all the kinetic parameters were estimated from a PET dynamic study in which the two radiotracers were injected with a 30-min delay from each other (Kadrmas et al., 2013). A longer delay between the two radiotracers' injections may be appropriate when short half-life radiotracers are used (Koeppe et al., 2001). Overall, our study is the first among the aforementioned ones which proposes a dual-radiotracer imaging methodology with radioiodinated molecules in the brain and a direct biological application.

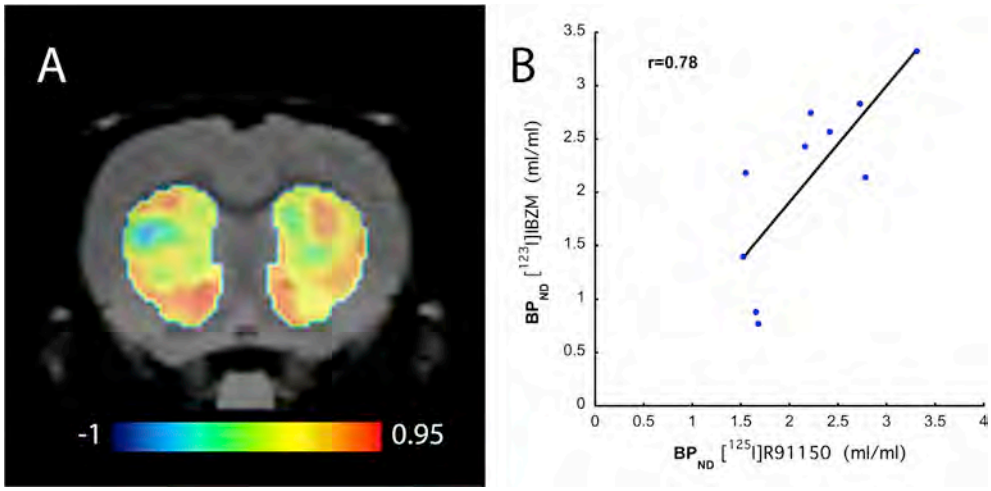

Fig. 9. (A) a coronal section of a parametric image of Pearson's r coefficients. Linear regression analysis was performed to compare $D_{2/3}$ and 5-HT_{2A} binding across the six rats of the experiment at the voxel level. The color bar represents r values. (B) Linear regression analysis for the comparison of $D_{2/3}$ and 5-HT_{2A} binding across ten rats at the VOI level (including average left and right NAcc for each rat).

Simultaneous study of $D_{2/3}$ and 5-HT_{2A} binding in the striatum

The *in vivo* study of multiple receptors or proteins in general, is an approach of great potential, as the understanding of brain physiology and pathology may not be limited to the study of one molecular target. In the present study, to emphasize on the feasibility of performing simultaneous, dual-radiotracer SPECT studies *in vivo,* we provide preliminary evidence for an association of $D_{2/3}$ and 5-HT_{2A} receptors in the NAcc. We employed Method 1 (DEW) to study the relationship between $D_{2/3}$ and 5-HT_{2A} binding because it is the most straightforward. $D_{2/3}$ and 5-HT_{2A} BP_{ND} values show a positive correlation, at the VOI level, in NAcc. In a preliminary evaluation of the same relationship at the voxel level, we find that $D_{2/3}$ and 5-HT_{2A} binding showed a good correlation in the NAcc across the rats. Given the fact that this is an exploratory analysis, with a primary purpose to validate the dual-radioligand approach (which is intended to use with any couple of molecular targets in the brain and not limited to $D_{2/3}$ and 5-HT_{2A}), with a limited number of rats and without any correction for the effects of noise, we did not perform any correction for multiple comparisons. In this context, formulating conclusions on the biological underpinnings of this voxel-wise correlation is out of the scope of this paper.

Evidently, one could hypothesize that there is no real correlation and that [^{123}I]IBZM contaminates [^{125}I]R91150 radioactivity measurements due to suboptimal correction of cross-talk. The simulation study described in section S2.3 shows that even in the "worst-case" scenario where both striatal and cerebellar α coefficient values have been miscalculated (by 20% that exceeds the variability of α coefficient estimates from [^{123}I]IBZM-only experiments as estimated in 2.5.1), the change of the slope of the regression line does not produce an artificial correlation. As a further proof, we performed the analysis in S2.3, in which radiolabeling with ^{123}I and ^{125}I was inversed for IBZM and R91150. In this case we evaluate the scenario where ^{123}I radioactivity in high [^{123}I]R91150-binding VOIs (such as in cortical VOIs) highly contaminates the signal from [^{125}I]IBZM which is virtually inexistent in the same regions. Knowing that no specific binding of [^{125}I]IBZM is observed out of the striatum, we safely assume that no correlation should be observed after the correction for cross-talk whatsoever. Before correction, voxel-wise BP_{ND} values between the two radiotracers correlated well (data not shown). This is not surprising, given the high level of ^{123}I-derived radioactivity that is measured at the ^{125}I energy spectrum. After correction for cross-talk, no voxel-wise correlation at any of the VOIs was observed, thus further confirming the validity of the DEW method that demonstrated this correlation between the two receptors. We also rule out the possibility that the observed correlation is in fact biased by the partial volume effects on [^{125}I]R91150 binding in NAcc from adjacent high-binding cortical VOIs. Indeed, no correlations are observed between $D_{2/3}$ binding in NAcc and 5-HT_{2A} binding in either of these cortical regions (S2.3). In addition, our *in vitro* autoradiography study (see Supplemental S1.4), shows that in NAcc, regional $D_{2/3}$ binding correlates with 5-HT_{2A} binding, further supporting the *in vivo* study.

Evidence in the literature on D_2 and 5-HT_{2A} interactions already exists: they may be co-expressed on the same cells (Ma et al., 2006) or form functional heterodimers (Albizu et al., 2011; Borroto-Escuela et al., 2014; Lukasiewicz et al., 2010) in physiological or pathological conditions (Varela et al., 2015). Nonetheless, the full extent of the biological implications of such an interaction remains elusive. In this context, dual-radiotracer imaging of $D_{2/3}$ and 5-HT_{2A} (as well as of other couples of molecular targets) may constitute a complementary means for the non-invasive, *in vivo* study of such complex biological phenomena.

Limitations

Our study has three main limitations. First, performing single- and dual-radiotracer experiments on the same rat at different time-points could provide a better comparison group for the validation of the methods proposed for the correction of cross-talk between ^{123}I and ^{125}I and further validation of the results with this approach is encouraged, especially if other couples of radiotracers are employed in future experiments. Indeed, averaging values across rats before comparison may diminish the effect of BP_{ND} variability. Nevertheless, we chose to use three independent groups of rats instead of using the same group and multiple scans for each animal to minimize stress for the animals. In addition, the use of the same rat at different time-points would still be subject to the test-retest variability. The scanning protocol employed in the study was quite long and this constituted a technical difficulty for using the same rats twice. Despite this limitation, the linear regression analysis results demonstrate a highly significant correlation between [^{125}I]R91150 values from dual-radiotracer and [^{123}I]R91150 values from single-radiotracer experiments.

Another limitation concerns the observed correlation between NAcc [^{123}I]IBZM and [^{125}I]R91150 BP_{ND} values. Despite support from literature, there is no direct study of the biological implications of this finding. However, this would be largely out of the scope of this paper, which intends to illustrate that using dual-radiotracer SPECT in translational research may reveal such relationships between different aspects of a biological phenomenon, to permit an *in vivo* longitudinal assessment and,

finally, to be coupled with studies at the cellular and molecular level. Furthermore, in the present paper, no assessment of this relationship in extra-striatal regions may be obtained given the absence of specific binding of [^{123}I]IBZM in these regions. Such a study may be performed with [^{123}I]epidepride, a high-affinity $D_{2/3}$ radiotracer presenting specific binding in extra-striatal regions. Our proposed methods may be directly applied in a dual-radiotracer [^{123}I]epidepride/[^{125}I]R91150 study, as with any couple of radio-iodinated molecules.

Finally, we did not perform either scatter or attenuation correction in our *in vivo* imaging studies. Both corrections should be important (Andersen et al., 2014), particularly with the DEW method (Lee et al., 2015). ^{125}I, in particular, is more subject to attenuation and scatter effects than ^{123}I (Feng et al., 2007; Gregor et al., 2007). Correcting for the effects of these phenomena should diminish the bias presented in BP_{ND} values of [^{125}I]R91150 compared to [^{123}I]R91150, which is evident from Fig. 8 and Table 2. In fact, despite excellent correlations, BP_{ND} values from dual-radiotracer experiments were overestimated with all three correction methods (with the values of the DEW and FA methods reaching statistically significant difference from [^{123}I]R91150 BP_{ND} values). This overestimation is, at least in its greatest part, the result of the effects of scatter and attenuation on ^{125}I imaging *per se* and not of any bias in the dual-radiotracer imaging approaches described here. As shown in supplemental Fig. S2, [^{125}I]R91150 BP_{ND} values from dual-radiotracer experiments correlate well with [^{125}I]R91150 BP_{ND} values from single-radiotracer experiments and do not differ significantly from them. Thus, it may be hypothesized that the origin of this overestimation, affecting both single- and dual-radiotracer studies with [^{125}I]R91150 is probably due to the aforementioned physical phenomena and a more pronounced effect of them on the radioactivity in reference region (CER) that in target VOI in the rat brain. As it may be observed in Fig. S5, VOI situated on the basis of the skull (i.e. those highlighted in red on the scatter plot) are less overestimated compared to [^{123}I]R91150 BP_{ND} values than the other, more superficial regions. This is probably due to a more pronounced effect of scatter and attenuation in these VOI. However, without CT data from our experiments, attenuation correction could not be performed. Regarding scatter correction, we performed a preliminary correction with DEW on the three rats of the dual radiotracer validation study (experiment 3 in Table 1) after having corrected data for scatter with the triple-energy window (TEW). This resulted in BP_{ND} values which correlated in an excellent manner with the corresponding BP_{ND} values from studies uncorrected for scatter. Given this result, the fact that scatter correction may be time-consuming and that scatter correction alone without attenuation correction may add further bias (Hutton et al., 2011), we chose not to implement scatter correction in our DEW methodology. In any case, our proposed methods may be substantially optimized with the correction of the scatter and attenuation effects (Lee et al., 2015), which was out of the scope of this paper.

Conclusion

Dual- and potentially multiple-radiotracer imaging may prove to be an invaluable tool in molecular imaging with both PET and SPECT. Numerous studies in neuropsychiatry already employ multiple-radiotracer imaging. Here, we provide three different methods for the correction of cross-talk produced by the overlap between the emission spectra of ^{123}I and ^{125}I. Among these methods, the DEW method is considered the most straightforward and computationally feasible. This applicability of this method was demonstrated in an experiment that showed that NAcc $D_{2/3}$ and 5-HT_{2A} binding are correlated at the voxel and VOI level.

Acknowledgments

This work was supported by the Swiss National Science Foundation (grant no. 310030_156829), by the Geneva Neuroscience Center and by the Maria Zaousi Memorial Foundation (Greece) through a scholarship of the Hellenic State Scholarship Foundation (ST) and by the "Swiss Association for Alzheimer's Research" which was created in 2009 to finance Swiss fundamental and clinical research programs on Alzheimer's disease. Dr Vallez-Garcia of the University Medical Center Groningen (UMCG) provided valuable expertise regarding the SAMIT Toolbox. Authors are grateful to Mrs Maria Surini-Demiri and Mr Marouane Ben Ammar for excellent technical assistance and declare that they have no conflict of interest.

Appendix A. Supplementary data

Supplementary data related to this article can be found at https://doi.org/10.1016/j.neuroimage.2018.04.063.

References

Akutsu, Y., Kaneko, K., Kodama, Y., Li, H.L., Nishimura, H., Hamazaki, Y., Suyama, J., Shinozuka, A., Gokan, T., Kobayashi, Y., 2009. Technetium-99m pyrophosphate/thallium-201 dual-isotope SPECT imaging predicts reperfusion injury in patients with acute myocardial infarction after reperfusion. Eur. J. Nucl. Med. Mol. Imaging 36, 230–236.

Akutsu, Y., Shinozuka, A., Kodama, Y., Li, H.L., Kayano, H., Hamazaki, Y., Yamanaka, H., Katagiri, T., 2004. Usefulness of simultaneous evaluations of contractile reserve, perfusion, and metabolism during dobutamine stress for predicting wall motion reversibility (myocardial stunning) after successful PTCA. Jpn. Heart J. 45, 195–204.

Albizu, L., Holloway, T., Gonzalez-Maeso, J., Sealfon, S.C., 2011. Functional crosstalk and heteromerization of serotonin 5-HT2A and dopamine D2 receptors. Neuropharmacology 61, 770–777.

Andersen, F.L., Ladefoged, C.N., Beyer, T., Keller, S.H., Hansen, A.E., Hojgaard, L., Kjaer, A., Law, I., Holm, S., 2014. Combined PET/MR imaging in neurology: MR-based attenuation correction implies a strong spatial bias when ignoring bone. Neuroimage 84, 206–216.

Antunes, M.L., Johnson, L.L., Seldin, D.W., Bhatia, K., Tresgallo, M.E., Greenspan, R.L., Vaccarino, R.A., Rodney, R.A., 1992. Diagnosis of right ventricular acute myocardial infarction by dual isotope thallium-201 and indium-111 antimyosin SPECT imaging. Am. J. Cardiol. 70, 426–431.

Baeken, C., D'Haenen, H., Flamen, P., Mertens, J., Terriere, D., Chavatte, K., Boumon, R., Bossuyt, A., 1998. 123I-5-I-R91150, a new single-photon emission tomography ligand for 5-HT2A receptors: influence of age and gender in healthy subjects. Eur. J. Nucl. Med. 25, 1617–1622.

Borroto-Escuela, D.O., Romero-Fernandez, W., Narvaez, M., Oflijan, J., Agnati, L.F., Fuxe, K., 2014. Hallucinogenic 5-HT2AR agonists LSD and DOI enhance dopamine D2R protomer recognition and signaling of D2-5-HT2A heteroreceptor complexes. Biochem. Biophys. Res. Commun. 443, 278–284.

Bruce, I.N., Burns, R.J., Gladman, D.D., Urowitz, M.B., 2000. Single photon emission computed tomography dual isotope myocardial perfusion imaging in women with systemic lupus erythematosus. I. Prevalence and distribution of abnormalities. J. Rheumatol. 27, 2372–2377.

Carson, R.E., Wu, Y., Lang, L., Ma, Y., Der, M.G., Herscovitch, P., Eckelman, W.C., 2003. Brain uptake of the acid metabolites of F-18-labeled WAY 100635 analogs. J. Cereb. Blood Flow. Metab. 23, 249–260.

Catafau, A.M., Bullich, S., Danus, M., Penengo, M.M., Cot, A., Abanades, S., Farre, M., Pavia, J., Ros, D., 2008. Test-retest variability and reliability of 123I-IBZM SPECT measurement of striatal dopamine D2 receptor availability in healthy volunteers and influence of iterative reconstruction algorithms. Synapse 62, 62–69.

Chang, C., Huang, W., Su, H., Chen, J., 2006. Separation of two radionuclides in simultaneous dual-isotope imaging with independent component analysis. Biomed. Eng. Appl. Basis Comm. 18, 264–269.

Constantinescu, C.C., Coleman, R.A., Pan, M.L., Mukherjee, J., 2011. Striatal and extrastriatal microPET imaging of D2/D3 dopamine receptors in rat brain with [(1)(8)F]fallypride and [(1)(8)F]desmethoxyfallypride. Synapse 65, 778–787.

Cselenyi, Z., Lundberg, J., Halldin, C., Farde, L., Gulyas, B., 2004. Joint explorative analysis of neuroreceptor subsystems in the human brain: application to receptor-transporter correlation using PET data. Neurochem. Int. 45, 773–781.

Cunha, L., Horvath, I., Ferreira, S., Lemos, J., Costa, P., Vieira, D., Veres, D.S., Szigeti, K., Summavielle, T., Mathe, D., Metello, L.F., 2014. Preclinical imaging: an essential ally in modern biosciences. Mol. Diagn Ther. 18, 153–173.

De Bruyne, S., Wyffels, L., Boos, T.L., Staelens, S., Deleye, S., Rice, K.C., De Vos, F., 2010. In vivo evaluation of [123I]-4-(2-(bis(4-fluorophenyl)methoxy)ethyl)-1-(4-iodobenzyl)piperidine, an iodinated SPECT tracer for imaging the P-gp transporter. Nucl. Med. Biol. 37, 469–477.

Di Paola, R., Bazin, J.P., Aubry, F., Aurengo, A., Cavailloles, F., Herry, J.Y., Kahn, E., 1982. Handling of dynamic sequences in nuclear medicine. IEEE Trans Nucl. Sci. N. S. 29, 1310–1321.

Du, Y., Frey, E.C., 2009. Quantitative evaluation of simultaneous reconstruction with model-based crosstalk compensation for 99mTc/123I dual-isotope simultaneous acquisition brain SPECT. Med. Phys. 36, 2021–2033.

Dumas, N., Moulin-Sallanon, M., Fender, P., Tournier, B.B., Ginovart, N., Charnay, Y., Millet, P., 2015. In vivo quantification of 5-HT2A brain receptors in Mdr1a KO rats with 123I-R91150 single-photon emission computed tomography. Mol. Imaging 14.

Dumas, N., Moulin-Sallanon, M., Ginovart, N., Tournier, B.B., Suzanne, P., Cailly, T., Fabis, F., Rault, S., Charnay, Y., Millet, P., 2014. Small-animal single-photon emission computed tomographic imaging of the brain serotoninergic systems in wild-type and mdr1a knockout rats. Mol. Imaging 13.

El Fakhri, G., Moore, S.C., Maksud, P., Aurengo, A., Kijewski, M.F., 2001. Absolute activity quantitation in simultaneous 123I/99mTc brain SPECT. J. Nucl. Med. 42, 300–308.

Fakhri, G.E., 2012. Ready for prime time? Dual tracer PET and SPECT imaging. Am. J. Nucl. Med. Mol. Imaging 2, 415–417.

Feng, B., Bai, B., Smith, A.M., Austin, D.W., Mintzer, R.A., Gregor, J., 2007. Reconstruction of multi-pinhole SPECT data with correction of attenuation, scatter and intrinsic detector resolution. In: 2007 IEEE Nuclear Science Symposium Conference Record, pp. 3482–3485.

Figueiras, F.P., Jimenez, X., Pareto, D., Gomez, V., Llop, J., Herance, R., Rojas, S., Gispert, J.D., 2011. Simultaneous dual-tracer PET imaging of the rat brain and its application in the study of cerebral ischemia. Mol. Imaging Biol. 13, 500–510.

Frankle, W.G., Laruelle, M., 2002. Neuroreceptor imaging in psychiatric disorders. Ann. Nucl. Med. 16, 437–446.

Frankle, W.G., Slifstein, M., Talbot, P.S., Laruelle, M., 2005. Neuroreceptor imaging in psychiatry: theory and applications. Int. Rev. Neurobiol. 67, 385–440.

Fukuchi, T., Okauchi, T., Shigeta, M., Yamamoto, S., Watanabe, Y., Enomoto, S., 2017. Positron emission tomography with additional gamma-ray detectors for multiple-tracer imaging. Med. Phys.

Ginovart, N., Kapur, S., 2012. Role of dopamine D(2) receptors for antipsychotic activity. Handb. Exp. Pharmacol. 27–52.

Gregor, J., Black, N., Wall, J., 2007. Monte Carlo study of scatter and attenuation effects in connection with I-125 pinhole imaging of mice. In: International Meeting on Fully 3D Image Reconstruction in Radiology and Nuclear Medicine (Lindau, Germany).

Hijnen, N.M., de Vries, A., Nicolay, K., Grull, H., 2012. Dual-isotope 111In/177Lu SPECT imaging as a tool in molecular imaging tracer design. Contrast Media Mol. Imaging 7, 214–222.

Howes, O.D., Kambeitz, J., Kim, E., Stahl, D., Slifstein, M., Abi-Dargham, A., Kapur, S., 2012. The nature of dopamine dysfunction in schizophrenia and what this means for treatment. Arch. Gen. Psychiatry 69, 776–786.

Hutton, B.F., Buvat, I., Beekman, F.J., 2011. Review and current status of SPECT scatter correction. Phys. Med. Biol. 56, R85–R112.

Ichihara, T., Ogawa, K., Motomura, N., Kubo, A., Hashimoto, S., 1993. Compton scatter compensation using the triple-energy window method for single- and dual-isotope SPECT. J. Nucl. Med. 34, 2216–2221.

Innis, R.B., Cunningham, V.J., Delforge, J., Fujita, M., Gjedde, A., Gunn, R.N., Holden, J., Houle, S., Huang, S.C., Ichise, M., Iida, H., Ito, H., Kimura, Y., Koeppe, R.A., Knudsen, G.M., Knuuti, J., Lammertsma, A.A., Laruelle, M., Logan, J., Maguire, R.P., Mintun, M.A., Morris, E.D., Parsey, R., Price, J.C., Slifstein, M., Sossi, V., Suhara, T., Votaw, J.R., Wong, D.F., Carson, R.E., 2007. Consensus nomenclature for in vivo imaging of reversibly binding radioligands. J. Cereb. Blood Flow. Metab. 27, 1533–1539.

Jack Jr., C.R., Knopman, D.S., Jagust, W.J., Petersen, R.C., Weiner, M.W., Aisen, P.S., Shaw, L.M., Vemuri, P., Wiste, H.J., Weigand, S.D., Lesnick, T.G., Pankratz, V.S., Donohue, M.C., Trojanowski, J.Q., 2013. Tracking pathophysiological processes in Alzheimer's disease: an updated hypothetical model of dynamic biomarkers. Lancet Neurol. 12, 207–216.

Ji, B., Chen, C.J., Bando, K., Ashino, H., Shiraishi, H., Sano, H., Kasahara, H., Minamizawa, T., Yamada, K., Ono, M., Zhang, M.R., Seki, C., Farde, L., Suhara, T., Higuchi, M., 2015. Distinct binding of amyloid imaging ligands to unique amyloid-beta deposited in the presubiculum of Alzheimer's disease. J. Neurochem. 135, 859–866.

Kadrmas, D.J., Rust, T.C., Hoffman, J.M., 2013. Single-scan dual-tracer FLT+FDG PET tumor characterization. Phys. Med. Biol. 58, 429–449.

Kessler, R.M., Ansari, M.S., de Paulis, T., Schmidt, D.E., Clanton, J.A., Smith, H.E., Manning, R.G., Gillespie, D., Ebert, M.H., 1991. High affinity dopamine D2 receptor radioligands. 1. Regional rat brain distribution of iodinated benzamides. J. Nucl. Med. 32, 1593–1600.

Koeppe, R.A., Raffel, D.M., Snyder, S.E., Ficaro, E.P., Kilbourn, M.R., Kuhl, D.E., 2001. Dual-[11C]tracer single-acquisition positron emission tomography studies. J. Cereb. Blood Flow. Metab. 21, 1480–1492.

Kung, H.F., Pan, S., Kung, M.P., Billings, J., Kasliwal, R., Reilley, J., Alavi, A., 1989. In vitro and in vivo evaluation of [123I]IBZM: a potential CNS D-2 dopamine receptor imaging agent. J. Nucl. Med. 30, 88–92.

Lammertsma, A.A., Hume, S.P., 1996. Simplified reference tissue model for PET receptor studies. Neuroimage 4, 153–158.

Laruelle, M., 2000. Imaging synaptic neurotransmission with in vivo binding competition techniques: a critical review. J. Cereb. Blood Flow. Metab. 20, 423–451.

Lee, S., Gregor, J., Kennel, S.J., Osborne, D.R., Wall, J., 2015. GATE validation of standard dual energy corrections in small animal SPECT-CT. PLoS One 10, e0122780.

Lee, S., Gregor, J., Osborne, D., Wall, J., 2013. Dual isotope SPECT imaging of I-123 and I-125. In: Nuclear Science Symposium and Medical Imaging Conference (NSS/MIC). IEEE, 2013 IEEE.

Lukasiewicz, S., Polit, A., Kedracka-Krok, S., Wedzony, K., Mackowiak, M., Dziedzicka-Wasylewska, M., 2010. Hetero-dimerization of serotonin 5-HT(2A) and dopamine D(2) receptors. Biochim. Biophys. Acta 1803, 1347–1358.

Ma, J., Ye, N., Cohen, B.M., 2006. Expression of noradrenergic α1, serotoninergic 5HT2a and dopaminergic D2 receptors on neurons activated by typical and atypical antipsychotic drugs. Prog. Neuro-Psychopharmacology Biol. Psychiatry 30, 647–657.

Mattner, F., Bandin, D.L., Staykova, M., Berghofer, P., Gregoire, M.C., Ballantyne, P., Quinlivan, M., Fordham, S., Pham, T., Willenborg, D.O., Katsifis, A., 2011. Evaluation of [(1)(2)(3)I]-CLINDE as a potent SPECT radiotracer to assess the degree of astroglia activation in cuprizone-induced neuroinflammation. Eur. J. Nucl. Med. Mol. Imaging 38, 1516–1528.

Mattner, F., Mardon, K., Katsifis, A., 2008. Pharmacological evaluation of [123I]-CLINDE: a radioiodinated imidazopyridine-3-acetamide for the study of peripheral benzodiazepine binding sites (PBBS). Eur. J. Nucl. Med. Mol. Imaging 35, 779–789.

McCormick, P.N., Ginovart, N., Wilson, A.A., 2011. Isoflurane anaesthesia differentially affects the amphetamine sensitivity of agonist and antagonist D2/D3 positron emission tomography radiotracers: implications for in vivo imaging of dopamine release. Mol. Imaging Biol. 13, 737–746.

Meikle, S.R., Kench, P., Kassiou, M., Banati, R.B., 2005. Small animal SPECT and its place in the matrix of molecular imaging technologies. Phys. Med. Biol. 50, R45–R61.

Millet, P., Moulin-Sallanon, M., Tournier, B.B., Dumas, N., Charnay, Y., Ibanez, V., Ginovart, N., 2012. Quantification of dopamine D(2/3) receptors in rat brain using factor analysis corrected [18F]Fallypride images. Neuroimage 62, 1455–1468.

Nestler, E.J., Hyman, S.E., 2010. Animal models of neuropsychiatric disorders. Nat. Neurosci. 13, 1161–1169.

Ordonez, A.A., Pokkali, S., DeMarco, V.P., Klunk, M., Mease, R.C., Foss, C.A., Pomper, M.G., Jain, S.K., 2015. Radioiodinated DPA-713 imaging correlates with bactericidal activity of tuberculosis treatments in mice. Antimicrob. Agents Chemother. 59, 642–649.

Pimlott, S.L., Ebmeier, K.P., 2007. SPECT imaging in dementia. Br. J. Radiol. 80 (2), S153–S159.

Schiffer, W.K., Mirrione, M.M., Biegon, A., Alexoff, D.L., Patel, V., Dewey, S.L., 2006. Serial microPET measures of the metabolic reaction to a microdialysis probe implant. J. Neurosci. Methods 155, 272–284.

Sehlin, D., Fang, X.T., Cato, L., Antoni, G., Lannfelt, L., Syvanen, S., 2016. Antibody-based PET imaging of amyloid beta in mouse models of Alzheimer's disease. Nat. Commun. 7, 10759.

Selvaraj, S., Arnone, D., Cappai, A., Howes, O., 2014. Alterations in the serotonin system in schizophrenia: a systematic review and meta-analysis of postmortem and molecular imaging studies. Neurosci. Biobehav Rev. 45, 233–245.

Tsartsalis, S., Dumas, N., Tournier, B.B., Pham, T., Moulin-Sallanon, M., Gregoire, M.C., Charnay, Y., Millet, P., 2015. SPECT imaging of glioma with radioiodinated CLINDE: evidence from a mouse GL26 glioma model. EJNMMI Res. 5, 9.

Tsartsalis, S., Moulin-Sallanon, M., Dumas, N., Tournier, B.B., Ghezzi, C., Charnay, Y., Ginovart, N., Millet, P., 2014a. Quantification of GABAA receptors in the rat brain with [(123)I]Iomazenil SPECT from factor analysis-denoised images. Nucl. Med. Biol. 41, 186–195.

Tsartsalis, S., Moulin-Sallanon, M., Dumas, N., Tournier, B.B., Ginovart, N., Millet, P., 2014b. A modified simplified reference tissue model for the quantification of dopamine D2/3 receptors with [18F]fallypride images. Mol. Imaging 13.

Tsartsalis, S., Toumier, B.B., Huynh-Gatz, T., Dumas, N., Ginovart, N., Moulin-Sallanon, M., Millet, P., 2016a. 5-HT2A receptor SPECT imaging with [I-123]R91150 under P-gp inhibition with tariquidar: more is better? Nucl. Med. Biol. 43, 81–88.

Tsartsalis, S., Tournier, B.B., Aoun, K., Habiby, S., Pandolfo, D., Dimiziani, A., Ginovart, N., Millet, P., 2017. A single-scan protocol for absolute D2/3 receptor quantification with [123I]IBZM SPECT. Neuroimage 147, 461–472.

Tsartsalis, S., Tournier, B.B., Huynh-Gatz, T., Dumas, N., Ginovart, N., Moulin-Sallanon, M., Millet, P., 2016b. 5-HT2A receptor SPECT imaging with [(1)(2)(3)I] R91150 under P-gp inhibition with tariquidar: more is better? Nucl. Med. Biol. 43, 81–88.

Vallez Garcia, D., Casteels, C., Schwarz, A.J., Dierckx, R.A., Koole, M., Doorduin, J., 2015. A standardized method for the construction of tracer specific PET and SPECT rat brain templates: validation and implementation of a toolbox. PLoS One 10, e0122363.

Varela, M.J., Lage, S., Caruncho, H.J., Cadavid, M.I., Loza, M.I., Brea, J., 2015. Reelin influences the expression and function of dopamine D2 and serotonin 5-HT2A receptors: a comparative study. Neuroscience 290, 165–174.

Wu, Y., Carson, R.E., 2002. Noise reduction in the simplified reference tissue model for neuroreceptor functional imaging. J. Cereb. Blood Flow. Metab. 22, 1440–1452.

Xi, W., Tian, M., Zhang, H., 2011. Molecular imaging in neuroscience research with small-animal PET in rodents. Neurosci. Res. 70, 133–143.

S1. Supplemental materials and methods

S1.1 Test-retest variability of [^{123}I]IBZM and [^{125}I]R91150 BP_{ND} values

The ten rats that participated in the experiment described in paragraph 2.7 underwent a second simultaneous [^{123}I]IBZM and [^{125}I]R91150 SPECT scan under the exact same conditions as described in 2.7. The mean doses of radioactivity injected were 36.96±10.09 and 27.28±3.79 MBq, respectively. Percentage test–retest variability for dual-radiotracer [^{123}I]IBZM and [^{125}I]R91150 BP_{ND} measurements (in the CPu for [^{123}I]IBZM and in the MPFC for [^{125}I]R91150) was calculated as follows: for each rat and each radiotracer, the absolute difference between the test and retest BP_{ND} value was divided by the average of these two values. The average of these ratios across the six rats gave the percent test-retest variability.

S1.2 Single-radiotracer [^{125}I]R91150 SPECT study

To evaluate the bias in binding parameters due to the use of ^{125}I in [^{125}I]R91150 *in vivo* we performed an *in vivo* [^{125}I]R91150 SPECT study. Three male *Mdr1a* KO rats, weighing between 493 and 573 g underwent a SPECT scan at t=100 min after injection of 40.45±9.73 MBq of [^{125}I]R91150. Scan procedures and image reconstruction were performed as described in sections 2.3 and 2.4, respectively. BP_{ND} was estimated with the SUR method with the CER as reference region. These values were compared with the corresponding values from the dual-radiotracer [^{125}I]R91150 study, as well as with the data corresponding to single-radiotracer [^{123}I]R91150 experiments described in section 2.5, by means of linear regression analysis and paired t-test analysis.

S1.3 Validation of the relationship between $D_{2/3}$ and 5-HT_{2A} binding in striatum using simulations

To validate the observed relationship between $D_{2/3}$ and 5-HT_{2A} binding in striatum and exclude any possible residual contamination from [^{123}I]IBZM on [^{125}I]R91150 after correction with the subtraction method, we performed a simulation study. The goal was to examine the hypothesis that a bias in the α coefficient either in striatum or in cerebellum could result in an overestimation of striatal [^{123}I]R91150 BP_{ND} values and thus produce an artificial observed correlation between the binding of the two radiotracers. We used radioactivity measurements from the CPu and NAcc (bilaterally, hence 4 VOIs) and cerebellum from one of the rats of the experiment of paragraph 2.7. These measurements were extracted from [^{123}I]IBZM images and uncorrected [^{125}I]R91150 images. Correction for cross-talk contamination was performed with the subtraction method as described in 2.5.1 using the actual α coefficient value of 0.34 for both striatal VOIs and cerebellum. Then, a -20% coefficient value in striatum and a +20% value in cerebellum was used simultaneously, to illustrate the case were bias in α coefficient values in both these regions would produce the maximal level of [^{125}I]R91150 BP_{ND} overestimation. Scatter plots of the correlation between [^{123}I]IBZM and [^{125}I]R91150 BP_{ND} values in the four striatal VOIs were produced for the baseline BP_{ND} values and the biased α coefficient case.

Secondly, because the bias in BP_{ND} values in case of an α coefficient miscalculation could depend on the absolute BP_{ND} value of [^{125}I]R91150 binding, we repeated the exact same simulation as above but changing the ground truth BP_{ND} value for the left CPu nucleus to a value +130% higher than its original value. Correction for cross-talk with an α coefficient value of 0.34 for both striatum and cerebellum was performed. Then, correction was performed with a +20% coefficient value for striatum and at the same time -20% value for cerebellum and the results were plotted as described above.

If a biased α coefficient value could result in biases in the ^{125}I-labelled radiotracer's BP_{ND} values, then a correlation between BP_{ND} values obtained with the two radiotracers should be observed at the voxel level, given that the DEW correction is applied voxel-wise. This correlation would be observed in numerous regions too, and not only in the striatum. In the case of [^{123}I]IBZM, given the very little binding outside the striatum, the effect of a possible residual activity on [^{125}I]R91150 may not be sufficiently marked to permit a confirmation or a rejection of this hypothesis. Thus, we performed another *in vivo* SPECT scan in which R91150 was radiolabelled with ^{123}I and IBZM with ^{125}I. Apart from this, we employed the exact same protocol for scanning and image analysis as in paragraph 2.3, 2.4 and cross-talk activity correction with the subtraction method as in 2.5.1. We estimated BP_{ND} at the voxel level and then we evaluated the scatter plots between voxel values of BP_{ND} with the two radiotracers for all the VOIs delineated in the Schiffer template (Schiffer et al., 2006).

A third hypothesis that should be excluded is that the observed correlation between $D_{2/3}$ and 5-HT_{2A} in NAcc binding derives from a contamination of [^{125}I]R91150 radioactivity from adjacent cortical high 5-HT_{2A}-binding VOIs. We thus performed correlation analysis of [^{123}I]IBZM binding in the NAcc and the CPu with the [^{125}I]R91150 binding in MPFC, MC and SSC across the six rats.

S1.4 Study of the relationship between $D_{2/3}$ and 5-HT_{2A} binding in NAcc using in vitro autoradiography

Finally, we studied the relationship between $D_{2/3}$ and 5-HT_{2A} receptor binding in NAcc, CPu and cortical regions of interest (ROIs) in a group of 8 Mdr1a KO rats using *in vitro* autoradiography. Rats were transcardially perfused with 0.9% saline under 3% isoflurane anesthesia. Anesthetized rats were euthanized by decapitation. Brains were removed and frozen in pre-cooled isopentane. Transverse sections (20 µm), including frontal cortical and striatal ROIs, as defined in the Paxinos' atlas (Paxinos and Watson, 2013), were cut on a cryostat and mounted as four series on gelatin-coated slides. Tris-$MgCl_2$ buffer (15 min, 50 mM Tris HCl, 50 mM $MgCl_2$, pH 7.4), then radioactive buffer (90 min) were applied and then slices were rinsed twice in 4°C Tris-$MgCl_2$ buffer (twice 3 min) and briefly washed in cold-water. The radioactive buffer consists of Tris-$MgCl_2$ buffer containing either [^{125}I]IBZM (0.11 MBq/ml) alone or in presence of 10 µM of unlabeled IBZM to determine the non-specific binding. The same procedure was performed using [^{125}I]R91150 (0.11 MBq/ml) instead of [^{125}I]IBZM, and unlabeled R91150 instead of unlabeled IBZM, on immediately adjacent slices. Slides were air-dried before exposure onto gamma-sensitive phosphor imaging plates (Fuji BAS-IP MS2325) for 30 min. Brain sections were then treated for acetylcholinesterase staining in order to delineate the following region of interests: CPu, NAcc, frontal cortex, MC, substancia nigra and ventral tegmental area.

Autoradiograms were analyzed with the Fujifilm BAS-1800II phosphorimager using Aida Software V4.06 (Raytest Isotopenmessgerate GmbH) in presence of homemade ^{125}I calibration curves. Specific binding ratio was calculated for each rat as follows: (Average radioactivity in ROI over 15 slices/ Average radioactivity in ROI over 8 slices in the presence of 10 µM of unlabeled tracer) – 1.

S2. Supplemental results

S2.1 Test-retest reliability

Average BP_{ND} values in the first series of SPECT scans were 5.18±1.09 for [^{123}I]IBZM in the CPu nucleus and 5.30±1.42 for [^{125}I]R91150 in the medial prefrontal cortex. In the second series of scans the respective values were 5.85±0.93 and 4.84±0.49. Percent test-retest variability for [^{123}I]IBZM was 16.80% and for [^{125}I]R91150 was 17.80%. Test and retest BP_{ND} values from one rat had an aberrantly high difference for both radiotracers. If this rat is excluded for the test-retest reliability analysis the reliability values are 14% for [^{123}I]IBZM and 14.10% for [^{125}I]R91150.

S2.2 Single-radiotracer [^{125}I]R91150 SPECT study

BP_{ND} values from single-radiotracer [^{125}I]R91150 experiments correlated well with the corresponding values from [^{123}I]R91150 experiments and with the ones from the dual-radiotracer [^{125}I]R91150 experiments ($r=0.92$, $p<0.001$ for both comparisons). As it can be shown in Figure S2, there is, overall, an overestimation for BP_{ND} values from single-radiotracer [^{125}I]R91150 experiments, which, nonetheless, is statistically non-significant ($p>0.05$, as determined by means of a paired samples t-test).

S2.3 Validation of the relationship between $D_{2/3}$ and 5-HT_{2A} binding in striatum using simulations

In the first simulated case, a concurrent bias of -20% in the striatum and of +20% in the cerebellum leads to a modification of the slope of the linear regression line from 0.048 to 0.117. Similarly, in the case where one of the CPu nuclei has an +130% higher ground truth BP_{ND} value than in the first case, the slope of the linear regression line went from -0.022 to 0.041. The absolute difference in the slope in the two cases were +0.069 and 0.063, respectively, which is quite similar.

Figure S1 presents the scatter plots of the correlation between [^{123}I]R91150 and [^{125}I]IBZM BP_{ND} for nine different VOIs from one rat. No correlation was observed in these nine VOIs and neither was for any other VOIs of the rat brain. However, before correction for cross-talk, a voxel-wise correlation was observed in most regions (data not shown).

Finally, the regression analysis of [^{123}I]IBZM binding in NAcc or CPu and the [^{125}I]R91150 binding in the cortical VOIs demonstrated very weak correlations: indeed, concerning the NAcc, all the regressions had slopes of less than 0.15 and associated r values of less than 0.17. Concerning the CPu, all regression had slopes of less than 0.30 and associated r values of less than 0.4.

S2.4 Study of the relationship between $D_{2/3}$ and 5-HT_{2A} binding in NAcc using in vitro autoradiography

BP_{ND} of [^{125}I]IBZM in NAcc correlated well with the corresponding [^{125}I]R91150 values across the eight rats ($r=0.81$, $p<0.001$), as presented in supplemental Figure S2. No other significant correlation was observed in the rest of the examined ROI (data not shown).

S3. Supplemental figure legends

Figure S1 Scatter plots of the correlation between [^{123}I]IBZM (A) and [^{125}I]R91150 (B) test and retest BP_{ND} values.

Figure S2 Scatter plot of the correlation between average [^{125}I]R91150 BP_{ND} values from single-injection experiments and average [^{123}I]R91150 BP_{ND} values from dual-injection experiments corrected with the DEW method.

Figure S3 Scatter plots of the correlation between [^{123}I]R91150 and [^{125}I]IBZM BP_{ND} for nine different VOIs of one rat.

Figure S4 Scatter plot of the correlation between *in vitro* [^{125}I]R91150 and [^{125}I]IBZM BP_{ND} in NAcc across eight rats.

Figure S5 Representative deep and superficial brain VOI from scatter plot of Figure 8A, depicting the correlation between [^{123}I]R91150 BP_{ND} values from single-radiotracer experiments and [^{125}I]R91150 values from DEW-corrected dual-radiotracer experiments. In this scatter plot, the dots corresponding to the deep VOI found on the basis of the skull (namely, NAcc, amygdala, entorhinal cortex, olfactory cortex, ventral tegmental area) are coloured red. The blue dots correspond to superficial VOI (namely, MPFC, MC, OFC, SSC, CC, anterodorsal and posterior hippocampi, hypothalamus, inferior and superior colliculi and the thalamus). Indeed, in these VOI, the BP_{ND} values of [^{125}I]R91150 are less overestimated compared to the corresponding values from more superficial VOI, suggesting a higher impact of attenuation and scatter in these VOI.

S4. Supplemental references

Paxinos, G., Watson, C., 2013. The Rat Brain in Stereotaxic Coordinates: Hard Cover Edition. Elsevier Science.

Schiffer, W.K., Mirrione, M.M., Biegon, A., Alexoff, D.L., Patel, V., Dewey, S.L., 2006. Serial microPET measures of the metabolic reaction to a microdialysis probe implant. J Neurosci Methods 155, 272-284.

Figure S1

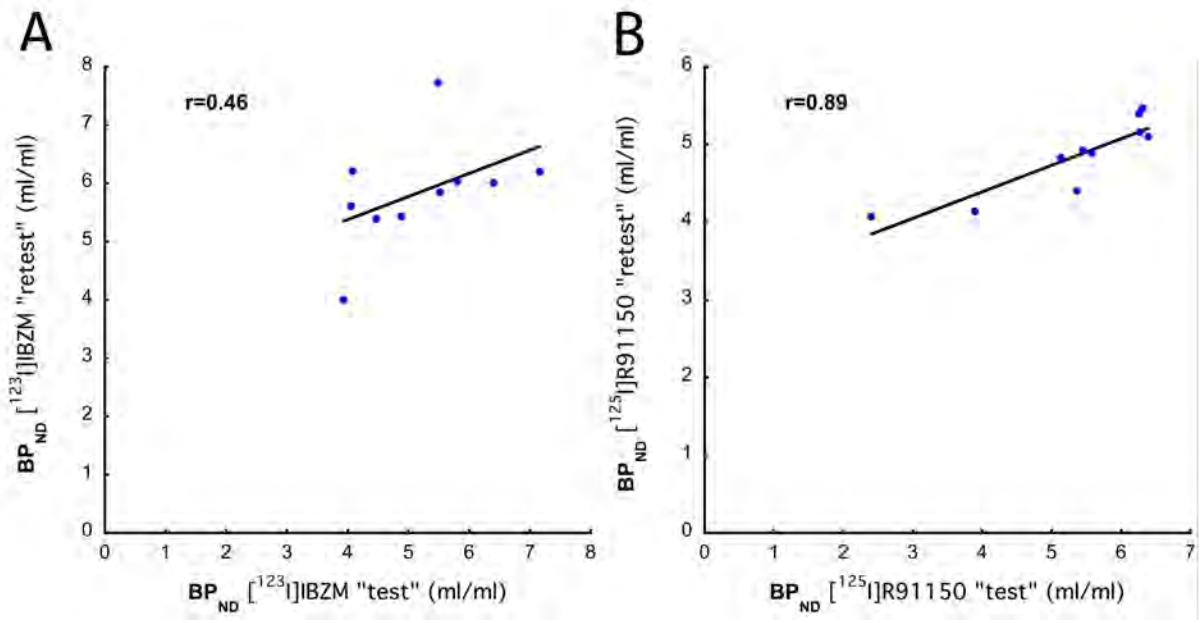
A
r=0.46
BP_ND [123I]IBZM "retest" (ml/ml)
BP_ND [123I]IBZM "test" (ml/ml)
B
r=0.89
BP_ND [125I]R91150 "retest" (ml/ml)
BP_ND [125I]R91150 "test" (ml/ml)

Figure S2

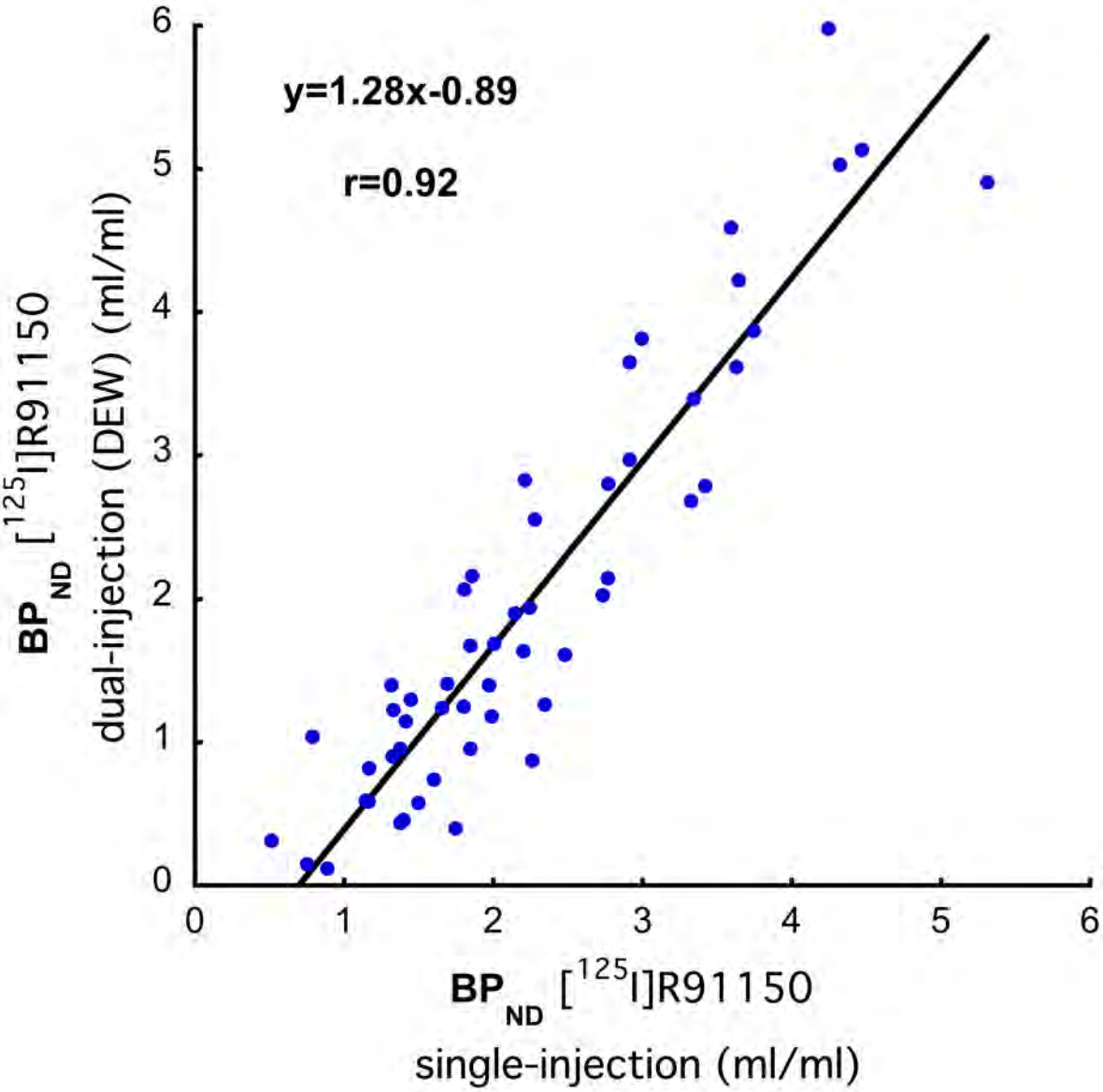
y=1.28x-0.89
r=0.92
BP ND [125I]R91150
dual-injection (DEW) (ml/ml)
BP ND [125I]R91150
single-injection (ml/ml)
0
1
2
3
4
5
6

Figure S3

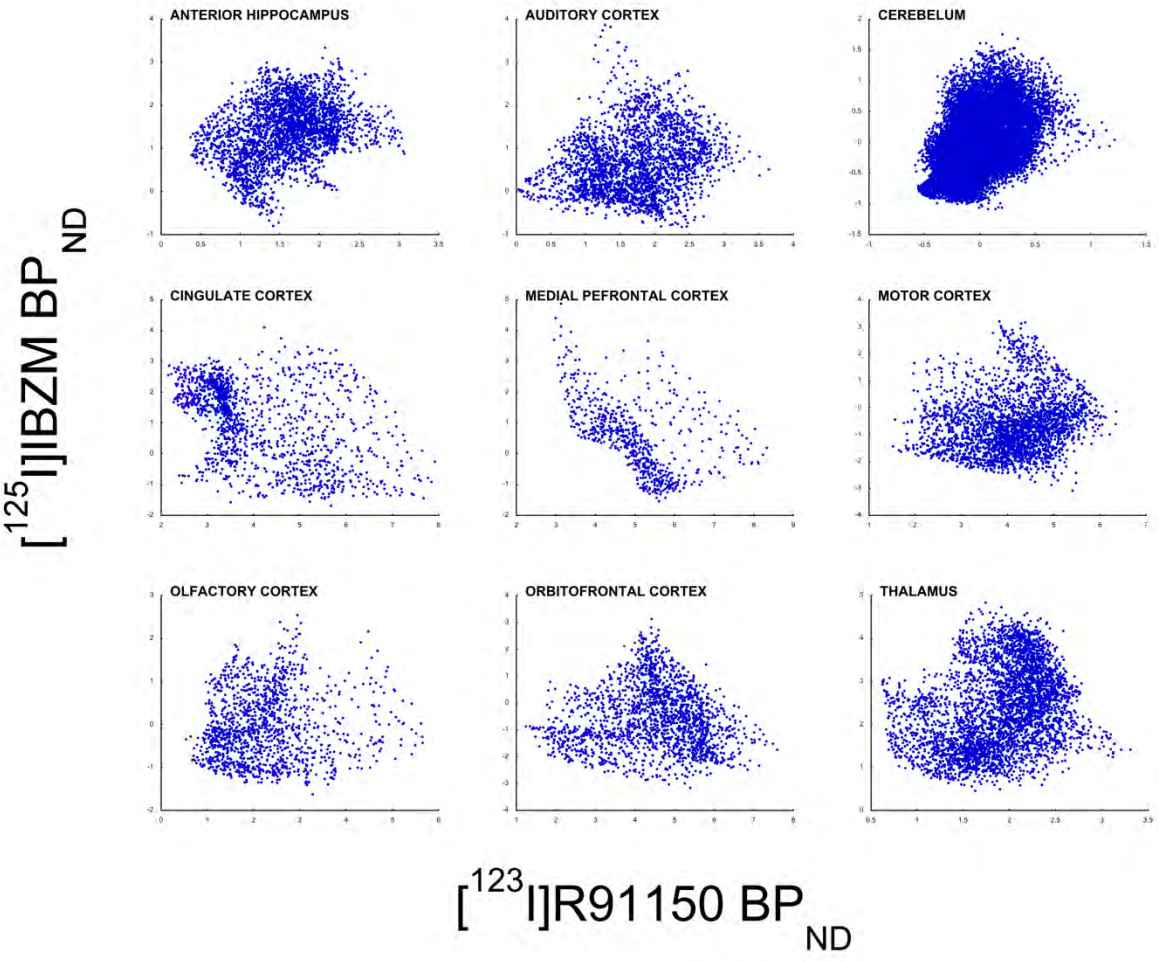
ANTERIOR HIPPOCAMPUS
AUDITORY CORTEX
CEREBELUM
CINGULATE CORTEX
MEDIAL PEFRONTAL CORTEX
MOTOR CORTEX
OLFACTORY CORTEX
ORBITOFRONTAL CORTEX
THALAMUS
[125I]IBZM BPND
[123I]R91150 BPND

Figure S4

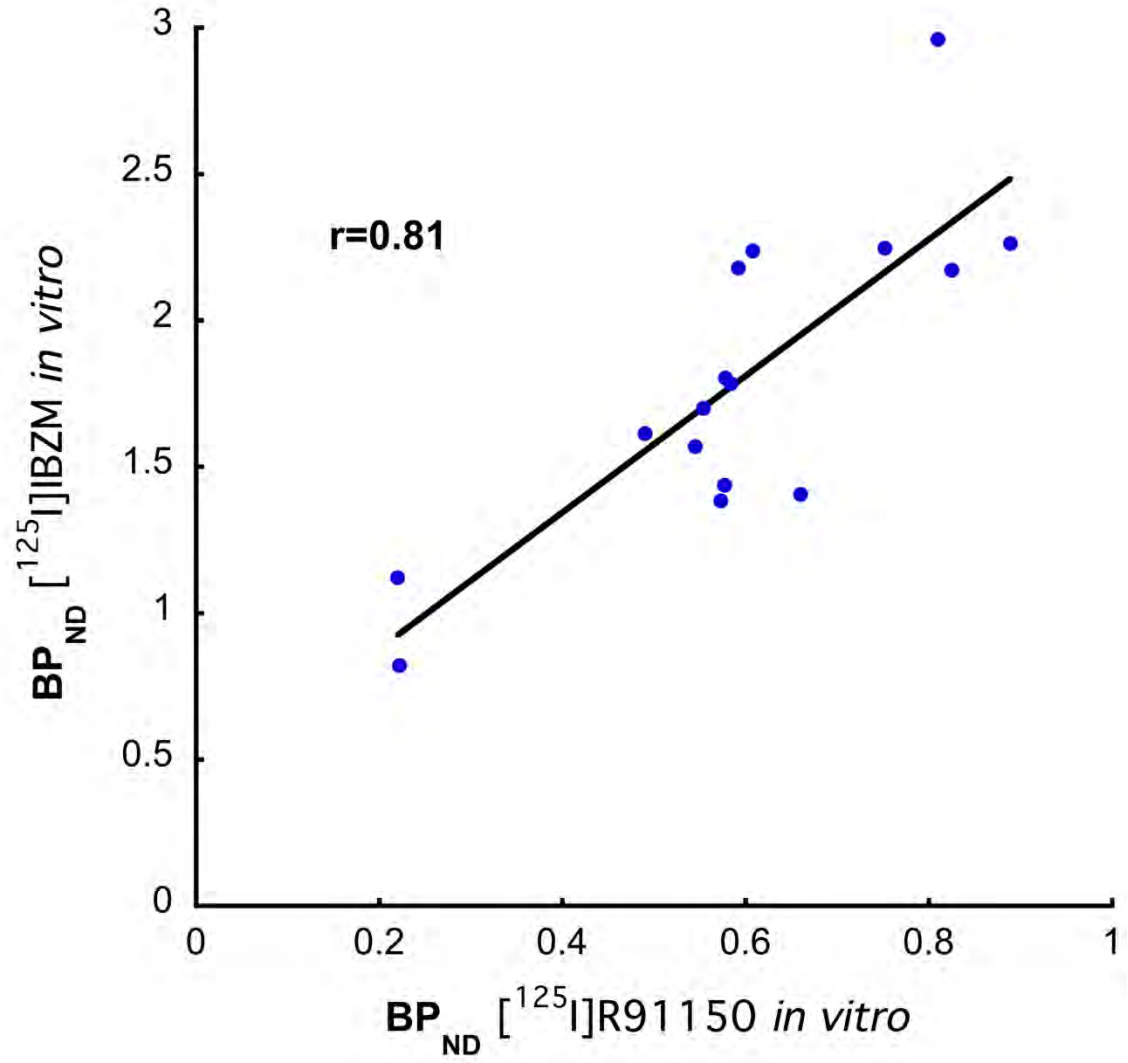
r=0.81
BP ND [125I]IBZM in vitro
BP ND [125I]R91150 in vitro
0
0.5
1
1.5
2
2.5
3
0
0.2
0.4
0.6
0.8
1

Figure S5

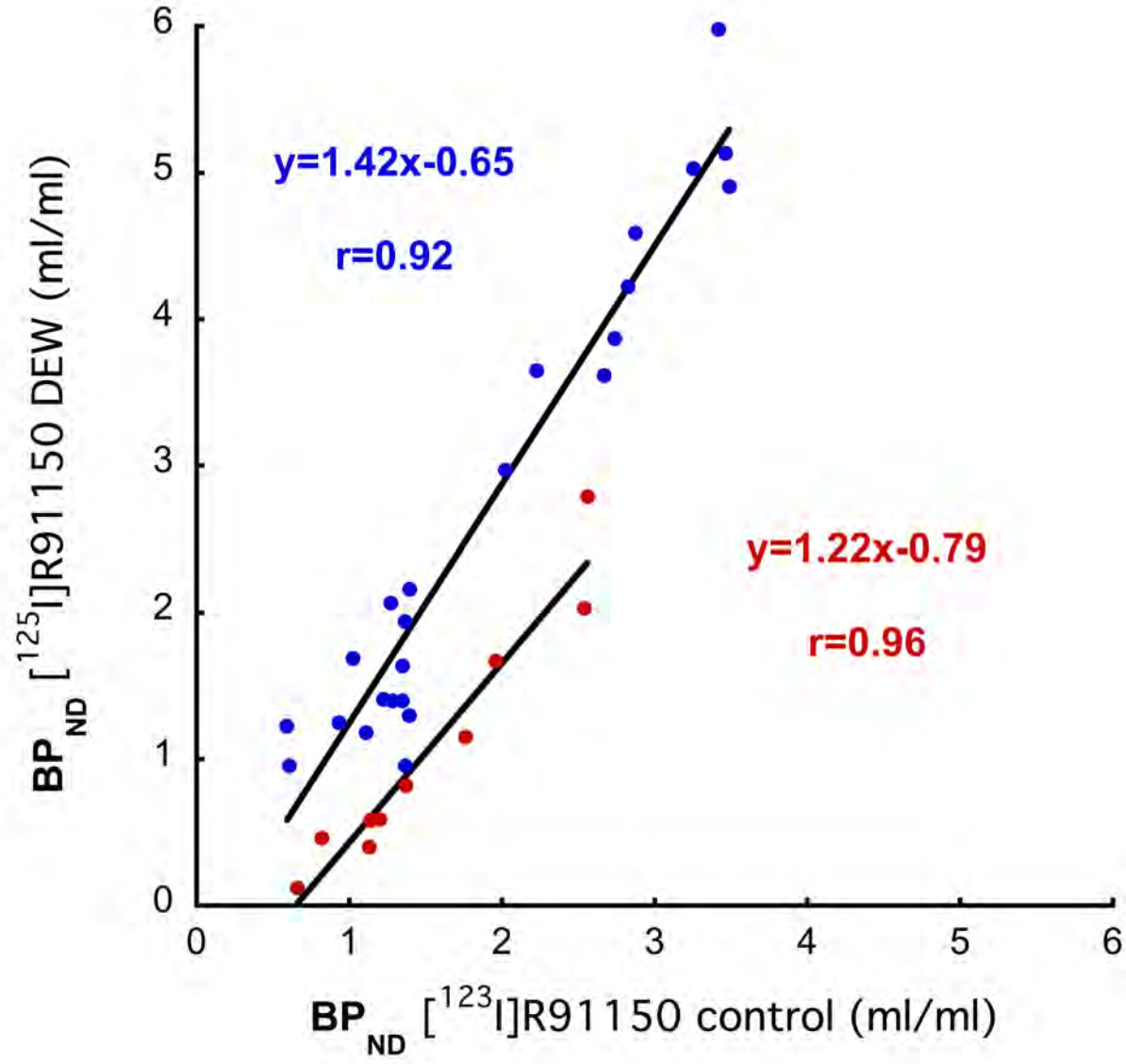
y=1.42x-0.65
r=0.92
y=1.22x-0.79
r=0.96
BP ND [125I]R91150 DEW (ml/ml)
BP ND [123I]R91150 control (ml/ml)
0
1
2
3
4
5
6

Article 5

Effect of 5-HT_{2A} receptor antagonism on levels of $D_{2/3}$ receptor occupancy and adverse behavioral side-effects induced by haloperidol: a SPECT imaging study in the rat

Stergios Tsartsalis[1,2], Benjamin B. Tournier[1], Yessica Gloria[1], Philippe Millet[1,3], Nathalie Ginovart[3,4]

1. Division of Adult Psychiatry, Department of Psychiatry, Geneva University Hospitals, Geneva, Switzerland
2. Division of Psychiatric Specialties, Department of Psychiatry, Geneva University Hospitals, Geneva, Switzerland
3. Department of Psychiatry, Faculty of Medicine, University of Geneva, Switzerland
4. Department of Basic Neurosciences, Faculty of Medicine, University of Geneva, Switzerland

Abstract

Several studies suggested that a 5-HT_{2A} blockade may provide a more favorable efficacy and side-effect profile to antipsychotic treatment. Here, we chronically treated male Mdr1a knock out rats with several doses of haloperidol alone or haloperidol with a saturating dose of a pure 5-HT_{2A} receptor antagonist, MDL-100,907. The occupancy of the receptors at clinically relevant levels was validated with a dual-radiotracer *in vivo* SPECT imaging procedure to assess $D_{2/3}$ and 5-HT_{2A} receptor occupancy. A series of experimental tests of efficacy and side effects was performed. Finally, a second dual-radiotracer *in vivo* SPECT scan assessed the neurochemical changes induced by the chronic treatments. Chronic haloperidol failed to reverse the disruption of the PPI by dizocilpine, whilst administration of MDL-100,907 along with haloperidol was associated with a reversal of the effect of dizocilpine. Haloperidol at 0.5 mg/kg/day and at 1 mg/kg/day induced catalepsy that was significantly alleviated (by approximately 50%) by the co-treatment with MDL-100,907 only in the case of the 0.5 mg/kg/day dose of haloperidol. Chronic haloperidol treatment, event at doses as low as 0.1 mg/kg/day induced a significant upregulation of the $D_{2/3}$ receptor in the striatum (by over 40% in the nucleus accumbens and over 20% in the caudate putamen nucleus), that was not reversed by MDL-100,907. Finally, an upregulation of the 5-HT_{2A} receptor after chronic haloperidol treatment at a moderate dose only (0.25 mg/kg/day) was demonstrated in several frontal cortical regions and the ventral tegmental area. Overall, a partial contribution of a 5-HT_{2A} antagonism to the efficacy and side-effect profile of antipsychotic agents is suggested.

1. Introduction

Antipsychotic medication constitutes the cornerstone of schizophrenia treatment. Antipsychotic agents are classified into typical (mainly D_2 receptor antagonists with relatively low affinity for other receptors) and atypical (with affinity for a wide spectrum of receptors, apart from the D_2 receptor) (reviewed in [1]). D_2 antagonism is a central element of antipsychotic activity [2]: indeed, for the majority of antipsychotic agents, a D_2 receptor occupancy between 65 and 80% of the total receptor pool in the striatum is associated with antipsychotic efficacy. An occupancy below this level produces no antipsychotic effects, whereas a higher occupancy is associated with the appearance of -mainly extrapyramidal- side effects (reviewed in [1]).

When compared to typical agents, atypical antipsychotics possess a lower propensity to cause extrapyramidal side effects [3,4]. This suggests that a better understanding of the mechanism of action of atypical antipsychotics could lead to the design of more tolerable, hence, a more efficient treatment of schizophrenia. Despite extensive efforts, the neurochemical and/or molecular bases of atypicality have long been a matter of debate. One popular theory proposes that a high 5-HT_{2A} receptor occupancy is a defining characteristic of atypical antipsychotics and indeed, the majority of them has a high affinity for the 5-HT_{2A} receptor [5]. Whereas 5-HT_{2A} receptor antagonism *per se* is not considered as conferring antipsychotic efficacy by itself [6], a combined blockade of D_2 and 5-HT_{2A} receptor has been proposed to be important for the efficacy and the reduced side effect liability of atypical versus typical drugs [1,2,7].

The existing literature on the subject is controversial and a systematic approach to the question of the implication of a 5-HT_{2A} antagonism on the antipsychotic atypicality is needed. Indeed, many studies have assessed the effect of a 5-HT_{2A} antagonism in association with a D_2 receptor blockade, notably by haloperidol, on a wide spectrum of behavioral paradigms of antipsychotic efficacy and side effect liability in rodents. However, in most studies, a single and, in most cases, saturating dose of haloperidol has been used. In addition, to our knowledge, no study has assessed multiple aspects of antipsychotic efficacy and side effect profile at the same time.

In the present study, we chronically treated male Mdr1a knock out rats with several doses of haloperidol alone or in combination with a saturating dose of a pure 5-HT_{2A} receptor antagonist, MDL-100,907. The occupancy of the receptors at clinically relevant levels was validated with a dual-radiotracer *in vivo* SPECT imaging to assess $D_{2/3}$ and 5-HT_{2A} receptor occupancy, simultaneously during the same scan session [8]. A series of well-validated experimental tests of efficacy and side effects was performed. Finally, a second dual-radiotracer *in vivo* SPECT scan was performed following a 4-weeks treatment period to assess neurochemical changes at the level of $D_{2/3}$ and 5-HT_{2A} receptor binding with respect to the chronic treatment regimes. Our hypothesis was that a 5-HT_{2A} antagonism, a putative substrate of antipsychotic atypicality, should enhance the efficacy of haloperidol at the experimental tasks and alleviate extrapyramidal side effects.

2. Materials and Methods

2.1 Animals

Figure 1 presents the timeline of the experiments. A total of 79 male adult Mdr1a knock out Sprague-Dawley rats, weighing 300 to 500 g, were employed in the main (*"in vivo"*) study. Two other groups of 38 and 19 rats of similar weights were employed in an *ex vivo* study for the establishment of the dose-occupancy curves of haloperidol and MDL-100,907, respectively. The animals were housed at constant room temperature (21±1 ^{o}C) and relative humidity (60±5 %) under a regular light/dark schedule (light 07:00–19:00). Food and water were freely available.

All experimental procedures were performed in accordance with the Swiss Federal Law on animal care under a protocol approved by the Ethical Committee on Animal Experimentation of the Canton of Geneva, Switzerland.

2.2 Osmotic minipump implantation procedure and chronic drug treatment

Haloperidol and MDL-100,907 (Sigma-Aldrich, Buchs, Switzerland) were diluted in a 50% DMSO solution in NaCl 0.9% (50 % v/v). MDL-100,907 was initially diluted in a small volume of a 10% acetic acid solution (constituting less than 5% of the final volume of the DMSO/NaCl solution). An initial *ex vivo* study was performed to determine the dose-occupancy curves for haloperidol and MDL-100,907. This study informed the choice of the concentration of the drugs for the chronic treatment of the animals in the main, *in vivo* study. The haloperidol/MDL-100,907 doses in the *in vivo* study (hereon abbreviated as Hx/My with x and y being the dose of each drug in mg/kg/day) and the number of rats (n) in each dosage were as follows: H0/M0 (n=12), H0.1/M0 (n=8), H0.1/M0.5 (n=7), H0.25/M0 (n=7), H0.25/M0.5 (n=7), H0.5/M0 (n=7), H0.5/M0.5 (n=7), H1/M0 (n=12) and H1/M0.5 (n=12). The doses employed in the *in vivo* study were informed by the *ex vivo* study described above and in detail in section 2.4.

Osmotic minipump (2ML4, Alzet, Cupertino, CA, USA) implantation was performed under isoflurane anesthesia (3% for induction, 2,5% for maintenance) and buprenorphine analgesia (0.02 mg/kg/8h sc; Temgesic, Reckitt Benckiser Pharmaceuticals Inc.). Body temperature was maintained at 37±1 °C by means of a thermostatically controlled heating blanket. After an incision made between the scapulae, a subcutaneous pocket was created using hemostatic forceps and a minipump loaded with a solution of the drug(s) was inserted. The incision was then closed with sutures.

At the end of the treatment period, the minipumps were removed with a similar operation as described above.

2.3 Behavioral tests

2.3.1. Dizocilpine-disrupted prepulse inhibition (PPI) of the startle reflex

In rodents, exposure to a strong acoustic stimulus provokes a startle response. If this strong stimulus is preceded by a milder acoustic stimulus, then the response of the animal to the startle-eliciting stimulus is attenuated and this phenomenon is termed prepulse inhibition (PPI) of the startle. It is disrupted by a dizocilpine (MK801) pretreatment. Antipsychotic agents reverse this disruption and this property is considered as a proxy of their efficacy against psychotic symptoms [9-11].

This test took place in sound-attenuating startle chambers (TSE Systems, Bad Homburg, Germany) which include enclosures (22.5x8x8.5cm) equipped with loudspeakers and a piezoelectric accelerometer that allow to deliver tone pulses and to measure animal startle responses, respectively. It took place on days 16 to 19 post-surgery. The first two days consist of habituation sessions (10 min and 30 min of 70dB background noise on day 1 and day 2, respectively). On day 3, PPI was measured (immediately after an i.p. injection of saline) as follows: after a 10 min acclimation period (70dB), the rat received, in a random fashion, 24 trials with a pulse-alone stimulus (120 dB, 40 ms), 12 trials with no stimulus (70-dB 200 ms), three types (3 × 12) of prepulse-and-pulse trials which include a 20-ms prepulse (75, 80, or 85-dB) followed 100 ms later by a 120-dB pulse stimulus, as described previously [12]. On day 4, PPI was measured as on day 3, using dizocilpine (0.15mg/kg) instead of saline as pretreatment. The amplitude of startle responses was recorded in all trials. The magnitude of PPI was calculated as a percent inhibition of the startle amplitude in the pulse-alone trial [11,13].

2.3.2 Catalepsy

Catalepsy is indicative of the potential of a pharmacological agent to induce extrapyramidal symptoms. It was performed on day 25 post-surgery. Catalepsy was assessed using a steel grid floor that is inclined at 60°. Rats were placed on the grid and the time elapsed in the same position (without leg movements) was recorded for a maximum of 3 min [14].

2.3.3 Y-maze

To evaluate the effects of the treatment on spatial working memory, the Y-maze test was performed [15-17] on day 26 post-surgery. Rats were placed on the center of the maze and were allowed to freely move between the arms during a 5-min session. Alternation was defined as successive entries into the three arms on overlapping triplet sets. The maximum number of possible spontaneous alternations was determined as the total number of arms entered minus 2. The results were expressed as the percentage of actual to possible alternations [17].

2.3.4 Vacuous chewing movements (VCM) test

Vacuous chewing movements (VCM) are purposeless, vertical jaw movements directed towards no object. They are considered a rodent model of antipsychotic drug-induced tardive dyskinesia. The VCM assessment took place 5 days after the removal of the osmotic minipumps, i.e. the end of the

treatment period. To assess VCM, rats were placed in a plexiglass restraining tube. After two minutes of habituation, VCM were recorded over a period of two minutes [18,19].

2.4 Ex vivo radioactive measurements and in vivo imaging

2.4.1 Radiotracer preparation

Preparation of [^{123}I]IBZM and [^{125}I]R91150 was performed as described previously by our group [8,20,21]. All chemicals for radiotracer preparation were purchased from Sigma-Aldrich (Buchs, Switzerland) unless otherwise specified. ^{123}I and ^{125}I radioiodide were purchased from Perkin Elmer (Basel, Switzerland). [^{123}I]IBZM was obtained by incubation, for 15 min at 68°C, of a mixture containing 5 µl of BZM precursor (ABX, Germany, 24 nmol/ µl in ethanol), 2 µl of glacial acetic acid, 1 µl of 30% H_2O_2 and 10 mCi of carrier-free ^{123}I sodium iodide in 0.05 M NaOH. The radiotracer was isolated by a linear gradient HPLC run (from 5% acetonitrile, ACN, to 95% ACN, 10 mM H_3PO_4, in 10 min). HPLC was equipped with a reverse-phase column (Phenomenex Bonclone C18, Phenomenex, Schlieren, Switzerland) and radiotracer was eluted at a flow of 3 ml/min. Fractions containing [^{123}I]IBZM were diluted in water and loaded on a Sep-Pak cartridge (Sep-Pak C18, Waters, Switzerland). [^{123}I]IBZM was eluted with 0.5 ml of 95% ACN, 10 mM H_3PO_4 and concentrated using a rotary evaporator, and the final product was diluted in saline prior to animal administration.

R91150 precursor preparation was described elsewhere [22]. For radiolabelling, 300 µg of R91150 precursor in 3 µL ethanol was mixed with 3 µL of glacial acetic acid, 15 µL of carrier-free ^{125}I sodium iodide (10 mCi) in 0.05 M NaOH, and 3 µL of 30% H_2O_2. [^{125}I]R91150 was isolated by an isocratic HPLC run (ACN/water 50/50, 10 mM acetic acid buffer pH 5) with a reversed-phase column (Bondclone C18 10 µm 300 X 7.8 mm, Phenomenex, Schlieren, Switzerland) at a flow rate of 3 mL/min.

2.4.2 Ex vivo and in vivo imaging experiments

An initial *ex vivo* study was performed to determine the dose-occupancy curves for haloperidol and MDL-100,907. This study informed on the choice of the respective concentration of each of each of the two drugs to be used for the chronic treatment of the animals in the main study. To estimate the dose-occupancy curve of haloperidol, 38 rats were employed in an *ex vivo* study. Rats were implanted with the procedure described in section 2.2 with osmotic minipumps containing various doses of haloperidol covering the range between 0 and 1 mg/kg/day over a 28-day treatment period. At the end of the treatment period rats were anesthetized using isoflurane anesthesia (4% for induction, 2.5% for maintenance) and injected with 6.48±0.34 MBq of [^{123}I]IBZM for the estimation of receptor occupancy and with 6.00±0.11 MBq of [^{125}I]R91150 for the estimation of 5-HT_{2A} receptor binding. 120 min later, they were decapitated, and brains were dissected to isolate the striatum, the frontal cortex and the cerebellum. The exact same procedure was carried out with another group of 19 rats employed in the estimation of the MDL100-907 dose-occupancy curve. Various doses of this antagonist ranging

between 0 and 1 mg/kg/day were employed. Rats were injected with 6.98±0.98 MBq of [^{123}I]R91150 at the end of the treatment period for the estimation of the 5-HT_{2A} receptor occupancy by MDL-100,907 and with 5.95±0.21 MBq of [^{125}I]IBZM for the estimation of $D_{2/3}$ receptor binding and their brains were dissected 120 min later as described above for the haloperidol study. Radioactivity in the dissected brain regions was immediately measured in an automated gamma counting system.

Dual-radiotracer SPECT imaging [8] was performed in the context of the main *in vivo* study described in this paper to assess the level of $D_{2/3}$ and 5-HT_{2A} occupancy by haloperidol and MDL-100,907 and the binding of $D_{2/3}$ and 5-HT_{2A} receptors after chronic treatment with these agents. *In vivo* dual radiotracer SPECT was performed as described previously [8]. At the end of the 28-day treatment period, the first dual-radiotracer SPECT scan was performed, to measure the occupancy of the $D_{2/3}$ and the 5-HT_{2A} receptor by their respective antagonists. One week later, an exactly similar dual-radiotracer SPECT scan was performed to index the density of the $D_{2/3}$ and the 5-HT_{2A} receptors. A polyethylene catheter (22G) was inserted in the tail vein for radiotracer injection, at a volume of 0.6 ml. Rats were simultaneously injected with both [^{123}I]IBZM (32.7±8.2 MBq) and [^{125}I]R91150 (26.9±6 MBq) over 30 sec. 80 minutes after the radiotracer administration, they were anesthetized using isoflurane (4% for induction and 2.5% for maintenance) and the scan was initiated in a U-SCAN-II SPECT camera (MiLabs, Utrecht, Netherlands) (using 4 frames of 10-min each). Body temperature was maintained at 37±1 °C by means of a thermostatically controlled heating blanket.

SPECT image reconstruction was performed using a pixel ordered subsets expectation maximization (P-OSEM, 0.4 mm voxels, 4 iterations, 6 subsets) algorithm using the MiLabs image reconstruction software. Reconstruction of dynamic SPECT images was performed using the radioactivity measured at each radioisotope's principal energy spectrum, that is at 143,1-179,9 keV for ^{123}I and at 15-45 keV for ^{125}I. Radioactive decay correction was performed while correction for attenuation or scatter was not.

2.4.3 Separation of the two distinct images from the dual-radiotracer SPECT scan

The co-injection of [^{123}I]IBZM with [^{125}I]R91150 induces a contamination of the [^{125}I]R91150 image. ^{123}I emits radioactivity principally at the 143,1-179,9 keV energy spectrum but also at a secondary energy spectrum, which is exactly the spectrum of ^{125}I (15-45 keV). To correct for this contamination, we employed a method described previously by our group [8]. Briefly, the secondary emission of ^{123}I is directly related to the principal one (34%). Contaminated [^{125}I]R91150 images were thus corrected by subtracting 34% of the radioactivity measured in the [^{123}I]IBZM images at the 143,1-179,9 keV energy spectrum.

2.4.4 Standardized uptake ratio (SUR) estimation in the ex vivo and in vivo experiments

For the *ex vivo* study, the standardized uptake ratio (SUR) for each radiotracer in the striatum and the frontal cortex was measured using the radioactivity measured in the gamma counting system as

follows: SUR=(radioactivity in the target-region)/(radioactivity in the cerebellum) – 1. The occupancy of the receptors from their respective antagonists was estimated as described in section 2.4.5.

For the *in vivo* study, SPECT images were processed using PMOD software (version 3.9, PMOD Technologies Ltd, Zurich, Switzerland). As previously validated by our group, the SUR of [^{123}I]IBZM is estimated over the static images corresponding to 80-110 min after the injection of the radiotracer [21], while the SUR of [^{125}I]R91150 at 100-120 min [20]. For each rat, static [^{125}I]R91150 SPECT images were spatially normalized on a [^{125}I]R91150 template-image (described here [8]) and filtered with a Gaussian filter of 0.6m^3 FWHM. The resulting transformation matrix was applied to the corresponding [^{123}I]IBZM images for each rat. A volume-of-interest (VOI) template (including 57 VOIs), incorporated in PMOD [23] was used to extract the radioactivity from each brain VOI and the cerebellum (CER), which was used as reference region. SUR values were estimated as follows: (Radioactivity in the target VOI)/(Radioactivity in CER)-1. The SUR values of the first dual-radiotracer SPECT scan for each rat (which is performed at the 27th day of the treatment period, while the rat is always under treatment with haloperidol and/or MDL-100,907) were used to estimate the occupancy of the receptor by their respective antagonists, as described below (section 2.4.5). The SUR values of the second SPECT scan for each rat (which is performed 7 days after the end of the treatment period) are direct indexes of the density of the respective receptor populations. For the [^{125}I]R91150 images of the second SPECT scans for each rat, SUR was also estimated at the voxel level using the same formula.

2.4.5 Receptor occupancy estimation

The % occupancy (O) of the $D_{2/3}$ and the 5-HT_{2A} receptors from their respective antagonists was estimated using the following formula: $O\ (\%)=(1-SUR/SUR_{CON})*100$, where SUR corresponds to the value obtained from an individual SPECT study in which a dose of antagonist was employed, while SUR_{CON} corresponds to the average value obtained from the control animals in which no antagonist was administered. In the estimations of occupancies for the $D_{2/3}$ receptor using [^{123}I]IBZM, a 0.55 value was subtracted from the SUR and SUR_{CON} values. This value corresponds to the difference in the non-displaceable binding between the striatum (target region) and the cerebellum (reference region) for this radiotracer, as described in a previous paper from our group [21].

2.5 Statistical analysis

For normally distributed data (assessed using the Shapiro-Wilk test) and for comparisons of means between multiple treatment groups, two-way analysis of variance (2-way ANOVA) was employed with haloperidol and MDL-100,907 dose as the independent factors and the variable under evaluation as the dependent variable. *Post-hoc* analysis was performed when appropriate. For the statistical analysis of the results of the PPI data (where multiple dependent variables were evaluated, i.e. the PPI after auditory stimuli of 75, 80 and 85 dB), as well as for the analysis of the alterations in the 5-HT_{2A} receptor binding in multiple brain VOI, a multi-variate analysis of variance (MANOVA) was employed. For non-normally distributed data, non-parametric tests (Kruskal-Wallis and Mann-Whitney) were employed. For

of 5-HT_{2A} receptor binding, parametric images of SUR were compared between groups using the SPM12 software (Wellcome Trust Centre for Neuroimaging, UCL, London, UK) and the Small Animal Molecular Imaging Toolbox [24] (SAMIT, Groningen, Netherlands) in Matlab (R2016, Mathworks Inc, USA). An uncorrected p at 0.001 with a cluster size threshold of 100 voxels was employed [25,26].

3. Results

3.1 Occupancy of the $D_{2/3}$ and the 5-HT_{2A} receptors by haloperidol and MDL-100,907

Figures 2a-b present the dose-occupancy curves for haloperidol from the *in vivo* and the *ex vivo* occupancy estimations, respectively. Figure 2c present the corresponding MDL-100,907 curve from the *ex vivo* experiment. Both approaches yielded similar results. For haloperidol, a 0.1 mg/kg/day dose leads to an occupancy of around 60% of the $D_{2/3}$ receptors. A dose of 0.25 mg/kg/day leads to an occupancy of a little less than 80% of the receptors, while the doses of 0.5 and 1 mg/kg/day leads towards saturations of more than 85-90% of the $D_{2/3}$ receptors in the Caudate/Putamen (CP). For the MDL-100,907, the dose of 0.5 mg/kg/day, which produces an almost total saturation of the frontal 5-HT_{2A} receptors, as estimated in the *ex vivo* occupancy measurement study, was employed in the main *in vivo* study.

3.2 Effect of chronic haloperidol and MDL-100,907 on the dizocilpine-disrupted prepulse inhibition (PPI) of the startle

Figure 3 presents the effect of the different treatment doses on the PPI: it includes the control group, i.e. H0M0 under the saline-pretreatment condition (the left most bar). All the other bars correspond to the PPI (%) values under the dizocilpine-pretreatment condition. The PPI (%) after a stimulus of 80 dB and 85 dB (presented in Figure 3a and 3b, respectively) were used as dependent variables. The PPI after a stimulus of 75 dB yielded aberrant results (not shown) and was discarded. In control animals (neither dizocilpine nor haloperidol/MDL-100,907 treatment) the PPI (both auditory stimuli volumes combined) was, by average, at 62%. Application of dizocilpine disrupted the PPI, diminishing it, by average, at 31%. Application of MDL-100,907 to the various doses of haloperidol was associated with a tendency to increase the average PPI under dizocilpine pretreatment, at least at the lowest doses of haloperidol. Given that the hypothesis under evaluation concerned the ability of the various combinations of haloperidol and MDL-100,907 to reverse the effect of dizocilpine on PPI, a MANOVA was performed only on the dizocilpine-treated rats, using the PPI (%) responses after the 80 and the 85 dB as dependent variables and the haloperidol and MDL-100,907 doses as factors. A significant effect of the MDL-100,907 treatment ($p<0.05$) as well as of the interaction of the haloperidol and MDL-100,907 factors was observed ($p<0.05$). *Post hoc* analysis using a protected Fischer's Least Significant Differences (LSD) test failed to demonstrate signification differences between any of the individual haloperidol and MDL-100,907 dosage combinations and the control group.

3.3 Haloperidol-induced catalepsy reversal by MDL-100,907

Figure 4 presents the effect of the various treatment schemes on the time elapsed between the placement of the animal on the grid and their first paw movements. Haloperidol doses of 0.5 mg/kg/day and 1 mg/kg/day induced a strong catalepsy (111.4±52.5 and 137.8±79.1 sec to first movement,

respectively), as the time to first movement is significantly higher than the one measured in of control animals (ie. H0/M0 dose) as indicated by a Kruskal Wallis test, $p<0.001$ and *post hoc* Mann Whitney tests $p<0.05$). Adding a 5-HT_{2A} antagonism alleviated the cataleptic effect of haloperidol at 0.5 mg/kg/day (40.3±26.9 sec, $p<0.05$) but not at 1 mg/kg/day (122.1±92.2 sec $p>0.05$).

3.4 Effect of haloperidol and MDL-100,907 treatments on spatial working memory

Spatial working memory, as evaluated by the Y maze test was unaltered across the different treatment groups (data not shown). Neither haloperidol, nor MDL-100,907 had an effect on the number of spontaneous alternations of the entrances in the different arms of the maze ($p>0.05$ for the main effects of factors "haloperidol", "MDL-100,907" and their interaction using 2-way ANOVA).

3.5 Haloperidol-induced vacuous VCM

Figure 5 presents the effect of the chronic treatment with haloperidol and MDL-100,907 on the induction of VCM. A chronic treatment with doses of haloperidol of 0.5 mg/kg/day and 1 mg/kg/day induced a significant increase in the number of the VCM (18.7±5.8 and 13.3±8.2, respectively) compared to saline-treated rats (2.4±2.11), as determined using the Kruskal Wallis, $p<0.001$ and the Mann Whitney test for *post hoc* comparisons, $p<0.05$ as compared to saline-treated animals. On the other hand, MDL-100,907 treatment had no effect on this phenomenon, i.e. did not manage to alleviate the haloperidol-induced VCM syndrome.

3.6 Alteration in in vivo $D_{2/3}$ and 5-HT_{2A} binding after chronic antagonism

Figures 6a and 6b shows the effect of chronic treatment with the various doses of haloperidol and MDL-100,907 on the $D_{2/3}$ receptor binding in the CP and the Nucleus Accumbens (NAc), respectively. All doses of haloperidol induced a significant up-regulation of $D_{2/3}$ binding in both these regions compared to the saline-treated groups, as measured with [^{123}I]IBZM, one week after the end of the treatment period. The SUR of [^{123}I]IBZM of control animals was at 2.62±0.64 in the NAc and 5.14±0.8 for the CP,in the control animals. Haloperidol-only-treated animals had an increase in SUR by +18 to +67% in the NAc and by +15 to +43% in the CP ($p<0.001$ for the effect of haloperidol at the 2-way ANOVA and significant *post hoc* tests of all doses against the saline-treated group). The addition of MDL-100,907 had no effect on this haloperidol-induced $D_{2/3}$ up-regulation in either the CP or the NAc. Haloperidol and MDL-100,907-treated animals had an average increase in the SUR by +11 to +52% NAc and by +15 to +27% in the CP. Regarding the 5-HT_{2A} binding, as measured with [^{125}I]R91150 SPECT, one week after the end of the treatment period, results of a MANOVA (with regional [^{125}I]R91150 SUR as the dependent variables and the haloperidol and MDL-100,907 doses as independent variables) showed a significant effect of haloperidol. To avoid a multiple tests problem and given the widespread binding of [^{125}I]R91150 over multiple brain regions, the statistical comparison between the individual haloperidol doses was performed at the voxel level using SPM. Only the dose

of 0.25 mg/kg/day has a significant effect on 5-HT_{2A} binding. Figure 7 demonstrates a significant increase in [^{125}I]R91150 binding in rats treated with 0.25 mg/kg/day of haloperidol, localized on a collection of frontal cerebral voxels, encompassing parts of the left orbitofrontal, piriform, insular and olfactory cortex, the right piriform and olfactory cortex as well as the left ventral tegmental area (VTA).

4. Discussion

4.1 Strengths of the in vivo imaging approach and design of the study

This study described a thorough evaluation of the impact of 5-HT_{2A} antagonism on multiple aspects of the efficacy and side effect profile of haloperidol. It presents a certain number of strengths regarding its design, the variety of outcome measures and the methods to evaluate these outcome measures: the major strength of the present study is, to our view, the carefully chosen the doses of haloperidol for the chronic treatment that were representative of what has been employed in the literature and clinically pertinent. Indeed, we employed doses ranging from relatively low (0.1 mg/kg/day) to particularly high (1 mg/kg/day). The 0.1 mg/kg/day produces an occupancy of around 60% of the $D_{2/3}$ receptors in the striatum, i.e. at the lowest end of the 65-80% occupancy window that is considered optimal in a clinical and a translational setting [1,7]. This occupancy was confirmed both *ex vivo* and *in vivo* (Figure 2a and 2b). At this occupancy, the 0.1 mg/kg/day dose is supposed to be marginally efficient, without any side effects. The 0.25 mg/kg/day produces a $D_{2/3}$ receptor occupancy that largely lies within the 60-85% occupancy window, thus being efficient and inducing minimal side effects. These two doses allowed to assess the hypothesis that the addition of an MDL-100,907 chronic treatment would ameliorate the efficacy of the haloperidol treatment (i.e. in the dizocilpine-disrupted PPI, as discussed in section 4.3). The two highest haloperidol doses (0.5 and 1 mg/kg/day) produce a maximal $D_{2/3}$ receptor occupancy, that lies largely beyond the highest end of the 65-80% occupancy window. Both doses induce side effects and were important for the assessment of the hypothesis that the addition of an MDL-100,907 chronic treatment would alleviate the haloperidol-induced side effects (as discussed in section 4.2). The 1 mg/kg/day dose, in particular, was included in this study to allow a direct comparison with the majority of previous studies. As discussed in the subsequent sections of this paper, the use of a 1 mg/kg/day dose of haloperidol in the literature (which has been criticized as unreasonably high [7]) may “conceal” any ameliorative effect of co-administered substances, such as the MDL-100,907. On the contrary, the use of a 0.5 mg/kg/day dose almost saturates the $D_{2/3}$ receptors in the striatum (Figure 2), induces clinically relevant side effects (e.g. catalepsy and VCM) and allows to demonstrate potential ameliorative effects of MDL-100,907, that were previously unappreciated in the literature (discussed thoroughly in section 4.2).

A chronic treatment scheme with the $D_{2/3}$ and 5-HT_{2A} antagonists was chosen. This is probably more clinically relevant for the evaluation of the effects of these antagonists firstly because antipsychotic agents are almost always employed chronically in patients. Secondly, the administration of these antagonists using osmotic minipumps and not via daily injections induces a stable occupancy of the receptors over time, resembling the temporal pattern of occupancy in patients. Indeed, the elimination of haloperidol in the rat is much faster than in human and a once-daily administration of the antagonists would lead to an intermittent occupancy of the receptors with steep peaks and decreases of the occupancy which are not clinically relevant [7,27,28].

The occupancy of the $D_{2/3}$ and the 5-HT_{2A} receptor is confirmed *in vivo* and *ex vivo* using a simultaneous, dual-radiotracer $D_{2/3}$ and 5-HT_{2A} imaging SPECT approach, previously validated by our

group [8]. The advantage of such a methodology lies on the fact that it allowed the *in vivo* study of the two receptors under the exact same physiological conditions and that it presents a highly acceptable test-retest variability of 14% for both radiotracers [8]. The neurochemical changes, at the level of $D_{2/3}$ and 5-HT_{2A} receptor binding, induced by chronic antagonism at these receptors was also allowed *in vivo* using the same dual-radiotracer approach. Finally, a strength of this study is also the fact that a variety of behavioral tests, relevant to the clinical actions of antipsychotic treatment were employed.

4.2 5-HT_{2A} antagonism partially alleviates haloperidol-induced catalepsy but has no effect on VCM

The present study confirms and extends the existing literature on the effect of a 5-HT_{2A} antagonism on the behavioral and neurochemical alterations induced by a $D_{2/3}$-specific antagonist. An interesting finding of our study concerns the effect of MDL-100,907 on the haloperidol-induced catalepsy. As expected, a high occupancy of the striatal $D_{2/3}$ receptors induces this acute extrapyramidal symptom. The groups of rats treated with the two higher haloperidol doses (0.5 and 1 mg/kg/day) presented a strong catalepsy, which confirms the current literature [29-33]. In accordance with this literature, 5-HT_{2A} antagonism failed to counteract the cataleptic effect of the highest dose of haloperidol (1 mg/kg/day). Interestingly, 5-HT_{2A} antagonism managed to significantly reduce the effect of the second highest dose of haloperidol, at 0.5 mg/kg/day, a finding that, to our knowledge, has never been reported before. Indeed, previous studies which evaluated the effect of MDL-100,907 on chronic haloperidol-induced catalepsy only employed high doses of haloperidol (1 mg/kg/day or higher) [29,31]. Regarding acute treatment regimes, Creed-Carson et al [31] employed a single subcutaneous 0.5 mg/kg dose of haloperidol. The resulting catalepsy was not reversed by a 0.5 mg/kg dose of MDL-100,907 (the exact same dose as in the present study). Similar results were observed with an acute administration of 0.63 mg/kg of haloperidol [34] and MDL100,907 at 0.1 mg/kg. However, this apparent discrepancy might be explained by the differential effects of an acutely vs a chronically administered dose of haloperidol and by the lower dose of MDL-100,907 employed in the latter study. Indeed, it is probable that the duration of treatment with an antagonist has an impact on the relationship between its dose and the resulting catalepsy: an acute dose of haloperidol of 0.25 mg/kg induces catalepsy, while the same dose administered chronically does not [35]. In addition, in a study comparing a continuous vs an once daily administration of haloperidol via subcutaneous injections, it was demonstrated that the same dose of haloperidol, when administered once-daily, produces steep peaks in occupancy that are considerably higher than the occupancy that is achieved with a continuous treatment via an osmotic minipump [28]. Regarding other possible pharmacological targets against antipsychotic-induced catalepsy, a chronically administered dose of haloperidol at 1 mg/kg/day produces a catalepsy that may be reversed by a 5-HT_{2C} antagonism [30,31,36] and 5-HT_{2C} antagonism may also reverse a raclopride (a highly selective $D_{2/3}$ antagonist)-induced catalepsy [37,38]. In light of the findings of the present study, a synergistic modulation of the nigrostriatal system by both 5-HT_{2A} and 5-HT_{2C} receptors may be hypothesized [39]. A 5-HT_{2A} antagonism may only be sufficient to prevent catalepsy at a limited range of $D_{2/3}$ blockade [40,41]. Overall, these results suggest that a 5-HT_{2A} antagonism could -at least

partially- underlie the clinically-observed lower prevalence of acute extrapyramidal symptoms with atypical antipsychotic agents [3].

The second aspect of motor side effects evaluated in this study was the haloperidol-induced VCM. In accordance with the literature [28,32,42], our results demonstrate that a high occupancy of the striatal $D_{2/3}$ receptors (induced by doses of 0.5 and 1 mg/kg/day) is associated with an induction of VCM. In the present study, the number of VCM that were recorded were somewhat higher than the number observed in other studies with similar doses of haloperidol [28,42]. This finding is expected, as animal restrain is associated with higher number of VCM compared to the VCM measured in freely moving rats [18]. A 5-HT_{2A} antagonism failed to alleviate this side effect of haloperidol (both at 0.5 mg/kg/day and 1 mg/kg/day). This finding is also in accordance with and extends the existing literature that, so far, has only evaluated the effect of 5-HT_{2A} antagonism on the VCM induced by the highest dose of haloperidol (1 mg/kg/day). Here, we extend this finding for a lower, but still supratherapeutic, dose of haloperidol (0.5 mg/kg/day). Interestingly, the effect of 5-HT_{2A} antagonism not only lacked any preventive effect on the VCM but was even associated with a tendency to increase the VCM induced by haloperidol (Figure 5, not reaching significance). This tendency excludes the possibility that the failure to demonstrate a favorable effect of 5-HT_{2A} antagonism on VCM could be due to a type II error (e.g. resulting from a lack of power). Consequently, 5-HT_{2A} antagonism is probably not implicated in the clinically and experimentally observed lower prevalence of VCM in animals treated with atypical antipsychotics that with typical agents [43-48] and other mechanisms might underlie this phenomenon. Several studies in the literature have indeed proposed a role for the 5-HT_{2C} receptor [31] and other neurotransmitter systems in the reduction of VCM in chronic haloperidol-treated rodents [47,49]. As a 5-HT_{2C} antagonism is a common feature of many atypical antipsychotic agents, this might be a more valid target of research for the prevention of antipsychotic-induced tardive dyskinesia.

4.3 5-HT_{2A} antagonism alters the dizocilpine-disruption of the PPI

In the present study, our hypothesis was that the chronic antagonism at the 5-HT_{2A} receptor will render the chronic haloperidol treatment capable of reversing the PPI-disruptive effect of dizocilpine. A haloperidol alone treatment has consistently been found ineffective in this experimental paradigm [50,51] (with only one study, to our knowledge, showing efficacy of a 14-day haloperidol treatment at 1 mg/kg/day in mice [52]). On the contrary, in the same test, atypical antipsychotics have been found effective [50,52-55]. Given that a 5-HT_{2A} antagonism alone has given positive results in one study [11], one might consider that a chronic MDL-100,907 treatment could render the haloperidol treatment capable of reversing the effect of dizocilpine and thus provide evidence that a 5-HT_{2A} antagonism could be the substrate of the superiority of atypical agents over typical ones in this experimental paradigm.

Given that our hypothesis was that the treatment with haloperidol and MDL-100,907 could augment the PPI in dizocilpine-pretreated rats, we evaluated the data that corresponded to these rats only, to obtain more statistical power. The results of the MANOVA showed a significant effect of the MDL-100,907 treatment, as well as the interaction of haloperidol and MDL-100,907 doses, pointing to an impact of MDL-100,907 on the PPI, likely dependent on the concurrently administered dose of

haloperidol. Subsequently, we performed *post hoc* pair-wise t-test comparisons (using a protected Fisher's correction). These comparisons failed to yield significant results, despite a tendency for the various treatments, particularly when an MDL-100,907 treatment is present, to augment the PPI (Figure 3). Given the variability of this data, it cannot be excluded that this part of our study lacked the necessary statistical power to clearly demonstrate significant differences in group-wise comparisons. On the other hand, as recently suggested in a recent study [56], a 5-HT_{2A} antagonism may partially contribute to the reversal of the effect of dizocilpine on the PPI, along with antagonism at other serotoninergic receptors, such as the 5-HT_{6}.

PPI is a physiological phenomenon observed both in human and rodents, while its actual neurophysiological substrates remain largely unknown. However, it has been demonstrated that that agents that efficiently treat positive psychotic symptoms, are able to reverse the disruption of PPI induced by various agents [9,10,57]. Here, we employed a NMDA antagonist, dizocilpine, as a PPI-disrupting agent. We did not use a dopaminergic agent, such as apomorphine, to induce the disruption of PPI because this would possibly not enable to assess the efficacy of 5-HT_{2A} antagonism, given that haloperidol, a $D_{2/3}$ antagonist would most likely already be quite efficient to reverse the apomorphine-induced disruption of PPI [13,58]. In addition, dizocilpine-disruption of PPI is probably more relevant for the study of the properties of atypicality [59]. Overall, the results of the PPI experiments provide further argument in favor of the efficacy of a 5-HT_{2A} antagonism in the reversal of dizocilpine-disruption of the PPI but further research is needed to confirm this hypothesis.

4.4 Spatial working memory is unaltered with either haloperidol or MDL-100,907 treatment

The present study failed to detect any significant effect of either antagonist, haloperidol or MDL-100,907 on the spatial working memory [60]. This contrasts findings of a part of the clinical and rodent studies on this subject, in which haloperidol, sulpiride and even some atypical agents [61], induced working memory deficits [17,32,62-68]. It is important to note, considering the preclinical studies that have demonstrated an impact of haloperidol on spatial working memory, that, for instance, in the Xu study [17], a particularly high and certainly clinically less pertinent dose of 2 mg/kg/day of haloperidol has been employed, while in the Karl study [32] spatial working memory was assessed with a test other than the Y maze. Other clinical studies found that antipsychotics (both typical and atypical) may in fact ameliorate cognitive deficits in schizophrenic patients [16,69-75], suggesting that, with respect to translational research on cognitive deficits induced or rescued by antipsychotics agents, animal models of schizophrenia would be more relevant, given the complexity of the phenomenon [76] and the probably differential effect of antipsychotics in healthy and schizophrenic individuals.

4.5 5-HT_{2A} antagonism fails to reverse the haloperidol-induced $D_{2/3}$ upregulation

At a neurochemical level, chronic $D_{2/3}$ antagonism by haloperidol led to a significant increase in the binding of this receptor in the CP and the NAc (Figure 6), an effect observed over the whole range of haloperidol doses. This is in accordance with the literature, in which a chronic $D_{2/3}$ antagonism (or

partial agonism in the case of aripiprazole) has been shown to lead to an upregulation of the $D_{2/3}$ receptors in the striatum [28,42,77-81]. The literature also suggests that this $D_{2/3}$ upregulation is present to a lesser extent, if at all, with atypical antipsychotics, notably clozapine [77,82-84]. A human study evaluating the $D_{2/3}$ receptor in human subjects found that this upregulation was present in patients treated with the typical agents haloperidol and perphenazine, as well as with the atypical risperidone [85]. Given the affinity for the 5-HT_{2A} receptor of the majority of the atypical agents that were evaluated in these studies, it was proposed that a 5-HT_{2A} antagonism could prevent this upregulation of the $D_{2/3}$. To our knowledge, no study so far has assessed the effect of a 5-HT_{2A} antagonism on this phenomenon, to directly test this hypothesis. In the present study, the co-administration of MDL-100,907 with any of the doses of haloperidol failed to significantly prevent the upregulation of the $D_{2/3}$ receptor. Ishikane et al [78] found that the D_2-receptor upregulation observed with low doses of haloperidol (0.1 mg/kg/day) were prevented with a parallel treatment with ritanserin, a mixed 5-HT_{2A}/5-HT_{2C} antagonist. Given that in the present study, a treatment with a pure 5-HT_{2A} antagonist, failed to prevent the $D_{2/3}$ upregulation, one could hypothesize that 5-HT_{2C} antagonist properties may play a more prominent role in the atypicality with respect to the chronic changes in $D_{2/3}$ binding.

It is also hypothesized that the upregulation of the $D_{2/3}$ receptors by haloperidol is implicated in the occurrence of the VCM [42]. The results of the present study suggest that the $D_{2/3}$ receptor upregulation is probably not a sufficient condition for the induction of VCM, as the animals treated with the 0.1 and the 0.25 mg/kg/day doses presented a $D_{2/3}$ upregulation without VCM. On the other hand, the failure of MDL-100,907 to prevent the haloperidol-induced $D_{2/3}$ upregulation coincided with its failure to prevent the VCM induced by the highest doses of haloperidol treatment. These results challenge the hypothesized causal link between $D_{2/3}$ upregulation and VCM induction and emphasize the need to conduct in-depth studies of these two phenomena.

4.6 Haloperidol at moderate doses upregulates the 5-HT_{2A} receptor in frontal cortical areas and the VTA

A surprising finding of the present study was the increase in the 5-HT_{2A} receptor binding in frontal cortical areas and in the VTA, induced by a moderate dose of haloperidol (0.25 mg/kg/day, that leads to an occupancy of the $D_{2/3}$ receptor mostly within the 65-80% occupancy window). It is important to note that only the rats treated with this dose presented this effect, which was unaltered by a 5-HT_{2A} antagonism. In fact, 5-HT_{2A} antagonism was not associated with any neurochemical change on either of the receptors studied. Higher doses of haloperidol had no impact on 5-HT_{2A} receptor binding in any brain region. This is a previously unappreciated finding, given that only a narrow range of haloperidol doses induced this upregulation and that the literature so far has not assessed the effect of such a moderate dose of haloperidol on 5-HT_{2A} binding. Indeed, only doses of 0.5 mg/kg/day or higher have been examined and showed, as this present study did, no effect. In fact, only atypical antipsychotics have been shown to alter 5-HT_{2A} binding, i.e. leading to a downregulation of this receptor [86-94]. Among the very few exceptions to the aforementioned results, Charron et al recently showed that haloperidol, at 0.5 mg/kg/day decreases [^{3}H]ketanserin binding in the frontal cortex and increases it in

the striatum. However, this radiotracer also binds to 5-HT_{2C} receptors, rendering the interpretation of these findings difficult. The downregulation of 5-HT_{2A}, shared by atypical agents and not by typical ones, was hypothesized as one of the substrates of atypicality, but no conclusive evidence linking it to the efficacy and side effect profile of atypical agents has been reported so far. The present study, given the absence of any 5-HT_{2A} antagonist properties of haloperidol, points to an indirect modulation of the 5-HT_{2A} binding possibly via an alteration of serotonin release. If serotonin release is diminished, this transmitter competes less with the [^{125}I]R91150 radiotracer for binding to the receptor and the binding of this radiotracer could be augmented. Indeed, there is evidence that the dopaminergic system, via the D_2 receptor may alter serotonin transmission [95-100]. Burnet et al and Bishnoi et al suggested that haloperidol treatment leads to a reduction in the concentration of a serotonin metabolite [101] and serotonin itself in the brain [102]. Another possible hypothesis would be to attribute this change of 5-HT_{2A} binding to alterations in D_2/5-HT_{2A} heteromers. Albizu et al [103] found that heteromers of D_2 and 5-HT_{2A} receptors produce allosteric modulations of the latter via D_2-mediated mechanisms and alter its affinity for 5-HT_{2A} binding radioligands. Finally, to explain the differential effect of moderate vs high doses of haloperidol on 5-HT_{2A} receptor binding, one could hypothesize that low doses of haloperidol may preferentially act on D_2 autoreceptors, while higher doses act both auto- and hetero-receptors. Interestingly, the dose of 0.25 mg/kg/day of haloperidol, is the dose in which the impact of 5-HT_{2A} antagonism shows the highest tendency towards a reversal of the dizocilpine-disruption of PPI (see section 4.3) suggesting that a possible involvement of this 5-HT_{2A} upregulation may be coupled to the fact that 5-HT_{2A} antagonism of this particular dose of haloperidol (0.25 mg/kg/day) may potentialize its efficacy in the PPI test.

From a methodological point of view, to confirm this finding, we first verified that haloperidol (from our *in vivo* SPECT studies) does not induce 5-HT_{2A} occupancy (data not shown). Secondly, we used our *ex vivo* experiments: indeed, as mentioned in the methods section, the group of rats treated with various doses of haloperidol to determine the dose-occupancy curve, was subjected to *ex vivo* radiotracer measurements with [^{125}I]R91150. Using the rats of this experiments that were treated with similar doses of haloperidol as in the *in vivo* study (0.2-0.4 mg/kg/day), we found that indeed a 5-HT_{2A} receptor upregulation was induced. This *ex vivo* study is also interesting because it confirms that this upregulation, measured *in vivo* 7 days after the end of the chronic treatments of the rats, is not a result of the drug withdrawal but of the treatment itself. This is because in the *ex vivo* study, the binding measurements were performed at the end of the 28 days treatment period, i.e. while the rats were still under treatment with haloperidol. Considering the *in vivo* methodology that was employed, we have previously conclusively demonstrated that the dual-radiotracer approach with simultaneous imaging with [^{123}I]IBZM and [^{125}I]R91150 does not induce any bias in the receptor binding estimation, excluding the possibility that this 5-HT_{2A} upregulation is a mere “artefact” of the SPECT scan methodology.

4.7 Limitations of the present study

Among the limitations of the study, first the use of a Mdr1a knock out strain has to be mentioned. We used this strain to be able to employ [^{125}I]R91150 for the *in vivo* imaging of 5-HT$_{2A}$. This radiotracer has minimal brain penetration in wild-type rats, impeding its *in vivo* use in SPECT imaging [20,22,104]. In this context, it is important to confirm that the use of Mdr1a knock out rats does not bias the behavioral and neurochemical responses to the chronic treatment with haloperidol and MDL-100,907. Arguments in favor of this hypothesis include the following observations: (1) Mdr1a knock out and wild-type rats present identical D$_{2/3}$ and 5-HT$_{2A}$ receptor binding in the brain (confirmed by *ex vivo* imaging that is possible with [^{125}I]R91150 even in wild-type rats), (2) the dose-occupancy curve of haloperidol shows no alterations compared to wild-type rats as estimated in previous studies [33,105], (3) the behavioral responses to haloperidol and dizocilpine were highly comparable to those observed in previous studies, notably the correspondence of the occupancy of the D$_{2/3}$ receptor by haloperidol and the induction of side effects. It also has to be noted that the results on 5-HT$_{2A}$ upregulation by moderate doses of haloperidol and not by high doses of this typical antipsychotic are mostly exploratory. No inference on a causal contribution on the effect of this antipsychotic agent may be formulated in the present study.

5. Conclusion

In conclusion, here, we provide evidence for the involvement of 5-HT_{2A} receptor antagonism in the alleviation of catalepsy induced by haloperidol, an effect that is dose-dependent. Similarly, preliminary evidence is provided for an involvement of 5-HT_{2A} receptor antagonism on the reversal of dizocilpine-disruption of PPI. 5-HT_{2A} receptor antagonism failed to prevent the upregulation of $D_{2/3}$ that is induced by a chronic haloperidol treatment, as well as the induction of VCM by high doses of this typical antipsychotic agent. A previously unappreciated dose-dependent effect of moderate doses of haloperidol on the *in vivo* and *ex vivo* frontal cortical 5-HT_{2A} binding has also been observed. The present work points to an involvement of a 5-HT_{2A} receptor antagonism in the modification of some aspects of the efficacy and side effect profile of haloperidol, suggesting that, at least partially, 5-HT_{2A} antagonism might be associated with atypicality. Based on the results of this study however, the role of the 5-HT_{2A} receptor antagonism as the sole (or even the major) determinant of antipsychotic atypicality can probably be rejected. The need to carefully choose clinically relevant antipsychotic doses (i.e. a dose of 0.5 mg/kg/day and not 1 mg/kg/day) and to further investigate the role of neurochemical changes induced by chronic antipsychotic treatment in the search for causal relationships with its clinical effect is warranted.

6. Acknowledgments

This work was supported by the Swiss National Science Foundation (grant no. 310030_156829), by the Geneva Neuroscience Centre and by the Maria Zaousi Memorial Foundation (Greece) through a scholarship of the Hellenic State Scholarship Foundation (ST) and by the “Swiss Association for Alzheimer’s Research" which was created in 2009 to finance Swiss fundamental and clinical research programs on Alzheimer’s disease. Author ST was supported by the Jean and Madeleine Vachoux Foundation. Dr Vallez-Garcia of the University Medical Center Groningen (UMCG) provided valuable expertise regarding the SAMIT Toolbox. Authors are grateful to Mrs Maria Surini-Demiri and Mr Marouane Ben Ammar for excellent technical assistance and declare that they have no conflict of interest.

Figure legends

Figure 1 Graphical presentation of the timeline of the present study.

Figure 2 Haloperidol *in vivo* (2a) and *ex vivo* (2b) dose-occupancy curves, estimated in the striatum. (2c) *Ex vivo* MDL-100,907 dose-occupancy curve, estimated in the frontal cortex.

Figure 3 The effect of the various haloperidol and MDL-100,907 combinations on the disruption of the PPI by dizocilpine using a (3a) 80 dB and a (3b) 85 dB auditory pulse (Mean±SEM values). The leftmost bar corresponds to the control group (H0/M0), not pre-treated with dizocilpine (baseline PPI). The rest correspond to rats pretreated with dizocilpine. The haloperidol and MDL-100,907 dosages are depicted below each bar. No significant differences were found in pairwise comparisons.

Figure 4 Results of the catalepsy tests under the various chronic treatment combinations (Mean±SEM). ‡Denotes significant differences between the mean time lapses between these four doses compared to the control (H0M0). *Denotes a significant difference between the H0.5M0 and the H0.5/M0.5 group.

Figure 5 The effect of the chronic treatment with haloperidol and MDL-100,907 on the induction of VCM/2 min (Mean±SEM). ‡Denotes a significant increase in the number of the VCM compared to saline-treated rats.

Figure 6 $D_{2/3}$ binding measured in the CP (6a) and NAc (6b) (Mean±SD). All groups present a significant increase compared to the controls (H0/M0).

Figure 7 Results of the voxel-wise comparison of the 5-HT_{2A} binding between the rats of the control group (H0/M0) and the rats treated with haloperidol at 0.25 mg/kg/day (Mean±SD).

References

1 Ginovart N, Kapur S. Role of dopamine D(2) receptors for antipsychotic activity. Handbook of experimental pharmacology. 2012(212):27-52.

2 Kapur S, Remington G. Dopamine D(2) receptors and their role in atypical antipsychotic action: still necessary and may even be sufficient. Biological psychiatry. 2001;50(11):873-83.

3 Martino D, Karnik V, Osland S, Barnes TRE, Pringsheim TM. Movement Disorders Associated With Antipsychotic Medication in People With Schizophrenia: An Overview of Cochrane Reviews and Meta-Analysis. Canadian journal of psychiatry Revue canadienne de psychiatrie. 2018:706743718777392.

4 Leucht S, Cipriani A, Spineli L, Mavridis D, Örey D, Richter F, et al. Comparative efficacy and tolerability of 15 antipsychotic drugs in schizophrenia: a multiple-treatments meta-analysis. The Lancet. 2013;382(9896):951-62.

5 Meltzer HY. What's atypical about atypical antipsychotic drugs? Current opinion in pharmacology. 2004;4(1):53-7.

6 Ebdrup BH, Rasmussen H, Arnt J, Glenthoj B. Serotonin 2A receptor antagonists for treatment of schizophrenia. Expert opinion on investigational drugs. 2011;20(9):1211-23.

7 Kapur S, Wadenberg ML, Remington G. Are animal studies of antipsychotics appropriately dosed? Lessons from the bedside to the bench. Canadian journal of psychiatry Revue canadienne de psychiatrie. 2000;45(3):241-6.

8 Tsartsalis S, Tournier BB, Habiby S, Ben Hamadi M, Barca C, Ginovart N, et al. Dual-radiotracer translational SPECT neuroimaging. Comparison of three methods for the simultaneous brain imaging of D2/3 and 5-HT2A receptors. Neuroimage. 2018;176:528-40.

9 Swerdlow NR, Weber M, Qu Y, Light GA, Braff DL. Realistic expectations of prepulse inhibition in translational models for schizophrenia research. Psychopharmacology. 2008;199(3):331-88.

10 Wadenberg MG, Sills TL, Fletcher PJ, Kapur S. Antipsychoticlike effects of amoxapine, without catalepsy, using the prepulse inhibition of the acoustic startle reflex test in rats. Biological psychiatry. 2000;47(7):670-6.

11 Varty GB, Bakshi VP, Geyer MA. M100907, a serotonin 5-HT2A receptor antagonist and putative antipsychotic, blocks dizocilpine-induced prepulse inhibition deficits in Sprague-Dawley and Wistar rats. Neuropsychopharmacology : official publication of the American College of Neuropsychopharmacology. 1999;20(4):311-21.

12 Tournier BB, Ginovart N. Repeated but not acute treatment with (9)-tetrahydrocannabinol disrupts prepulse inhibition of the acoustic startle: reversal by the dopamine D(2)/(3) receptor antagonist haloperidol. European neuropsychopharmacology : the journal of the European College of Neuropsychopharmacology. 2014;24(8):1415-23.

13 Martinez ZA, Oostwegel J, Geyer MA, Ellison GD, Swerdlow NR. "Early" and "late" effects of sustained haloperidol on apomorphine- and phencyclidine-induced sensorimotor gating deficits. Neuropsychopharmacology : official publication of the American College of Neuropsychopharmacology. 2000;23(5):517-27.

14 Gobira PH, Ropke J, Aguiar DC, Crippa JA, Moreira FA. Animal models for predicting the efficacy and side effects of antipsychotic drugs. Rev Bras Psiquiatr. 2013;35 Suppl 2:S132-9.

15 Tyson PJ, Roberts KH, Mortimer AM. Are the cognitive effects of atypical antipsychotics influenced by their affinity to 5HT-2A receptors? The International journal of neuroscience. 2004;114(6):593-611.

16 Williams GV, Rao SG, Goldman-Rakic PS. The physiological role of 5-HT2A receptors in working memory. The Journal of neuroscience : the official journal of the Society for Neuroscience. 2002;22(7):2843-54.

17 Xu H, Yang H-J, Rose GM. Chronic haloperidol-induced spatial memory deficits accompany the upregulation of D1 and D2 receptors in the caudate putamen of C57BL/6 mouse. Life sciences. 2012;91(9-10):322-28.

18 Glenthoj B. Persistent vacuous chewing in rats following neuroleptic treatment: relationship to dopaminergic and cholinergic function. Psychopharmacology. 1993;113(2):157-66.

19 Crowley JJ, Adkins DE, Pratt AL, Quackenbush CR, van den Oord EJ, Moy SS, et al. Antipsychotic-induced vacuous chewing movements and extrapyramidal side effects are highly heritable in mice. The pharmacogenomics journal. 2012;12(2):147-55.

20 Dumas N, Moulin-Sallanon M, Fender P, Tournier BB, Ginovart N, Charnay Y, et al. In Vivo Quantification of 5-HT2A Brain Receptors in Mdr1a KO Rats with 123I-R91150 Single-Photon Emission Computed Tomography. Molecular imaging. 2015;14.

21 Tsartsalis S, Tournier BB, Aoun K, Habiby S, Pandolfo D, Dimiziani A, et al. A single-scan protocol for absolute D2/3 receptor quantification with [123I]IBZM SPECT. NeuroImage. 2017;147:461-72.
22 Dumas N, Moulin-Sallanon M, Ginovart N, Tournier BB, Suzanne P, Cailly T, et al. Small-animal single-photon emission computed tomographic imaging of the brain serotoninergic systems in wild-type and mdr1a knockout rats. Molecular imaging. 2014;13(1).
23 Schiffer WK, Mirrione MM, Biegon A, Alexoff DL, Patel V, Dewey SL. Serial microPET measures of the metabolic reaction to a microdialysis probe implant. J Neurosci Methods. 2006;155(2):272-84.
24 Vallez Garcia D, Casteels C, Schwarz AJ, Dierckx RA, Koole M, Doorduin J. A standardized method for the construction of tracer specific PET and SPECT rat brain templates: validation and implementation of a toolbox. PLoS One. 2015;10(3):e0122363.
25 Bennett CM, Wolford GL, Miller MB. The principled control of false positives in neuroimaging. Soc Cogn Affect Neurosci. 2009;4(4):417-22.
26 Tsartsalis S, Tournier BB, Graf CE, Ginovart N, Ibanez V, Millet P. Dynamic image denoising for voxel-wise quantification with Statistical Parametric Mapping in molecular neuroimaging. PLoS One. 2018;13(9):e0203589.
27 Ginovart N, Wilson AA, Hussey D, Houle S, Kapur S. D2-Receptor Upregulation is Dependent upon Temporal Course of D2-Occupancy: A Longitudinal [11C]-Raclopride PET Study in Cats. Neuropsychopharmacology : official publication of the American College of Neuropsychopharmacology. 2008;34(3):662-71.
28 Turrone P, Remington G, Kapur S, Nobrega JN. Differential effects of within-day continuous vs. transient dopamine D2 receptor occupancy in the development of vacuous chewing movements (VCMs) in rats. Neuropsychopharmacology : official publication of the American College of Neuropsychopharmacology. 2003;28(8):1433-9.
29 McOmish CE, Lira A, Hanks JB, Gingrich JA. Clozapine-induced locomotor suppression is mediated by 5-HT2A receptors in the forebrain. Neuropsychopharmacology : official publication of the American College of Neuropsychopharmacology. 2012;37(13):2747-55.
30 Reavill C, Kettle A, Holland V, Riley G, Blackburn TP. Attenuation of haloperidol-induced catalepsy by a 5-HT2C receptor antagonist. British journal of pharmacology. 1999;126(3):572-4.
31 Creed-Carson M, Oraha A, Nobrega JN. Effects of 5-HT(2A) and 5-HT(2C) receptor antagonists on acute and chronic dyskinetic effects induced by haloperidol in rats. Behavioural brain research. 2011;219(2):273-9.
32 Karl T, Duffy L, O'Brien E, Matsumoto I, Dedova I. Behavioural effects of chronic haloperidol and risperidone treatment in rats. Behavioural brain research. 2006;171(2):286-94.
33 Wadenberg ML, Soliman A, VanderSpek SC, Kapur S. Dopamine D(2) receptor occupancy is a common mechanism underlying animal models of antipsychotics and their clinical effects. Neuropsychopharmacology : official publication of the American College of Neuropsychopharmacology. 2001;25(5):633-41.
34 Mombereau C, Arnt J, Mork A. Involvement of presynaptic 5-HT1A receptors in the low propensity of brexpiprazole to induce extrapyramidal side effects in rats. Pharmacology, biochemistry, and behavior. 2017;153:141-46.
35 Osborne PG, O'Connor WT, Beck O, Ungerstedt U. Acute versus chronic haloperidol: relationship between tolerance to catalepsy and striatal and accumbens dopamine, GABA and acetylcholine release. Brain research. 1994;634(1):20-30.
36 Di Giovanni G, De Deurwaerdere P. New therapeutic opportunities for 5-HT2C receptor ligands in neuropsychiatric disorders. Pharmacology & therapeutics. 2016;157:125-62.
37 Wadenberg ML, Ahlenius S. Antagonism by the 5-HT2A/C receptor agonist DOI of raclopride-induced catalepsy in the rat. European journal of pharmacology. 1995;294(1):247-51.
38 Wadenberg MG, Browning JL, Young KA, Hicks PB. Antagonism at 5-HT(2A) receptors potentiates the effect of haloperidol in a conditioned avoidance response task in rats. Pharmacology, biochemistry, and behavior. 2001;68(3):363-70.
39 Egerton A, Ahmad R, Hirani E, Grasby PM. Modulation of striatal dopamine release by 5-HT2A and 5-HT2C receptor antagonists: [11C]raclopride PET studies in the rat. Psychopharmacology. 2008;200(4):487-96.
40 Lucas G, De Deurwaerdere P, Caccia S, Umberto S. The effect of serotonergic agents on haloperidol-induced striatal dopamine release in vivo: opposite role of 5-HT(2A) and 5-HT(2C) receptor subtypes and significance of the haloperidol dose used. Neuropharmacology. 2000;39(6):1053-63.

41 Liegeois JF, Ichikawa J, Meltzer HY. 5-HT(2A) receptor antagonism potentiates haloperidol-induced dopamine release in rat medial prefrontal cortex and inhibits that in the nucleus accumbens in a dose-dependent manner. Brain research. 2002;947(2):157-65.
42 Turrone P, Remington G, Kapur S, Nobrega JN. The relationship between dopamine D2 receptor occupancy and the vacuous chewing movement syndrome in rats. Psychopharmacology. 2003;165(2):166-71.
43 Carbon M, Kane JM, Leucht S, Correll CU. Tardive dyskinesia risk with first- and second-generation antipsychotics in comparative randomized controlled trials: a meta-analysis. World Psychiatry. 2018;17(3):330-40.
44 Marchese G, Bartholini F, Casu MA, Ruiu S, Casti P, Congeddu E, et al. Haloperidol versus risperidone on rat "early onset" vacuous chewing. Behavioural brain research. 2004;149(1):9-16.
45 Ikeda H, Adachi K, Hasegawa M, Sato M, Hirose N, Koshikawa N, et al. Effects of chronic haloperidol and clozapine on vacuous chewing and dopamine-mediated jaw movements in rats: evaluation of a revised animal model of tardive dyskinesia. Journal of neural transmission. 1999;106(11-12):1205-16.
46 Egan MF, Hyde TM, Kleinman JE, Wyatt RJ. Neuroleptic-induced vacuous chewing movements in rodents: incidence and effects of long-term increases in haloperidol dose. Psychopharmacology. 1995;117(1):74-81.
47 Naidu PS, Kulkarni SK. Effect of 5-HT1A and 5-HT2A/2C receptor modulation on neuroleptic-induced vacuous chewing movements. European journal of pharmacology. 2001;428(1):81-6.
48 Rosengarten H, Quartermain D. The effect of chronic treatment with typical and atypical antipsychotics on working memory and jaw movements in three- and eighteen-month-old rats. Progress in neuro-psychopharmacology & biological psychiatry. 2002;26(6):1047-54.
49 Ceretta APC, de Freitas CM, Schaffer LF, Reinheimer JB, Dotto MM, de Moraes Reis E, et al. Gabapentin reduces haloperidol-induced vacuous chewing movements in mice. Pharmacology, biochemistry, and behavior. 2018;166:21-26.
50 Varty GB, Higgins GA. Examination of drug-induced and isolation-induced disruptions of prepulse inhibition as models to screen antipsychotic drugs. Psychopharmacology. 1995;122(1):15-26.
51 Feifel D, Priebe K. The effects of subchronic haloperidol on intact and dizocilpine-disrupted sensorimotor gating. Psychopharmacology. 1999;146(2):175-9.
52 Li C, Tang Y, Yang J, Zhang X, Liu Y, Tang A. Sub-chronic Antipsychotic Drug Administration Reverses the Expression of Neuregulin 1 and ErbB4 in a Cultured MK801-Induced Mouse Primary Hippocampal Neuron or a Neurodevelopmental Schizophrenia Model. Neurochemical research. 2016;41(8):2049-64.
53 Bubenikova V, Votava M, Horacek J, Palenicek T, Dockery C. The effect of zotepine, risperidone, clozapine and olanzapine on MK-801-disrupted sensorimotor gating. Pharmacology, biochemistry, and behavior. 2005;80(4):591-6.
54 Zangrando J, Carvalheira R, Labbate G, Medeiros P, Longo BM, Melo-Thomas L, et al. Atypical antipsychotic olanzapine reversed deficit on prepulse inhibition of the acoustic startle reflex produced by microinjection of dizocilpine (MK-801) into the inferior colliculus in rats. Behavioural brain research. 2013;257:77-82.
55 Hudson MR, Rind G, O'Brien TJ, Jones NC. Reversal of evoked gamma oscillation deficits is predictive of antipsychotic activity with a unique profile for clozapine. Translational psychiatry. 2016;6:e784.
56 Fijal K, Popik P, Nikiforuk A. Co-administration of 5-HT6 receptor antagonists with clozapine, risperidone, and a 5-HT2A receptor antagonist: effects on prepulse inhibition in rats. Psychopharmacology. 2014;231(1):269-81.
57 Bakshi VP, Geyer MA. Multiple limbic regions mediate the disruption of prepulse inhibition produced in rats by the noncompetitive NMDA antagonist dizocilpine. The Journal of neuroscience : the official journal of the Society for Neuroscience. 1998;18(20):8394-401.
58 Zhang M, Ballard ME, Unger LV, Haupt A, Gross G, Decker MW, et al. Effects of antipsychotics and selective D3 antagonists on PPI deficits induced by PD 128907 and apomorphine. Behavioural brain research. 2007;182(1):1-11.
59 Geyer MA, Krebs-Thomson K, Braff DL, Swerdlow NR. Pharmacological studies of prepulse inhibition models of sensorimotor gating deficits in schizophrenia: a decade in review. Psychopharmacology. 2001;156(2-3):117-54.
60 Ott T, Nieder A. Dopamine D2 Receptors Enhance Population Dynamics in Primate Prefrontal Working Memory Circuits. Cerebral Cortex. 2016.

61 Nielsen RE, Levander S, Kjaersdam Telléus G, Jensen SOW, Østergaard Christensen T, Leucht S. Second-generation antipsychotic effect on cognition in patients with schizophrenia-a meta-analysis of randomized clinical trials. Acta psychiatrica Scandinavica. 2015;131(3):185-96.
62 Csomor PA, Stadler RR, Feldon J, Yee BK, Geyer MA, Vollenweider FX. Haloperidol Differentially Modulates Prepulse Inhibition and P50 Suppression in Healthy Humans Stratified for Low and High Gating Levels. Neuropsychopharmacology : official publication of the American College of Neuropsychopharmacology. 2007;33(3):497-512.
63 Hutchings EJ, Waller JL, Terry AV. Differential Long-Term Effects of Haloperidol and Risperidone on the Acquisition and Performance of Tasks of Spatial Working and Short-Term Memory and Sustained Attention in Rats. Journal of Pharmacology and Experimental Therapeutics. 2013;347(3):547-56.
64 Sakurai H, Bies RR, Stroup ST, Keefe RS, Rajji TK, Suzuki T, et al. Dopamine D2 receptor occupancy and cognition in schizophrenia: analysis of the CATIE data. Schizophrenia bulletin. 2013;39(3):564-74.
65 Nørbak-Emig H, Ebdrup BH, Fagerlund B, Svarer C, Rasmussen H, Friberg L, et al. Frontal D2/3Receptor Availability in Schizophrenia Patients Before and After Their First Antipsychotic Treatment: Relation to Cognitive Functions and Psychopathology. International Journal of Neuropsychopharmacology. 2016;19(5):pyw006.
66 Lustig C, Meck WH. Chronic treatment with haloperidol induces deficits in working memory and feedback effects of interval timing. Brain and cognition. 2005;58(1):9-16.
67 Naef M, Muller U, Linssen A, Clark L, Robbins TW, Eisenegger C. Effects of dopamine D2/D3 receptor antagonism on human planning and spatial working memory. Translational psychiatry. 2017;7(4):e1107.
68 Kim E, Howes OD, Turkheimer FE, Kim BH, Jeong JM, Kim JW, et al. The relationship between antipsychotic D2 occupancy and change in frontal metabolism and working memory : A dual [(11)C]raclopride and [(18) F]FDG imaging study with aripiprazole. Psychopharmacology. 2013;227(2):221-9.
69 Steen NE, Aas M, Simonsen C, Dieset I, Tesli M, Nerhus M, et al. Serum levels of second generation antipsychotics are associated with cognitive function in psychotic disorders. The World Journal of Biological Psychiatry. 2016:1-33.
70 Shin S, Kim S, Seo S, Lee JS, Howes OD, Kim E, et al. The relationship between dopamine receptor blockade and cognitive performance in schizophrenia: a [(11)C]-raclopride PET study with aripiprazole. Translational psychiatry. 2018;8(1):87.
71 Takano H. Cognitive Function and Monoamine Neurotransmission in Schizophrenia: Evidence From Positron Emission Tomography Studies. Frontiers in psychiatry / Frontiers Research Foundation. 2018;9:228.
72 Zhang G, Stackman RW. The role of serotonin 5-HT2A receptors in memory and cognition. Frontiers in pharmacology. 2015;6.
73 Goozee R, Reinders A, Handley R, Marques T, Taylor H, O'Daly O, et al. Effects of aripiprazole and haloperidol on neural activation during the n-back in healthy individuals: A functional MRI study. Schizophrenia research. 2016;173(3):174-81.
74 Zhou Y, Li G, Li D, Cui H, Ning Y. Dose reduction of risperidone and olanzapine can improve cognitive function and negative symptoms in stable schizophrenic patients: A single-blinded, 52-week, randomized controlled study. J Psychopharmacol. 2018;32(5):524-32.
75 Desamericq G, Schurhoff F, Meary A, Szoke A, Macquin-Mavier I, Bachoud-Levi AC, et al. Long-term neurocognitive effects of antipsychotics in schizophrenia: a network meta-analysis. European journal of clinical pharmacology. 2014;70(2):127-34.
76 Castner SA, Williams GV, Goldman-Rakic PS. Reversal of antipsychotic-induced working memory deficits by short-term dopamine D1 receptor stimulation. Science. 2000;287(5460):2020-2.
77 Kusumi I, Takahashi Y, Suzuki K, Kameda K, Koyama T. Differential effects of subchronic treatments with atypical antipsychotic drugs on dopamine D2 and serotonin 5-HT2A receptors in the rat brain. Journal of neural transmission. 2000;107(3):295-302.
78 Ishikane T, Kusumi I, Matsubara R, Matsubara S, Koyama T. Effects of serotonergic agents on the up-regulation of dopamine D2 receptors induced by haloperidol in rat striatum. European journal of pharmacology. 1997;321(2):163-9.
79 Varela FA, Der-Ghazarian T, Lee RJ, Charntikov S, Crawford CA, McDougall SA. Repeated aripiprazole treatment causes dopamine D2 receptor up-regulation and dopamine supersensitivity in young rats. J Psychopharmacol. 2014;28(4):376-86.

80 Inoue A, Miki S, Seto M, Kikuchi T, Morita S, Ueda H, et al. Aripiprazole, a novel antipsychotic drug, inhibits quinpirole-evoked GTPase activity but does not up-regulate dopamine D2 receptor following repeated treatment in the rat striatum. European journal of pharmacology. 1997;321(1):105-11.
81 Mahmoudi S, Levesque D, Blanchet PJ. Upregulation of dopamine D3, not D2, receptors correlates with tardive dyskinesia in a primate model. Movement disorders : official journal of the Movement Disorder Society. 2014;29(9):1125-33.
82 Tarazi FI, Yeghiayan SK, Baldessarini RJ, Kula NS, Neumeyer JL. Long-term effects of S(+)N-n-propylnorapomorphine compared with typical and atypical antipsychotics: differential increases of cerebrocortical D2-like and striatolimbic D4-like dopamine receptors. Neuropsychopharmacology : official publication of the American College of Neuropsychopharmacology. 1997;17(3):186-96.
83 Tarazi FI, Florijn WJ, Creese I. Differential regulation of dopamine receptors after chronic typical and atypical antipsychotic drug treatment. Neuroscience. 1997;78(4):985-96.
84 Lidow MS, Goldman-Rakic PS. A common action of clozapine, haloperidol, and remoxipride on D1- and D2-dopaminergic receptors in the primate cerebral cortex. Proceedings of the National Academy of Sciences of the United States of America. 1994;91(10):4353-6.
85 Silvestri S, Seeman MV, Negrete JC, Houle S, Shammi CM, Remington GJ, et al. Increased dopamine D2 receptor binding after long-term treatment with antipsychotics in humans: a clinical PET study. Psychopharmacology. 2000;152(2):174-80.
86 Amato D, Natesan S, Yavich L, Kapur S, Muller CP. Dynamic regulation of dopamine and serotonin responses to salient stimuli during chronic haloperidol treatment. Int J Neuropsychopharmacol. 2011;14(10):1327-39.
87 Yadav PN, Kroeze WK, Farrell MS, Roth BL. Antagonist functional selectivity: 5-HT2A serotonin receptor antagonists differentially regulate 5-HT2A receptor protein level in vivo. The Journal of pharmacology and experimental therapeutics. 2011;339(1):99-105.
88 Lian J, Huang X-F, Pai N, Deng C. Effects of olanzapine and betahistine co-treatment on serotonin transporter, 5-HT2A and dopamine D2 receptor binding density. Progress in Neuro-Psychopharmacology and Biological Psychiatry. 2013;47:62-68.
89 Moreno JL, Holloway T, Umali A, Rayannavar V, Sealfon SC, Gonzalez-Maeso J. Persistent effects of chronic clozapine on the cellular and behavioral responses to LSD in mice. Psychopharmacology. 2013;225(1):217-26.
90 Tarazi FI, Zhang K, Baldessarini RJ. Long-term effects of olanzapine, risperidone, and quetiapine on serotonin 1A, 2A and 2C receptors in rat forebrain regions. Psychopharmacology. 2002;161(3):263-70.
91 Steward LJ, Kennedy MD, Morris BJ, Pratt JA. The atypical antipsychotic drug clozapine enhances chronic PCP-induced regulation of prefrontal cortex 5-HT2A receptors. Neuropharmacology. 2004;47(4):527-37.
92 Choi YK, Adham N, Kiss B, Gyertyan I, Tarazi FI. Long-term effects of aripiprazole exposure on monoaminergic and glutamatergic receptor subtypes: comparison with cariprazine. CNS spectrums. 2017:1-11.
93 Kurita M, Holloway T, Garcia-Bea A, Kozlenkov A, Friedman AK, Moreno JL, et al. HDAC2 regulates atypical antipsychotic responses through the modulation of mGlu2 promoter activity. Nature neuroscience. 2012;15(9):1245-54.
94 Huang X-F, Tan YY, Huang X, Wang Q. Effect of chronic treatment with clozapine and haloperidol on 5-HT2A and 2C receptor mRNA expression in the rat brain. Neuroscience research. 2007;59(3):314-21.
95 Mendlin A, Martin FJ, Jacobs BL. Involvement of dopamine D2 receptors in apomorphine-induced facilitation of forebrain serotonin output. European journal of pharmacology. 1998;351(3):291-8.
96 Amargos-Bosch M, Adell A, Artigas F. Antipsychotic drugs reverse the AMPA receptor-stimulated release of 5-HT in the medial prefrontal cortex. Journal of neurochemistry. 2007;102(2):550-61.
97 Amargos-Bosch M, Lopez-Gil X, Artigas F, Adell A. Clozapine and olanzapine, but not haloperidol, suppress serotonin efflux in the medial prefrontal cortex elicited by phencyclidine and ketamine. Int J Neuropsychopharmacol. 2006;9(5):565-73.
98 Amargós-Bosch M, Adell A, Bortolozzi A, Artigas F. Stimulation of α1-adrenoceptors in the rat medial prefrontal cortex increases the local in vivo 5-hydroxytryptamine release: reversal by antipsychotic drugs. Journal of neurochemistry. 2004;87(4):831-42.

99 Amargos-Bosch M, Adell A, Bortolozzi A, Artigas F. Stimulation of alpha1-adrenoceptors in the rat medial prefrontal cortex increases the local in vivo 5-hydroxytryptamine release: reversal by antipsychotic drugs. Journal of neurochemistry. 2003;87(4):831-42.
100 Maejima T, Masseck OA, Mark MD, Herlitze S. Modulation of firing and synaptic transmission of serotonergic neurons by intrinsic G protein-coupled receptors and ion channels. Frontiers in integrative neuroscience. 2013;7:40.
101 Burnet PW, Chen CP, McGowan S, Franklin M, Harrison PJ. The effects of clozapine and haloperidol on serotonin-1A, -2A and -2C receptor gene expression and serotonin metabolism in the rat forebrain. Neuroscience. 1996;73(2):531-40.
102 Bishnoi M, Chopra K, Kulkarni SK. Neurochemical changes associated with chronic administration of typical antipsychotics and its relationship with tardive dyskinesia. Methods and findings in experimental and clinical pharmacology. 2007;29(3):211-6.
103 Albizu L, Holloway T, Gonzalez-Maeso J, Sealfon SC. Functional crosstalk and heteromerization of serotonin 5-HT2A and dopamine D2 receptors. Neuropharmacology. 2011;61(4):770-7.
104 Tsartsalis S, Tournier BB, Huynh-Gatz T, Dumas N, Ginovart N, Moulin-Sallanon M, et al. 5-HT2A receptor SPECT imaging with [(1)(2)(3)I]R91150 under P-gp inhibition with tariquidar: More is better? Nuclear medicine and biology. 2016;43(1):81-8.
105 Natesan S, Reckless GE, Nobrega JN, Fletcher PJ, Kapur S. Dissociation between In Vivo Occupancy and Functional Antagonism of Dopamine D2 Receptors: Comparing Aripiprazole to Other Antipsychotics in Animal Models. Neuropsychopharmacology : official publication of the American College of Neuropsychopharmacology. 2005;31(9):1854-63.

Figure 1

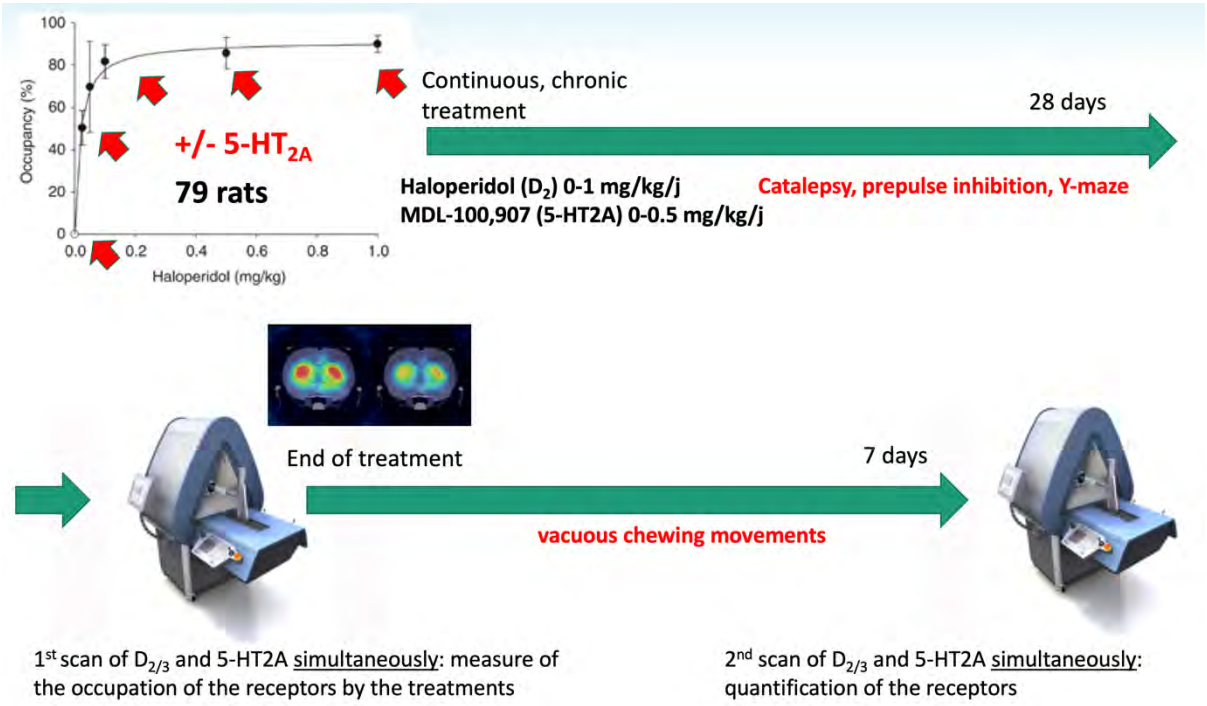
100
80
60
40
20
0
Occupancy (%)
0.0
0.2
0.4
0.6
0.8
1.0
Haloperidol (mg/kg)
+/- 5-HT2A
79 rats
Continuous, chronic treatment
28 days
Haloperidol (D2) 0-1 mg/kg/j
MDL-100,907 (5-HT2A) 0-0.5 mg/kg/j
Catalepsy, prepulse inhibition, Y-maze
End of treatment
7 days
vacuous chewing movements
1st scan of D2/3 and 5-HT2A simultaneously: measure of the occupation of the receptors by the treatments
2nd scan of D2/3 and 5-HT2A simultaneously: quantification of the receptors

Figure 2

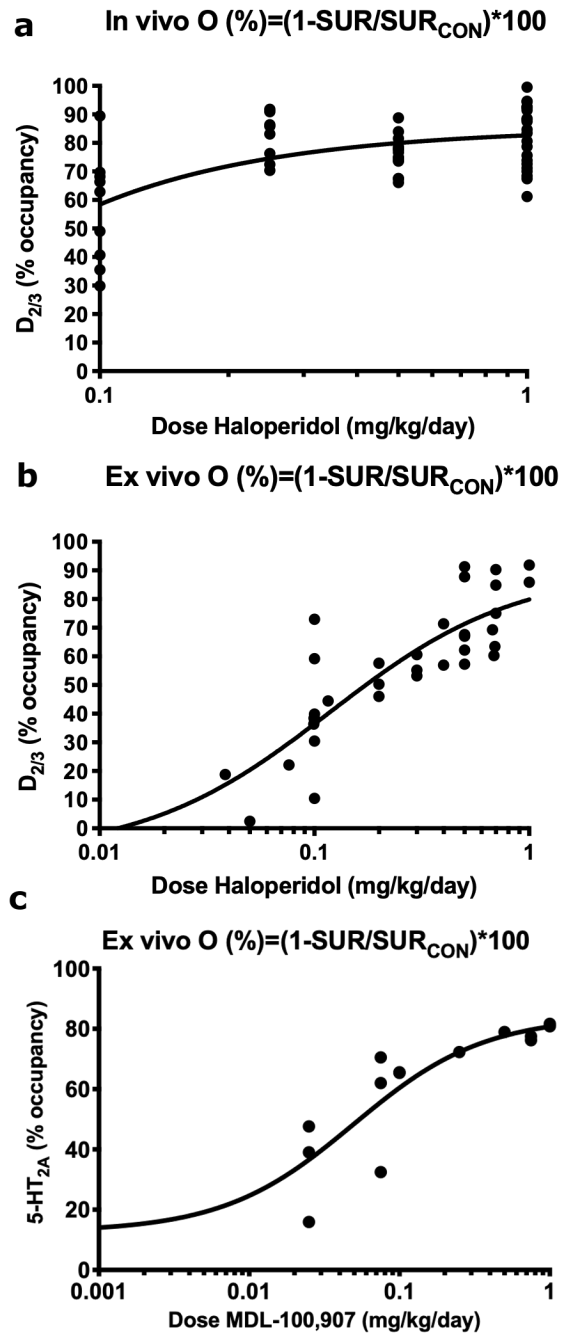
a
In vivo O (%)=(1-SUR/SUR$_{CON}$)*100
D$_{2/3}$ (% occupancy)
Dose Haloperidol (mg/kg/day)
b
Ex vivo O (%)=(1-SUR/SUR$_{CON}$)*100
D$_{2/3}$ (% occupancy)
Dose Haloperidol (mg/kg/day)
c
Ex vivo O (%)=(1-SUR/SUR$_{CON}$)*100
5-HT$_{2A}$ (% occupancy)
Dose MDL-100,907 (mg/kg/day)

Figure 3

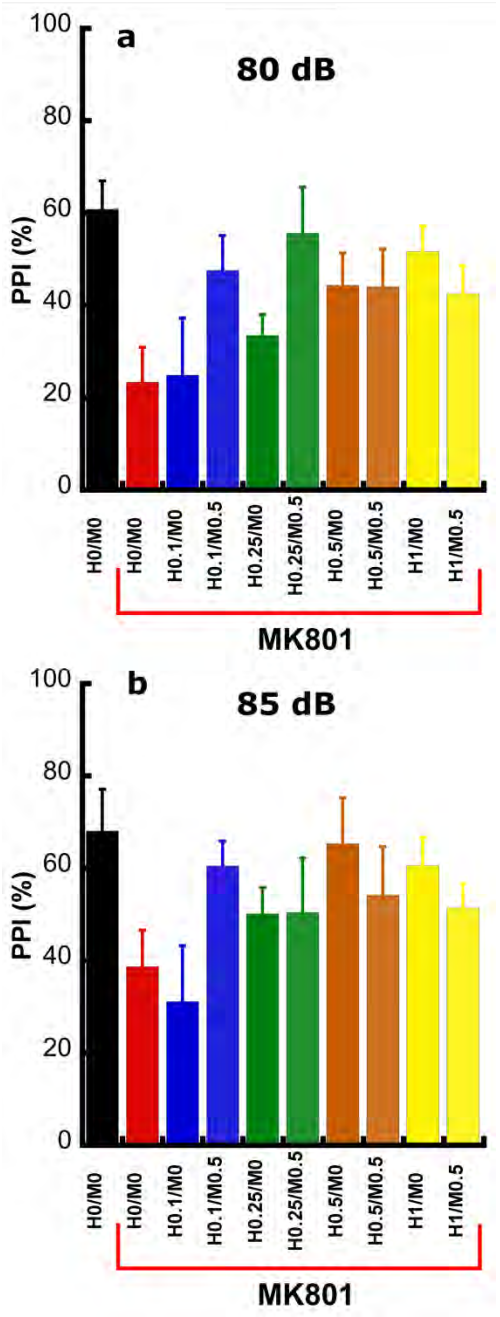
a
80 dB
PPI (%)
100
80
60
40
20
0
H0/M0
H0/M0
H0.1/M0
H0.1/M0.5
H0.25/M0
H0.25/M0.5
H0.5/M0
H0.5/M0.5
H1/M0
H1/M0.5
MK801
b
85 dB
PPI (%)
100
80
60
40
20
0
H0/M0
H0/M0
H0.1/M0
H0.1/M0.5
H0.25/M0
H0.25/M0.5
H0.5/M0
H0.5/M0.5
H1/M0
H1/M0.5
MK801

Figure 4

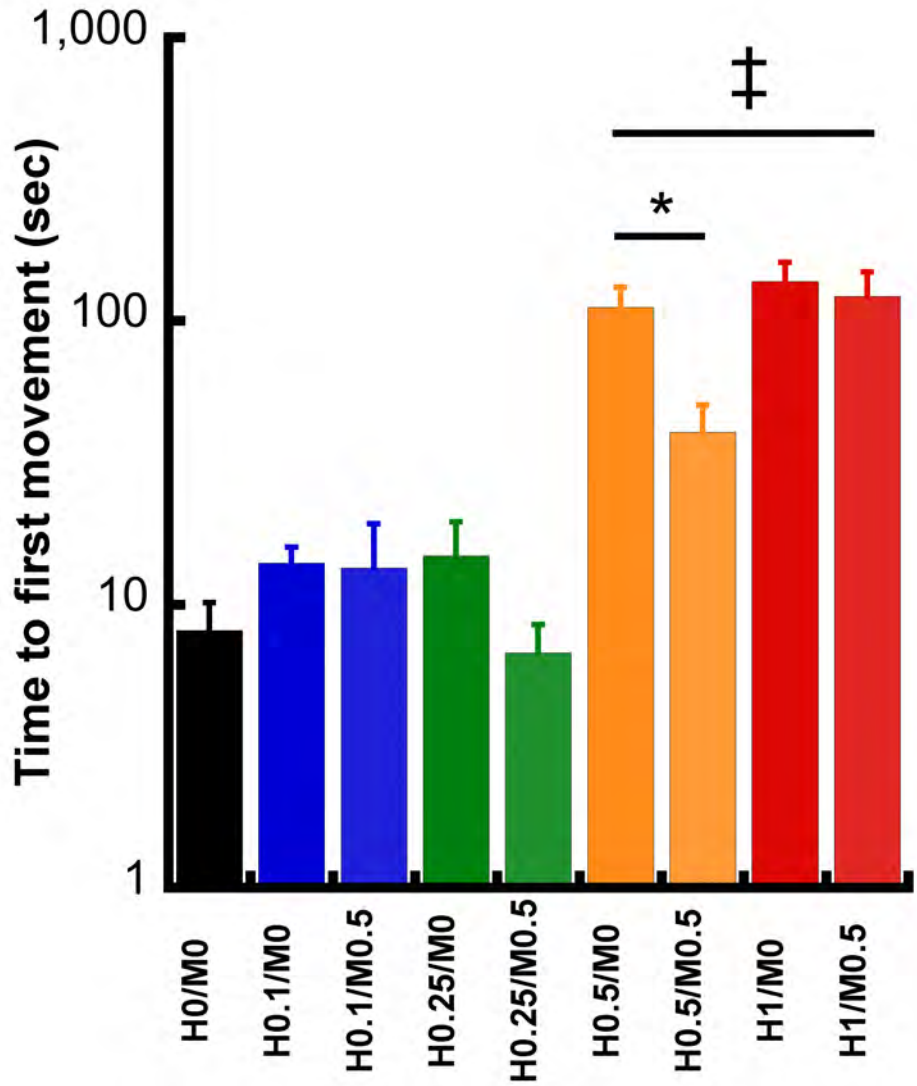
1,000
100
10
1
Time to first movement (sec)
*
‡
H0/M0
H0.1/M0
H0.1/M0.5
H0.25/M0
H0.25/M0.5
H0.5/M0
H0.5/M0.5
H1/M0
H1/M0.5

Figure 5

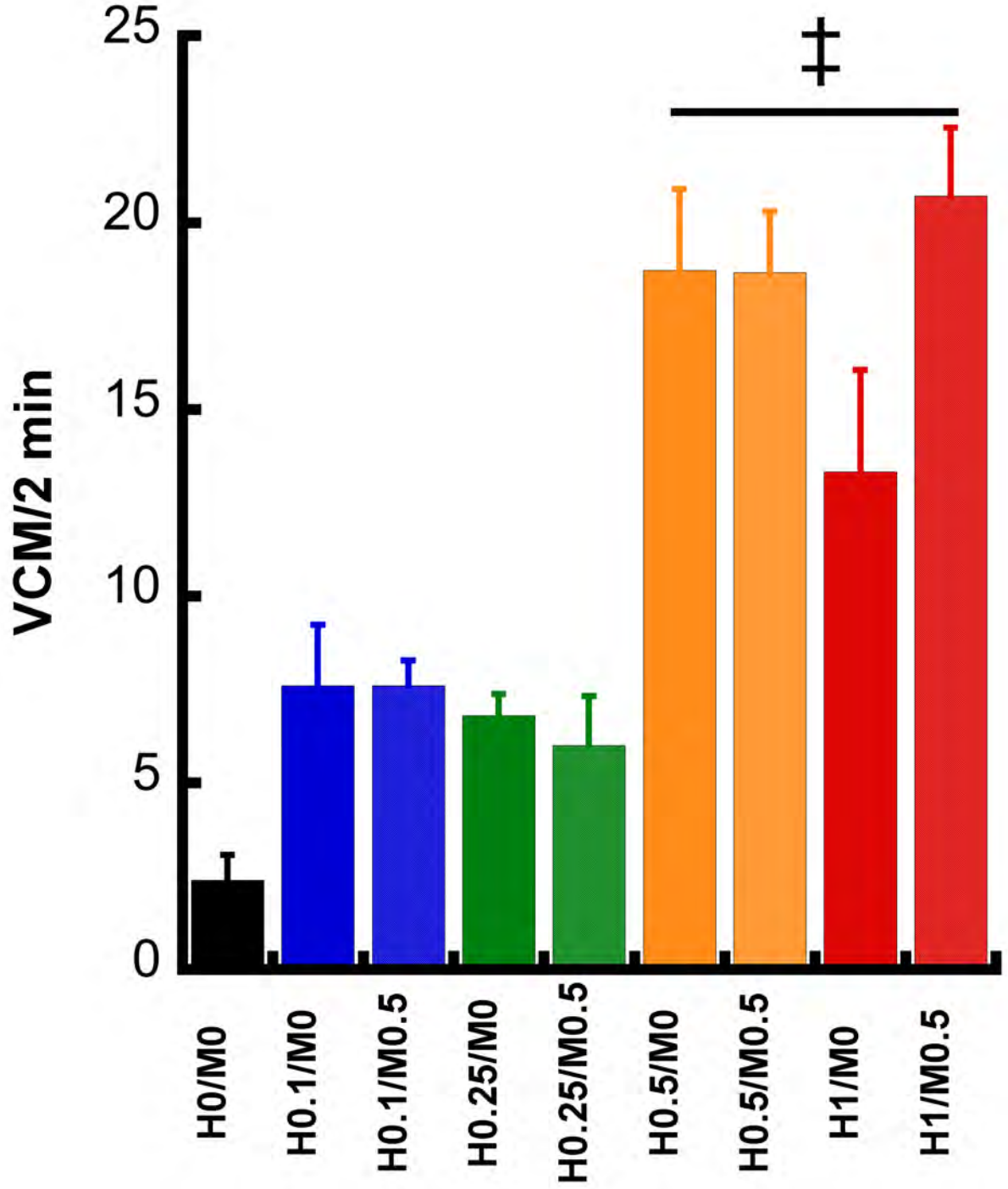
25
20
15
10
5
0
VCM/2 min
‡
H0/M0
H0.1/M0
H0.1/M0.5
H0.25/M0
H0.25/M0.5
H0.5/M0
H0.5/M0.5
H1/M0
H1/M0.5

Figure 6

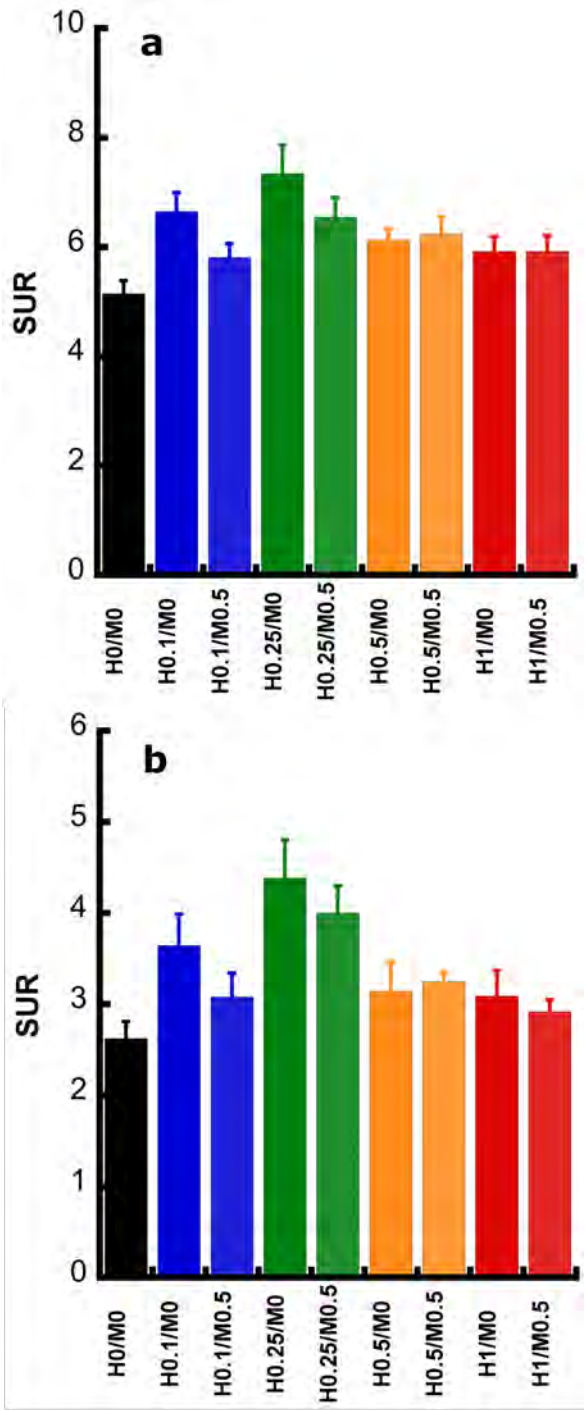
a
SUR
10
8
6
4
2
0
H0/M0
H0.1/M0
H0.1/M0.5
H0.25/M0
H0.25/M0.5
H0.5/M0
H0.5/M0.5
H1/M0
H1/M0.5
b
SUR
6
5
4
3
2
1
0
H0/M0
H0.1/M0
H0.1/M0.5
H0.25/M0
H0.25/M0.5
H0.5/M0
H0.5/M0.5
H1/M0
H1/M0.5

Figure 7